

Università degli Studi di Milano

Department of Chemistry



Doctorate School in Chemical Science and Technologies

Ph.D Course in Chemical Science - XXXII Cycle

Hybrid Catalysts for Carbene and Nitrene Transfer Reactions

**Ph.D Thesis of:
Caterina Damiano
Matr. n. R11651**

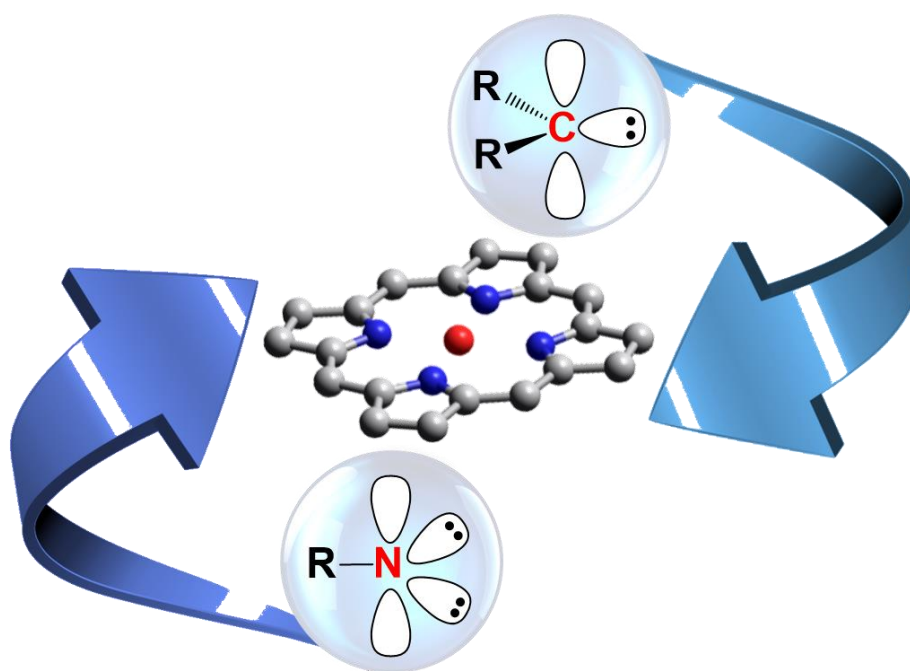
**Tutor: Prof. Emma Gallo
Coordinator: Prof. Emanuela Licandro**

Academic Year 2018/2019

Chapter I: General Introduction	7
1. Metal catalysed carbene and nitrene transfer reactions	8
1.1. C-C and C-N bond formation: three-membered ring compounds	9
2. Metal porphyrin complexes	10
2.1. The porphyrin ligand	10
3. Porphyrins and biomolecules	15
3.1. Metal porphyrin complexes in nature	15
3.2. Engineered heme proteins for catalytic application	17
4. Aim and outline of the thesis	19
5. References	21
Chapter II: Glycoconjugated porphyrins	25
1. Introduction	26
1.1. Glycoporphyrins: synthetic approach	26
1.2. Glycoporphyrins as ligands in catalysis	28
2. Results and Discussion	32
2.1. Glycoporphyrins synthesis	32
2.2. Glycoporphyrin complexes in alkene cyclopropanation reactions	36
2.3. Glycoporphyrin complexes in alkene aziridination reactions	38
3. Conclusion	41
4. Experimental section	42
4.1. Synthesis of porphyrin ligands	42
4.2. Synthesis of porphyrin complexes	49
4.3. Synthesis of diazo compounds	57
4.4. Synthesis of azides	58
4.5. Synthesis of cyclopropanes	60
4.6. Synthesis of aziridines	63
4.7. ¹ H-NMR, ¹⁹ F-NMR and ¹³ C-NMR of isolated compounds	66
5. References	82
Chapter III: Hybrid <i>bis</i>-strapped porphyrin	85
1. Introduction	86
1.1. Single and double-face porphyrins	86
1.2. <i>Bis</i> -strapped porphyrins as ligand for carbene transfer reactions	88
2. Discussion	92
2.1. Preliminary studies	92
2.2. Hybrid <i>bis</i> -strapped ligand for alkenes cyclopropanation	96
3. Conclusion	99
4. Experimental section	100
4.1. Synthesis of organic precursors	100
4.2. Synthesis of porphyrin ligands	102
4.3. Synthesis of porphyrin complex	106
4.4. Synthesis of cyclopropanes	106
4.5. ¹ H-NMR and 2D NMR of isolated compounds	109
5. References	114

Chapter IV: Porphyrins for conjugation with macromolecules	117
1. Introduction	118
1.1. B-lactoglobulines as host proteins	118
1.2. Bio-cellulose as solid support	121
1.3. A ₃ B-type porphyrins	123
2. Discussion	126
2.1. Synthesis of A ₃ B-porphyrins	126
2.2. Preliminary studies with cellulose	128
3. Conclusion	130
4. Experimental section	131
4.1. Synthesis of porphyrin ligands	131
4.2. Synthesis of solid supported catalyst	135
4.3. Synthesis of cyclopropane	136
4.4. ¹ H-NMR and ¹³ C-NMR of isolated compounds	137
5. References	140
Chapter V: Ruthenium porphyrins for CO₂ cycloaddition to three-membered ring compounds	143
1. Introduction	144
1.1. CO ₂ as renewable C1 building block	145
1.2. Mechanism of CO ₂ cycloaddition to epoxides and aziridines	146
2. Discussion	150
2.1. CO ₂ cycloaddition to aziridines	150
2.2. CO ₂ cycloaddition to epoxides	152
2.3. Hypothesis of the CO ₂ cycloaddition mechanism	154
3. Conclusion	156
4. Experimental section	157
4.1. Synthesis of ruthenium complexes	157
4.2. Synthesis of oxazolidin-2-ones	159
4.3. Competitive reaction between aziridines and epoxides	160
4.4. Synthesis of cyclic carbonates	160
5. References	164
Summary	167
List of publications	175

Chapter I: General Introduction



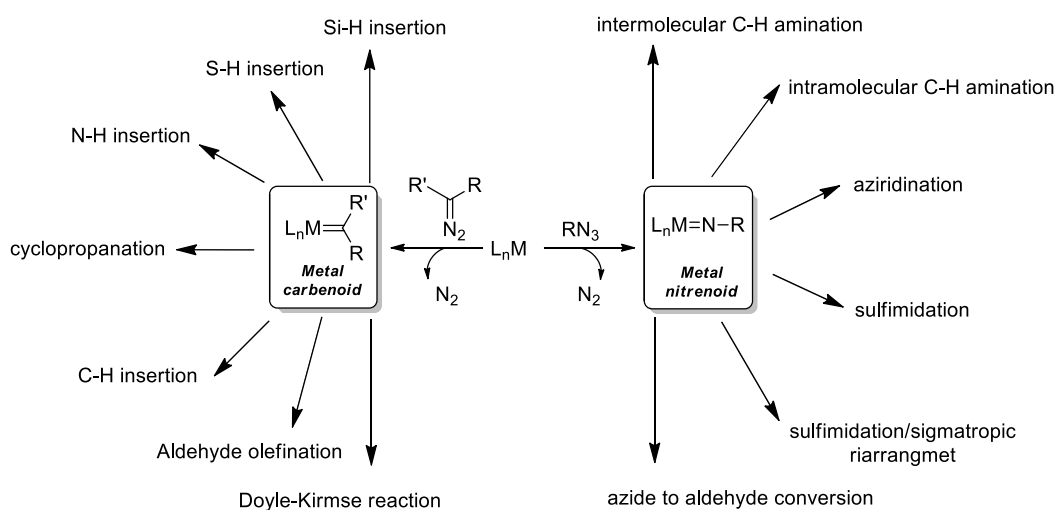
1. Metal catalysed carbene and nitrene transfer reactions

Current society is increasingly focused on environment and sustainability. Accordingly, chemical industry is ever more interested to develop sustainable and selective procedures for the synthesis of high-added fine chemicals.

A chemical transformation can be considered clean and sustainable only if it does not produce large amounts of side-products and waste, avoiding the use of toxic reagents, and if it shows a high atom economy^{1,2}. In this context, metal catalysed reactions are a powerful tool to achieve the purpose especially if the chosen catalytic system shows high selectivity, activity and stability and it can be recycled and reused³.

Reasons mentioned above prompted the research community to identify the most attractive reactions and efficient catalytic systems to apply in synthetic methodologies, natural products synthesis and functionalization of complex molecules.

The metal catalysed carbene and nitrene transfer reactions have proved to be an excellent strategy to achieve the goal⁴, due to their ability to form C-C, C-N and C-heteroatom bond^{5,6}. Metallo-carbene/nitrene mediated reactions proceed, under mild conditions, with high stereo- and regioselectivity and their performances can also be modulated by changing the metal ion or the ligand of the catalyst. In addition, a good choice of carbene and nitrene precursors can increase the sustainability and the atom efficiency of the methodology, as in the case of diazo compounds⁷ and azides,⁸ which produce molecular nitrogen as the only by-product of carbene and nitrene transfer reactions (Scheme 1).



Scheme 1: Metal catalysed carbene and nitrene transfer reactions

1.1. C-C and C-N bond formation: three-membered ring compounds

Among all the metal catalysed carbene and nitrene transfer reactions, the formation of three-membered ring compounds, such as cyclopropanes and aziridines, is one of the most attractive topics in organic chemistry due to their use as building blocks and biological and/or pharmaceutical activity.

Cyclopropane are contained in many natural and synthetic products such as insecticides and pharmaceutical drugs and the aziridines, the smallest *N*-heterocycle compounds, are contained in antitumor compounds, antibiotics and enzyme inhibitors (Figure 1)⁹⁻¹¹. Thanks to the energy associated to the strained three-membered ring, they have a prominent role as building blocks for the synthesis of challenging complex molecules.

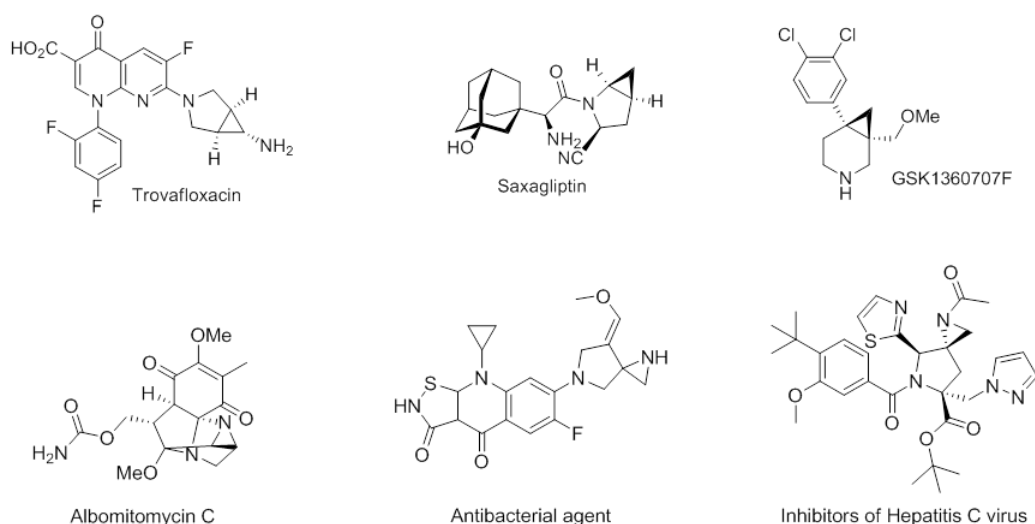
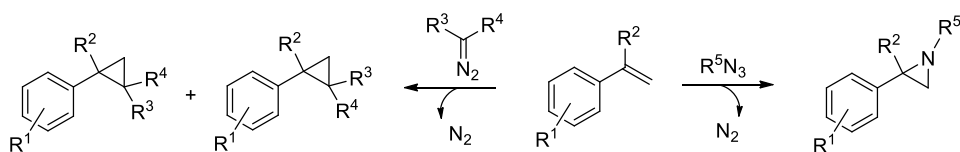


Figure 1: Examples of cyclopropanes and aziridines containing compounds

Due to the high interest in the synthesis of three-membered ring compounds, several synthetic procedures have been developed during the years and the direct transfer reaction of carbene and nitrene is one of the most interesting ones. In particular, the use of the one-pot reaction between alkenes and either azides or diazo compounds increase the process sustainability (Scheme 2)^{7,12}. Among all the metal complexes which are used as catalysts for cyclopropanation and aziridination reactions, metal porphyrin complexes are the most promising ones, because of their high catalytic activity and chemical stability.



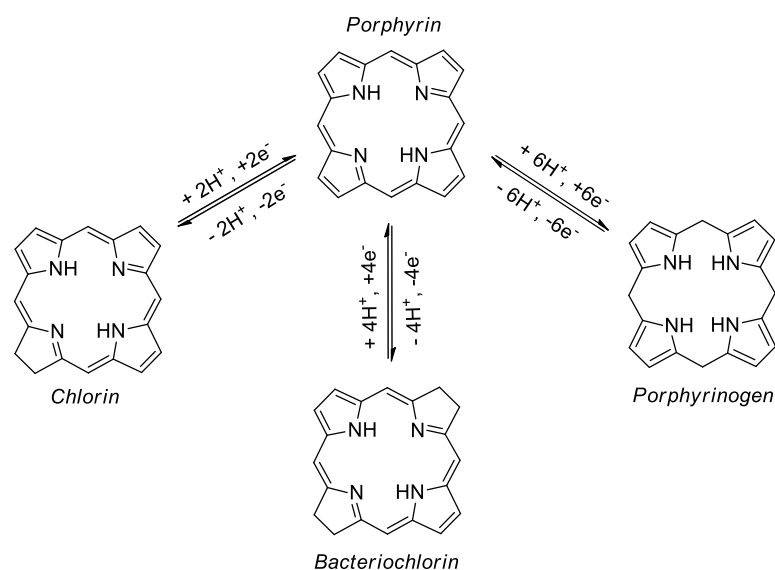
Scheme 2: Direct reaction of styrenes with diazo compounds or aryl azides

2. Metal porphyrin complexes

2.1. The porphyrin ligand

Porphyrin ligands, generally called “pigment of life”, are high stable macrocycles that play an important role in biology as well as in chemical, industrial and technological fields. Porphyrin ligands are, in fact, fundamental component of several proteins and their corresponding metal complexes are responsible for photosynthesis (chlorophyll), oxygen transport (hemoglobin) and oxygen activation (cytochrome).

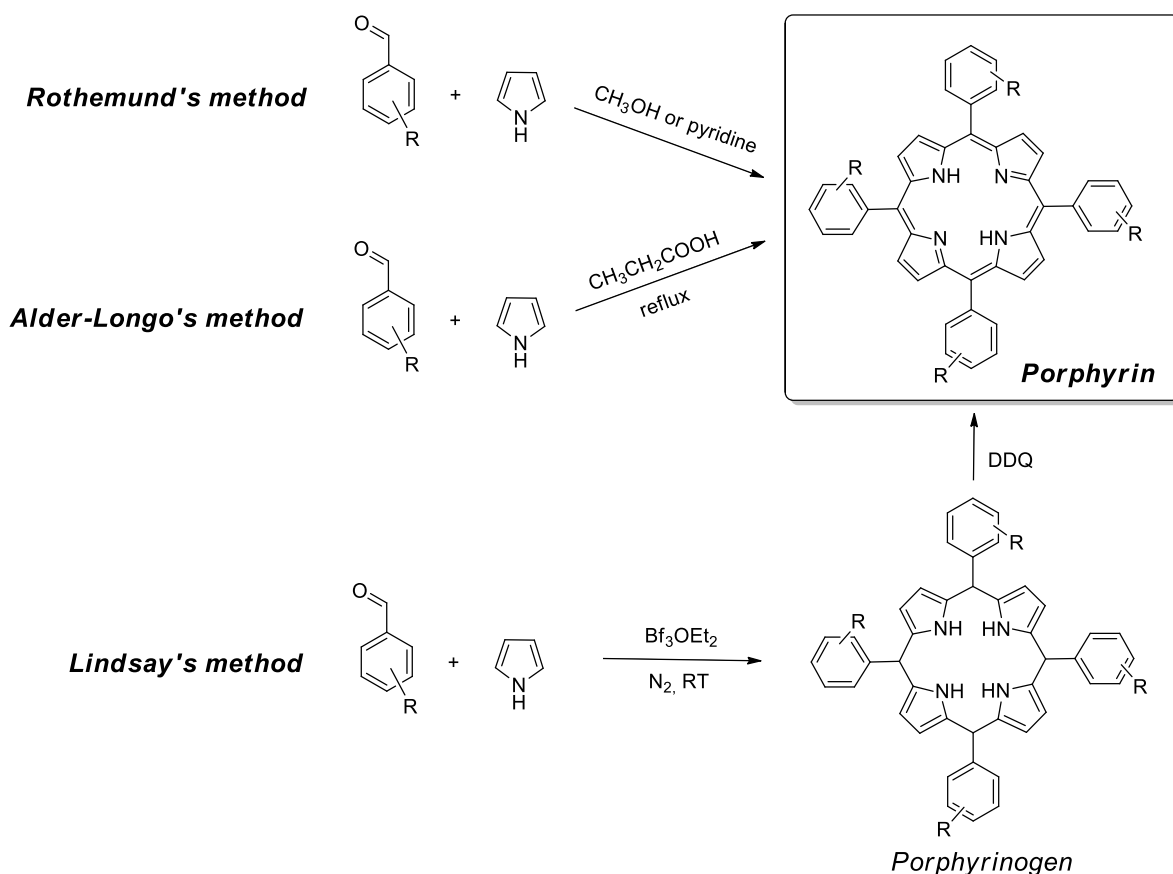
In structural terms, the high stable porphyrinic ring is arranged in four pyrrole units bridged by methine groups and with its 11 conjugate double bonds and 26 π -electrons delocalized all over the ring, it respects the Huckel rule ($4n+2$). The structure also lends itself to possible modifications, a large variety of substituents can be attached at pyrrolic β sites or linked to the *meso*-positions at the methine bridges and the addition of a different number of protons can produce different pyrrolic cycles with different properties (Scheme 3).



Scheme 3: Porphyrin and other related macrocycles

Even though the β -substituted porphyrins are in the majority of natural macrocycles, the *meso*-substituted porphyrins display a promising role both in chemistry and biology and present a simpler synthetic route for their production. The first synthetic approach for the synthesis of *meso*-substituted porphyrin ligands was developed by Rothmund in 1935, reacting pyrrole and the desired aldehyde in methanol or pyridine in a sealed tube (Scheme 4)¹³⁻¹⁵. In subsequent years, Alder and Longo optimized the strategy refluxing the same reagents in propionic acid at atmospheric pressure¹⁶. On the one hand, the Alder-Longo strategy permits the conversion of a variety of substituted benzaldehydes for obtaining the desired *meso*-porphyrin with good yield (15-20%) as a crystalline precipitate. On the other hand, the required harsh reaction conditions and the large amount of by-products don't allow the synthesis of

derivatives containing sensitive functional groups. To overcome this impediment, in 1987, Lindsay significantly improved the synthetic procedure with the introduction of the two-steps one-pot porphyrinogen methodology¹⁷. At room temperature and under anaerobic conditions, the acid catalysed reaction between pyrrole and aldehydes affords the *meso*-porphyrinogen, which is subsequently oxidized in the presence of an oxidizing agent, such as 2,3-dichloro-5,6-dicyano-1,4-benzoquinone (DDQ), giving the desired porphyrin in good yields up to 40%.



Scheme 4: Methodologies for the synthesis of porphyrins

Thanks to the flexibility and the improvements of the Alder and Lindsay methodology a plethora of *meso* and/or β -substituted porphyrins can be synthesised with different structural and electronics properties.

2.2. Metal porphyrin complexes

Porphyrins are a unique class of ligands. In their neutral form, usually called “free base”, they present two protonated pyrrolic units. When the two protons are removed, the porphyrin becomes a tetradentate

dianionic ligand that can accommodate several metals or semimetals forming the metal porphyrin complexes listed in the so-called “*periodic table of metalloporphyrins*”¹⁸.

The various kinds of metal porphyrin complexes show significantly different structures and chemical reactivities depending on the oxidation state, configuration and spin state of the metal ions. The obtained complexes can be classified according to the stoichiometry or geometry, or both. Usually, the porphyrin core is big enough to accommodate the metal atom giving rise the most common geometries (square planar or octahedral). In presence of too large atoms, they are placed outside of the plane, but metals with particular electronic properties may also give rise unusual *out of plane* geometries (Figure 2).

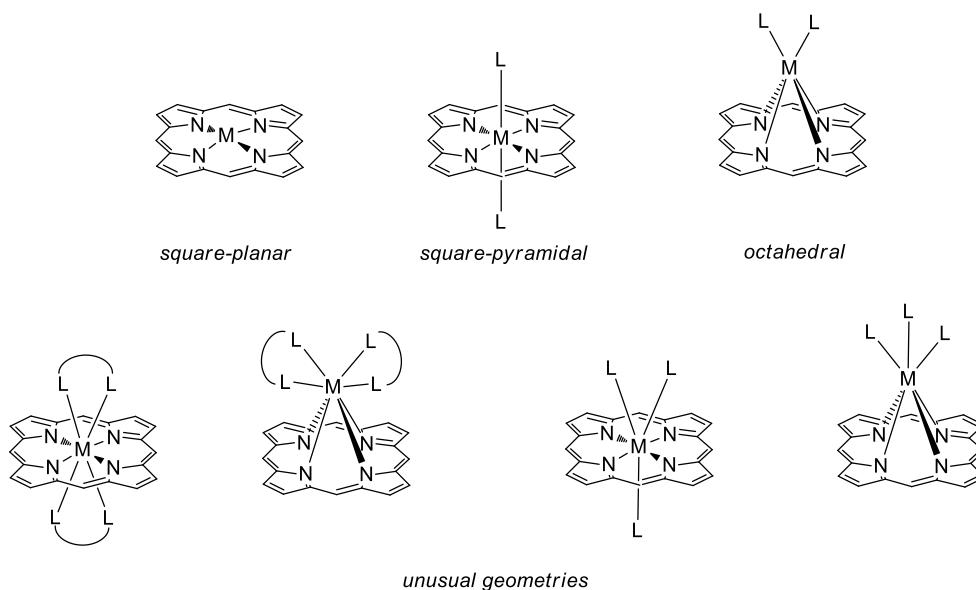
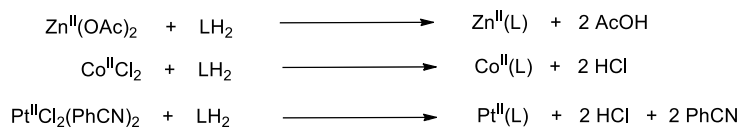


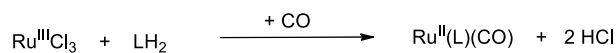
Figure 2: Geometries of metal porphyrin complexes

Several synthetic procedures were developed for the synthesis of metal porphyrin complexes that involved the coordination, reduction or oxidation of the metal, depending from the nature of the metal sources. The oxidation step may be achieved spontaneously thanks to the reaction conditions but, in some cases, the introduction of an external oxidant reagent is necessary. All the possible strategies for the synthesis of metal porphyrin complexes can be classified in four classes: I) coordination of the metal from a MX_2 salt, II) reduction of a metal salt, III) oxidation from an external oxidant agent and IV) spontaneous oxidation of the metal starting from a $\text{M}(0)$ cluster (Scheme 5)¹⁹.

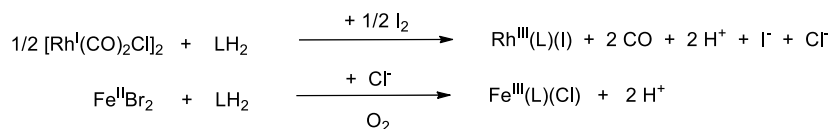
I) Coordination of the metal from a MX_2 salt:



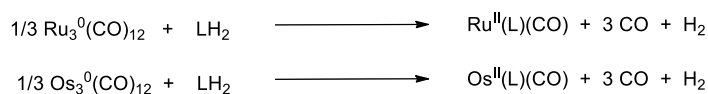
II) Reduction of a metal salt:



III) Oxidation by an external oxidant:



III) Spontaneous oxidation of the metal from $M(0)$ cluster:



Scheme 5: Methods for the synthesis of metal porphyrin complexes

I) Coordination of the metal from a MX_2 salt: the synthetic procedure consists in the reaction between a divalent metal salt and the porphyrin ligand, in the opportune solvent, in order to simultaneously react the two substrates in reactive conditions. The main problem that rises from this strategy is the choice of the solvent because, in most cases, a good porphyrin solvent is not suitable for solubilising the metal salts. Among all the solvents tested for the reaction, *N,N*-dimethylformamide (DMF) proved to be an excellent medium in which several porphyrins and metals are soluble. By using this method, a variety of metals (Zn, Co, Cu, Ni, Fe, Cr, Mn, Pb, Pd, Hg, Cd etc.) can react with the porphyrin ligand giving the desired product in very good yields. In addition, the use of a weak Brønsted base promotes the reaction rate, removing the two free base pyrrolic protons.

II) Reduction of a metal salt: the synthetic procedure provides the metal insertion starting from a metal precursor in higher oxidation state, like in the case of the insertion of Ru-CO moiety from the RuCl_3 . The reaction is performed under carbon monoxide atmosphere that acts both as a reductant and ligand in order to complete the coordination sphere of the metal. A complete stoichiometry of this reaction is not reported but it seems to be not so different from the *in situ* formation of the $\text{Ru}_3\text{CO}_{12}$ cluster that subsequently reacts with the ligand.

III) Oxidation from an external oxidant agent: the method requires the introduction of an external oxidant reagent in order to promote the oxidation state variation of the metal centre obtaining an isolable and stable product. The most common example of this strategy is the iron insertion in which the initially formed Fe(II)(porphyrin) is oxidized to the corresponding Fe(III) compound during the

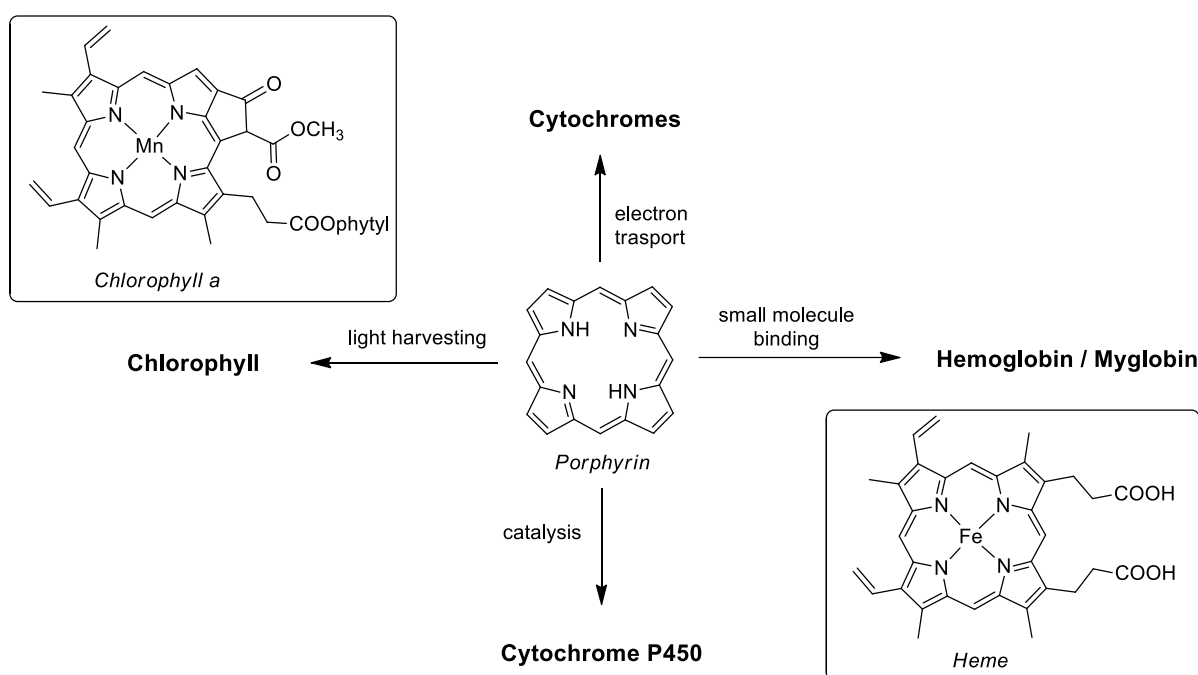
work-up runs at the air and in presence of a donor ligand (for example Cl^- from an aqueous HCl/NaCl solution).

IV) Spontaneous oxidation of the metal starting from a $M(0)$ cluster: the procedure consists in the reaction between the neutral cluster $\text{M}_3(\text{CO})_{12}$ and the free-base in a high boiling point solvent in which the spontaneous oxidation of the metal is promoted by the formation of molecular hydrogen derived from the two inner pyrrolic protons of the porphyrin. This strategy is generally used for the insertion of ruthenium and osmium and the solubility of the reagents is not crucial for a successful reaction. That is the reason why several solvents have been used depending on the stability and conformation of the free-base at high temperatures.

3. Porphyrins and biomolecules

3.1. Metal porphyrin complexes in nature

Porphyrins and some of their metal complex salts play an important role as natural pigments for life on earth. Two classes of natural metal porphyrins can be distinguished depending on the metal and the nature of the porphyrin ligand: the chlorophyll molecule²⁰ and the heme group containing molecules (Scheme 6)²¹.



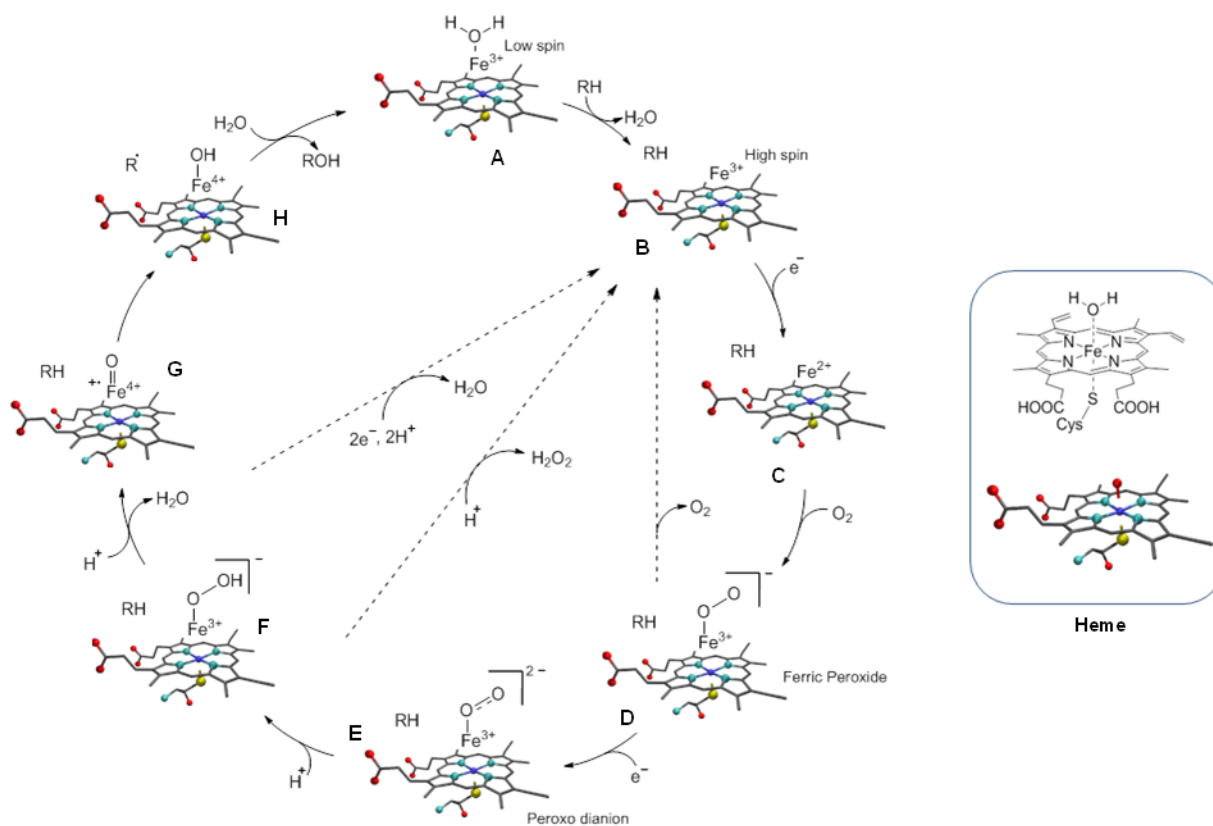
Scheme 6: Metalloporphyrins and related functions in nature

Chlorophyll, a magnesium-containing porphyrin, is an important photosynthetic pigment in plants with a high ability to absorb light related to the structure of the porphyrin ring. The magnesium ion plays a bifunctional role, a structural one to provide the necessary rigidity to the system and the second role is the facilitation of the energy transfer of an absorbed photon's energy.

The iron complex of protoporphyrin IX, also known as heme, it's an essential component of various hemoproteins involved in the oxygen transport and storage (hemoglobin, myoglobin), electron transfer, drug and steroid metabolism (cytochromes), degradation of hydrogen peroxide (catalases, peroxidases) and signal transduction (nitric oxide synthases, guanylate cyclases).

Among the heme-containing proteins, the cytochrome P450²² represents one of the most interesting enzyme contained in several monooxygenase. This enzyme is able to catalyse a series of oxidative reactions by the insertion of activated oxygen and it's also able to promote the oxidation of non-activated hydrocarbons at a physiological temperature. Several studies on different cytochromes

P450 revealed that the iron atom, placed in the porphyrin ring, is bound to a cysteine residue and a water molecule, which is involved in the oxygen activation cycle, is the sixth ligand of the low spin iron atom. The catalytic cycle (Scheme 7) starts from the resting state (A), in which the low-spin ferric enzyme is bonded to the water molecule and the cysteine residue. The addition of the substrate (R–H) and the displacement of the water ligand induces the change of the iron spin state, giving an high-spin penta-coordinated ferric complex (B). At this step, the electron, originated by the NAD(P)H and shuttled by the protein, reduces the Fe(III) complex to the corresponding Fe(II) complex (C) that it's able to bond the ambient oxygen forming the ferric peroxide (D). The second electron reduction produces the ferric-peroxo intermediate (E), a super-nucleophilic compound that is quickly protonated giving the ferric-hydroperoxo intermediate (F). The addition of another proton leads to the release of a water molecule and a very reactive oxoferryl intermediate, the radical cation species (G), which is stabilised by the donation of one electron from the porphyrin ligand. This highly reactive species takes a hydrogen atom from the substrate, generating the ferryl-hydroxo compound (H) which hydroxylates the substrate according to a radical mechanism. At this point, the product is released and the resting state (A) is regenerated to rebound the water molecule.



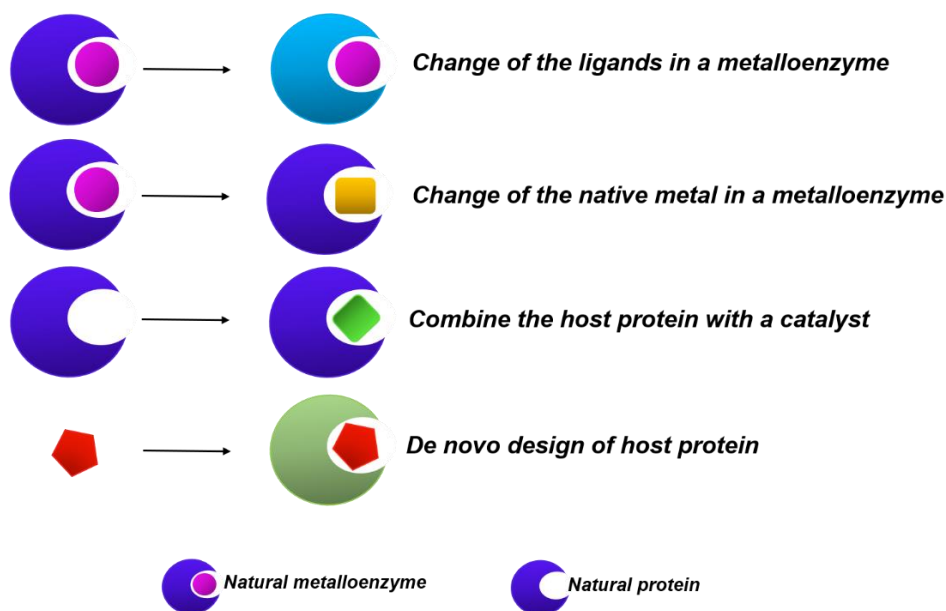
Scheme 7. Catalytic oxygen activation cycle of cytochrome P450

The example of cytochrome P450 shows the ability of metalloenzymes to perform reactions with uniquely high selectivities and specificities. Inspired by the remarkable catalytic activity of heme-containing enzymes, many efforts have been made to synthesize new catalytic systems able to reproduce or expand the enzymatic performances reusing what nature offers. Over the years, the catalysis has been approaching a new idea that exploits the biomolecules and their properties in order to bring out the gap between the synthetic catalysts and the natural enzyme.

3.2. Engineered heme proteins for catalytic application

Traditionally, catalysts have always been classified in three different categories: heterogeneous, homogeneous and enzymes. Nowadays the concept of bio-based hybrid catalysts and artificial metalloenzymes has been introduced in order to combine the properties of synthetic catalysts and natural systems²³.

Several approaches have been explored to develop artificial enzymes and they can be classified in four types: replacement of the native metallic ion; change of the ligands in the metalloenzyme; *de novo* design of artificial metalloenzymes and incorporation of coordination complexes in host molecules (Scheme 8)²⁴⁻³⁰.



Scheme 8: Approaches for the synthesis of bio-hybrid catalysts

The replacement of the native metallic ion represents one of the easiest ways to obtain an artificial metalloenzyme with different catalytic properties. It consists in the replacement of the native metal with another one in order to change the catalytic activity. Sreenilayam et al.³¹ reported the recombinant

expression of myoglobin (oxygen-transport hemoprotein) variants incorporating first, second and third row transition metal cofactors (Mn, Co, Ru, Rh, Ir). The resulting artificial metalloenzyme showed high catalytic activity towards the cyclopropanation, N–H and S–H insertion reactions. In addition, the Mn-substituted and Co-substituted variants showed activity for the intermolecular carbene C–H insertion, a non supported reaction by the iron-containing myoglobins³¹.

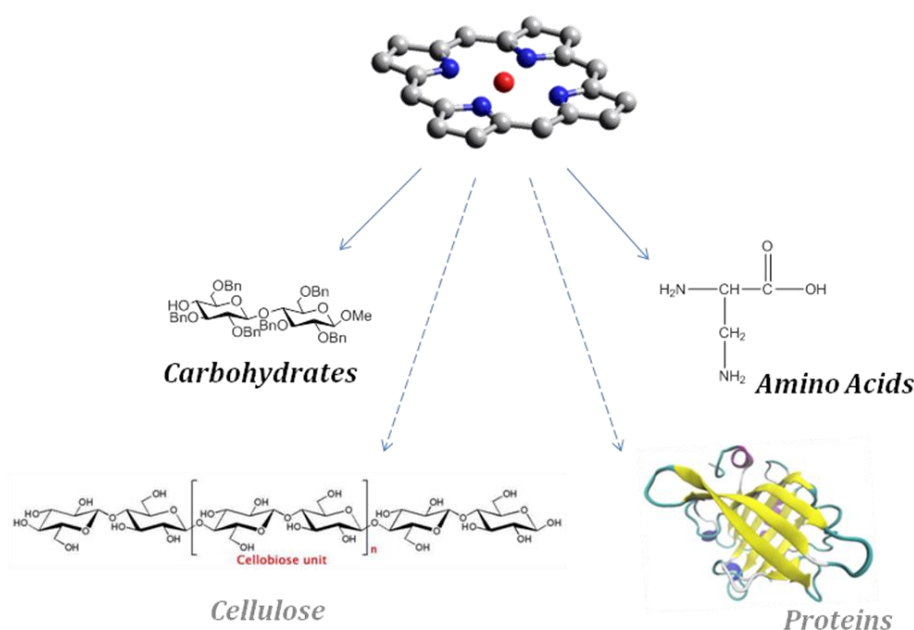
An alternative strategy, often used in the case of heme-proteins, aims to modify the native enzyme function through the mutation of some amino-acids involved in the catalytic process^{32–34}, in order to alter the reactivity and improve the substrate scope. This approach usually benefits from the support of molecular modelling in order to avoid the coordination of remote aminoacids to the metal and foster the active site. An example of this strategy is reported by Fasan et al. They replaced the cysteine apical ligand of the cytochrome P450 with a serine residue. This mutation, combined with other substitutions in the protein scaffold, makes the enzyme able to catalyse the intramolecular amination (C–N bond formation) and the carbene transfers to alkenes with good yields and selectivities^{35,36}.

The rational or *de novo* design of metalloenzymes involves the construction of a peptide sequence that spontaneously folds in a specific three-dimensional structure. The goal of this approach consists in the development of a stable protein constructs with functions and properties either comparable to or better than those of native proteins.

The last method for the synthesis of bio-hybrid catalysts is represented by the incorporation of coordination complexes in host proteins or biomolecules. The engineered enzyme can derive from the insertion of a synthetic catalyst in the apo-form of the protein, like in the case of the cytochrome P450 developed by Hartwing et al., in which the heme group is replaced by an Ir(Me)-*mesoporphyrin IX* in order to expand the reactivity towards C–H insertions^{37,38}. But synthetic metalloporphyrins are not the only ones that can be introduced in the apo-form of a hemeprotein: Schiff base complexes were considered good candidates as well to replace the hemic group because of their planar structure and their high catalytic efficiency^{26,39–42}.

4. Aim and outline of the thesis

Considering the catalytic activity of metal porphyrin complexes in promoting cyclopropanation and aziridination reactions of alkenes, the following PhD project aims to develop a new class of hybrid catalysts able to perform carbene and nitrene transfer reactions under mild experimental conditions. In order to confer chiral recognition properties and modulate the catalyst solubility, the approach is the conjugation of metal porphyrin complexes with bio-scaffolds such as carbohydrates, amino acids, cellulose and β -lactoglobulins (Scheme 9).



Scheme 9: Approaches for the synthesis of bio-hybrid catalysts

In **Chapter II** the synthesis of novel *mono* and *tetra*substituted glycoporphyrin ligands is reported. The catalytic activity of their corresponding iron (III) and ruthenium (II) complexes, towards cyclopropanation and aziridination reactions, is discussed focusing the attention on the influence of sugar moieties on the catalytic performances.

In **Chapter III** the synthesis of a new hybrid *bis*-strapped porphyrin, derived from the conjugation with an aminoacidic residue, is described. Symmetry considerations and NMR characterizations of the new hybrid ligand are discussed together with the catalytic activity of the corresponding iron (III) complex in cyclopropanation reaction.

In **Chapter IV** the synthesis of different *mono*-substituted porphyrins, suitable for the conjugation with cellulose and proteins, is reported. Preliminary studies conducted on the conjugation with cellulose are described together with the first catalytic test in cyclopropanation reaction.

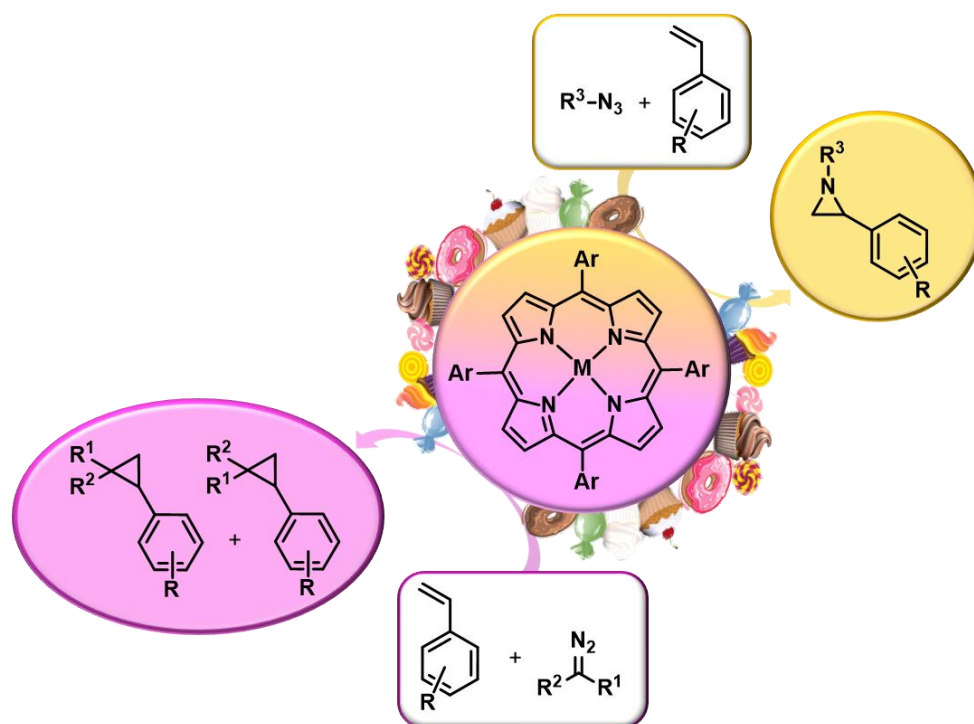
In **Chapter V** the use of ruthenium porphyrins as catalyst for the CO₂ cycloaddition to three membered-ring compounds, like aziridines and epoxides, is reported. Mechanistic considerations and future perspectives of this system for the synthesis of added-value compounds are discussed.

5. References

- (1) Centi, G.; Perathoner, S. *Catal. Today* **2003**, 77 (4), 287–297.
- (2) Sheldon, R. A. *Chem. Soc. Rev.* **2012**, 41 (4), 1437–1451.
- (3) Trindade, A. F.; Gois, P. M. P.; Afonso, C. A. M. *Chem. Rev.* **2009**, 109 (2), 418–514.
- (4) Empel, C.; Koenigs, R. M. *Synlett* **2019**, 30 (17), 1929–1934.
- (5) Intriери, D.; Carminati, D. M.; Gallo, E. In *Handbook of Porphyrin Science; Handbook of Porphyrin Science*; World Scientific Publishing Company, **2016**; 38, 1–99.
- (6) Zhu, S.-F.; Zhou, Q.-L. *Acc. Chem. Res.* **2012**, 45 (8), 1365–1377.
- (7) Intriери, D.; Caselli, A.; Gallo, E. *Eur. J. Inorg. Chem.* **2011**, 33, 5071–5081.
- (8) Intriери, D.; Zardi, P.; Caselli, A.; Gallo, E. *Chem. Commun.* **2014**, 50 (78), 11440–11453.
- (9) Kumari, G.; Nutan; Modi, M.; Gupta, S. K.; Singh, R. K. *Eur. J. Med. Chem.* **2011**, 46 (4), 1181–1188.
- (10) Nikitjuka, A.; Jirgensons, A. *Chem. Heterocycl. Compd.* **2014**, 49 (11), 1544–1559.
- (11) Talele, T. T. *J. Med. Chem.* **2016**, 59 (19), 8712–8756.
- (12) Damiano, C.; Intriери, D.; Gallo, E. *Inorganica Chim. Acta* **2018**, 470, 51–67.
- (13) Rothmund, P. *J. Am. Chem. Soc.* **1935**, 57 (10), 2010–2011.
- (14) Rothmund, P. *J. Am. Chem. Soc.* **1936**, 58 (4), 625–627.
- (15) Rothmund, P.; Menotti, A. R. *J. Am. Chem. Soc.* **1941**, 63 (1), 267–270.
- (16) Adler, A. D.; Longo, F. R.; Finarelli, J. D.; Goldmacher, J.; Assour, J.; Korsakoff, L. *J. Org. Chem.* **1967**, 32 (2), 476.
- (17) Lindsey, J. S.; Schreiman, I. C.; Hsu, H. C.; Kearney, P. C.; Marguerettaz, A. M. *J. Org. Chem.* **1987**, 52 (5), 827–836.
- (18) Dolphin, D. *The Porphyrins VI: Structure and Synthesis*; Elsevier Science, **2012**.
- (19) Kadish, K.; Smith, K. M.; Guillard, R. *The Porphyrin Handbook*; Raymond F. Boyer Library Collection; Elsevier Science, **2000**.
- (20) Katz, J. J.; Norris, J. R.; Shipman, L. L.; Thurnauer, M. C.; Wasielewski, M. R. *Annu. Rev. Biophys. Bioeng.* **1978**, 7 (1), 393–434.
- (21) Smith, L. J.; Kahraman, A.; Thornton, J. M. *Proteins Struct. Funct. Bioinforma.* **2010**, 78 (10), 2349–2368.
- (22) De Montellano, P. R. O.; Fund, R. E. C. M. *Cytochrome P450: Structure, Mechanism, and Biochemistry*; Springer US, **2005**.
- (23) Hoarau, M.; Hureau, C.; Gras, E.; Faller, P. *Coord. Chem. Rev.* **2016**, 308, 445–459.
- (24) Lu, Y.; Berry, S. M.; Pfister, T. D. *Chem. Rev.* **2001**, 101 (10), 3047–3080.
- (25) Ward, T. R. *Acc. Chem. Res.* **2011**, 44 (1), 47–57.
- (26) Dürrenberger, M.; Ward, T. R. *Curr. Opin. Chem. Biol.* **2014**, 19 (1), 99–106.
- (27) Yu, F.; Cangelosi, V. M.; Zastrow, M. L.; Tegoni, M.; Plegaria, J. S.; Tebo, A. G.; Mocny, C. S.;

- Ruckthong, L.; Qayyum, H.; Pecoraro, V. L. *Chem. Rev.* **2014**, *114* (7), 3495–3578.
- (28) Matsuo, T.; Hirota, S. *Bioorganic Med. Chem.* **2015**, *22* (20), 5638–5656.
- (29) Korendovych, I. V.; DeGrado, W. F. *Curr. Opin. Struct. Biol.* **2014**, *27* (1), 113–121.
- (30) Markel, U.; Sauer, D. F.; Schiffels, J.; Okuda, J.; Schwaneberg, U. *Angew. Chemie - Int. Ed.* **2019**, *58* (14), 4454–4464.
- (31) Sreenilayam, G.; Moore, E. J.; Steck, V.; Fasan, R. *Adv. Synth. Catal.* **2017**, *359* (12), 2076–2089.
- (32) Kuchner, O.; Arnold, F. H. *Trends Biotechnol.* **1997**, *15* (12), 523–530.
- (33) Romero, P. A.; Arnold, F. H. *Nat. Rev. Mol. Cell Biol.* **2009**, *10* (12), 866–876.
- (34) Brandenburg, O. F.; Fasan, R.; Arnold, F. H. *Curr. Opin. Biotechnol.* **2017**, *47*, 102–111.
- (35) Singh, R.; Bordeaux, M.; Fasan, R. *ACS Catal.* **2014**, *4* (2), 546–552.
- (36) Singh, R.; Kolev, J. N.; Sutura, P. A.; Fasan, R. *ACS Catal.* **2015**, *5* (3), 1685–1691.
- (37) Dydio, P.; Key, H. M.; Nazarenko, A.; Rha, J. Y.-E.; Seyedkazemi, V.; Clark, D. S.; Hartwig, J. F. *Science* **2016**, *354* (6308), 102 – 106.
- (38) Key, H. M.; Dydio, P.; Clark, D. S.; Hartwig, J. F. *Nature* **2016**, *534*, 534.
- (39) Ohashi, M.; Koshiyama, T.; Ueno, T.; Yanase, M.; Fujii, H.; Watanabe, Y. *Angew. Chemie Int. Ed.* **2003**, *42* (9), 1005–1008.
- (40) Letondor, C.; Ward, T. R. *ChemBioChem* **2006**, *7* (12), 1845–1852.
- (41) Pordea, A.; Creusa, M.; Panek, J.; Duboc, C.; Mathis, D.; Novic, M.; Ward, T. R. *J. Am. Chem. Soc.* **2008**, *130* (25), 8085–8088.
- (42) Ema, T.; Yokoyama, M.; Watanabe, S.; Sasaki, S.; Ota, H.; Takaishi, K. *Org. Lett.* **2017**, *19* (15), 4070–4073.

Chapter II: Glycoconjugated porphyrins



Parts of this chapter have been published and are reproduced here from:

C. Damiano, S. Gadolini, D. Intrieri, L. Lay, C. Colombo and E. Gallo, "Iron and Ruthenium Glycoporphyrins: Active Catalysts for the Synthesis of Cyclopropanes and Aziridines", *Eur. J. Inorg. Chem.*, article in press DOI:10.1002/ejic.201900829

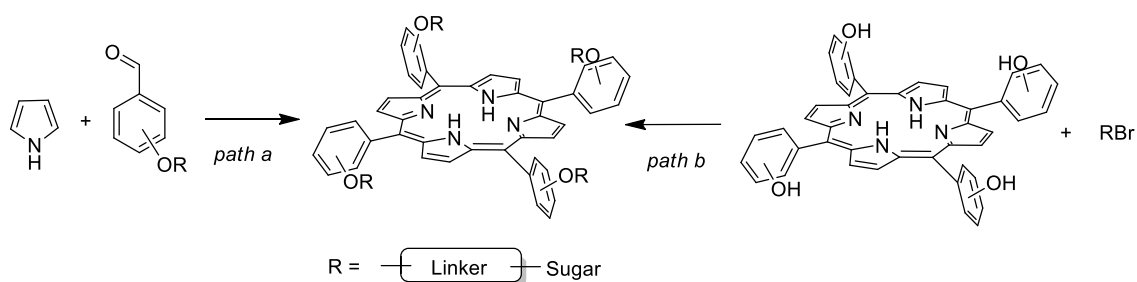
1. Introduction

Carbohydrates are chiral polyhydroxylated compounds found in abundance in Nature where they play critical roles in biological processes including energy storage, cellular communication and recognition, and immune system maintenance^{1,2}. The glyco-modification of the porphyrin unit can modulate the chemical and physical characteristics of the tetrapyrrolic ring conferring chiral recognition properties and variable solubility (depending on the nature of hydroxyl protecting groups on the carbohydrate fragment). During the years, glycoporphyrin derivatives prompted the attention in medical applications due to the carbohydrates cell-permeability and their binding properties that can lead to better pharmacological treatment³⁻⁵. Indeed one of the most widespread glycoporphyrins applications is in the photodynamic therapy (PDT)⁶⁻⁸ that combines the high efficiency of porphyrin rings as photosensitizers with sugar moiety's ability to recognize over-expressed receptors in certain malignant cells.

However, carbohydrates are promising tools for the rational design of enantioselective and water-soluble catalysts thanks to their defined spatial arrangement and the presence of several stereogenic centres^{9,10}. A great range of examples of phosphorous ligands functionalized with sugar moieties are reported in literature¹⁰ but the application of glycoporphyrins as ligands for catalytic purposes is still limited.

1.1. Glycoporphyrins: synthetic approach

The porphyrin macrocycle can be substituted in β -pyrrolic or *meso* positions but one of the most common glycoporphyrin classes, generally used for PDT, is represented by glycoconjugated *meso*-tetrarylporphyrins, which can be prepared by using two different strategies (Scheme 1).



Scheme 1: Strategies for the synthesis of glycoconjugated porphyrins

The first procedure follows the Lindsay's protocol reacting pyrrole with the desired glycoconjugated benzaldehyde (*path a*, Scheme 1). The alternative strategy is the two-steps reaction in which the pre-formed porphyrin (that usually shows hydroxyl groups) reacts with the sugar fragments opportunely protected and functionalized with halogen atoms (*path b*, Scheme 1). The choice of the synthetic procedure depends on the final glycoporphyrin structure. The glycoconjugated *meso*-tetrarylporphyrins

are classified in three different families: glycoconjugated porphyrins with a constrained structure (**A**), glycoconjugated porphyrins with flexible structure (**B**) and glycodendrimeric porphyrins (**C**) (Figure 1)⁸.

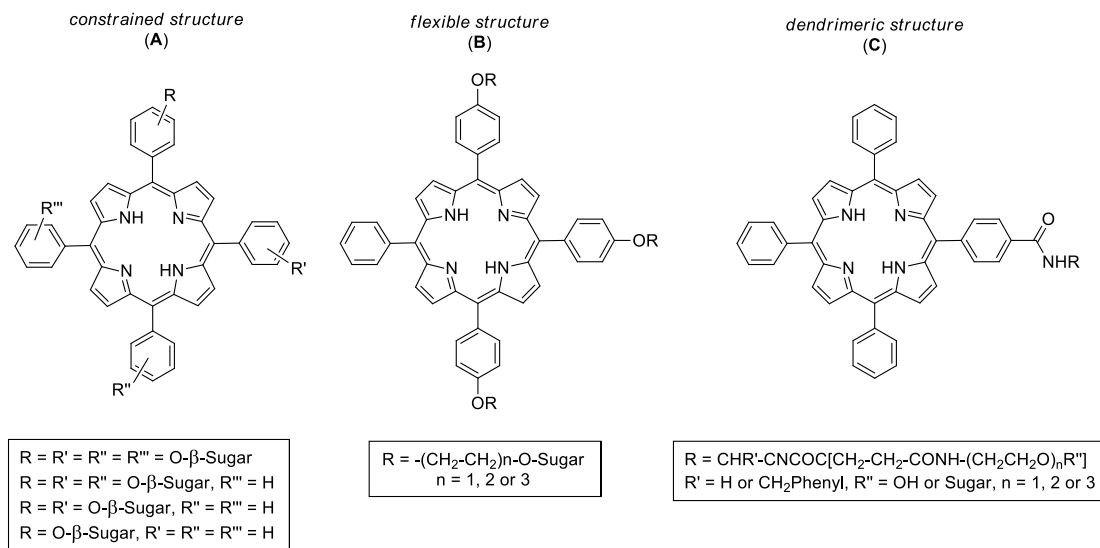


Figure 1: Examples of *meso*-tetrarylporphyrins: A) porphyrins with constrained structure; B) porphyrins with flexible structure; C) dendrimeric porphyrins

The synthesis of constrained *meso*-O-glycoconjugated-aryl porphyrins (**A**) can be performed with both general strategies depending on the electronic nature of the desired product. Electron-rich glycoporphyrins are prepared by the one-pot condensation of pyrrole and commercial or synthetic *para*, *meta*- or *ortho*-O-β-glycosylated benzaldehydes. This approach allows the preparation of mixed *meso*-glycosylated aryl-alkyl or -pentafluoroaryl porphyrins. The latter are instead necessary for the synthesis of electron poor conjugates due to the presence of fluoride rings which are susceptible to nucleophilic attack by sugar moieties.

Flexible O-glycosylated porphyrins (**B**), presenting a spacer between the sugar fragment and the porphyrin core, are usually prepared following the *path b* (Scheme 1) reacting the *tri*- or *tetra*-(*para*-hydroxyphenyl)porphyrin with a glycoside fragment functionalized with opportune spacers. This strategy is more convenient than the synthesis of aldehydes functionalized with variable sugars and lengths of the spacer.

Dendrimeric glycoporphyrins (**C**) are the most flexible glycoconjugates due to the presence of a hybrid component made of sugars and aminoacidic residues (glycyl or L-phenylalanyl). The synthesis of these compounds requires the use of *mono*-substituted porphyrins presenting at least one carboxylic group able to react with the *N*-terminus of the aminoacidic fragment.

1.2. Glycoporphyrins as ligands in catalysis

Few examples are reported in literature about the use of glycoconjugated porphyrins for catalytic applications even though they are desirable ligands for organometallic synthesis.

At the end of the 90's Momenteau M., a pioneer in the use of glycoporphyrins as ligands in catalysis, reported the synthesis of different glycoconjugated porphyrins and the catalytic activity of their corresponding manganese complexes towards the epoxidation of 4-chlorostyrene¹¹. All the porphyrins were synthesized by the direct condensation of pyrrole with the desired glycosylated benzaldehydes in order to obtain the *ortho*- and *meta*-substituted ligands (Figure 2).

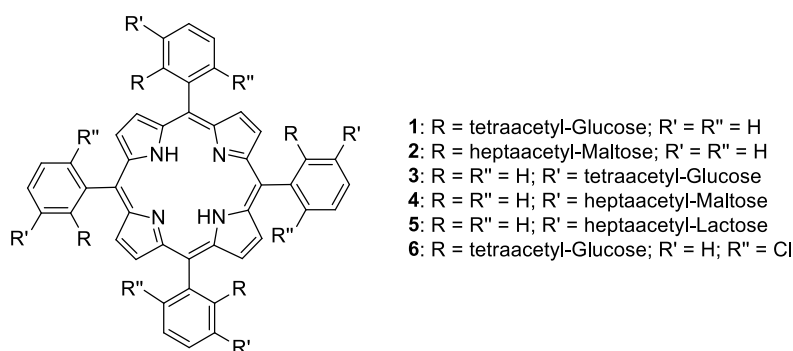
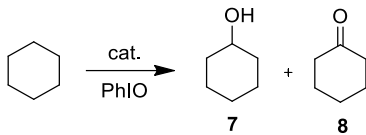


Figure 2: *Ortho*- and *meta*-substituted glycoporphyrin ligands

The corresponding manganese (III) complexes turned out to be efficient, enantioselective and stable catalysts for the epoxidation of 4-chlorostyrene in presence of different oxygen sources. The results achieved showed that the enantioselectivity is heavily dependent on the position of sugar fragments. The *meta*-substituted porphyrins (**3**, **4**, **5**) didn't afford the epoxidation product with enantiocontrol as opposed to the *ortho*-substituted ones (**1**, **2**), which gave higher enantioselectivity thanks to the proximity of the chiral moieties to the active metal site. The subsequent optimization of the *ortho*-substituted porphyrin (**3**) with the introduction of chloride atoms in the *ortho*' positions (**6**) gave a more robust Mn(III) catalyst able to perform the asymmetric epoxidation of 4-chlorostyrene in presence of H₂O₂ without significant degradation of the complex. The latter was also be reused in several catalytic cycles¹².

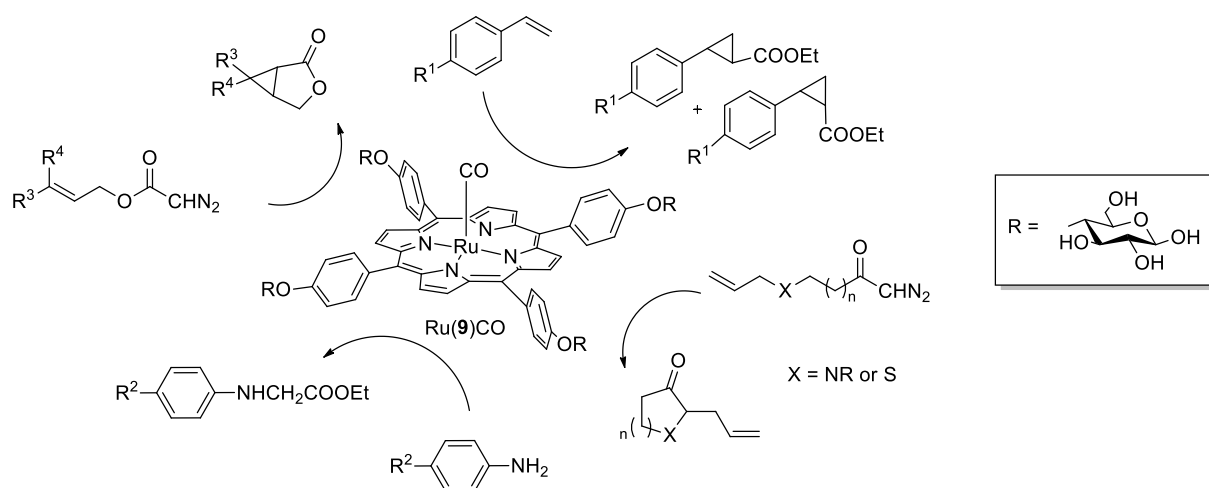
During the same years, Zhang and co-workers reported the catalytic activity of iron and manganese glycoporphyrins towards the cyclohexane oxidation¹³. In order to shade some light on the role of saccharide units, they compared the activity of metal glycoporphyrins with that of the parents Fe(TPP)Cl and Mn(TPP)Cl (TPP = dianion of tetraphenyl porphyrin) complexes in the formation of cyclohexanol (**7**) (Table 1).

Table 1: Synthesis of **7** and **8** catalysed by iron and manganese glycoporphyrins


entry	cat.	yield(%) of 7	yield (%) of 8	7:8	Turnover
1	Fe(TPP)Cl	15.1	1.7	9.0	4.9
2	Fe(1)Cl	31.3	2.2	14.4	9.8
3	Fe(3)Cl	28.3	2.0	14.2	8.9
4	Mn(TPP)Cl	14.3	1.8	8.1	4.7
5	Mn(1)Cl	34.4	3.1	11.1	11.0
6	Mn(3)Cl	34.0	3.0	11.4	10.9

Collected data show that the acetylglycosylated metalloporphyrins have stronger catalytic power than metalloporphyrins without sugar fragments (compare entry 1, 2, 4 and 5). The higher ratio between cyclohexanol (**7**) and cyclohexanone (**8**) as well as the yield, the reaction rate and the turnover number indicates a better stability of the glycosylated porphyrins than the unsubstituted ones. In addition, the kinetic study revealed the ability of acetylglycosylated metalloporphyrins to catalyse the cyclohexane oxidation with a mechanism similar to that of the cytochrome P450 monooxygenase.

The promising results obtained in the oxidation reactions catalysed by iron and manganese glycoporphyrins, prompted the research community to investigate the applicability and catalytic efficiency of different glycoconjugated metal complexes. Che and co-workers reported the first example of water-soluble ruthenium glycosylated porphyrins as catalysts for carbenoid transfer reactions¹⁴. The water-soluble Ru(**9**)CO complex was obtained by deprotection of the tetraacetylated precursor and was tested in alkene cyclopropanations, ylide formations/[2,3]sigmatropic rearrangements and carbenoid insertions in X-H (X = C, N, S) bonds (Scheme 2).

**Scheme 2:** Catalytic applications of Ru(**9**)CO

The glycosylated ruthenium porphyrin demonstrated high activity and selectivity in the above-mentioned reactions but it can also be applied for the side-selective modification of proteins and peptides. In fact the Ru(**9**)CO complex is able to modify the *N*-terminus of several peptides by carbenoid N-H insertion in water media with high site selectivity and moderate substrate conversions. Recently, Gallo and co-workers studied the activity of different electron poor and electron rich glycoporphyrin complexes as catalysts for amination reactions¹⁵. Three different glycoconjugated porphyrins were synthesized, directly modifying the porphyrin precursors and they were used for the synthesis of the corresponding cobalt (II), ruthenium (II) and iron (III) complexes (Figure 3).

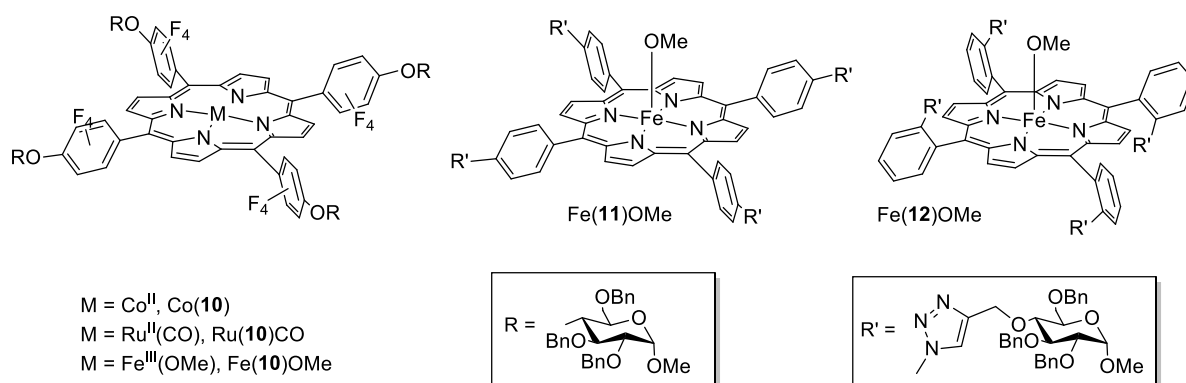


Figure 3: Cobalt (II), ruthenium (II) and iron (III) glycoporphyrin complexes

The study of the catalytic activity towards the formation of the benzylic amine **13** showed the high activity and selectivity of the electron poor iron and ruthenium glycoporphyrin complexes (Table 2).

Table 2: Synthesis of **13** catalysed by iron, ruthenium and cobalt glycoporphyrins

entry	cat.	time (h)	yield (%)
1	Fe(12)OMe	25	10
2	Fe(11)OMe	30	15
3	Co(10)	4	56
4	Fe(10)OMe	0.25	90
5	Ru(10)CO	0.25	92
6	Fe(F₂₀TPP)OMe	0.33	68
7	Ru(F₂₀TPP)CO	0.75	82

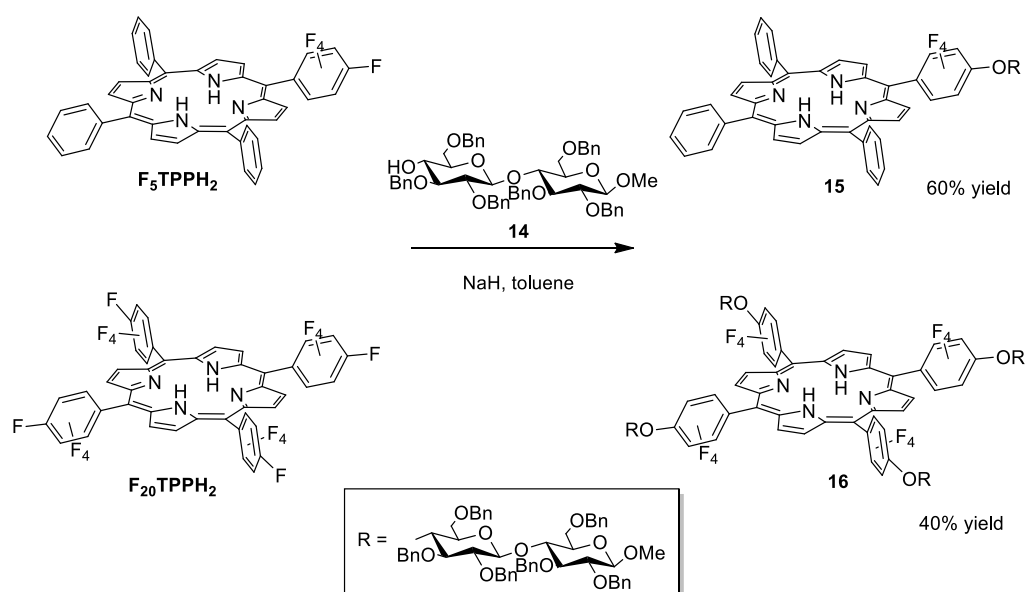
The comparison between catalytic results obtained employing Fe(**10**)OMe and Ru(**10**)CO and those achieved by Fe(**F₂₀TPP**)OMe and Ru(**F₂₀TPP**)CO (**F₂₀TPP** = dianion of *meso*-tetrakis(pentafluorophenyl)porphyrin) indicates the positive role of carbohydrates units both in terms of yields and reaction times (Table 2). Fe(**10**)OMe and Ru(**10**)CO also showed the ability to catalyse the benzylic amination with several organic azides confirming the applicability of these systems as catalysts for eco-friendly reactions.

2. Results and Discussion

To assess how differently glycosylated porphyrin ligands can influence the catalytic activity of their relative ruthenium and iron complexes, different *meso* glycosyl-conjugated porphyrins were synthesised. The number and the position of the carbohydrate units onto the porphyrin ring play an important role to determine the ligand's chemo-physical properties. *Mono* and *tetra* glycosyl derivative porphyrins were obtained and the corresponding iron and ruthenium complexes were tested in cyclopropanation and aziridination reactions.

2.1. Glycoporphyrins synthesis

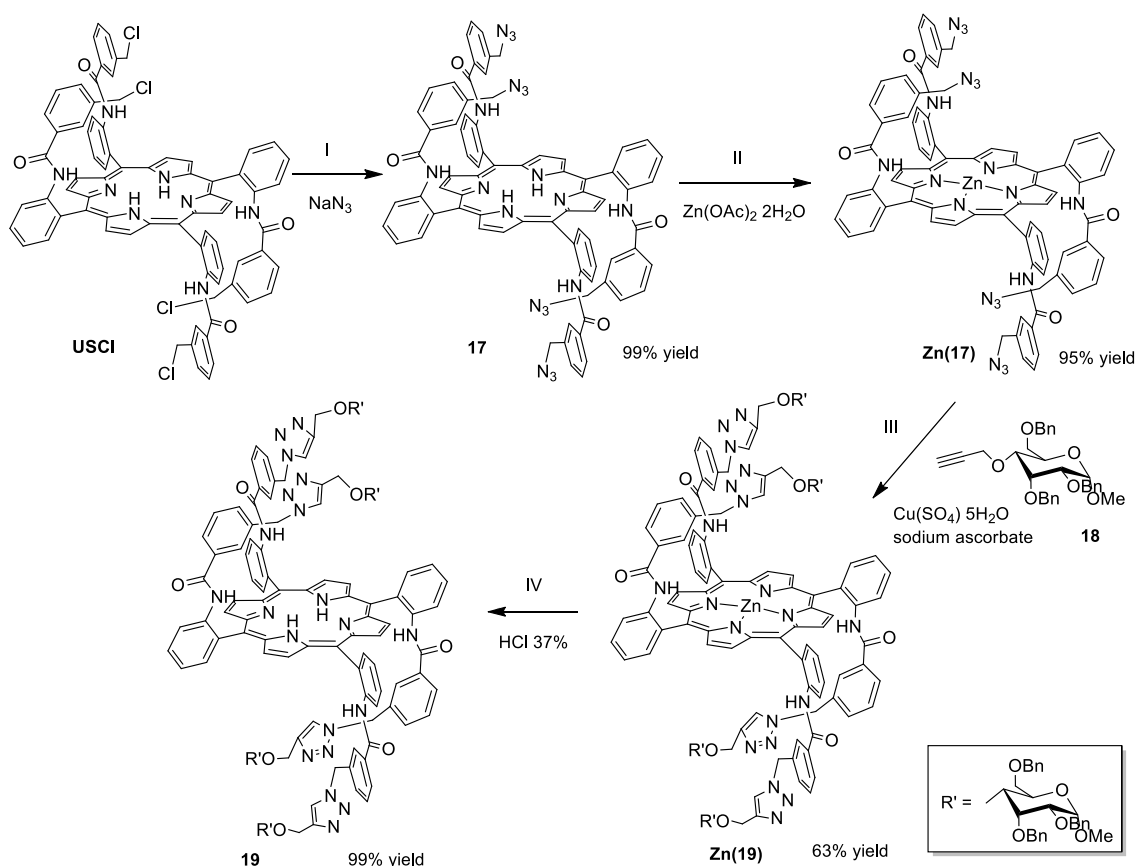
Porphyrins **15** and **16**, which show respectively one and four carbohydrate units on the *para* position of the *meso*-aryl group, were obtained by the C₆F₅ moiety *para* fluorine atom nucleophilic substitution¹⁵. The direct reaction of the disaccharide **14**¹⁶ either with F₅TPPH₂¹⁷ and F₂₀TPPH₂¹⁸ afforded the desired compounds **15** and **16** respectively in 60 % and 40 % yields (Scheme 3).



Scheme 3: Synthesis of ligands **15** and **16**

The *tetra*-carbohydrate porphyrin **19** was obtained by a multistep reaction (Scheme 4) starting from the $\alpha_2\beta_2$ *meso-tetra*{2-[(3-chloromethyl)benzoylamido]phenyl}porphyrin (**USCI**)¹⁹ precursor. In the first step (I, scheme 4) the porphyrin **17** was obtained by nucleophilic substitution of the chloride atoms with azide groups. The obtained porphyrin was subsequently used for the synthesis of the Zn(**17**) complex (II, scheme 4). The introduction of the zinc atom in the porphyrin core is necessary to protect the porphyrin ring during the “click reaction” with the saccharide **18**²⁰ which involves the use of Cu(SO₄) (III, scheme 4). The final porphyrin **19** was obtained in a quantitative yield by the demetallation of

Zn(**19**) complex in acidic conditions. Although the synthetic procedure to obtain **19** requires four steps, three of them occurred in quantitative yields and one in yield up to 63%. All the reaction steps for the synthesis of **19** were performed at low temperatures (under 50°C) to avoid the formation of the statistical distribution of C₂ porphyrin atropoisomers^{19,21}.

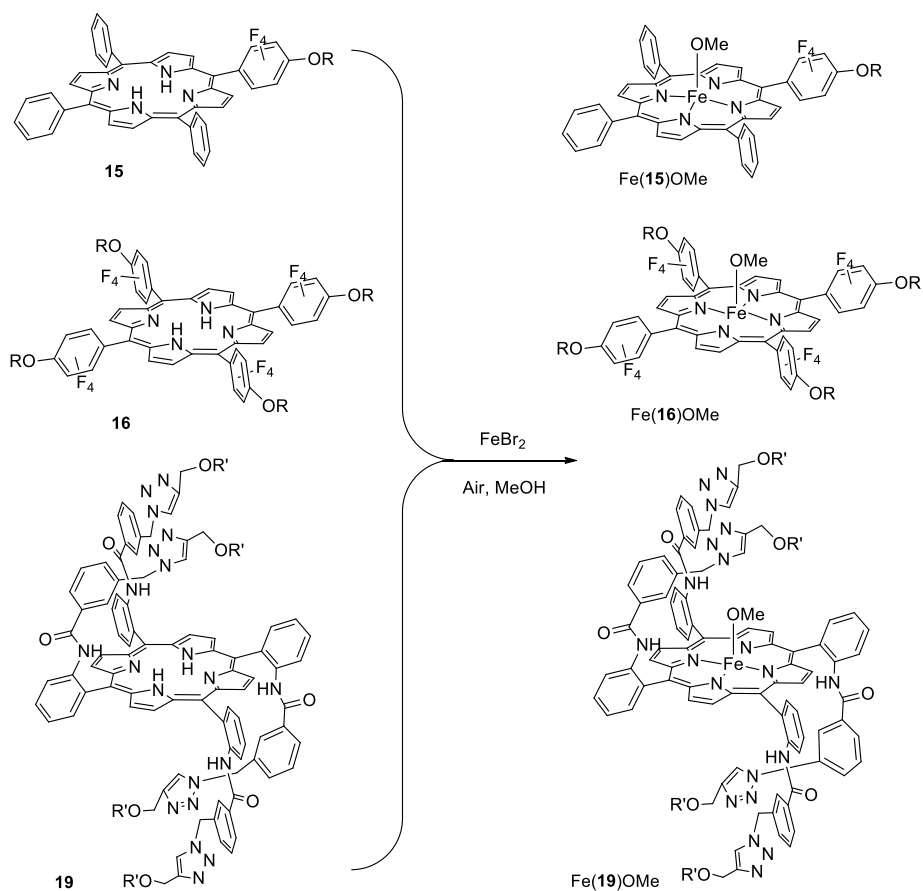


Scheme 4: Synthesis of ligand **19**

The glycoconjugated porphyrins **15**, **16** and **19** were used for the synthesis of their corresponding iron (III) and ruthenium (II) complexes.

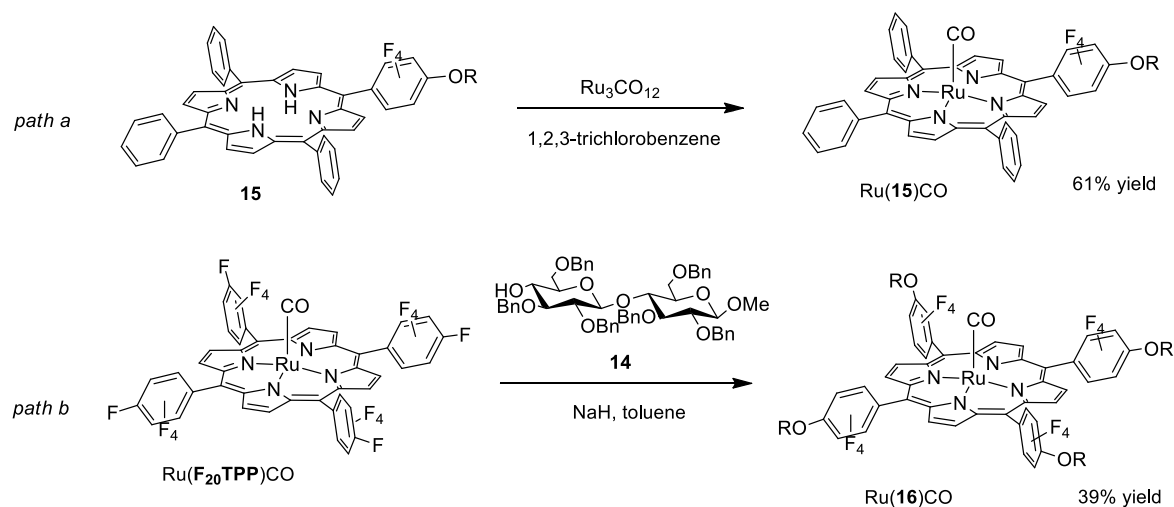
All the iron complexes were prepared with the same synthetic strategy, refluxing the free ligand with an excess of FeBr₂ and obtaining the desired complexes in quantitative yields (Scheme 5). The introduction of the methoxy axial ligand occurred by MeOH-based chromatography purification and the treatment of the final complexes in MeOH at 50°C.

Different strategies were used for the ruthenium insertion, which usually requires experimental conditions more drastic than those employed for the iron metal. Ru(**15**)CO was obtained in 61 % yield by refluxing the free ligand **15** with an excess of Ru₃(CO)₁₂ in 1,2,3-trichlorobenzene as the reaction solvent (*path a*, Scheme 6).

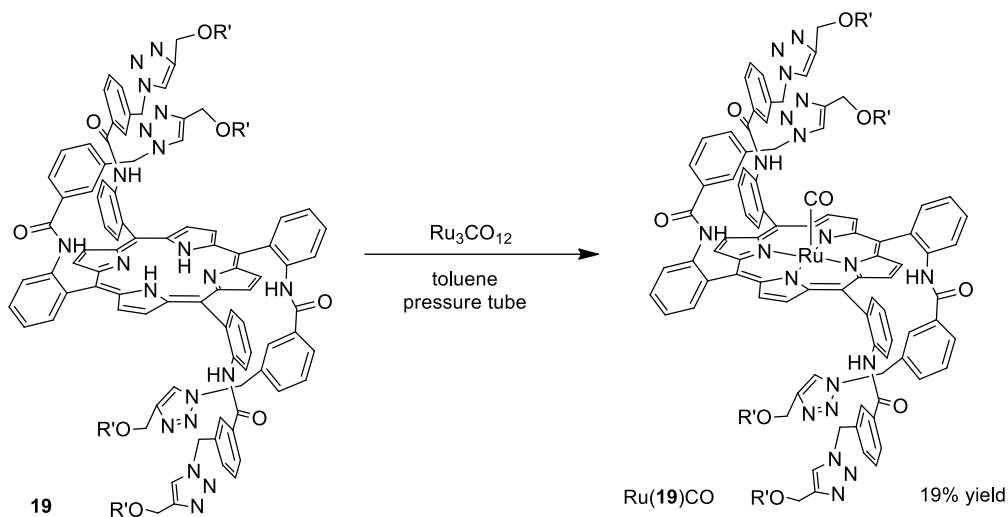


Scheme 5: Synthesis of iron glycoporphyrins

Considering that Ru(**16**)CO was not obtained simply treating ligand **16** with Ru₃(CO)₁₂, an alternative strategy was applied. In the same conditions used for the synthesis of Ru(**15**)CO, the Ru(**F₂₀TPP**)CO complex was synthesised and after it was reacted with **14** in presence of sodium hydride to yield Ru(**16**)CO in 39% yield (*path b*, Scheme 6).


 Scheme 6: Synthesis of Ru(**15**)CO and Ru(**16**)CO

All the above described procedures failed for the insertion of ruthenium into porphyrin **19** and the Ru(**19**)CO complex was obtained in 19% yield reacting the free porphyrin with Ru₃(CO)₁₂ in a pressure tube at 150°C, using toluene as a reaction solvent (Scheme 7). The high temperature required for this procedure is responsible for the atropisomerization of the desired compound and it justifies the Ru(**19**)CO low yield.

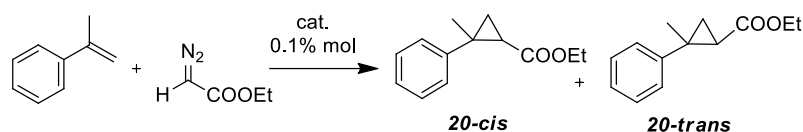


Scheme 7: Synthesis of Ru(**19**)CO

2.2. Glycoporphyrin complexes in alkene cyclopropanation reactions

All the synthesised iron and ruthenium glycoporphyrins were initially tested in the model cyclopropanation reaction between α -methylstyrene and ethyl diazoacetate (EDA) forming cyclopropane **20**. The activity of all glycoconjugated complexes was also compared with that of the unsubstituted ones in order to understand the effect of saccharide units on the catalytic performances (Table 3).

Table 3: Synthesis of **20** catalysed by iron and ruthenium glycoporphyrins



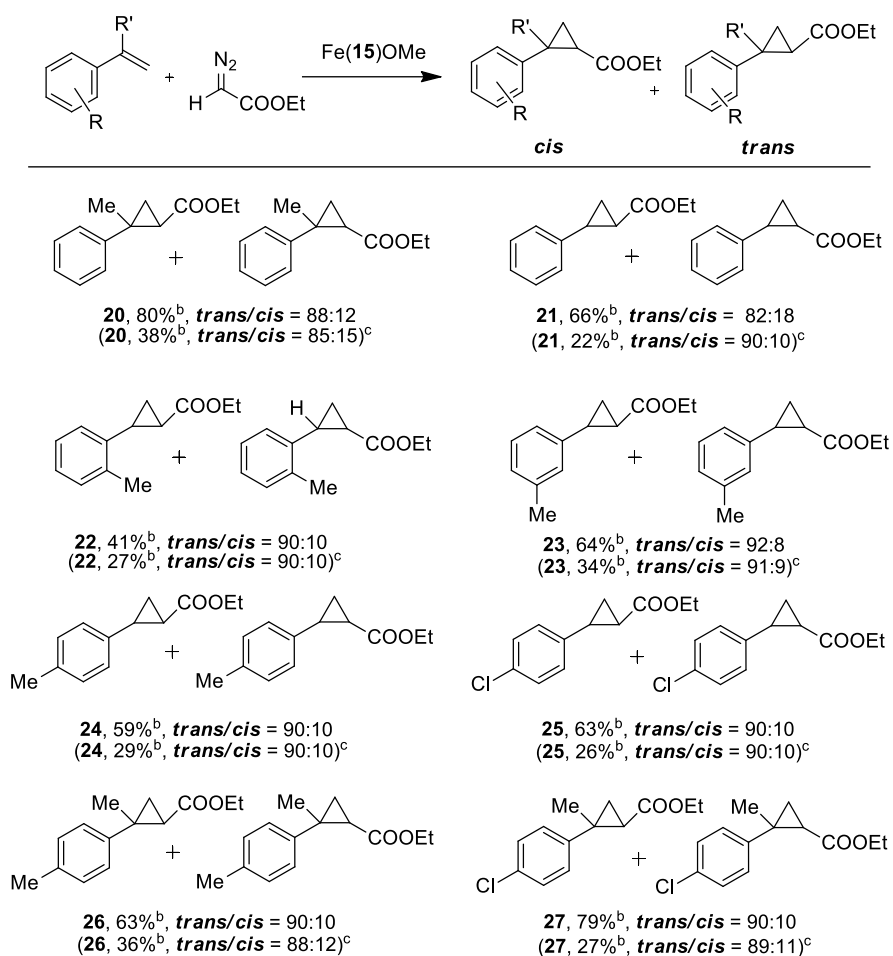
entry	cat.	yield (%) ^b	<i>trans/cis</i> ^b
1	Fe(F₅TPP)OMe	80	87:13
2	Fe(15)OMe	80	88:12
3	Ru(F₅TPP)CO	70	88:12
4	Ru(15)CO	68	90:10
5	Fe(F₂₀TPP)OMe	60	60:40
6	Fe(16)OMe	71	80:20
7	Ru(F₂₀TPP)CO	45	60:40
8	Ru(16)CO	61	78:22
9	Fe(19)OMe	69	95:5
10	Ru(19)CO	66	95:5

^aReactions were stirred in toluene for 2 h at 25°C by using catalyst/EDA/ α -methylstyrene = 1:1100:5000. ^bDetermined by ¹H NMR spectroscopy using 2,4-dinitrotoluene as the internal standard.

In the cyclopropanation model reaction all the Fe(porphyrin)OMe complexes showed higher activity than the parents Ru(porphyrin)CO and the obtained data display how the diastereoselective trend depends on the ligand structure (Table 3). The addition of one saccharide unit onto the porphyrin ring didn't affect the yield and the diastereoselectivity (entries 1 and 2, table 3) but the introduction of four sugars onto the **F₂₀TPPH₂** had a positive effect both in terms of yield and diastereoselectivity (entries 5 and 6, Table 3). The best *trans/cis* selectivity was obtained with the ligand **19** which shows a C₂-symmetry of the porphyrinic skeleton. The different location of the four carbohydrate units did not influence the reaction yields (compare entries 6 and 9, table 3) but it had a relevant effect on the reaction diastereoselectivity. In fact the C₂-symmetry of ligand **19** was responsible for the highest diastereocontrol, regardless of the active metal's nature (compare entries 6 and 8 with 9 and 10, table 3). Furthermore, the synthesis of **19** required a long synthetic procedure and the cyclopropanation yields with this ligand were lower than the other glycoporphyrin complexes.

Based on these results, Fe(**15**)OMe was chosen as the best complex forming the compound **20** due to the good compromise between yield, diastereoselectivity and synthetic procedure. The activity of the Fe(**15**)OMe was evaluated with different styrenes affording the compounds listed in table 4 in very good yields (up to 80%) and diastereoselectivities (up to 98:2).

Table 4: Synthesis of compounds **20-27** catalysed by Fe(**15**)OMe



^aReactions were stirred in toluene for 2 h at 25°C by using Fe(**15**)OMe/EDA/styrene = 1:1100:5000. ^bDetermined by ¹H NMR spectroscopy using 2,4-dinitrotoluene as the internal standard. ^cFe(**15**)OMe/EDA/styrene = 1:1100:1000.

Catalytic tests were performed using two different molar ratios between EDA and styrenes, the molar ratio Fe(**15**)OMe/EDA/alkene = 1:1100:5000 and the slight EDA excess with respect to the substrate (Fe(**15**)OMe/EDA/alkene = 1:1100:1000). The obtained data show that the alkene excess is necessary to suppress the EDA homo-coupling process which can decrease the cyclopropane yields.

The steric hinderance on the styrene substrate can strongly influence the catalytic productivity, as proved by the low yield obtained for the product **22**, which shows a methyl substituent in the *ortho* position of the aromatic moiety. Better yields were obtained using a *meta*-substituted styrene as

substrate (product **23**) but the best ones were achieved by using *para*-substituted styrenes, regardless of the alkene substituents' electronic nature (products **24** - **27**).

The steric hindrance and electronic properties of different diazo derivatives were also evaluated as previously done for styrene substrates. Styrene and α -methylstyrene were reacted with diazo compounds **28-30** (Figure 4) in the presence of Fe(**15**)OMe using the same reaction conditions reported in table 4.

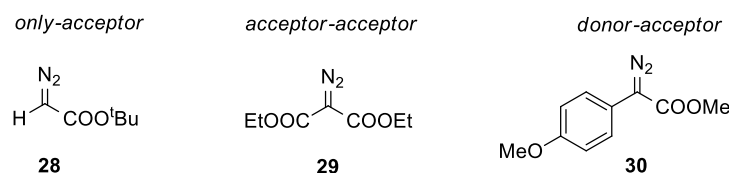
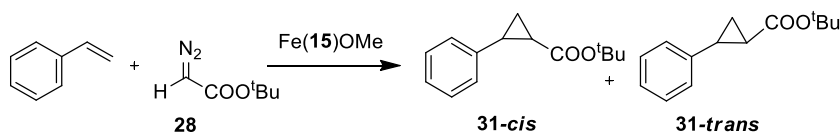


Figure 4: Diazo compounds tested in cyclopropanation reactions

The reaction with acceptor-acceptor (**29**) and donor-acceptor (**30**) diazo compounds didn't afford the desired cyclopropanes either with styrene and α -methylstyrene. Using the only-acceptor diazo derivative (**28**), the desired cyclopropane was obtained only with styrene substrate in 48 % yield and *trans/cis* ratio of 88:12 (Scheme 8). No reaction occurred using α -methylstyrene and **28** due to the steric hindrance generated by the methyl group.

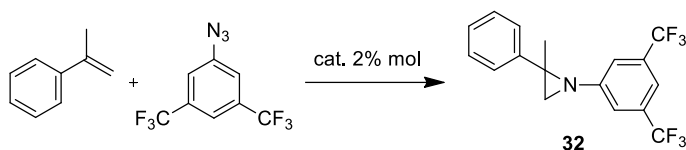


Scheme 8: Synthesis of **31** catalysed by Fe(**15**)OMe

2.3. Glycoporphyrin complexes in alkene aziridination reactions

All the iron and ruthenium glycoconjugated porphyrins were tested in the aziridination reaction model between α -methylstyrene and 3,5-*bis*(trifluoromethyl)phenyl azide forming aziridine **32**. Unfortunately, Fe(III)OMe complexes didn't catalyse the aziridination reaction; furthermore, **32** was obtained in a very good yield (up to 83%) in presence of Ru(porphyrin)CO complexes (Table 5).

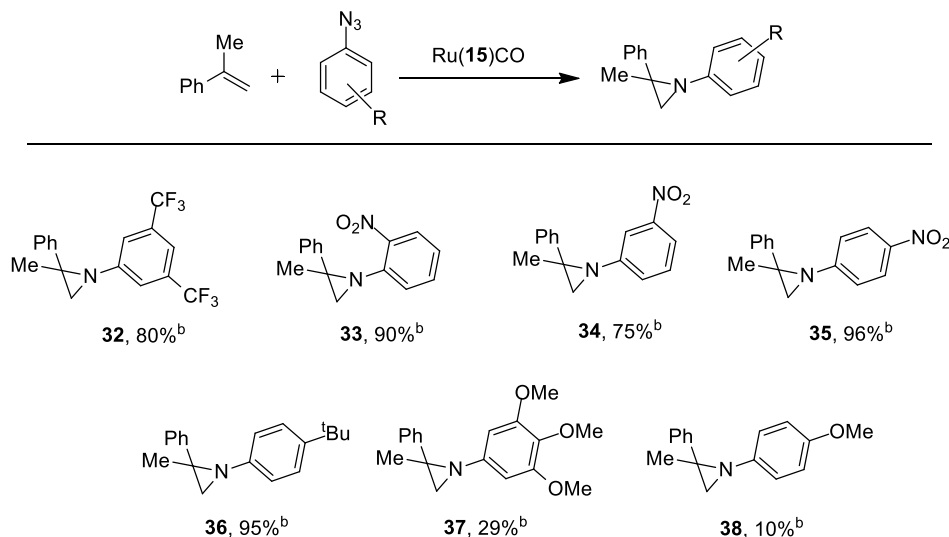
The unsubstituted Ru(**F₅TPP**)CO and Ru(**F₂₀TPP**)CO mediated the synthesis of **32** in analogous yields (entries 1 and 2, Table 5) and a comparable yield was also obtained with the glycoconjugated Ru(**15**)CO complex. The *tetra*-substituted glycoporphyrin Ru(**16**)CO showed lower catalytic performances in forming **32** but a complete inactivity was observed using Ru(**19**)CO (entry 5, Table 5). The inactivity of Ru(**19**)CO could be attributed to the ligand's three-dimensional arrangement, which probably hampers the interaction of the substrate with the active ruthenium metal centre.

Table 5: Synthesis of **32** catalysed by ruthenium glycoporphyrins


entry	cat.	yield (%) ^b
1	Ru(F₅TPP)CO	81
2	Ru(F₂₀TPP)CO	83
3	Ru(15)CO	80
4	Ru(16)CO	17
5	Ru(19)CO	-

^aReactions were refluxed in benzene for 2 h by using catalyst/azide/ α -methylstyrene = 1:50:250. ^bDetermined by ¹H NMR spectroscopy using 2,4-dinitrotoluene as the internal standard.

Considering the good results obtained with Ru(**15**)CO and the deployment in the near future of glycoconjugated porphyrins for catalytic applications, the Ru(**15**)CO complex was tested for the synthesis of aziridines starting from α -methylstyrene and different aryl azides (Table 6).

Table 6: Synthesis of compounds **32-28** catalysed by Ru(**15**)CO


^aReactions were refluxed in benzene for 2 h by using catalyst/azide/ α -methylstyrene = 1:50:250.

^bDetermined by ¹H NMR spectroscopy using 2,4-dinitrotoluene as the internal standard.

The obtained results indicate that the starting aryl azide steric nature could affect the Ru(**15**)CO catalytic activity. Indeed compounds **33** and **35**, showing respectively the nitro group on the *ortho* and *para* positions of the aryl moiety, were obtained in comparable yields. A lower yield was obtained using

the *meta*-substituted starting azide (product **34**), because the presence of substituents close to the reactive N₃ group could hamper the formation of the desired aziridine. Moreover, the aromatic azide electronic nature does not appear to strongly affect the Ru(**15**)CO catalytic activity. Compounds **35** and **36**, demonstrating respectively an electron withdrawing and an electron donating substituent, were obtained in very good yields (up to 96 %).

The lowest yields were obtained in presence of methoxy substituents (products **37** and **38**) which are able to coordinate the ruthenium metal and are responsible for the catalyst deactivation. The negative effect is more marked using the *para*-methoxy aryl azide as substrate due to a better coordinative capability of the unhindered methoxy group compared to the three contiguous ones (compare yields of **37** and **38**)²².

3. Conclusion

The synthesis and catalytic activity of different iron and ruthenium glycoporphyrins and their related precursors have been reported. From the synthetic point of view, the nucleophilic substitution in *para* positions of fluorinated aryl moieties represents an efficient strategy to obtain *mono* and *tetra* glycosylated ligands in good yields.

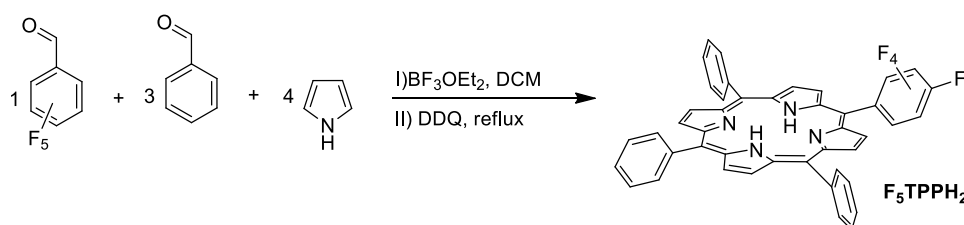
The collected catalytic data established the ability of iron (III) complexes to efficiently promote cyclopropanation reactions and showed the possibility to use ruthenium (II) complexes for the synthesis of aziridines. Among all synthesised catalysts, the catalytic activity of Fe(**15**)OMe and Ru(**15**)CO was investigated because the free porphyrin **15** can be considered a useful ligand to perform catalysis in a biphasic systems, after the deprotection of the sugar moieties. In addition, the precursor **F₅TPPH₂** can be used for anchoring the porphyrinic system to polysaccharides fragments or solid supports in order to provide sustainable catalysts that can be tested under more eco-compatible reaction conditions.

4. Experimental section

General conditions: Unless otherwise specified, all reactions were carried out under nitrogen atmosphere employing standard Schlenk techniques and vacuum-line manipulations. All the solvents were dried by using standard procedures and stored under nitrogen atmosphere. All the other starting materials were commercial products and used as received. NMR spectra were recorded at room temperature either on a Bruker Avance 300-DRX, operating at 300 MHz for ^1H , at 75 MHz for ^{13}C and at 282 MHz for ^{19}F , or on a Bruker Avance 400-DRX spectrometers, operating at 400 MHz for ^1H , 100 MHz for ^{13}C and 376 MHz for ^{19}F . Chemical shifts (ppm) are reported relative to TMS. The ^1H -NMR signals of the compounds described in the following were attributed by 2D NMR techniques. Assignments of the resonance in ^{13}C -NMR were made by using the APT pulse sequence, HSQC and HMBC techniques. Infrared spectra were recorded on a Varian Scimitar FTS 1000 spectrophotometer. UV/Vis spectra were recorded on an Agilent 8453E instrument. MALDI-TOF spectra were acquired either on a Bruker Daltonics Microflex or on a Bruker Daltonics Autoflex III TOF/TOF at C.I.G.A., University of Milan. High resolution MS (HR-MS) spectra were obtained on a Bruker Daltonics ICR-FTMS APEX II at C.I.G.A., University of Milan. Microanalysis was performed on a Perkin Elmer 2400 CHN Elemental Analyzer instrument.

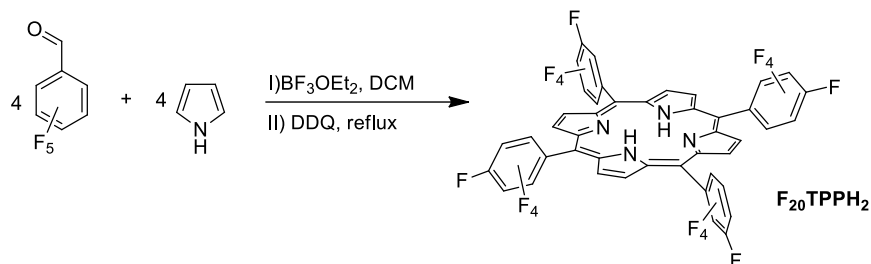
4.1. Synthesis of porphyrin ligands

4.1.1. Synthesis of F_5TPPH_2



Pentafluorobenzaldehyde (0.16 mL, 1.25×10^{-3} mol), benzaldehyde (0.38 mL, 3.75×10^{-3} mol) and pyrrole (0.35 mL, 5.00×10^{-3} mol) were dissolved in CH_2Cl_2 (400 mL) and $\text{BF}_3\cdot\text{Et}_2\text{O}$ (0.63 mL, $5.00 \cdot 10^{-4}$ mol) was added under nitrogen. The reaction was stirred at room temperature over night and then 2,3-dichloro-5,6-dicyano-1,4-benzoquinone (DDQ) (0.56 mg, 2.51×10^{-3} mol) was added. The reaction mixture was refluxed for 12 hours. At the end of the reaction TEA was added and the solvent was evaporated to dryness. The crude was purified by flash chromatography (SiO_2 , gradient elution from *n*-hexane to *n*-hexane/ CH_2Cl_2 = 85:15) to yield purple solid (180.0 mg, 21%). The collected analytical data are in accordance with those reported in literature¹⁷.

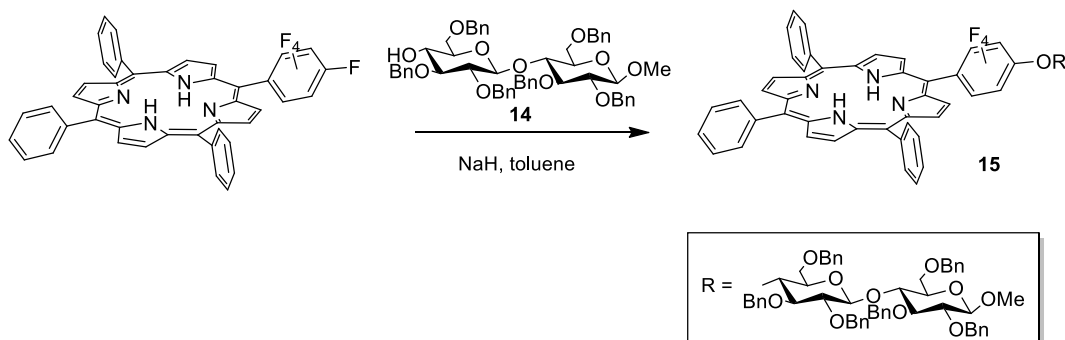
^1H NMR (300 MHz, CDCl_3): δ 9.01 (d, J = 4.8 Hz, 2H, $\text{H}_{\beta\text{pyr}}$), 8.92 (s, 4H, $\text{H}_{\beta\text{pyr}}$), 8.85 (d, J = 4.6 Hz, 2H, $\text{H}_{\beta\text{pyr}}$), 8.27 (m, 6H, H_{Ar}), 7.80 – 7.75 (m, 9H, H_{Ar}), -2.66 (s, 2H, NH_{pyr}).

4.1.2. Synthesis of F₂₀TPPH₂

Pentafluorobenzaldehyde (0.64 mL, 5.00×10^{-3} mol) and pyrrole (0.35 mL, 5.00×10^{-3} mol) were dissolved in CH₂Cl₂ (250 mL) and BF₃·Et₂O (0.19 mL, $1.5 \cdot 10^{-3}$ mol) was added under nitrogen. The reaction was refluxed for 4 hours and then 2,3-dichloro-5,6-dicyano-1,4-benzoquinone (DDQ) (0.56 mg, 2.51×10^{-3} mol) was added. The reaction mixture was refluxed for other 12 hours. At the end of the reaction TEA was added and the solvent was evaporated to dryness. The crude was purified by flash chromatography (SiO₂, gradient elution from *n*-hexane to *n*-hexane/CH₂Cl₂ = 95:5) to yield purple solid (150.0 mg, 12%). The collected analytical data are in accordance with those reported in literature¹⁸.

¹H NMR (400 MHz, CDCl₃): δ 8.97 (s, 4H, H_{βpyrr}), -2.85 (s, 2H, NH_{pyrr}).

4.1.3. Synthesis of porphyrin 15

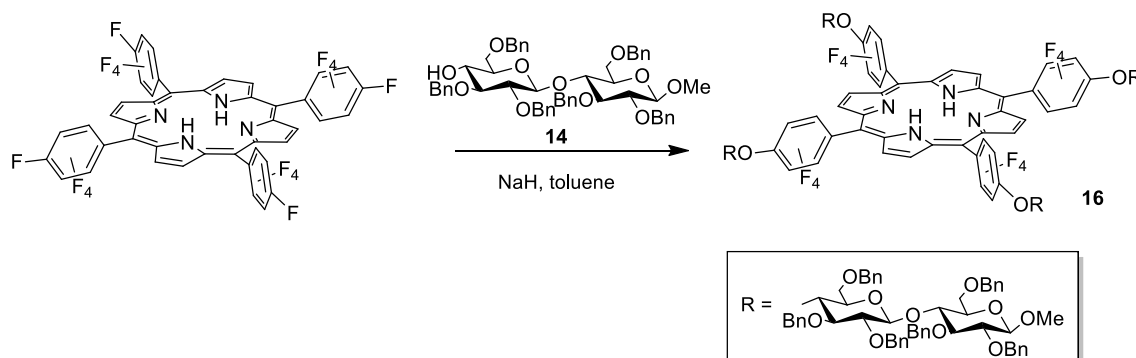


NaH 60% (128.0 mg, 5.32 mmol) was added under nitrogen to a toluene (28.0 mL) solution of F₅TPPH₂ (150.0 mg, 2.13×10^{-1} mmol) and **14** (380.0 mg, 4.33×10^{-1} mmol). The resulting solution was refluxed for 50 hours until the complete consumption of the starting porphyrin was observed by TLC (SiO₂, *n*-hexane/AcOEt = 7:3). Residual NaH was quenched with HCl 1.0 N and then CH₂Cl₂ (50.0 mL) was added to the mixture. The organic phase was extracted with H₂O until pH = 7, then dried over Na₂SO₄ and filtered. The solvent was evaporated to dryness under vacuum and the residue purified by flash chromatography (SiO₂, gradient elution from *n*-hexane to *n*-hexane/AcOEt = 7:3) to yield a purple solid **2** (130.0 mg, 59%).

¹H NMR (300 MHz, CDCl₃): δ 8.90 (s, 4H, H_{βpyrr}), 8.84 (d, *J* = 5.4 Hz, 2H, H_{βpyrr}), 8.51 (d, *J* = 4.8 Hz, 2H, H_{βpyrr}), 8.26 (t, *J* = 6.3 Hz, 6H, H_{Ar}), 7.89 – 7.73 (m, 9H, H_{Ar}), 7.45 - 7.19 (m, 46H, H_{Ar} + H_{solvent}), 5.15 (dd, *J* = 13.4, 11.2 Hz, 2H, H_{sugar}), 5.03 – 4.73 (m, 12H, H_{sugar}), 4.73 – 4.60 (m, 2H H_{sugar}), 4.36 (dd,

$J = 17.7, 7.6$ Hz, 2H, H_{sugar}), 4.20 (t, $J = 9.3$ Hz, 1H, H_{sugar}), 4.12 (dd, $J = 11.4, 1.9$ Hz, 1H, H_{sugar}), 4.06 – 3.86 (m, 3H, H_{sugar}), 3.85 – 3.74 (m, 3H, H_{sugar}), 3.73 – 3.56 (m, 7H, H_{sugar}), 3.54 – 3.27 (m, 4H, H_{sugar}), -2.73 (s, 2H, NH_{pyrr}). ^{19}F NMR (282 MHz, CDCl_3): δ -139.36 (dd, $J = 24.5, 8.1$ Hz, 2F), -156.83 (dd, $J = 23.7, 8.7$ Hz, 2F). ^{13}C NMR (75 MHz, CDCl_3): δ 142.38, 142.22, 139.58, 139.05, 138.63, 138.52, 135.01, 134.93, 129.05, 128.98, 128.85, 128.82, 128.78, 128.72, 128.70, 128.65, 128.56, 128.52, 128.48, 128.43, 128.40, 128.37, 128.28, 128.23, 128.19, 128.17, 128.13, 128.08, 128.04, 128.00, 127.95, 127.80, 127.76, 127.70, 127.62, 127.51, 127.16, 127.10, 105.18, 105.08, 102.79, 102.53, 85.23, 84.73, 84.36, 84.10, 83.34, 83.14, 83.07, 82.44, 82.18, 82.11, 81.13, 76.84, 75.43, 75.29, 74.86, 74.38, 73.32, 71.98, 71.51, 57.56, 57.49, 57.44. IR ν_{max} (CH_2Cl_2)/ cm^{-1} : 1089, 1200, 1362, 1497, 1453, 1430, 1712, 1989, 3063. UV-Vis: λ_{max} (CH_2Cl_2)/nm (log ϵ): 418 (4.7), 513 (3.6), 548 (3.2), 588 (3.1), 645 (3.1). LR-MS (ESI): m/z ($\text{C}_{99}\text{H}_{85}\text{F}_4\text{N}_4\text{O}_{11}$) calcd. 1582.77; found $[M+H]^+$ 1583.6. Elemental analysis calc. for $\text{C}_{99}\text{H}_{85}\text{F}_4\text{N}_4\text{O}_{11}$ C, 75.13; H, 5.41; N, 3.54; found: C, 75.35; H, 5.70; N, 3.45

4.1.4. Synthesis of porphyrin 16

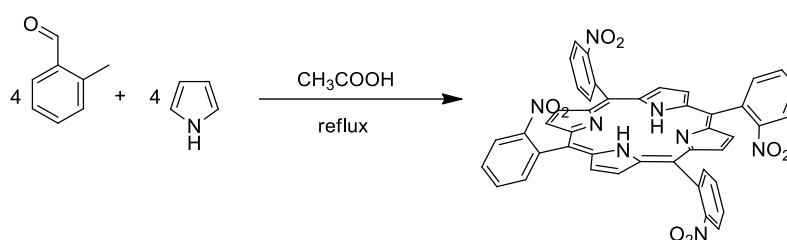


NaH 60% (123.0 mg, 3.08 mmol) was added under nitrogen to a toluene (9.0 mL) solution of **F₂₀TPPH₂** (50.0 mg, 5.13×10^{-2} mmol) and **14** (368.0 mg, 4.15×10^{-1} mmol). The resulting solution was refluxed for 50 hours until the complete consumption of the starting porphyrin was observed by TLC (SiO_2 , n -hexane/ $\text{AcOEt} = 7:3$). Residual NaH was quenched with HCl 1.0 N and then CH_2Cl_2 (15.0 mL) was added to the mixture. The organic phase was extracted with H_2O until pH = 7, then dried over Na_2SO_4 and filtered. The solvent was evaporated to dryness under vacuum and the residue purified by flash chromatography (SiO_2 , gradient elution from n -hexane to n -hexane/ $\text{AcOEt} = 7:3$) to yield a purple solid **3** (89.0 mg, 39%).

^1H NMR (400 MHz, CDCl_3): δ 8.44 (s, 8H, $H_{\beta\text{pyrr}}$), 7.46 (m, 30H, H_{Ar}), 7.39 – 7.19 (m, 109H, $H_{\text{Ar}} + H_{\text{solvent}}$), 7.13 (t, $J = 7.2$ Hz, 4H, H_{Ar}), 5.13 (dd, $J = 16.0, 11.4$ Hz, 8H, H_{sugar}), 4.95 – 4.75 (m, 34H, H_{sugar}), 4.66 (dd, $J = 22.7, 9.9$ Hz, 9H, H_{sugar}), 4.52 (d, $J = 12.1$ Hz, 8H, H_{sugar}), 4.36 (d, $J = 7.6$ Hz, 4H, H_{sugar}), 4.20 – 4.11 (m, 8H, H_{sugar}), 4.01 – 3.56 (m, 43H, H_{sugar}), 3.52 – 3.39 (m, 8H, H_{sugar}), -3.02 (s, 2H, NH_{pyrr}). ^{19}F NMR (376 MHz, CDCl_3): δ -138.80 – -138.87 (m, 8F), -156.04 (d, $J = 17.2$ Hz, 8F). ^{13}C NMR (100 MHz, CDCl_3): δ 147.74, 145.35, 141.87, 141.70, 139.39, 139.23, 138.70, 138.59,

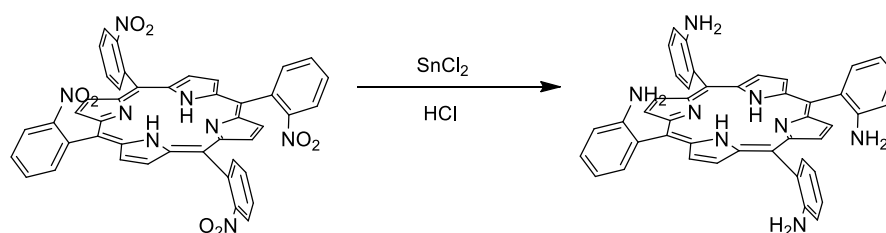
138.49, 138.19, 138.13, 128.66, 128.57, 128.46, 128.34, 128.31, 128.12, 128.08, 128.03, 127.88, 127.82, 127.78, 127.57, 127.45, 127.42, 127.39, 127.33, 113.88, 113.69, 113.50, 104.84, 104.03, 102.16, 83.80, 83.01, 82.71, 81.78, 80.99, 76.72, 76.46, 75.36, 75.24, 75.02, 74.96, 74.93, 74.52, 73.71, 73.61, 69.49, 68.07, 57.13. **IR** ν_{\max} (CH₂Cl₂)/cm⁻¹: 1004, 1060, 1209, 1361, 1399, 1432, 1497, 2626, 2870, 2926, 3061. **UV-Vis**: λ_{\max} (CH₂Cl₂)/nm (log ϵ): 416 (5.9), 509 (4.2), 538 (4.4), 584 (3.7.), 639 (2.8). **LR-MS** (MALDI): m/z (C₂₆₄H₂₄₈F₁₆N₄O₄₄) calcd. 4481.70; found [M] 4481.3. **Elemental analysis** calc. for (C₂₆₄H₂₄₈F₁₆N₄O₄₄) C, 70.73; H, 5.53; N, 1.25; found: C, 70.84; H, 5.66; N, 1.24.

4.1.5. Synthesis of *o*-TNPPH₂



2-Nitrobenzaldehyde (500 mg, 1,68 x 10⁻¹ mol) was dissolved in acetic acid (500 mL) in air. The solution was slowly brought to reflux and then distilled pyrrole (11.5 mL, 1.65 x 10⁻¹ mol) was added dropwise in about 15 minutes. The mixture was refluxed for 45 minutes and during this period the mixture turned to red at first, then to deep black. The dark solution was allowed to cool at 60°C and then chloroform (150 mL) was gradually added obtaining a dark suspension. The obtained solid was filtered, washed with dichloromethane and dried *in vacuo* (2.50 g, 8%).

4.1.6. Synthesis of $\alpha_2\beta_2$ *o*-TAPPH₂



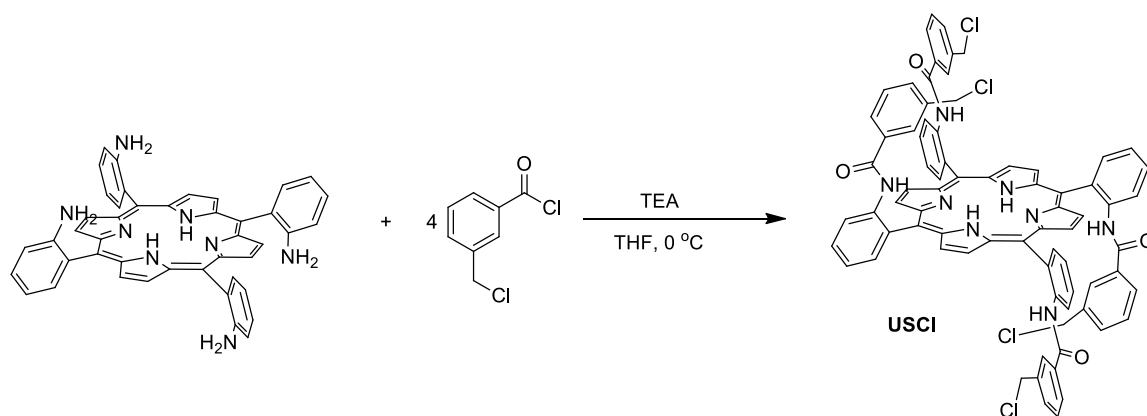
o-TNPPH₂ (10.0 g, 1.26 x 10⁻² mol) was dissolved in HCl 37% (500 mL) under vigorous magnetic stirring and then SnCl₂·2H₂O (50 g, 1.89 x 10⁻¹ mol) was slowly added. The resulting green mixture was stirred at room temperature in air for 48 hours, then chloroform (300 mL) was added. After 15 minutes the solution was cooled to 0°C and a saturated solution of KOH was added dropwise until a pH=10. The solid was filtered off and the aqueous phase was extracted several times with chloroform. The combined organic phases were dried over Na₂SO₄, filtered and the solvent was evaporated under reduced pressure to yield a dark purple solid containing the four atropoisomers.

The four atropoisomers were separated by flash chromatography (SiO₂, 15 μ m, gradient elution with CH₂Cl₂ and CH₃OH) with CH₂Cl₂ for $\alpha\beta$ (12.5%), 0.5% CH₃OH for $\alpha_2\beta_2$ (25%), 3% CH₃OH for $\alpha_3\beta$

(50%) and 5% CH₃OH for α_4 (12.5%). The collected analytical data are in accordance with those reported in literature¹⁹.

¹H NMR (400 MHz, CDCl₃) $\alpha_2\beta_2$ -*o*-TAPPH₂: δ 8.92 (s, 8H, H_{βpyrr}), 7.86 (d, J = 7.4 Hz, 4H, H_{Ar}), 7.26 (t, J = 7.8 Hz, 4H, H_{Ar}), 7.18 (t, J = 7.4 Hz, 4H, H_{Ar}), 7.14 (d, J = 8.1 Hz, 2H, H_{Ar}), 3.58 (s, 8H, NH₂), -2.65 (s, 2H, NH_{pyrr}).

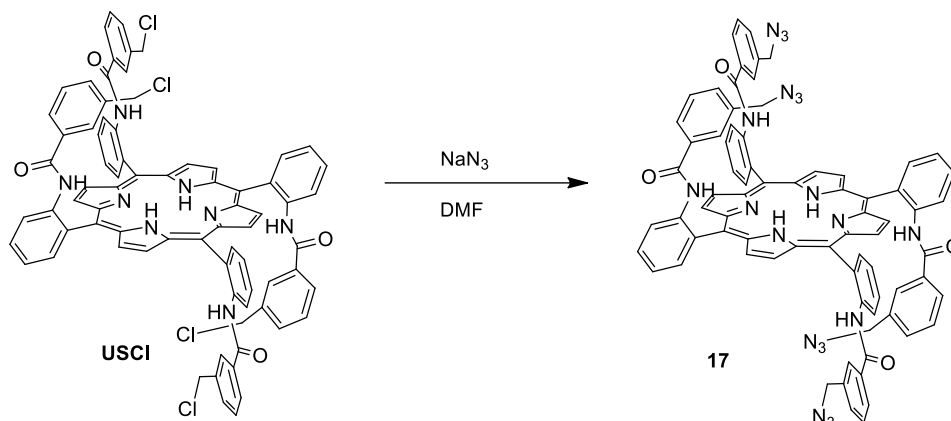
4.1.7. Synthesis of USCl porphyrin



The $\alpha_2\beta_2$ -*o*-TAPPH₂ (700 mg, 1.03×10^{-3} mol) was dissolved in fresh distilled THF (35.0 mL) at room temperature followed by the addition of TEA (1.23 mL, 8.24×10^{-3} mol). The dark solution was cooled to 0°C and 3-(chloromethyl)benzoyl chloride (0.95 mL, 6.18×10^{-3} mol) was added dropwise. The solution was stirred for 45min and then CH₃OH was added to quench the reaction. The solvent was removed under reduced pressure and the crude was purified by flash chromatography (SiO₂, 15 μ m, gradient elution from CH₂Cl₂ to CH₂Cl₂/CH₃OH = 99.5:0.5) to yield a purple solid (852 mg, 65%). The collected analytical data are in accordance with those reported in literature¹⁹.

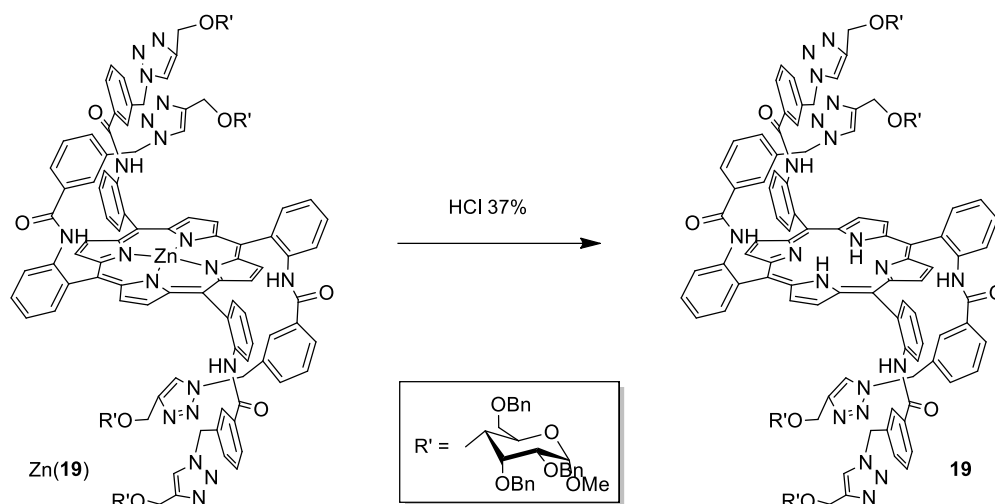
¹H NMR (400 MHz, CDCl₃): δ 8.96 (d, J = 4.1 Hz, 8H, H_{βpyrr}), 8.86 (d, 4H, J = 8.4 Hz, H_{Ar}), 8.04 (d, J = 6.3 Hz, 4H, H_{Ar}), 7.90 (t, J = 7.3 Hz, 4H, H_{Ar}), 7.62 (s, 4H, H_{NH}), 7.58 (t, J = 8.0 Hz, 4H, H_{Ar}), 6.71 (d, J = 7.7 Hz, 4H, H_{Ar}), 6.54 – 6.42 (m, 8H, H_{Ar}), 6.36 (t, J = 7.7 Hz, 4H, H_{Ar}), 3.54 – 3.46 (m, 8H, H_{CH2}), -2.55 ppm (s, 2H, NH_{pyrr}).

4.1.8. Synthesis of porphyrin 17



Sodium azide (28.0 mg, 4.31 mmol) was added to a DMF (10.0 mL) solution of **USCI** porphyrin (100.0 mg, 7.71×10^{-2} mmol). The resulting solution was stirred at 85 °C for 3 hours until the complete consumption of the porphyrin was observed by TLC (SiO_2 , $\text{CH}_2\text{Cl}_2/\text{CH}_3\text{OH} = 99:1$), then distilled water (30.0 mL) was added and the mixture was extracted with CH_2Cl_2 (3 x 50.0 mL). The organic phase was washed with a saturated solution of NH_4Cl (3 x 50.0 mL), dried over Na_2SO_4 and filtered. The solvent was evaporated to dryness under vacuum and the residue purified by flash chromatography (SiO_2 , gradient elution from CH_2Cl_2 to $\text{CH}_2\text{Cl}_2/\text{CH}_3\text{OH} = 95:5$) to yield a purple solid **5** (150.0 mg, 95%).

^1H NMR (400 MHz, CDCl_3): δ 8.98 – 8.82 (m, 11H, $\text{H}_{\text{pyrr}} + \text{H}_{\text{Ar}}$), 8.04 - 7.88 (m, 9H, H_{Ar}), 7.70 – 7.45 (m, 8H, H_{Ar}), 6.76 – 6.18 (m, 16H, H_{Ar}), 3.35 – 3.06 (m, 8H, $\text{H}_{\text{CH}_2\text{-N}_3}$), -2.49 (s, 2H, NH_{pyrr}). **^{13}C NMR** (100 MHz, CDCl_3 , 298 K): δ 165.30, 157.39, 138.98, 135.76, 135.63, 135.53, 135.37, 135.08, 130.70, 128.81, 128.56, 126.57, 126.44, 126.16, 126.04, 123.92, 115.54, 53.76, 53.64, 53.55, 53.47. **IR** ν_{max} (CH_2Cl_2)/ cm^{-1} : 1091, 1222, 1362, 1428, 1712, 2100, 2962, 3004, 3061, 3407. UV-Vis λ_{max} (CH_2Cl_2)/nm (log ϵ): 421 (4.7), 483 (3.3), 517 (3.8), 548 (3.4), 592 (3.4), 647 (3.2). **LR-MS** (ESI): m/z ($\text{C}_{76}\text{H}_{54}\text{N}_{20}\text{O}_4$) calcd. 1311.37; found $[\text{M}+\text{H}]^+$ 1312.4. **Elemental analysis** calc. for $\text{C}_{76}\text{H}_{54}\text{N}_{20}\text{O}_4$: C, 69.61; H, 4.15; N, 21.36; found: C, 69.72; H, 4.15; N, 21.36.

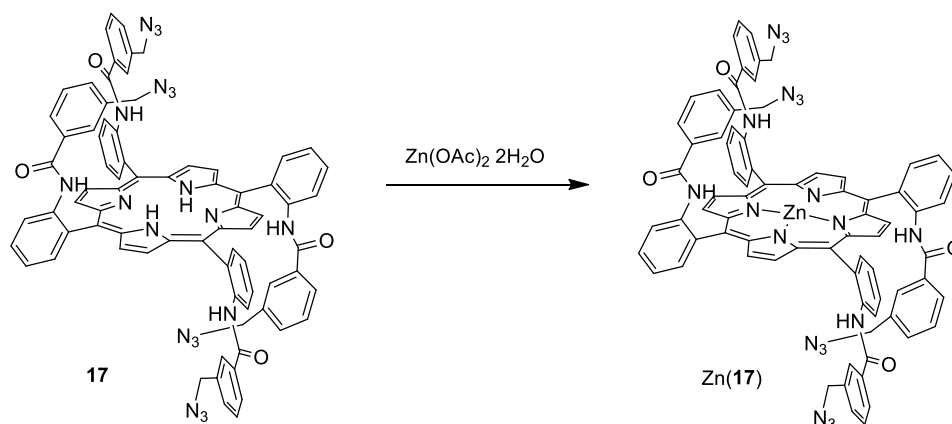
4.1.9. Synthesis of porphyrin **19**

HCl 37% (30.0 mL) was added to a AcOEt (120.0 mL) solution of Zn(**19**) (200.0 mg, 5.92×10^{-2} mmol). The resulting solution was stirred for 3 hours at room temperature until the complete consumption of Zn^{II}(**19**) was observed by TLC (SiO₂, CH₂Cl₂/CH₃OH = 97:3), then H₂O (100.0 mL) was added to the mixture. The organic phase was extracted with H₂O (3 x 100.0 mL) until pH = 7. The resulting solution was dried over Na₂SO₄ and filtered. The solvent was evaporated to dryness under vacuum to yield the purple solid **19** (195.0 mg, 99%).

¹H NMR (400 MHz, CDCl₃, 298 K): δ 8.91 - 8.82 (m, 8H, H_{pyrr}), 8.77 - 8.59 (m, 4H, H_{Ar}), 7.93 - 7.83 (m, 9H, H_{Ar}), 7.72 (s, 2H, H_{triazole}), 7.51 - 7.48 (m, 5H, H_{Ar} + H_{triazole}), 7.31 - 7.07 (m, 63H, H_{Ar} + H_{solvent}), 6.89 - 5.86 (m, 19H, H_{Ar}), 4.91 - 4.26 (m, 46H, H_{sugar}), 3.85 - 3.79 (t, $J = 9.2$ Hz, 4H, H_{sugar}), 3.59 - 3.49 (m, 20H, H_{sugar}), 3.33 (s, 12H, H_{OMe}), -2.64 (s, 2H, NH_{pyrr}). **¹³C NMR** (100 MHz, CDCl₃, 298 K): δ 165.14, 145.69, 145.57, 139.16, 138.73, 138.54, 138.67, 138.45, 138.38, 138.35, 135.89, 135.55, 135.49, 135.35, 135.20, 130.91, 130.67, 130.60, 128.86, 128.78, 128.75, 128.70, 128.64, 128.52, 128.33, 128.25, 128.20, 128.13, 128.07, 127.95, 127.90, 127.85, 127.79, 127.74, 127.33, 126.97, 126.04, 125.56, 124.21, 122.85, 122.48, 115.88, 115.62, 98.52, 82.22, 82.18, 80.18, 78.13, 78.07, 75.87, 73.75, 70.24, 68.78, 66.26, 55.60, 52.82. **IR** ν_{max} (CH₂Cl₂)/cm⁻¹: 1047, 1096, 1266, 1306, 1449, 1518, 1582, 1680, 2929, 2960, 3033, 3417. **UV-Vis** λ_{max} (CH₂Cl₂)/nm (log ϵ): 424 (5.50), 521 (4.24), 549 (3.70), 591 (3.76), 647 (3.51). **HR-MS** (MALDI): m/z (C₂₀₀H₁₉₀N₂₀O₂₈) calcd. 3321.41, found [M+Na]⁺ 3344.3. **Elemental analysis** calc. for C₂₀₀H₁₉₀N₂₀O₂₈: C, 72.32; H, 5.77; N, 8.43; found: C, 72.01; H, 5.88; N, 8.31.

4.2. Synthesis of porphyrin complexes

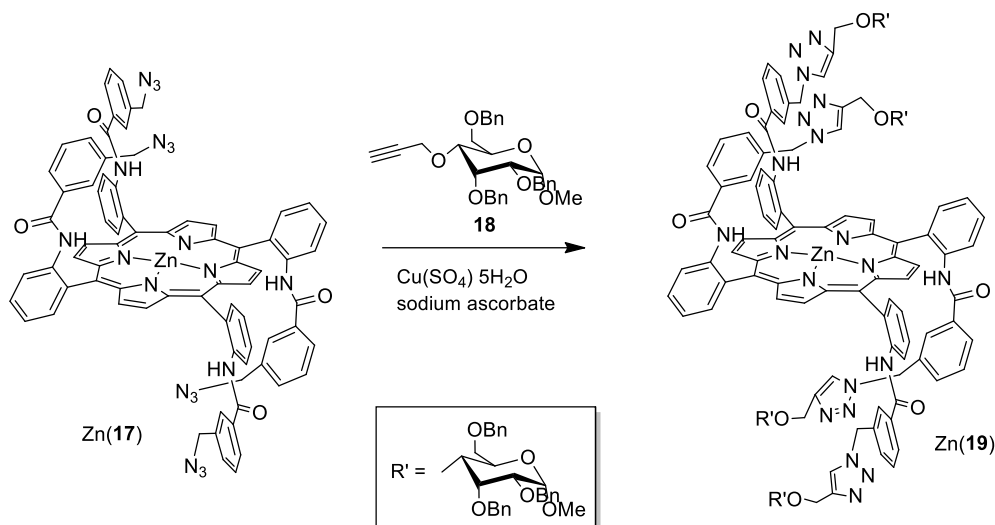
4.2.1. Synthesis of Zn(17)



A solution of $\text{Zn}(\text{OAc})_2 \cdot 2\text{H}_2\text{O}$ (375.0 mg, 1.71 mmol) in CH_3OH (8.0 mL) was added to a CH_2Cl_2 (60.0 mL) solution of **17** (150.0 mg, 1.14×10^{-1} mmol). The resulting solution was stirred overnight at room temperature until the complete consumption of the starting porphyrin was observed by TLC (SiO_2 , $\text{CH}_2\text{Cl}_2/\text{CH}_3\text{OH} = 99:1$), then H_2O (50.0 mL) was added to the mixture. The organic phase was extracted with H_2O (3 x 50.0 mL), dried over Na_2SO_4 and filtered. The solvent was evaporated to dryness under vacuum to give the purple compound **Zn(17)** (155.0 mg, 99%).

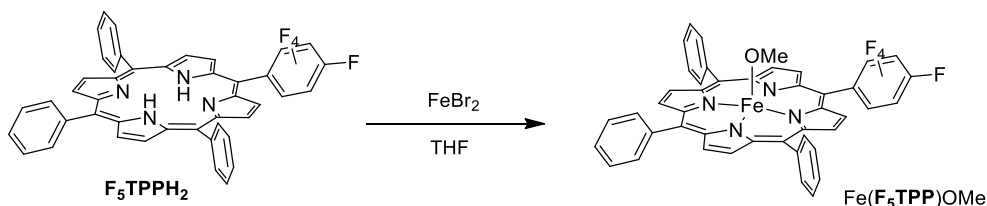
^1H NMR (400 MHz, CDCl_3 , 298 K): δ 9.04 – 8.96 (m, 8H, $\text{H}_{\beta\text{pyr}}$), 8.82 – 8.72 (m, 4H, H_{Ar}), 8.11 – 8.09 (m, 1H, H_{Ar}), 8.05 (d, $J = 7.4$ Hz, 1H, H_{Ar}), 8.02 – 7.96 (m, 2H, H_{Ar}), 7.91 – 7.84 (m, 5H, H_{Ar}), 7.68 (s, 1H, H_{NH}), 7.61 – 7.52 (m, 5H, $\text{H}_{\text{Ar}} + \text{H}_{\text{NH}}$), 7.47 (s, 1H, H_{NH}), 7.30 (s, 1H, H_{NH}), 6.75 (d, $J = 7.5$ Hz, 1H, H_{Ar}), 6.62 – 6.57 (m, 3H H_{Ar}), 6.50 – 6.39 (m, 4H, H_{Ar}), 6.38 – 6.29 (m, 4H, H_{Ar}), 6.01 – 5.94 (m, 2H, H_{Ar}), 5.66 – 5.61 (m, 2H, H_{Ar}), 2.97 (s, 1H, $\text{H}_{\text{CH}_2\text{-N}_3}$), 2.81 (m, 2H, $\text{H}_{\text{CH}_2\text{-N}_3}$), 2.65 (d, $J = 13.8$, 1H, $\text{H}_{\text{CH}_2\text{-N}_3}$), 2.55 (m, 3H, $\text{H}_{\text{CH}_2\text{-N}_3}$), 2.12 (s, 1H, $\text{H}_{\text{CH}_2\text{-N}_3}$). **^{13}C NMR** (300 MHz, CDCl_3 , 298 K): δ 164.75, 152.00, 151.26, 150.78, 138.75, 132.88, 130.28, 123.39, 126.36, 123.58, 121.08, 115.88, 52.82, 52.69, 52.38. **IR** ν_{max} (CH_2Cl_2)/ cm^{-1} : 996, 1250, 1308, 1447, 1518, 1581, 1681, 2101, 2340, 2360, 3415. **UV-Vis** λ_{max} (CH_2Cl_2)/nm (log ϵ): 425 (5.58), 556 (4.30), 592 (1.20), 626 (2.78) (1.20). **LR-MS** (ESI): m/z ($\text{C}_{76}\text{H}_{52}\text{N}_{20}\text{O}_4\text{Zn}$) calcd. 1372.38; found $[\text{M}+\text{Na}]^+$ 1396.4. **Elemental Analysis** calc. for $\text{C}_{76}\text{H}_{54}\text{N}_{20}\text{O}_4\text{Zn}$: C, 66.30; H, 3.95; N, 20.35; found: C, 66, 54; H, 3.99; N, 20.16.

4.2.2. Synthesis of Zn(19)



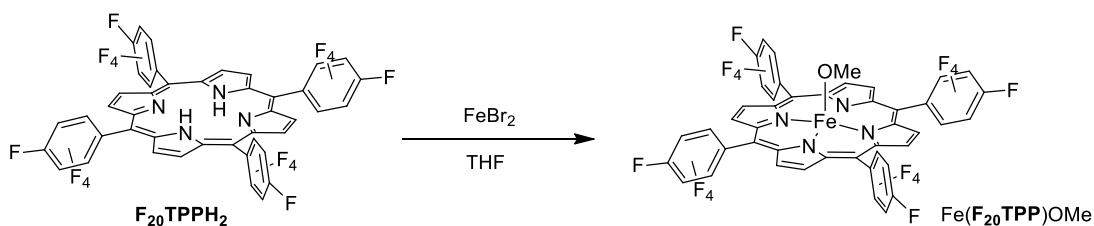
Zn(17) (150.0 mg, 1.11×10^{-1} mmol) and **18** (276.0 mg, 5.54×10^{-1} mmol) were dissolved in THF (20.0 mL) and then a solution of $\text{CuSO}_4 \cdot 5\text{H}_2\text{O}$ (137.0 mg, 5.54×10^{-1} mmol) in H_2O (5.0 mL) was added. A solution of sodium ascorbate (109.0 mg, 5.54×10^{-1} mmol) in H_2O (5 mL) was added and the resulting mixture was stirred for 5 hours at 50°C until the complete consumption of the zinc porphyrin was observed by TLC (SiO_2 , $\text{CH}_2\text{Cl}_2/\text{CH}_3\text{OH} = 97:3$). The mixture was extracted with CH_2Cl_2 (3 x 20.0 mL), dried over Na_2SO_4 and filtered. The solvent was evaporated to dryness under vacuum and the residue purified by flash chromatography (SiO_2 , gradient elution from CH_2Cl_2 to $\text{CH}_2\text{Cl}_2/\text{CH}_3\text{OH}$ 98:2) to yield the purple solid Zn(19) (232.0 mg, 63%).

^1H NMR (400 MHz, CDCl_3 , 298 K): δ 8.98 - 8.75 (m, 12 H, $\text{H}_{\beta\text{pyrr}} + \text{H}_{\text{Ar}}$), 8.09 (t, $J = 6.6$ Hz, 4H, H_{Ar}), 7.85 - 7.81 (m, 8H, $\text{H}_{\text{Ar}} + \text{H}_{\text{NH}}$), 7.75 (s, 1H, H_{NH}), 7.61 (s, 1H, H_{NH}), 7.52 - 6.94 (m, 88H, $\text{H}_{\text{Ar}} + \text{H}_{\text{solvent}}$), 6.82 - 6.74 (m, 4H, H_{Ar}), 6.66 - 6.47 (m, 12H, H_{Ar}), 6.26 - 6.18 (m, 3H, H_{Ar}), 5.84 - 5.72 (m, 4H, H_{CH_2}), 5.52 - 5.48 (m, 2H, H_{CH_2}), 5.41 - 5.34 (m, 2H, H_{CH_2}), 5.01 - 4.92 (m, 1H, H_{sugar}), 4.84 (d, $J = 11.2$ Hz, 2H, H_{sugar}), 4.72 (q, $J = 9.5, 7.8$ Hz, 6H, H_{sugar}), 4.66 - 4.52 (m, 9H, H_{sugar}), 4.49 - 4.24 (m, 12H, H_{sugar}), 4.22 - 4.14 (m, 2H, H_{sugar}), 4.05 - 3.97 (m, 2H, H_{sugar}), 3.78 (t, $J = 9.2$ Hz, 2H, H_{sugar}), 3.69 - 3.62 (m, 1H, H_{sugar}), 3.57 - 3.39 (m, 8H, H_{sugar}), 3.31 - 3.29 (m, 12H, H_{sugar}), 3.23 - 3.13 (m, 1H, H_{sugar}), 3.04 (d, $J = 11.6$ Hz, 1H, H_{sugar}), 2.93 (t, $J = 9.4$ Hz, 1H, H_{sugar}). **^{13}C NMR** (100 MHz, CDCl_3 , 298 K): δ 139.42, 139.10, 138.41, 128.86, 128.68, 128.50, 128.34, 128.05, 127.89, 119.49, 99.34, 98.47, 82.28, 81.98, 81.42, 80.17, 73.75, 70.67, 70.15, 68.77, 65.58, 65.45, 63.73, 55.99, 52.76. **IR** ν_{max} (CH_2Cl_2)/ cm^{-1} : 1047, 1091, 1223, 1273, 1362, 1446, 1519, 1582, 1712, 2928, 3060, 3411. **UV-Vis** λ_{max} (CH_2Cl_2)/nm (log ϵ): 434 (5.20), 563 (4.08), 602 (3.51). **HR-MS** (MALDI): m/z ($\text{C}_{200}\text{H}_{188}\text{N}_{20}\text{O}_{28}\text{Zn}$) calcd. 3383.33, found [M] 3383.6. **Elemental Analysis** calc. for $\text{C}_{200}\text{H}_{188}\text{N}_{20}\text{O}_{28}\text{Zn}$: C, 70.96; H, 5.60; N, 8.28; found: C, 71.06; H, 5.70; N, 8.20.

4.2.3. Synthesis of Fe(F₅TPP)OMe

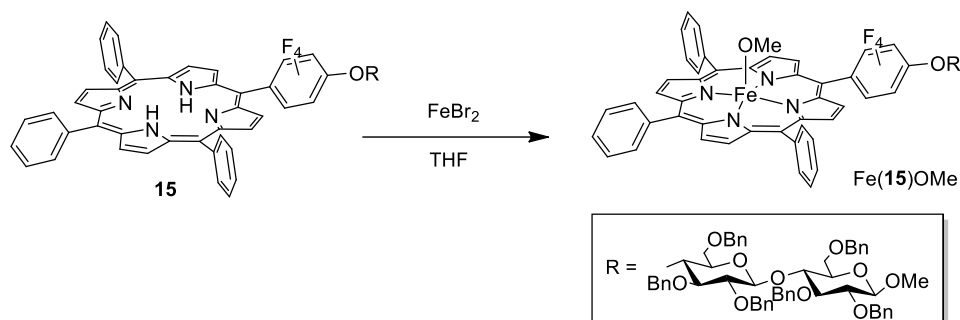
FeBr₂ (305.0 mg, 1.42 mmol) was added to a THF (20.0 mL) solution of **F₅TPPH₂** (50.0 mg, 7.12 x 10⁻² mmol) under nitrogen. The solution was refluxed at 75°C for 5 hours until the complete consumption of the starting porphyrin was observed by TLC (Al₂O₃, CH₂Cl₂/CH₃OH = 97:3). The solvent was evaporated to dryness under vacuum and the residue purified by chromatography (Al₂O₃, eluent CH₂Cl₂/CH₃OH 97:3) to yield the brown solid Fe(**F₅TPP**)OMe (56.0 mg, 92%).

IR ν_{\max} (CH₂Cl₂)/cm⁻¹: 1091, 1277, 1273, 1420, 2854, 2927, 3054, 3059. **UV-Vis** λ_{\max} (CH₃OH)/nm (log ϵ): 413 (3.7), 478 (2.8), 484 (2.8). **LR-MS** (ESI): m/z (C₄₅H₂₆F₅FeN₄O) calcd. 789.14; found [M-OMe] 759.18. **Elemental analysis** calc. for C₄₅H₂₆FeN₄O: calcd. C, 68.45; H, 3.32; N, 7.10; found C, 68.67; H, 3.63; 6.96.

4.2.4. Synthesis of Fe(F₂₀TPP)OMe

FeBr₂ (219.0 mg, 1.02 mmol) was added to a THF (20.0 mL) solution of **F₂₀TPPH₂** (50.0 mg, 5.13 x 10⁻² mmol) under nitrogen. The solution was refluxed at 75°C for 5 hours until the complete consumption of the starting porphyrin was observed by TLC (Al₂O₃, CH₂Cl₂/CH₃OH = 97:3). The solvent was evaporated to dryness under vacuum and the residue purified by chromatography (Al₂O₃, eluent CH₂Cl₂/CH₃OH 97:3) to yield the brown solid Fe(**F₂₀TPP**)OMe (49.0 mg, 90%). The collected analytical data are in accordance with those reported in literature.

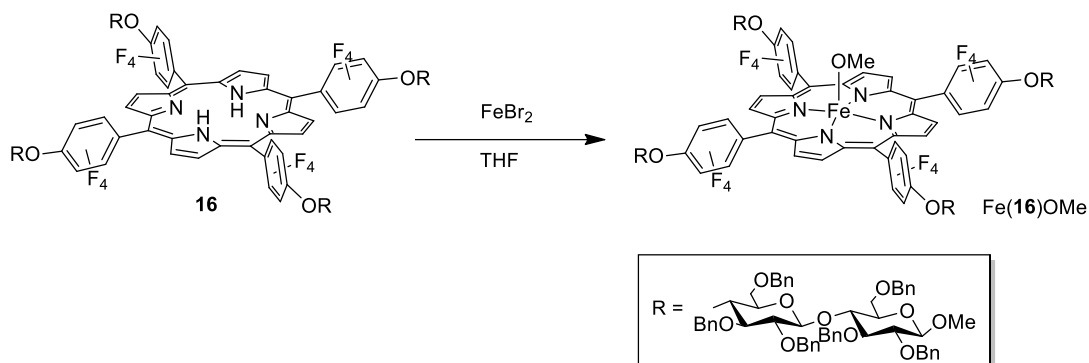
4.2.5. Synthesis of Fe(15)OMe



FeBr₂ (136.0 mg, 6.33 × 10⁻¹ mmol) was added to a THF (20.0 mL) solution of porphyrin **15** (50.0 mg, 3.16 × 10⁻² mmol) under nitrogen. The solution was refluxed at 75°C for 5 hours until the complete consumption of the starting porphyrin was observed by TLC (Al₂O₃, CH₂Cl₂/CH₃OH = 97:3). The solvent was evaporated to dryness under vacuum and the residue purified by chromatography (Al₂O₃, eluent CH₂Cl₂/CH₃OH 97:3) to yield the brown solid Fe(**15**)OMe (47.0 mg, 90%).

IR ν_{max} (CH₂Cl₂)/cm⁻¹: 1026, 1092, 1271, 1280, 1422, 2927, 2961, 3056. **UV-Vis** λ_{max} (CH₃OH)/nm (log ε): 413 nm (5.7), 495 (3.6), 600 (3.4). **LR-MS** (ESI) m/z: (C₁₀₀H₈₅F₄FeN₄O₁₂) calcd. 1665.54, found [M+Na]⁺ 1688.59. **Elemental analysis** calc. for C₁₀₀H₈₅F₄FeN₄O₁₂ C 72.07, H 5.14, N 3.36; found: C, 72.25; H, 5.35; N, 3.30

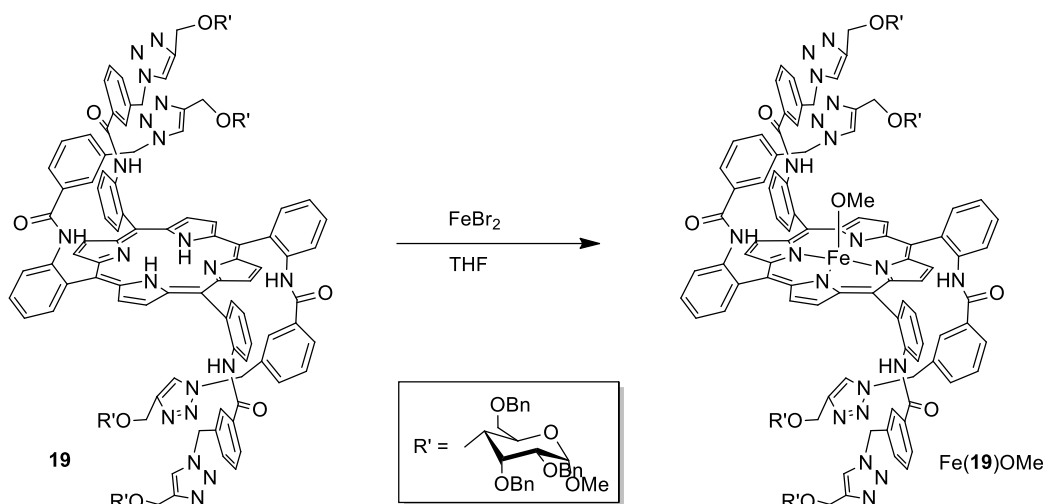
4.2.6. Synthesis of Fe(16)OMe



FeBr₂ (47.0 mg, 2.23 × 10⁻¹ mmol) was added to a THF (20.0 mL) solution of porphyrin **16** (50.0 mg, 1.12 × 10⁻² mmol) under nitrogen. The solution was refluxed at 75°C for 5 hours until the complete consumption of the starting porphyrin was observed by TLC (Al₂O₃, CH₂Cl₂/CH₃OH = 97:3). The solvent was evaporated to dryness under vacuum and the residue purified by chromatography (Al₂O₃, eluent CH₂Cl₂/CH₃OH 97:3) to yield the brown solid Fe(**16**)OMe (48.0 mg, 95%).

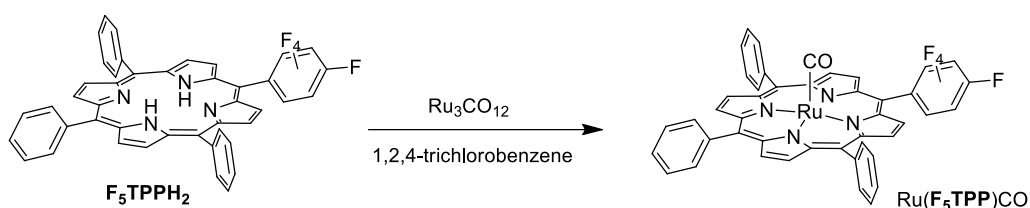
IR ν_{max} (CH₂Cl₂)/cm⁻¹: 1081, 1259, 1266, 1278, 2857, 2926, 3058. **UV-Vis** λ_{max} (CH₃OH)/nm (log ε): 410 (5.1), 519 (3.8), 580 (3.7). **HR-MS** (MALDI): m/z (C₂₆₅H₂₄₉F₁₆FeN₄O₄₅) calcd. 4566.64, found [M-OMe+Na]⁺ 4559.2. **Elemental analysis** calc. for C₂₆₅H₂₄₉F₁₆FeN₄O₄₅ C, 69.65; H, 5.49; N, 1.23; found: C, 69.83; H, 5.62; N, 1.21.

4.2.7. Synthesis of Fe(19)OMe



FeBr₂ (48.0 mg, 2.24 × 10⁻¹ mmol) was added to a THF (20.0 mL) solution of porphyrin **19** (50.0 mg, 1.51 × 10⁻² mmol) under nitrogen. The solution was refluxed at 75°C for 5 hours until the complete consumption of the starting porphyrin was observed by TLC (Al₂O₃, CH₂Cl₂/CH₃OH = 97:3). The solvent was evaporated to dryness under vacuum and the residue purified by chromatography (Al₂O₃, eluent CH₂Cl₂/CH₃OH 97:3) to yield the brown solid Fe(**19**)OMe (47.0 mg, 92%).

IR ν_{\max} (CH₂Cl₂)/cm⁻¹: 1447, 1452, 1512, 1582, 1680, 2867, 2928, 2960, 3417. **UV-Vis** λ_{\max} (CH₂Cl₂)/nm (log ϵ) 421 (5.43), 478 (4.78), 581 (4.39). **HR-MS** (MALDI): *m/z* (C₂₀₁H₁₉₁FeN₂₀O₂₈) calcd. 3406.35, found [M-OMe] 3375.0. **Elemental analysis** calc. for C₂₀₁H₁₉₁FeN₂₀O₂₈: C 70.87, H 5.65, N 8.22; found C 70.97, H 5.75, N 8.15.

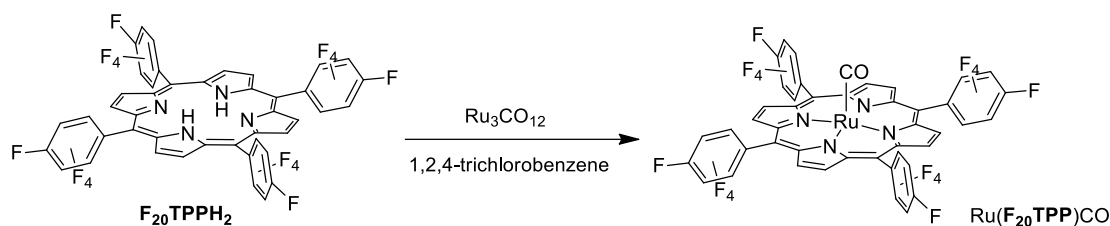
4.2.8. Synthesis of Ru(F₅TPP)CO

Ru₃CO₁₂ (92.0 mg, 1.42 × 10⁻¹ mmol) was added to a 1,2,4-trichlorobenzene (20.0 mL) solution of **F₅TPPH₂** (50.0 mg, 7.12 × 10⁻² mmol) under nitrogen. The solution was refluxed for 5 hours until the complete consumption of the starting porphyrin was observed by TLC (SiO₂, *n*-hexane/AcOEt = 7:3). The solvent was evaporated to dryness under vacuum and the residue purified by chromatography (SiO₂, gradient elution from *n*-hexane to *n*-hexane/AcOEt = 7:3) to yield a red solid Ru(**F₅TPP**)CO (42.0 mg, 68%).

¹H NMR (300 MHz, CDCl₃): δ 8.78 (d, *J* = 4.9 Hz, 2H, H_{βpyr}), 8.69 (s, 4H, H_{βpyr}), 8.61 (d, *J* = 4.9 Hz, 2H, H_{βpyr}), 8.25 – 8.09 (m, 6H, H_{Ar}), 7.82 – 7.67 (m, 9H, H_{Ar}). **¹⁹F NMR** (282 MHz, CDCl₃): δ -136.62 (dd, *J* = 24.2, 9.0 Hz, 1F), -138.24 (d, *J* = 24.3 Hz, 1F), -153.73 (t, *J* = 21.0 Hz, 1F), -162.48 (t, *J* = 23.4

Hz, 1F), -163.06 (d, $J = 23.9$ Hz, 1F). ^{13}C NMR (75 MHz, CDCl_3): δ 144.59, 144.18, 144.15, 143.16, 142.09, 142.03, 138.76, 134.41, 133.81, 133.37, 132.24, 131.90, 129.48, 128.04, 127.56, 126.97, 126.70, 126.64, 126.49, 123.97, 123.54, 122.53. **IR** ν_{max} (CH_2Cl_2)/ cm^{-1} : 1010, 1094, 1273, 1282, 1494, 1520, 1942, 2962, 3004, 3056, 3063, 3415. **UV-Vis** λ_{max} (CH_2Cl_2)/nm (log ϵ): 408 (3.9), 528 (2.9), 553 (2.7). **LR-MS** (ESI): m/z ($\text{C}_{45}\text{H}_{23}\text{F}_5\text{N}_4\text{ORu}$) calcd. 832.08 found $[\text{M}-\text{CO}]$ 804.04. **Elemental analysis** calc. for $\text{C}_{45}\text{H}_{23}\text{F}_5\text{N}_4\text{ORu}$ C, 64.98; H, 2.79; F, 6.74; found C, 65.25; H, 3.09; N, 6.62.

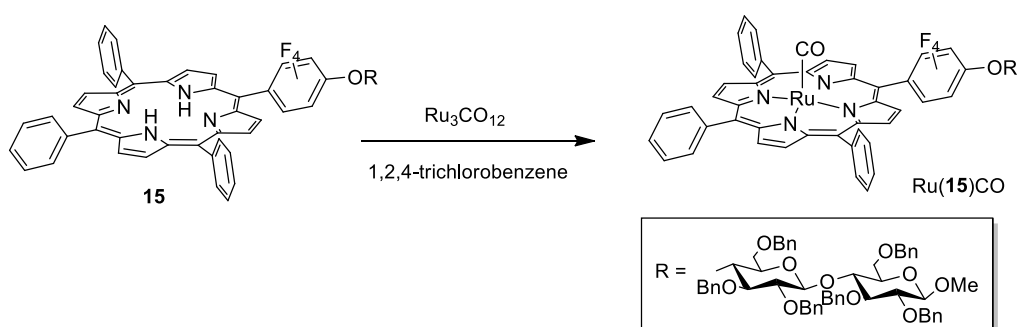
4.2.9. Synthesis of $\text{Ru}(\text{F}_{20}\text{TPP})\text{CO}$



$\text{Ru}_3\text{CO}_{12}$ (130.0 mg, 2.06×10^{-1} mmol) was added to a 1,2,4-trichlorobenzene (20.0 mL) solution of $\text{F}_{20}\text{TPPH}_2$ (100.0 mg, 1.03×10^{-1} mmol) under nitrogen. The solution was refluxed for 5 hours until the complete consumption of the starting porphyrin was observed by TLC (SiO_2 , n -hexane/ $\text{AcOEt} = 7:3$). The solvent was evaporated to dryness under vacuum and the residue purified by chromatography (SiO_2 , gradient elution from n -hexane to n -hexane/ $\text{AcOEt} = 7:3$) to yield a red solid $\text{Ru}(\text{F}_{20}\text{TPP})\text{CO}$ (91.0 mg, 81%). The collected analytical data are in accordance with those reported in literature.

^1H NMR (300 MHz, CDCl_3): δ 8.73 (s, 8H, $\text{H}_{\beta\text{pyrr}}$).

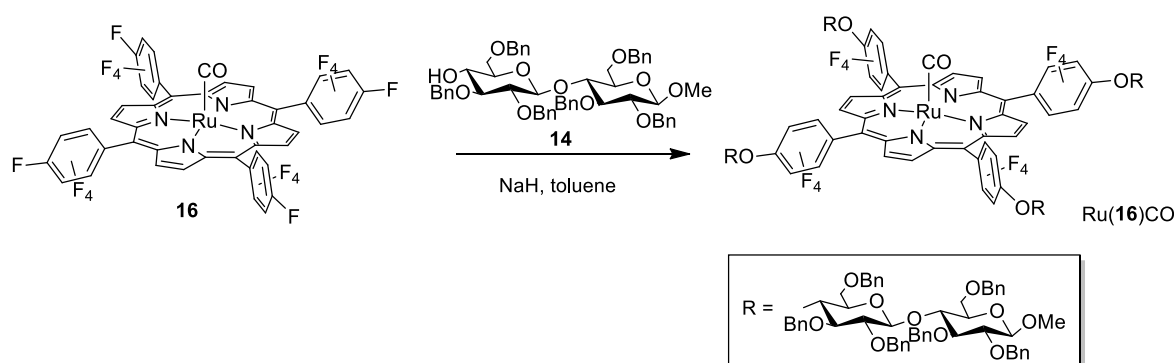
4.2.10. Synthesis of $\text{Ru}(\mathbf{15})\text{CO}$



$\text{Ru}_3\text{CO}_{12}$ (38.0 mg, 5.76×10^{-2} mmol) was added to a 1,2,4-trichlorobenzene (20.0 mL) solution of porphyrin **15** (45.0 mg, 2.84×10^{-2} mmol) under nitrogen. The solution was refluxed for 5 hours until the complete consumption of the starting porphyrin was observed by TLC (SiO_2 , n -hexane/ $\text{AcOEt} = 7:3$). The solvent was evaporated to dryness under vacuum and the residue purified by chromatography (SiO_2 , gradient elution from n -hexane to n -hexane/ $\text{AcOEt} = 7:3$) to yield a red solid $\text{Ru}(\mathbf{15})\text{CO}$ (32.0 mg, 61%).

$^1\text{H NMR}$ (300 MHz, CDCl_3): δ 8.71 – 8.36 (m, 8H, H_{pyrr}), 8.34 – 8.12 (m, 9H, H_{Ar}), 7.80 – 7.58 (m, 16H, H_{Ar}), 7.40 – 7.26 (m, 77H, H_{Ar} + $\text{H}_{\text{solvent}}$), 5.16 – 3.67 (br, 29H, H_{sugar}). $^{19}\text{F NMR}$ (282 MHz, CDCl_3): δ -137.94 – -140.21 (m, 2F), -156.17 – -157.34 (m, 2F). $^{13}\text{C NMR}$ (75 MHz, CDCl_3): δ 135.01, 134.93, 129.05, 128.98, 128.85, 128.82, 128.78, 128.72, 128.70, 128.65, 128.56, 128.52, 128.48, 128.43, 128.40, 128.37, 128.28, 128.23, 128.19, 128.17, 128.13, 128.08, 128.04, 128.00, 127.95, 127.80, 127.76, 127.70, 127.62, 127.51, 127.16, 127.10, 105.18, 105.08, 102.79, 102.53, 85.23, 84.73, 84.36, 84.10, 83.34, 83.14, 83.07, 82.44, 82.18, 82.11, 81.13, 75.43, 75.29, 74.86, 74.38, 73.32, 71.98, 71.51, 57.56, 57.49, 57.44. **IR** ν_{max} (CH_2Cl_2)/ cm^{-1} : 1009, 1095, 1262, 1275, 1282, 1941, 2926, 2960, 2986, 3051, 3060. **UV-Vis** λ_{max} (CH_2Cl_2)/nm (log ϵ): 406 (5.1), 527 (3.8), 550 (3.6). LR-MS (ESI) m/z ($\text{C}_{100}\text{H}_{82}\text{F}_4\text{N}_4\text{O}_{12}\text{Ru}$) calcd. 1708.40, found $[\text{M}+\text{K}]^+$ 1746.7. **Elemental analysis** calc. for $\text{C}_{100}\text{H}_{82}\text{F}_4\text{N}_4\text{O}_{12}\text{Ru}$ C, 70.29; H, 4.84; N, 3.28; found: C, 70.49; H, 5.05; N, 3.22.

4.2.11. Synthesis of Ru(16)CO

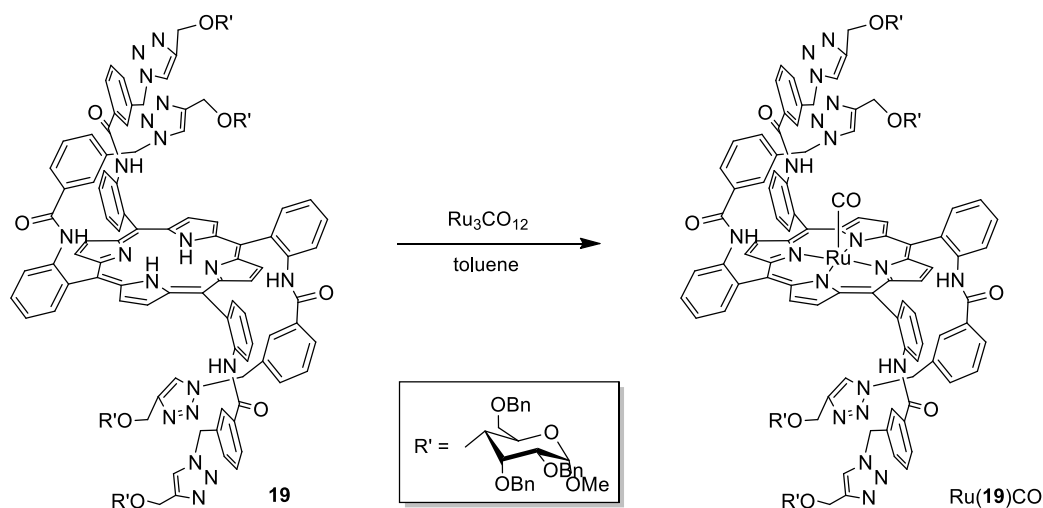


NaH 60% wt (166.4 mg, 4.16 mmol) was added under nitrogen to a toluene (14.0 mL) solution of $\text{Ru}(\text{F}_{20}\text{TPP})\text{CO}$ (115.0 mg, 0.104 mmol) and **14** (290.0 mg, 0.624 mmol). The solution was refluxed for 50 hours until the complete consumption of $\text{Ru}(\text{F}_{20}\text{TPP})\text{CO}$ was observed by TLC (SiO_2 , n -hexane/ AcOEt = 7:3) and then residual NaH was quenched with HCl 1.0 N. CH_2Cl_2 (20.0 mL) was added to the mixture, the organic phase was extracted with H_2O until pH = 7, dried over Na_2SO_4 and filtered. The solvent was evaporated to dryness under vacuum and the resulting residue was purified by flash chromatography (SiO_2 , gradient elution from n -hexane to n -hexane/ AcOEt = 6:4) to yield the red solid $\text{Ru}(\text{16})\text{CO}$ (197.0 mg, 39%).

$^1\text{H NMR}$ (400 MHz, CDCl_3): δ 8.30 - 8.24 (m, 8H, H_{pyrr}), 7.44 – 7.23 (m, 187H, H_{Ar} + $\text{H}_{\text{solvent}}$), 5.10 (t, J = 11.9 Hz, 9H, H_{sugar}), 4.92 – 4.73 (m, 40H, H_{sugar}), 4.64 (dd, J = 20.9, 9.4 Hz, 14H, H_{sugar}), 4.50 (d, J = 11.6 Hz, 10H, H_{sugar}), 4.34 (d, J = 7.5 Hz, 6H, H_{sugar}), 4.17 – 4.08 (m, 9H, H_{sugar}), 3.96 – 3.87 (m, 10H, H_{sugar}), 3.78 – 3.60 (m, 15H, H_{sugar}), 3.58 – 3.48 (m, 25H, H_{sugar}), 3.46 – 3.39 (m, 12H, H_{sugar}). $^{19}\text{F NMR}$ (376 MHz, CDCl_3): δ -138.18 – -140.32 (m, 8F), -155.84 – -156.90 (m, 8F). $^{13}\text{C NMR}$ (100 MHz, CDCl_3) δ 144.00, 139.21, 138.68, 138.49, 138.25, 138.16, 128.65, 128.59, 128.43, 128.30, 128.12, 128.07, 128.01, 127.79, 127.75, 127.56, 127.39, 127.31, 104.81, 102.12, 83.73, 83.00, 82.67, 81.76,

80.94, 76.43, 75.31, 75.20, 75.00, 74.97, 74.90, 74.55, 73.64, 73.58, 69.46, 68.05, 57.11. **IR** ν_{\max} (CH_2Cl_2)/ cm^{-1} : 1080, 1270, 1360, 1420, 1497, 1954, 2871, 2987, 3052. **UV-Vis** λ_{\max} (CH_2Cl_2)/nm (log ϵ): 408 (5.1), 528 (3.9), 550 (3.7). **HR-MS** (MALDI) m/z : ($\text{C}_{265}\text{H}_{246}\text{F}_{16}\text{N}_4\text{O}_{45}\text{Ru}$) calcd. 4609.59, found [M-CO] 4581.8. **Elemental analysis** calc. for $\text{C}_{265}\text{H}_{246}\text{F}_{16}\text{N}_4\text{O}_{45}\text{Ru}$: C, 69.01; H, 5.38; N, 1.21, found C, 69.30; H, 5.56, N, 1.19.

4.2.12. Synthesis of Ru(19)CO

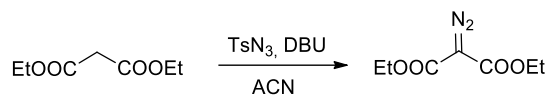


$\text{Ru}_3\text{CO}_{12}$ (30.0 mg, 4.53×10^{-2} mmol) was added to a toluene (15.0 mL) solution of **19** (50.0 mg, 1.51×10^{-2} mmol) under nitrogen. The solution was refluxed in pressure tube for 8 hours until the complete consumption of the porphyrin was observed by TLC (SiO_2 , $\text{CH}_2\text{Cl}_2/n$ -hexane = 1:1). The solvent was evaporated to dryness under vacuum and the resulting residue was purified by flash chromatography (SiO_2 , gradient elution from n -hexane/AcOEt = 7:3 to n -hexane/AcOEt = 1:1) to yield the brown solid Ru(**19**)CO (15.0 mg, 19%).

^1H NMR (400 MHz, CDCl_3): δ 9.21 – 8.91 (m, 12H, $\text{H}_{\text{ppyr}} + \text{H}_{\text{Ar}}$), 8.33 – 6.74 (m, 127H, $\text{H}_{\text{Ar}} + \text{H}_{\text{solvent}}$), 5.49 – 4.59 (m, 60H, H_{sugar}), 4.11 – 2.92 (m, 30H, H_{sugar}). **^{13}C NMR** (100 MHz, CDCl_3): δ 201.32, 163.80, 163.40, 144.74, 144.07, 138.70, 138.23, 137.99, 128.65, 128.10, 127.97, 127.55, 127.13, 127.00, 123.20, 98.29, 97.86, 97.41, 81.81, 80.15, 73.15, 69.78, 69.46, 68.41, 65.94, 55.31. **IR** ν_{\max} (CH_2Cl_2)/ cm^{-1} : 1094, 1420, 1520, 1582, 1680, 1681, 1948, 2023, 2305, 2855, 2958, 3054. **UV-Vis** λ_{\max} (CH_2Cl_2)/nm (log ϵ): 417 (5.1), 535 (4.1), 598 (3.7). **HR-MS** (MALDI) m/z : ($\text{C}_{201}\text{H}_{189}\text{N}_{20}\text{O}_{29}\text{Ru}$) calcd. 3448.30, found [M-CO] 3418.2 **Elemental Analysis** calc. for $\text{C}_{201}\text{H}_{189}\text{N}_{20}\text{O}_{29}\text{Ru}$ C, 70.00; H, 5.49; N, 8.12; found: C, 70.29; H, 5.70; N, 7.96.

4.3. Synthesis of diazo compounds

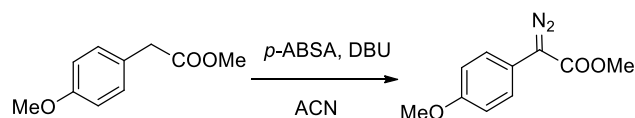
4.3.1. Synthesis of diethyl-2-diazomalonate (29)



Diethylmalonate (50 mmol) and tosyl azide (55 mmol) were dissolved in CH₃CN (100 mL) and the mixture was cooled to 0°C. DBU (55 mmol) was added dropwise and the reaction mixture was stirred for 5h. The solvent was removed and the residue was dissolved in CH₂Cl₂ (50 mL), then distilled water (50 mL) was added and the mixture was extracted with CH₂Cl₂. The organic phase was washed with brine and dried over Na₂SO₄ and concentrated *in vacuo*. The solvent was evaporated to dryness under vacuum and the residue purified by flash chromatography (SiO₂, gradient elution from *n*-hexane to *n*-hexane/AcOEt = 8:2) to yield a yellow oil (80%). The collected analytical data are in accordance with those reported in literature²³.

¹H NMR (300 MHz, CDCl₃): δ 4.30 (q, *J* = 7.1 Hz, 4H, H_{CH2}), 1.32 (t, *J* = 7.1 Hz, 6H, H_{CH3}).

4.3.2. Synthesis of methyl-2-diazo-2-(4-methoxyphenyl)acetate (30)

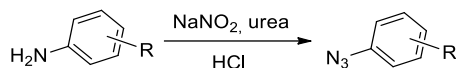


Methyl 2-(4-methoxyphenyl)acetate (100 mmol) and *p*-ABSA (113 mmol) were dissolved in CH₃CN (70 mL), the mixture was cooled to 0°C and DBU (55 mmol) was added in one portion. The mixture was allowed to reach room temperature and further stirred for 4 hours. The reaction was quenched with a saturated solution of NH₄Cl and the aqueous phase was extracted by diethyl ether (3 x 75 mL) and the obtained organic phase was dried over MgSO₄. The solvent was removed under reduced pressure and residue was triturated with 50% diethyl ether/petroleum ether. The solid was filtered off and the solvent was removed under reduced pressure. The crude was purified by flash chromatography (SiO₂, gradient elution from *n*-hexane to *n*-hexane/AcOEt = 88:2) to yield an orange solid (35%). The collected analytical data are in accordance with those reported in literature²⁴.

¹H NMR (400 MHz, CDCl₃): δ 7.38 (d, 2H, *J* = 9.2, H_{Ar}), 6.94 (d, 2H, *J* = 9.2, H_{Ar}), 3.85 (s, 3H, H_{OCH3}), 3.81 (s, 3H, H_{OCH3}).

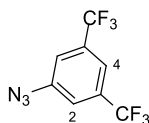
4.4. Synthesis of azides

General procedure for the synthesis of azides



The desired aniline (3.80×10^{-2} mol) was dissolved in a solution of HCl 37% (75 mL) and water (75 mL). The mixture was cooled at 0° C in an ice bath and a solution of NaNO₂ (3.98×10^{-2} mol) in 25.0 mL of water was added. The reaction was stirred for 30 minutes and then urea (2.16×10^{-2} mol) was added in one portion. Under vigorous magnetic stirring a solution of sodium azide (5.38×10^{-2} mol) in 20.0 mL of water was added to the cold mixture in about 15 minutes. The mixture was stirred for 30 minutes and then allowed to reach room temperature and further stirred for 3 hours. The aqueous phase was extracted by diethyl ether (3 x 75 mL) and the obtained organic phase was dried over Na₂SO₄, filtered and concentrated *in vacuo*²⁵.

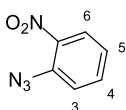
4.4.1. Synthesis of 3,5-bis(trifluoromethyl) phenylazide



The general procedure for the synthesis of azides was followed using 3,5-bis(trifluoromethyl)aniline (83% yield). The collected analytical data are in accordance with those reported in literature²⁵.

¹H NMR (300 MHz, CDCl₃): δ 7.64 (s, 1H, H⁴), 7.44 (s, 2H, H²).

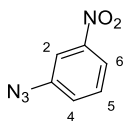
4.4.2. Synthesis of 2-nitrophenylazide



The general procedure for the synthesis of azides was followed using 2-nitroaniline (80% yield). The collected analytical data are in accordance with those reported in literature²⁵.

¹H NMR (300 MHz, CDCl₃): δ 7.94 (d, 1H, *J* = 8.2 Hz, H³), 7.63 (t, 1H, *J* = 7.8 Hz, H⁵), 7.35 (d, 1H, *J* = 8.1 Hz, H⁶), 7.26 (t, 1H, *J* = 7.8 Hz, H⁴).

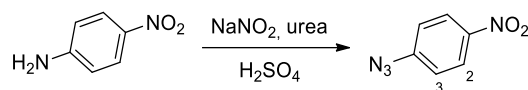
4.4.3. Synthesis of 3-nitrophenylazide



The general procedure for the synthesis of azides was followed using 3-nitroaniline (78% yield). The collected analytical data are in accordance with those reported in literature²⁶.

¹H NMR (300 MHz, CDCl₃): δ 8.00 (ddd, 1H, *J* = 8.2, 2.2, 1.0 Hz, H⁴), 7.89 (t, 1H, *J* = 2.0 Hz, H²), 7.54 (t, 1H, *J* = 8.0 Hz, H⁵), 7.35 (ddd, 1H, *J* = 8.1, 2.3, 1.0 Hz, H⁶).

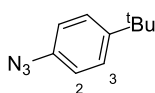
4.4.4. Synthesis of 4-nitrophenylazide



4-Nitroaniline (5.20 g, 3.80 x 10⁻² mol) was dissolved in a solution of H₂SO₄ 30% (75.0 mL) under air. The yellow mixture was cooled at 0° C in an ice bath and a solution of NaNO₂ (2.75 g, 3.98 x 10⁻² mol) in 25.0 mL of water was added. The reaction was stirred for 30 minutes and then urea (1.30 g, 2.16 x 10⁻² mol) was added in one portion. Under vigorous magnetic stirring a solution of sodium azide (3.50 g, 5.38 x 10⁻² mol) in 20.0 mL of water was added to the cold mixture in about 15 minutes. The resulting mixture was then allowed to reach room temperature and further stirred for 30 minutes. Dichloromethane (100 mL) was added and the phases were separated. The aqueous phase was washed twice with 50.0 mL of dichloromethane and the combined organic phases were dried over Na₂SO₄. The solvent was evaporated under reduced pressure up to 10 mL and hexane (15.0 mL) was added. The yellow precipitate was collected by filtration and dried *in vacuo* (70% yield). The collected analytical data are in accordance with those reported in literature²⁵.

¹H NMR (300 MHz, CDCl₃): δ 7.62 (d, 2H, *J* = 9.1 Hz, H³), 6.15 (d, 2H, *J* = 9.1 Hz, H²).

4.4.5. Synthesis of 4-tertbutylphenylazide

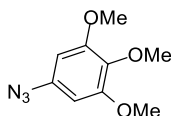


The general procedure for the synthesis of azides was followed using 4-tertbutylaniline (92% yield).

The collected analytical data are in accordance with those reported in literature²⁵.

¹H NMR (300 MHz, CDCl₃): δ 7.37 (d, 2H, *J* = 7.2 Hz, H³), 6.98 (d, 2H, *J* = 7.2 Hz, H²), 1.32 (s, 9H, H_{tBu}).

4.4.6. Synthesis of 1,2,3-trimethoxyphenylazide

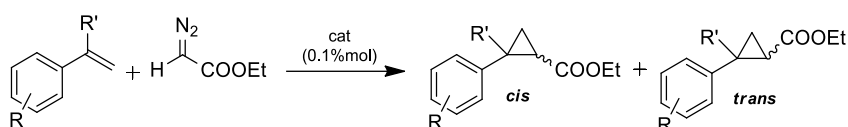


The general procedure was followed using 1,2,3-trimethoxyaniline (70% yield). The collected analytical data are in accordance with those reported in literature²⁶.

¹H NMR (300 MHz, CDCl₃): δ 6.24 (s, 2H, H_{Ar}), 3.84 (s, 6H, H_{OCH3}), 3.81 (s, 3H, H_{OCH3}).

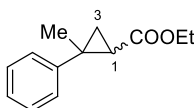
4.5. Synthesis of cyclopropanes

General catalytic procedure for the synthesis of cyclopropanes



Method A: In a typical run, the catalyst (6.79×10^{-4} mmol) was dissolved in 2.0 mL of dry toluene before adding the alkene (3.39 mmol) and the diazo compound (7.47×10^{-1} mmol) under nitrogen. The reaction was stirred for 2 hours at 25°C. The solution was then evaporated to dryness and the reaction crude was analysed by ¹H-NMR spectroscopy using 2,4-dinitrotoluene as the internal standard. *Method B:* the procedure illustrated for method A was followed using 6.79×10^{-1} mmol of alkene.

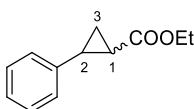
4.5.1. Synthesis of *trans*-ethyl-2-methyl-2-phenylcyclopropanecarboxylate (20)



The general catalytic procedure for the synthesis of cyclopropanes was followed using α -methylstyrene and EDA. The collected analytical data are in accordance with those reported in literature²⁷.

¹H NMR (300 MHz, CDCl₃): δ 7.31 (d, 4H, $J = 4.4$ Hz, H_{Ar}), 7.22 (m, 1H, H_{Ar}), 4.20 (q, 2H, $J = 7.1$ Hz, H_{CH2Et}), 1.97 (dd, 1H, $J = 8.2, 6.1$ Hz, H¹), 1.54 (s, 3H, H_{CH3}), 1.49 – 1.39 (m, 2H, H³), 1.31 (t, 3H, $J = 7.1$ Hz, H_{CH3Et}).

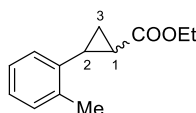
4.5.2. Synthesis of *trans*-ethyl-2-phenylcyclopropanecarboxylate (21)



The general catalytic procedure for the synthesis of cyclopropanes was followed using styrene and EDA. The collected analytical data are in accordance with those reported in literature²⁷.

$^1\text{H NMR}$ (300 MHz, CDCl_3): δ 7.09 – 7.31 (m, 5H, H_{Ar}), 4.17 (q, 2H, $J = 7.2$ Hz, $\text{H}_{\text{CH}_2\text{Et}}$), 2.57 – 2.52 (m, 1H, H^2), 1.94 – 1.90 (m, 1H, H^1), 1.64 – 1.60 (m, 1H, H^3), 1.35-1.30 (m, 1H, $\text{H}^{3'}$), 1.28 (t, 3H, $J = 7.2$ Hz, $\text{H}_{\text{CH}_3\text{Et}}$).

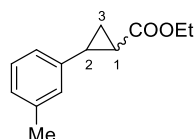
4.5.3. Synthesis of *trans*-ethyl-2-(2-methylphenyl)cyclopropane carboxylate (22)



The general catalytic procedure for the synthesis of cyclopropanes was followed using 2-methylstyrene and EDA. The collected analytical data are in accordance with those reported in literature²⁸.

$^1\text{H NMR}$ (300 MHz, CDCl_3): δ 7.14 (m, 3H, H_{Ar}), 6.99 (m, 1H, H_{Ar}), 4.20 (q, 2H, $J = 7.2$ Hz, $\text{H}_{\text{CH}_2\text{Et}}$), 2.51 (m, 1H, H^2), 2.38 (s, 3H, H_{CH_3}), 1.78 (m, 1H, H^1), 1.57 (m, 1H, H^3), 1.31 (m, 1H, $\text{H}^{3'}$), 1.29 (t, 3H, $J = 7.2$ Hz, $\text{H}_{\text{CH}_3\text{Et}}$).

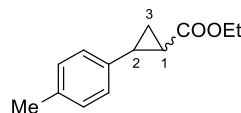
4.5.4. Synthesis of *trans*-ethyl-2-(3-methylphenyl)cyclopropane carboxylate (23)



The general catalytic procedure for the synthesis of cyclopropanes was followed using 3-methylstyrene and EDA. The collected analytical data are in accordance with those reported in literature²⁸.

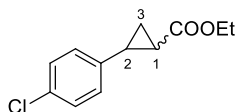
$^1\text{H NMR}$ (300 MHz, CDCl_3): δ 6.88 – 7.19 (m, 4H, H_{Ar}), 4.16 (q, 2H, $J = 7.2$ Hz, $\text{H}_{\text{CH}_2\text{Et}}$), 2.48 (m, 1H, H^2), 2.32 (s, 3H, H_{CH_3}), 1.89 (m, 1H, H^1), 1.58 (m, 1H, H^3), 1.29 (m, 1H, $\text{H}^{3'}$), 1.27 (t, 3H, $J = 7.2$ Hz, $\text{H}_{\text{CH}_3\text{Et}}$).

4.5.5. Synthesis of *trans*-ethyl-2-(4-methylphenyl)cyclopropane carboxylate (24)



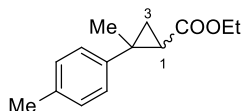
The general catalytic procedure for the synthesis of cyclopropanes was followed using 4-methylstyrene and EDA. The collected analytical data are in accordance with those reported in literature²⁸.

$^1\text{H NMR}$ (400 MHz, CDCl_3): δ 7.10 (d, 2H, $J = 7.9$ Hz, H_{Ar}), 7.01 (d, 2H, $J = 8.1$ Hz, H_{Ar}), 4.18 (q, 2H, $J = 7.1$ Hz, $\text{H}_{\text{CH}_2\text{Et}}$), 2.53 – 2.48 (m, 1H, H^2), 2.32 (s, 3H, H_{CH_3}), 1.86 (m, 1H, H^1), 1.58 (m, 1H, H^3), 1.28 (t, 3H, $J = 7.1$ Hz, $\text{H}_{\text{CH}_3\text{Et}}$), 1.27 (m, 1H, $\text{H}^{3'}$).

4.5.6. Synthesis of *trans*-ethyl-2-(4-chlorophenyl)cyclopropane carboxylate (25)

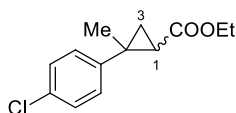
The general catalytic procedure for the synthesis of cyclopropanes was followed using 4-chlorostyrene and EDA. The collected analytical data are in accordance with those reported in literature²⁹.

¹H NMR (300 MHz, CDCl₃): δ 7.22 (d, 2H, *J* = 8.5 Hz, H_{Ar}), 7.01 (d, 2H, *J* = 8.4 Hz, H_{Ar}), 4.16 (q, 2H, *J* = 7.1 Hz, H_{CH₂Et}), 2.51-2.44 (m, 1H, H²), 1.90 – 1.80 (m, 1H, H¹), 1.60 – 1.57 (m, 1H, H³), 1.27 (t, 3H, *J* = 7.1 Hz, H_{CH₃Et}), 1.25 (m, 1H, H³).

4.5.7. Synthesis of *trans* ethyl-2-methyl-(4-methylphenyl)cyclopropane carboxylate (26)

The general catalytic procedure for the synthesis of cyclopropanes was followed using 4-methyl- α -methylstyrene and EDA. The crude was purified by flash chromatography (silica gel, 60 μ m, *n*-hexane/AcOEt 98:2) to give a yellow oil.

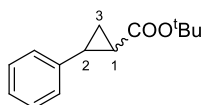
¹H NMR (300 MHz, CDCl₃): δ 7.23 – 7.18 (m, 2H, H_{Ar}), 7.16 – 7.09 (m, 2H, H_{Ar}), 4.20 (qd, 2H, *J* = 7.1, 1.8 Hz, H_{CH₂Et}), 2.33 (s, 3H, H_{CH₃}), 1.95 (dd, 1H, *J* = 8.3, 6.0 Hz, H¹), 1.52 (s, 3H, H_{CH₃}), 1.46 – 1.37 (m, 2H, H³), 1.31 (t, 3H, *J* = 7.1 Hz, H_{CH₃Et}). **¹³C NMR** (75 MHz, CDCl₃): δ 172.42, 143.15, 136.18, 129.24, 127.32, 60.59, 30.45, 29.84, 27.98, 21.10, 20.96, 20.09, 14.56. **IR** ν_{max} (CH₂Cl₂)/cm⁻¹: 1271, 1420, 1720, 2305, 2987, 3058, 3060. **UV-Vis** λ_{max} (CH₂Cl₂)/nm (log ϵ): 243 (2.2), 265 (1.9). **LR-MS** (ESI): *m/z* (C₁₄H₁₈O₂) calcd. 218.29; found [M+H]⁺ 219.03.

4.5.8. Synthesis of *trans*-ethyl-2-methyl-(4-chlorophenyl)cyclopropane carboxylate (27)

The general catalytic procedure for the synthesis of cyclopropanes was followed using 4-chloro- α -methylstyrene and EDA. The collected analytical data are in accordance with those reported in literature³⁰.

¹H NMR (400 MHz, CDCl₃): δ 7.26 (q, 4H, *J* = 8.5 Hz, H_{Ar}), 4.26 – 4.18 (m, 2H, H_{CH₂Et}), 1.94 (dd, 1H, *J* = 8.3, 6.1 Hz, H¹), 1.52 (s, 3H, H_{CH₃}), 1.47 (m, 1H, H³), 1.39 (dd, 1H, *J* = 8.4, 4.8 Hz, H³), 1.32 (t, 3H, *J* = 7.1 Hz, H_{CH₃Et}).

4.5.9. Synthesis of *trans-tert*-butyl 2-phenylcyclopropanecarboxylate (31)

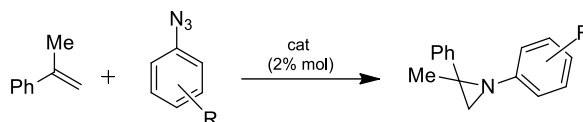


The general catalytic procedure for the synthesis of cyclopropanes was followed using styrene and *tert*-butyl diazoacetate (**28**). The collected analytical data are in accordance with those reported in literature³¹.

¹H NMR (400 MHz, CDCl₃): δ 7.07 - 7.28 (m, 5H, H_{Ar}), 2.47 – 2.41 (m, 1H, H²), 1.85 – 1.81 (m, 1H, H¹), 1.56 – 1.51 (m, 1H, H³), 1.46 (s, 9H, H_{tBu}), 1.25 – 1.20 (m, 1H, H^{3'}).

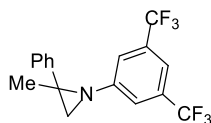
4.6. Synthesis of aziridines

General catalytic procedure for the synthesis of aziridines



In a typical run, the catalyst (2.72×10^{-2} mmol) was dissolved in 6.0 mL of dry benzene before adding the azide (1.34×10^{-1} mmol) and the alkene (6.79×10^{-1} mmol) under nitrogen. The resulting solution was refluxed using a preheated oil bath for two 2 hours. The solution was then evaporated to dryness and the reaction crude was analysed by ¹H-NMR spectroscopy using 2,4-dinitrotoluene as the internal standard.

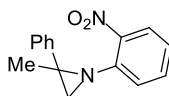
4.6.1. Synthesis of 1-(3,5-bis(trifluoromethyl)phenyl)-2-methyl-2-phenylaziridine (32)



The general catalytic procedure for the synthesis of aziridines was followed using α -methylstyrene and 3,5-bis(trifluoromethyl)phenyl azide (80% yield). The collected data are in accordance with those reported in literature²².

¹H NMR (300 MHz, CDCl₃): δ 7.55 – 7.51 (m, 3H, H_{Ar}), 7.44 (m, 5H, H_{Ar}), 2.70 (s, 1H, H_{CH2}), 2.42 (s, 1H, H_{CH2}), 1.50 (s, 3H, H_{CH3}).

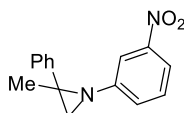
4.6.2. Synthesis of 2-methyl-1-(2-nitrophenyl)-2-phenylaziridine (33)



The general catalytic procedure for the synthesis of aziridines was followed using α -methylstyrene and 2-nitrophenylazide (90% yield). The collected data are in accordance with those reported in literature²².

¹H NMR (300 MHz, CDCl₃): δ 7.66 – 7.62 (m, 1H, H_{Ar}), 7.41 – 7.37 (m, 2H, H_{Ar}), 7.20 – 7.09 (m, 3H, H_{Ar}), 6.81 – 6.78 (m, 1H, H_{Ar}), 6.48 – 6.46 (m, 1H, H_{Ar}), 6.44 – 6.39 (m, 1H, H_{Ar}), 2.29 (s, 1H, H_{CH2}), 1.70 (s, 1H, H_{CH2}), 1.12 (s, 3H, H_{CH3}).

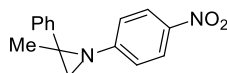
4.6.3. Synthesis of 2-methyl-1-(3-nitrophenyl)-2-phenylaziridine (34)



The general catalytic procedure for the synthesis of aziridines was followed using α -methylstyrene and 3-nitrophenylazide (75% yield). The crude was purified by flash chromatography (SiO₂, 60 μ m, *n*-hexane/AcOEt 90:10 with 0.5% of TEA) to give a yellow oil.

¹H NMR (300 MHz, CDCl₃): δ 7.87 – 7.83 (m, 1H, H_{Ar}), 7.79 (t, 2H, $J = 2.2$ Hz, H_{Ar}), 7.56 – 7.46 (m, 2H, H_{Ar}), 7.46 – 7.22 (m, 5H, H_{Ar}), 2.64 (s, 1H, H_{CH2}), 2.38 (s, 1H, H_{CH2}), 1.45 (s, 3H, H_{CH3}). **¹³C NMR** (75 MHz, CDCl₃): δ 151.92, 149.09, 142.29, 129.68, 128.61, 127.47, 127.04, 126.39, 117.00, 115.34, 56.56, 54.15, 44.54, 42.45. **IR** ν_{\max} (CH₂Cl₂)/cm⁻¹: 1285, 1353, 1429, 1530, 2305, 2988, 3055. **UV-Vis** λ_{\max} (CH₂Cl₂)/nm (log ϵ): 246 (4.0), 357 (3.6). **LR-MS** (ESI): m/z (C₁₅H₁₄N₂O₂) calcd. 254.11; found [M+H]⁺ 255.20.

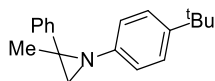
4.6.4. Synthesis of 2-methyl-1-(4-nitrophenyl)-2-phenylaziridine (35)



The general catalytic procedure for the synthesis of aziridines was followed using α -methylstyrene and 4-nitrophenylazide (96% yield). The collected data are in accordance with those reported in literature²².

¹H NMR (300 MHz, CDCl₃): δ 8.19 (d, 2H, $J = 9.0$ Hz, H_{Ar}), 7.51 (d, 2H, $J = 7.2$ Hz, H_{Ar}), 7.40 (pst, 2H, $J = 7.2$ Hz, H_{Ar}), 7.34 (t, 1H, $J = 7.2$ Hz, H_{Ar}), 7.02 (d, 2H, $J = 9.0$ Hz, H_{Ar}), 2.69 (s, 1H, H_{CH2}), 2.42 (s, 1H, H_{CH2}), 1.50 (s, 3H, H_{CH3}).

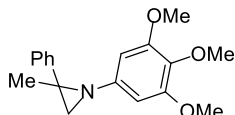
4.6.5. Synthesis of 1-(4-(tert-butyl)phenyl)-2-methyl-2-phenylaziridine (36)



The general catalytic procedure for the synthesis of aziridines was followed using α -methylstyrene and 4-(tert-butyl)phenylazide (95% yield). The collected data are in accordance with those reported in literature²².

¹H NMR (300 MHz, CDCl₃): δ 7.56 – 7.53 (m, 2H, H_{Ar}), 7.40 – 7.35 (m, 2H, H_{Ar}), 7.31 – 7.25 (m, 3H, H_{Ar}), 6.92 – 6.88 (m, 2H, H_{Ar}), 2.46 (s, 1H, H_{CH2}), 2.25 (s, 1H, H_{CH2}), 1.38 (s, 3H, H_{CH3}), 1.31 (s, 9H, H_{tBu}).

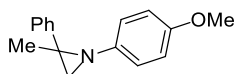
4.6.6. Synthesis of 2-methyl-2-phenyl-1-(3,4,5-trimethoxyphenyl)aziridine (37)



The general catalytic procedure for the synthesis of aziridines was followed using α -methylstyrene and 3,4,5-trimethoxyphenylazide (29% yield). The collected data are in accordance with those reported in literature²².

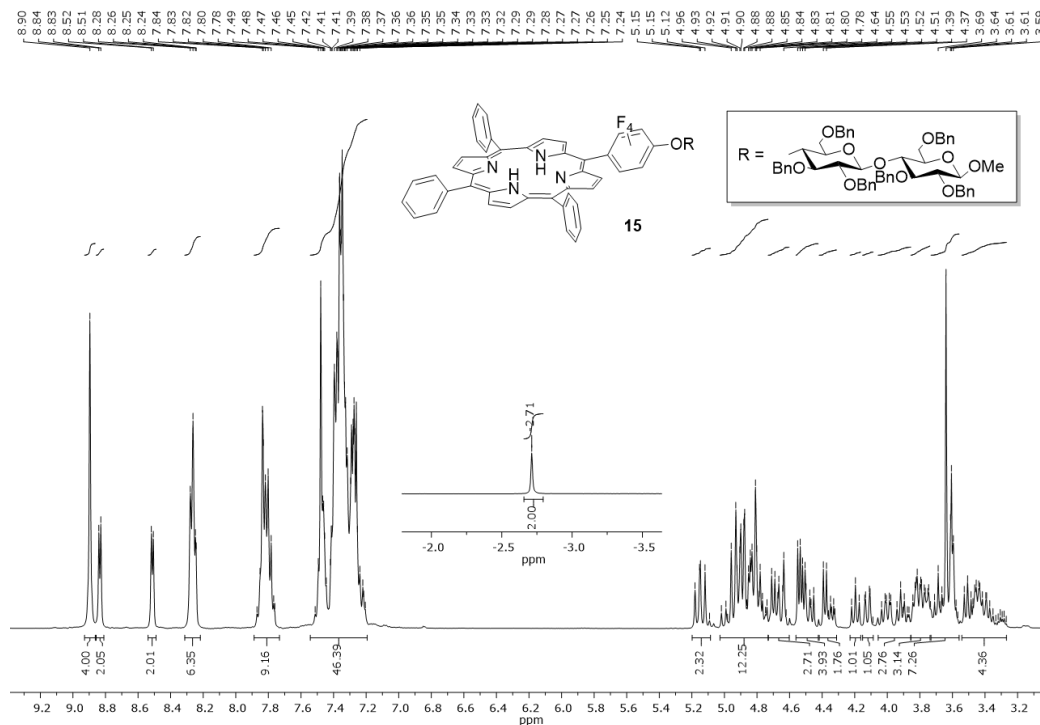
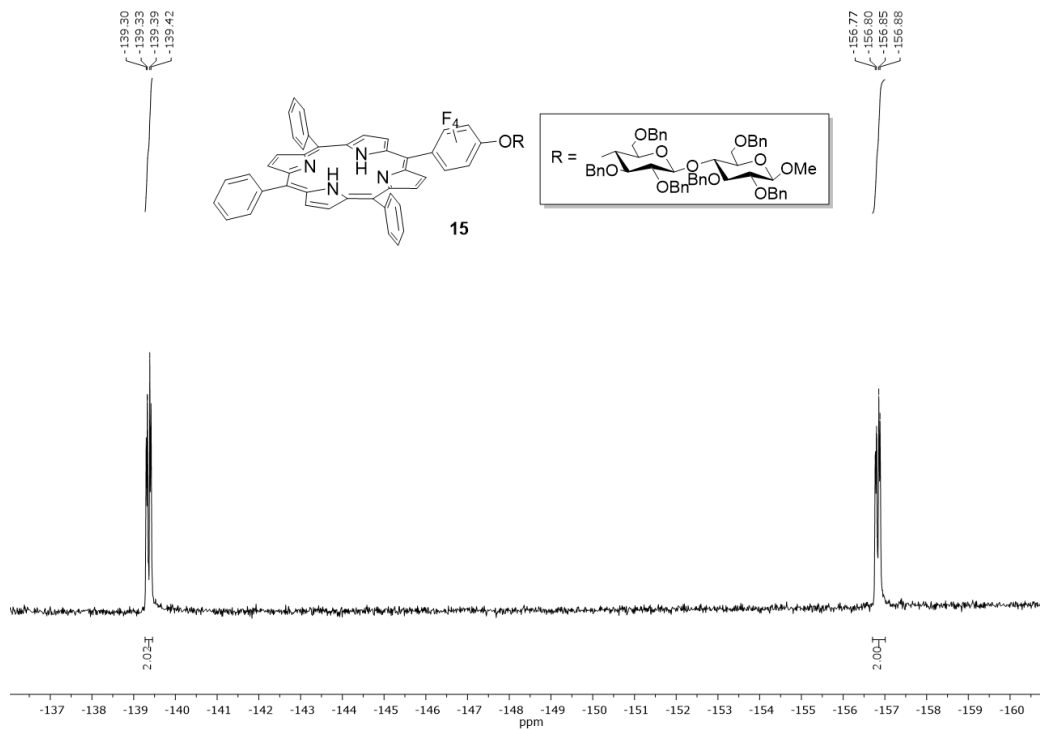
¹H NMR (300 MHz, CDCl₃): δ 7.51 (d, 2H, $J = 7.4$ Hz, H_{Ar}), 7.37 (pst, 2H, $J = 7.4$ Hz, H_{Ar}), 7.29 (t, 1H, $J = 7.4$ Hz, H_{Ar}), 6.16 (s, 2H, H_{Ar}), 3.84 (s, 6H, HOCH₃), 3.81 (s, 3H, HOCH₃), 2.46 (s, 1H, H_{CH2}), 2.28 (s, 1H, H_{CH2}), 1.44 (s, 3H, H_{CH3}).

4.6.7. Synthesis of 1-(4-methoxyphenyl)-2-methyl-2-phenylaziridine (38)

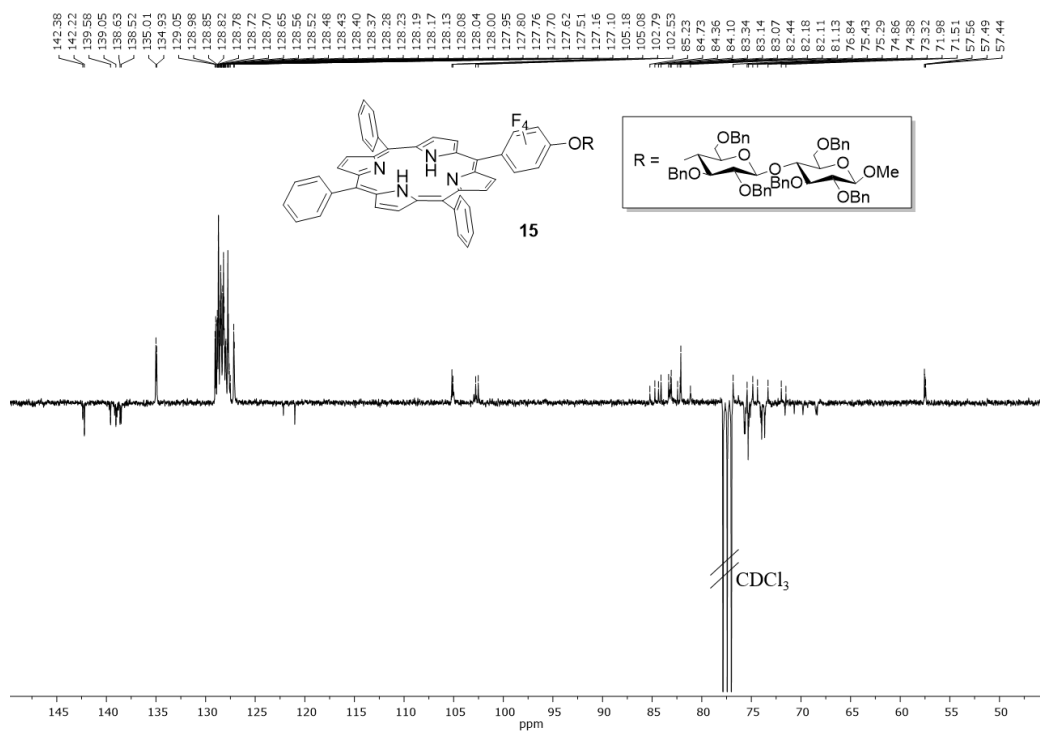


The general catalytic procedure for the synthesis of aziridines was followed using α -methylstyrene and 4-methoxyphenylazide (10% yield). The collected data are in accordance with those reported in literature²².

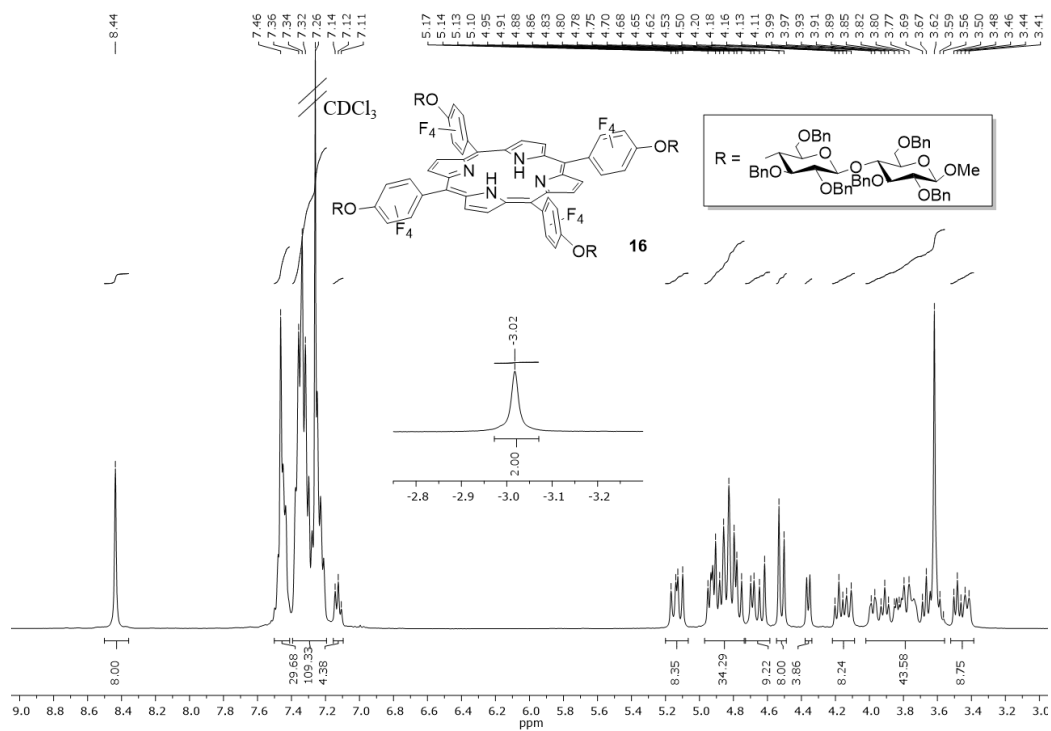
¹H NMR (300 MHz, CDCl₃): δ 7.51 (d, 2H, $J=6.5$ Hz, H_{Ar}), 7.34 (pst, 2H, $J=6.5$ Hz, H_{Ar}), 7.28 (t, 1H, $J=6.5$ Hz, H_{Ar}), 6.88 (d, 2H, $J=8.8$ Hz, H_{Ar}), 6.82 (d, 2H, $J=8.8$ Hz, H_{Ar}), 3.79 (s, 3H, HOCH₃), 2.46 (s, 1H, H_{CH2}), 2.24 (s, 1H, H_{CH2}), 1.34 (s, 3H, H_{CH3}).

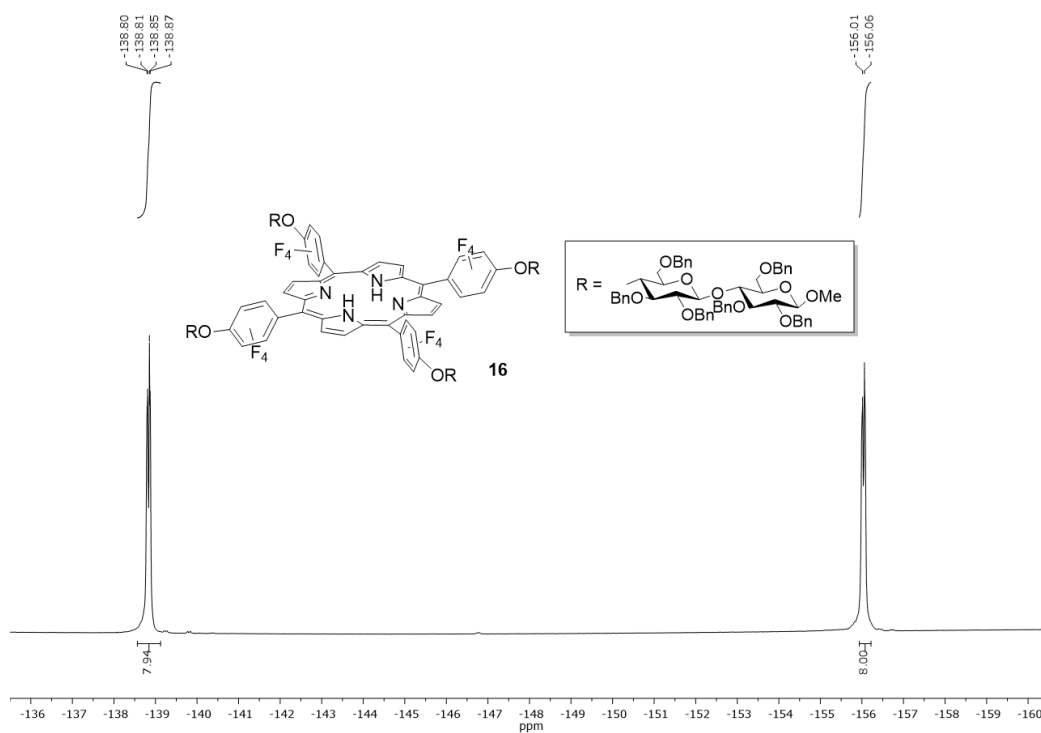
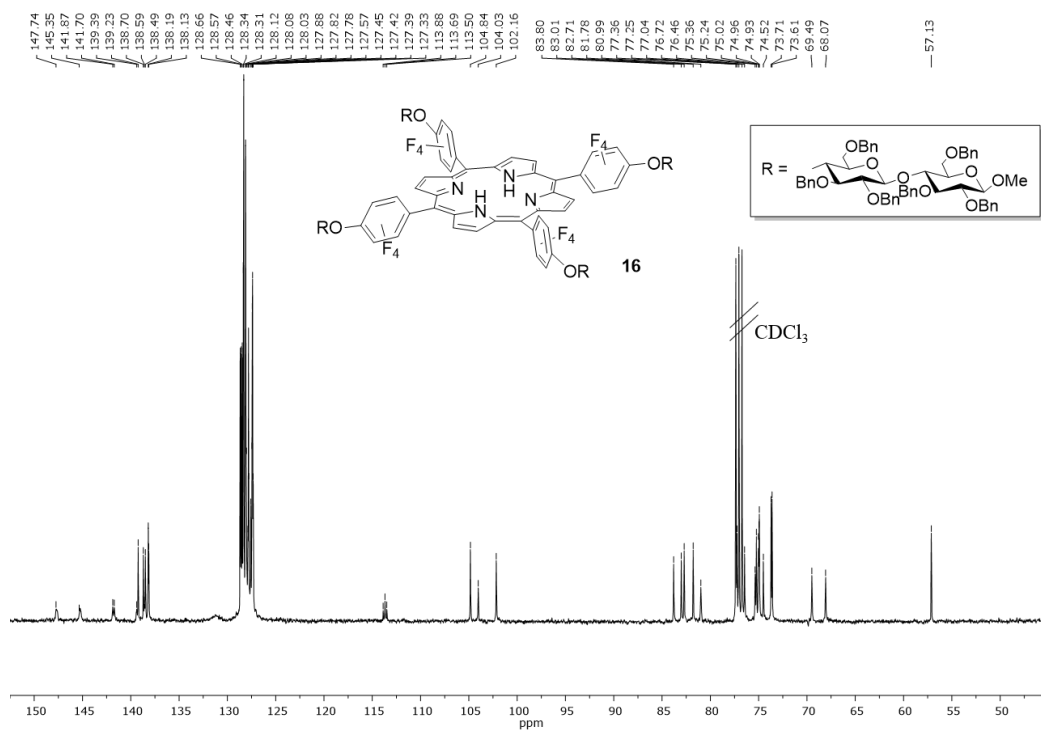
4.7. ^1H -NMR, ^{19}F -NMR and ^{13}C -NMR of isolated compounds ^1H NMR spectrum (400 MHz, CDCl_3 , 298 K) of porphyrin 15 ^{19}F NMR spectrum (376 MHz, CDCl_3 , 298 K) of porphyrin 15

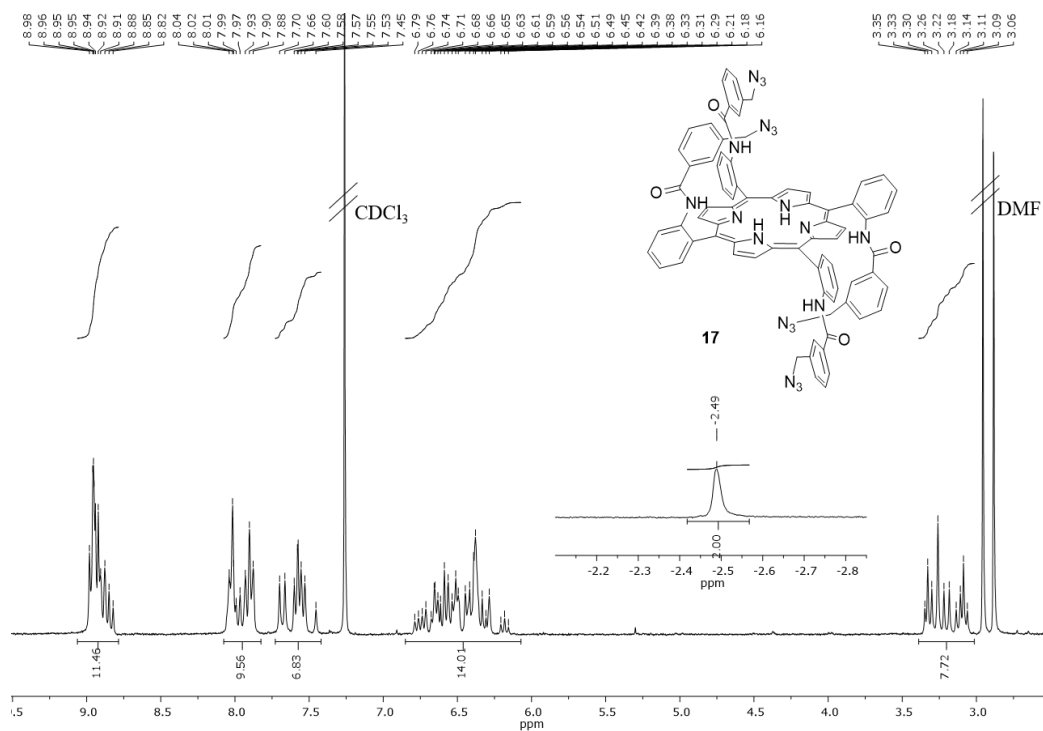
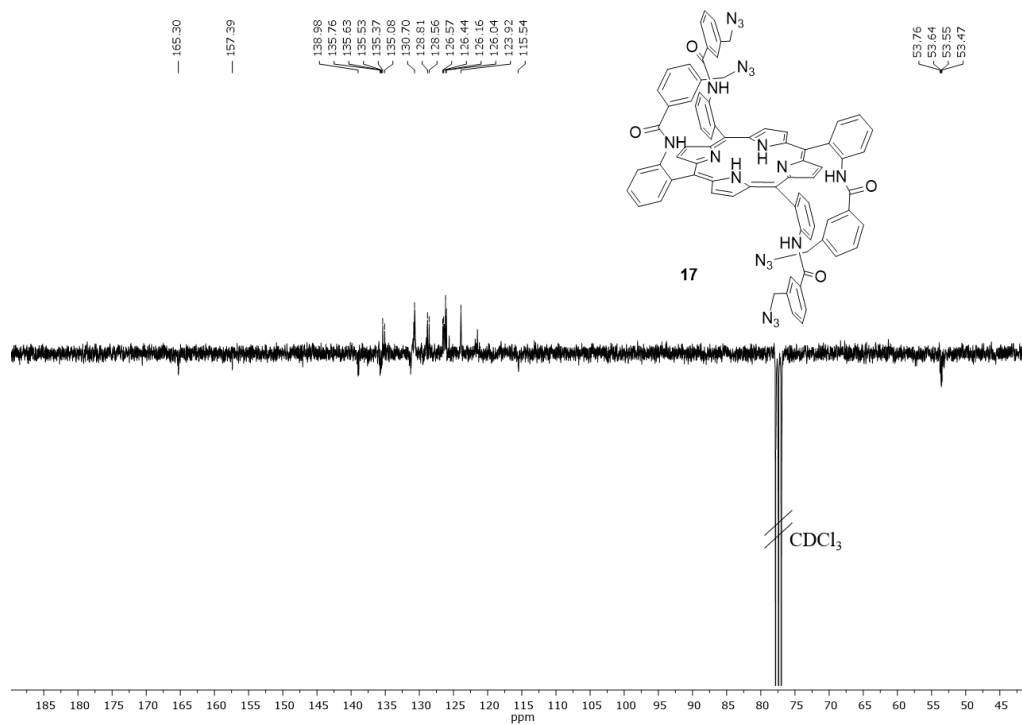
^{13}C NMR spectrum (100 MHz, CDCl_3 , 298 K) of porphyrin 15

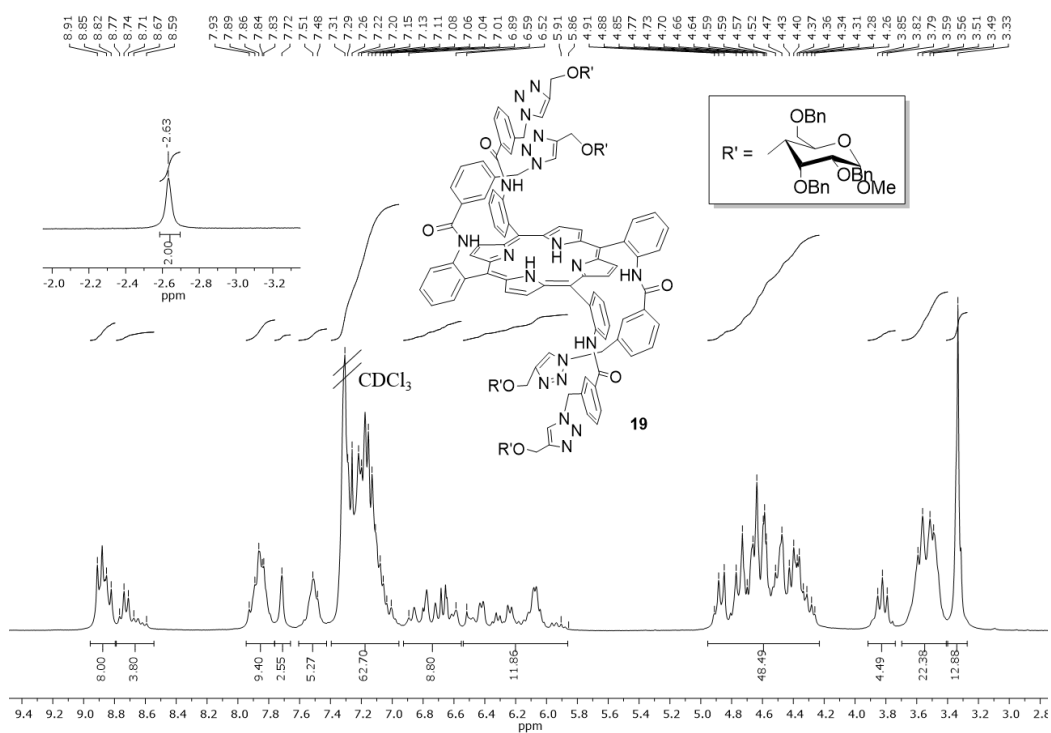
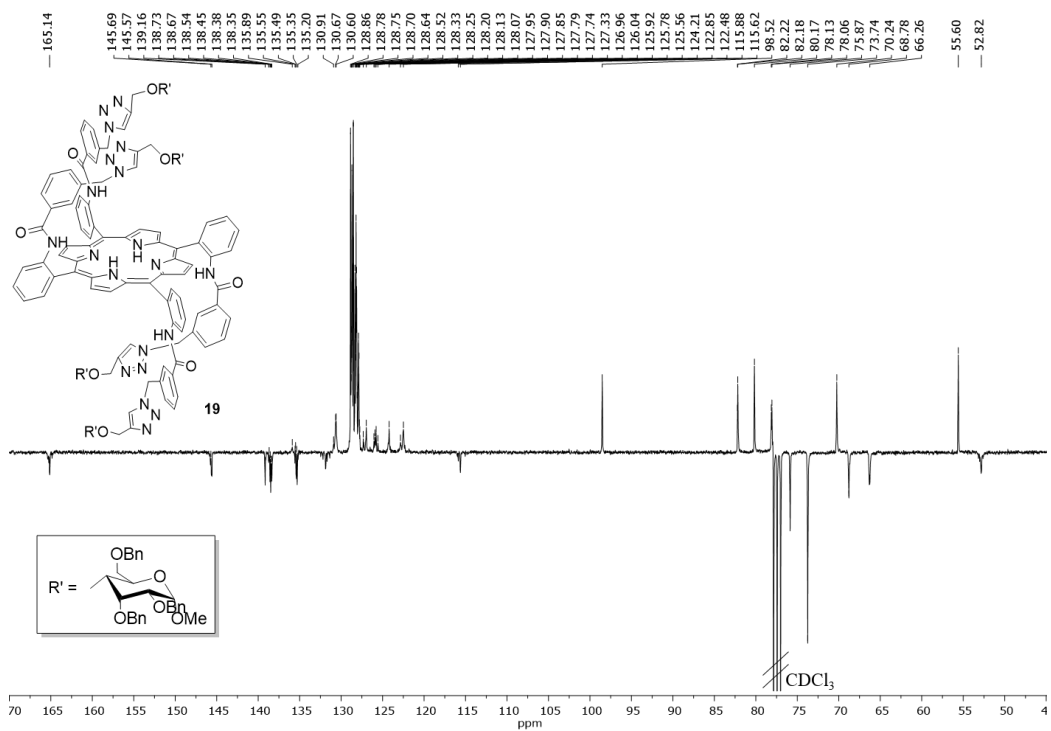


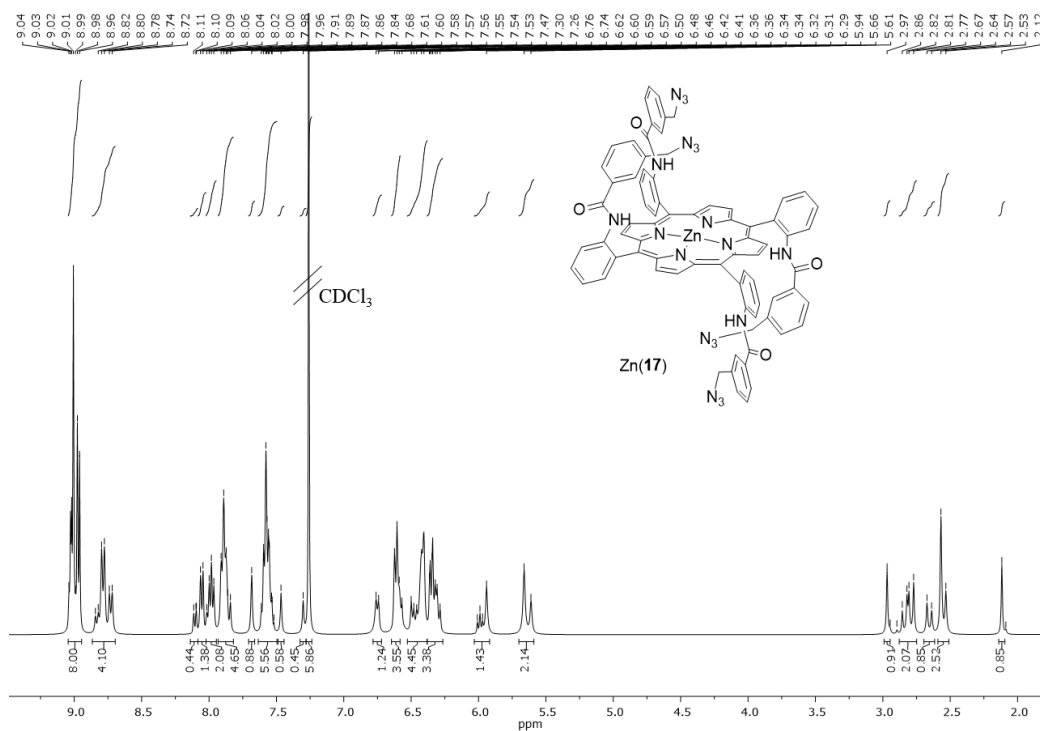
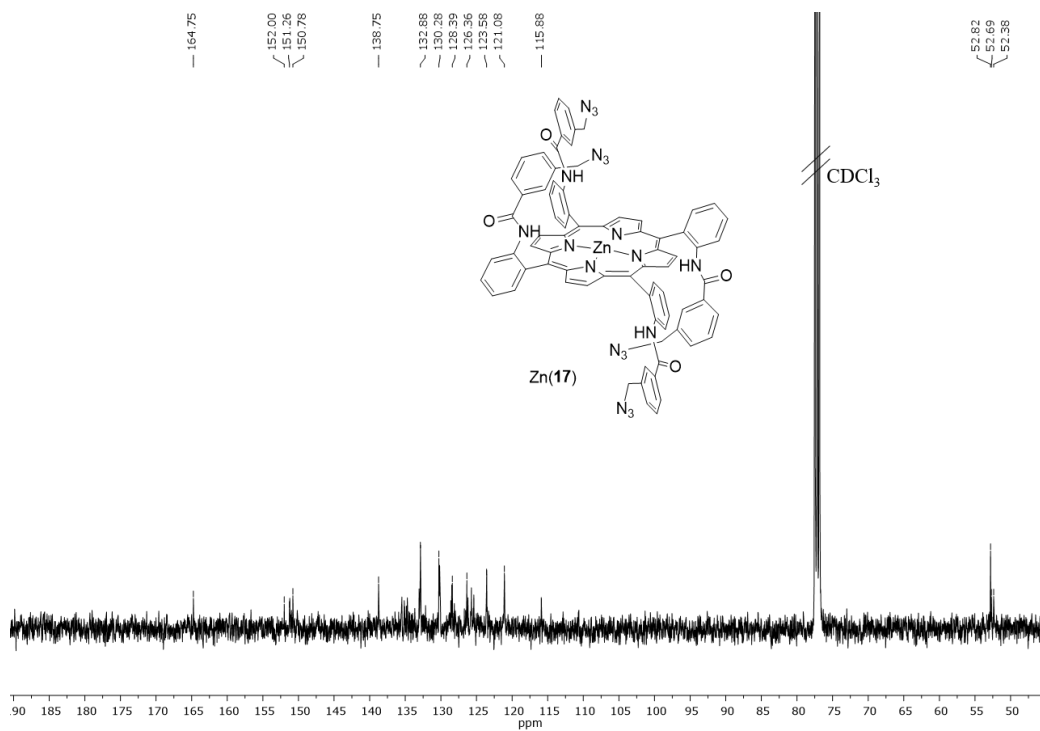
^1H NMR spectrum (400 MHz, CDCl_3 , 298 K) of porphyrin 16

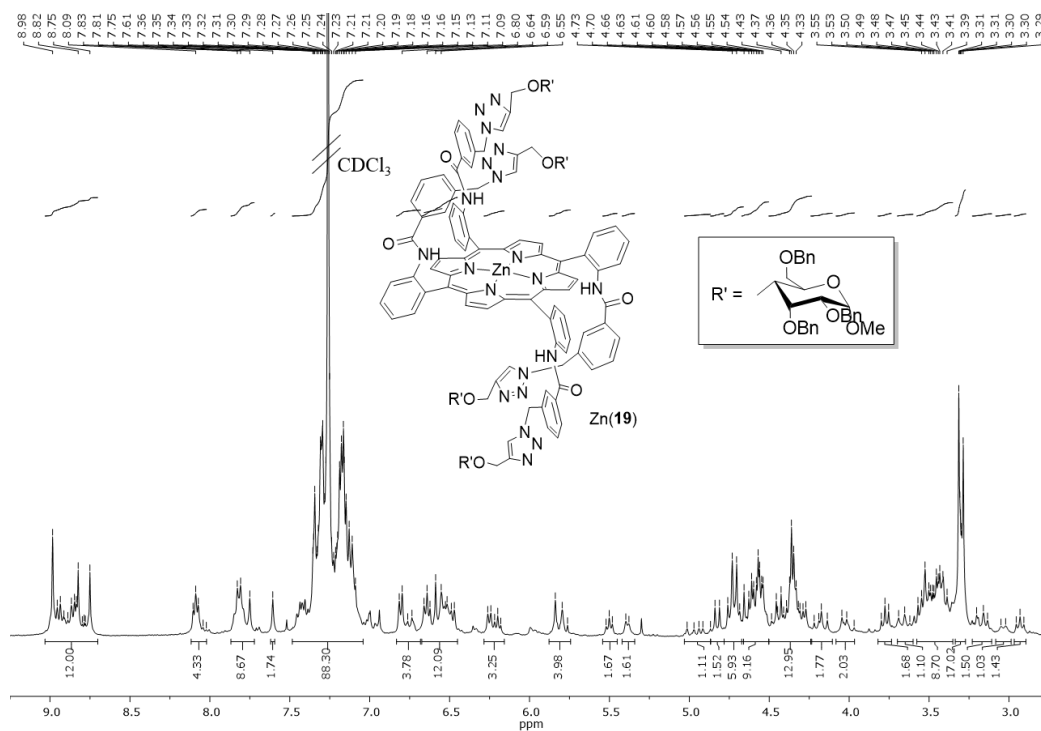
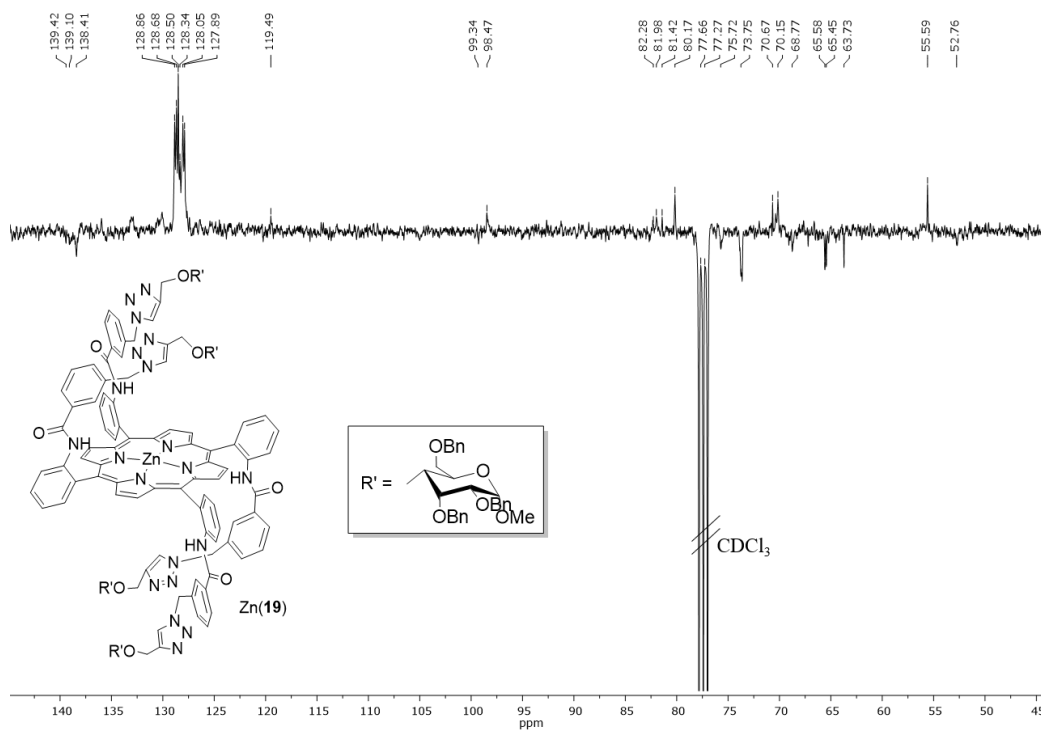


^{19}F NMR spectrum (376 MHz, CDCl_3 , 298 K) of porphyrin 16 **^{13}C NMR spectrum (100 MHz, CDCl_3 , 298 K) of porphyrin 16**

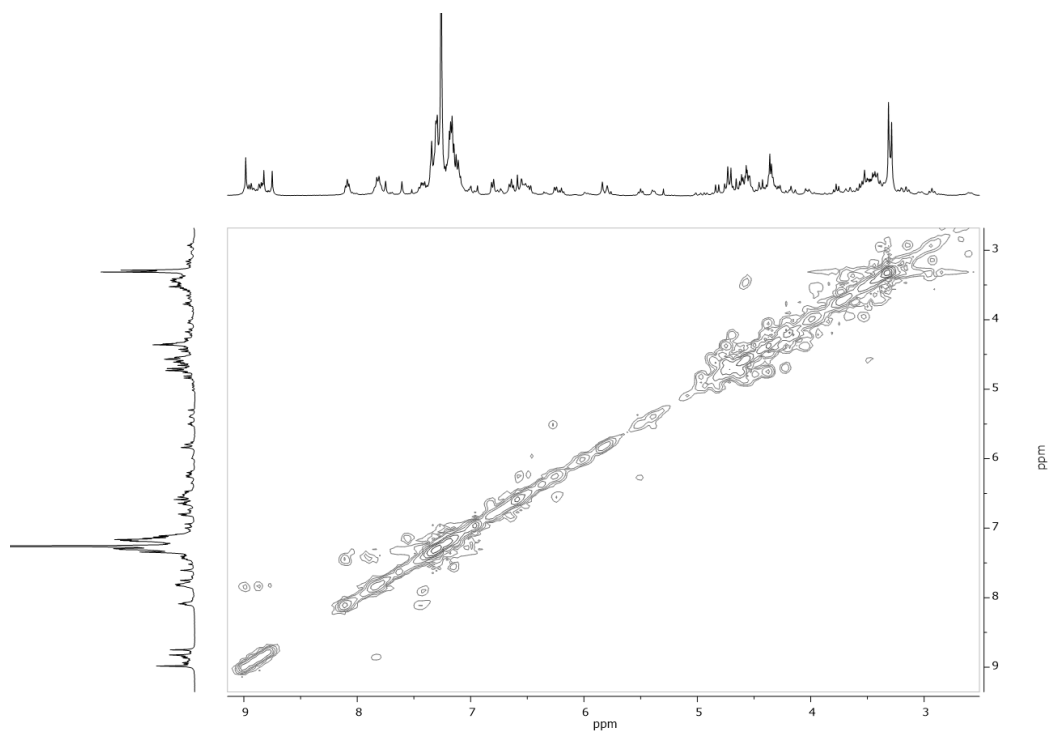
^1H NMR spectrum (400 MHz, CDCl_3 , 298 K) of porphyrin 17 **^{13}C NMR spectrum (100 MHz, CDCl_3 , 298 K) of porphyrin 17**

¹H NMR spectrum (400 MHz, CDCl₃, 298 K) of porphyrin 19**¹³C NMR spectrum (100 MHz, CDCl₃, 298 K) of porphyrin 19**

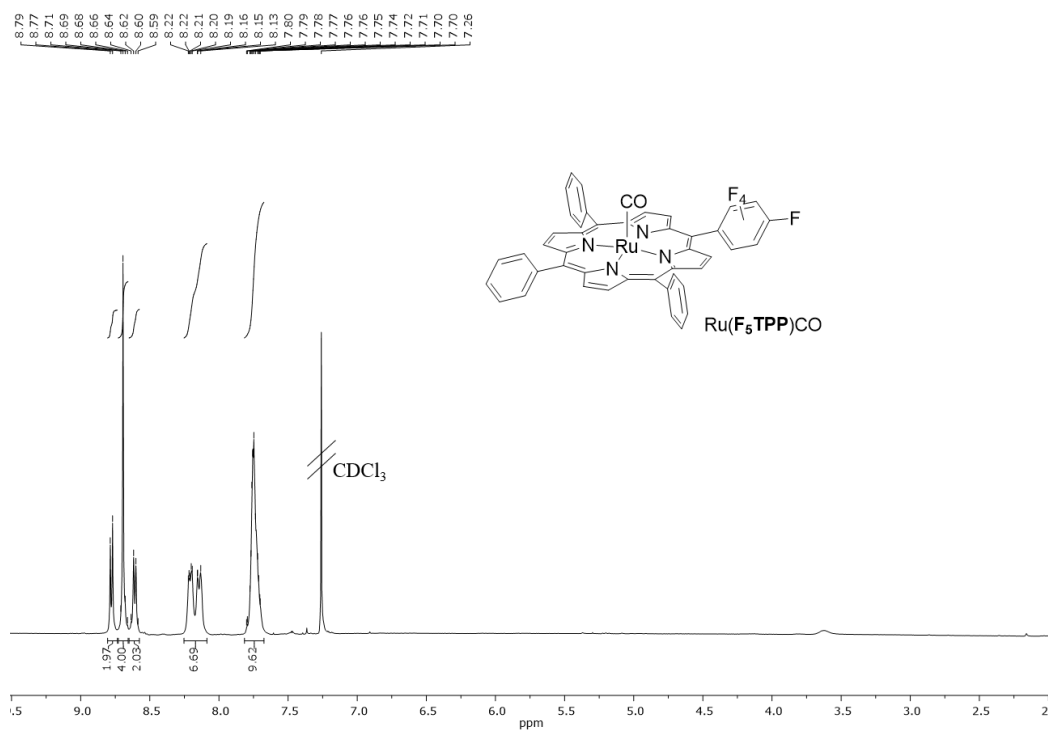
^1H NMR spectrum (400 MHz, CDCl_3 , 298 K) of Zn(17) ^{13}C NMR spectrum (100 MHz, CDCl_3 , 298 K) of Zn(17)

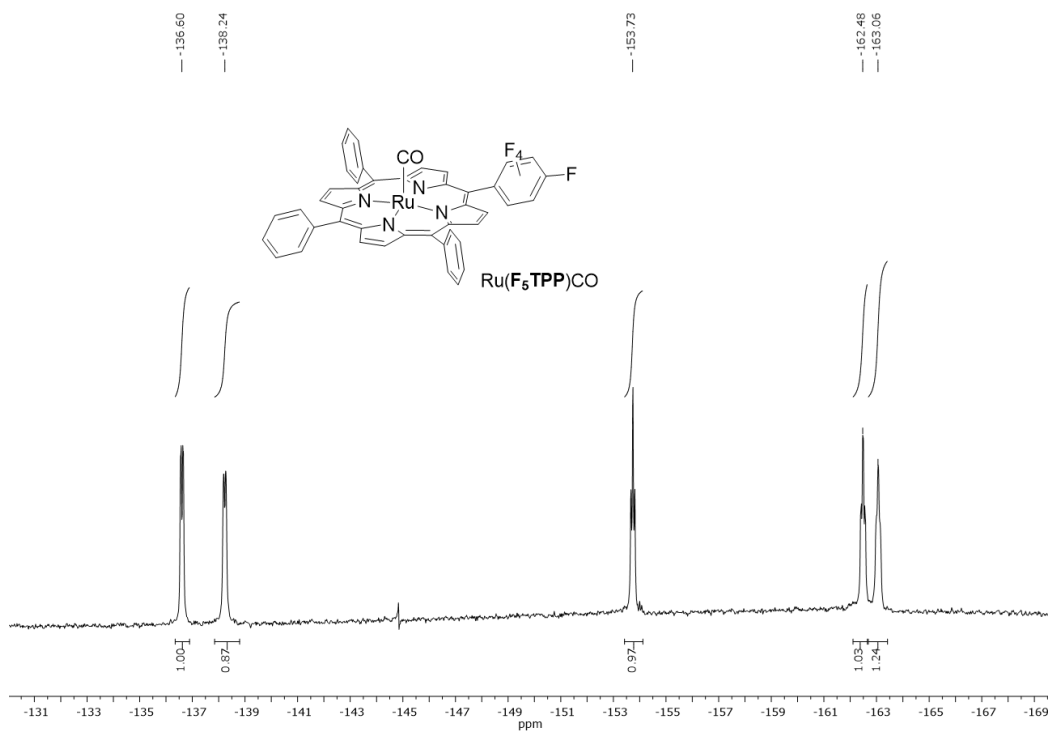
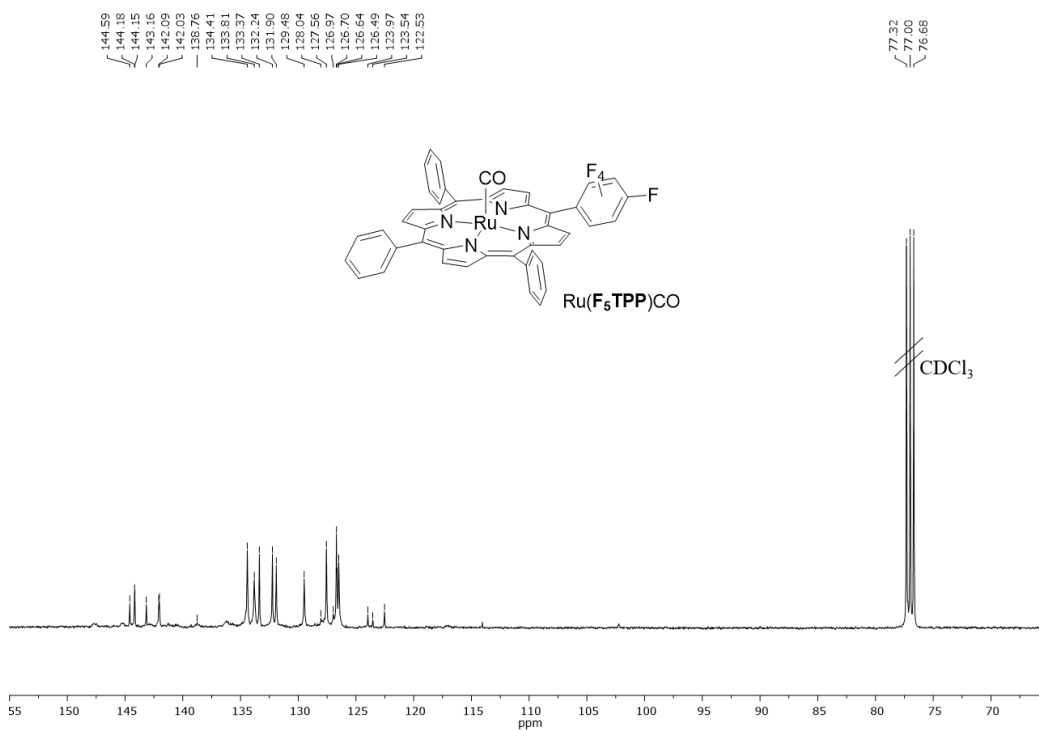
¹H NMR spectrum (400 MHz, CDCl₃, 298 K) of Zn(19)**¹³C NMR spectrum (100 MHz, CDCl₃, 298 K) of Zn(19)**

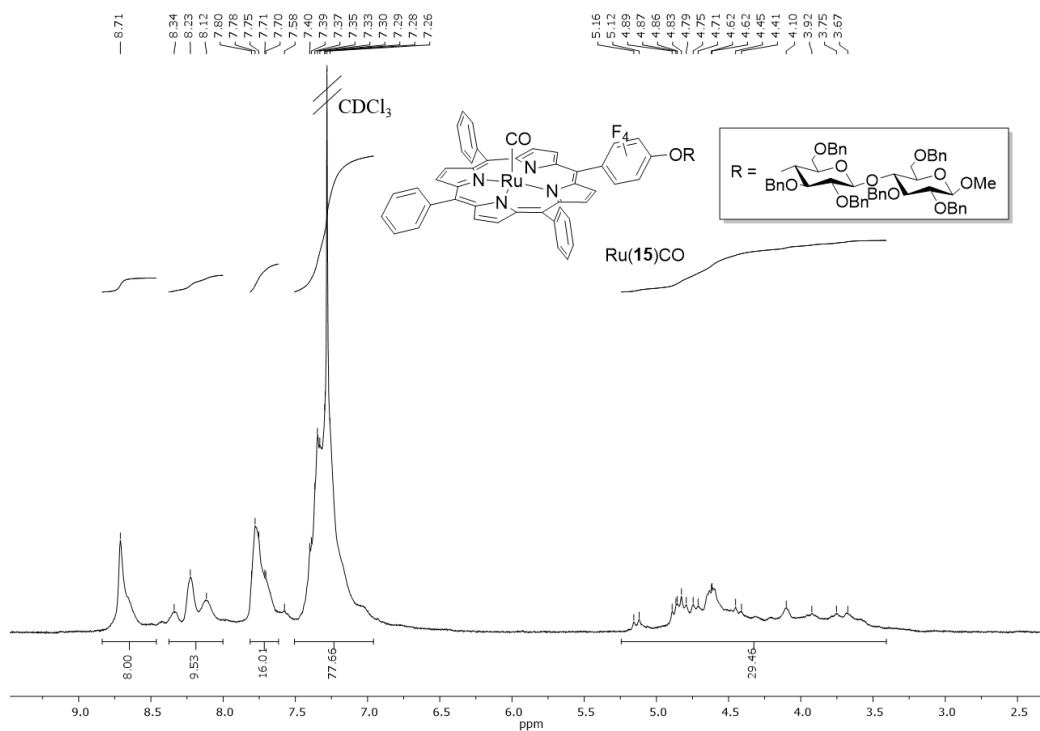
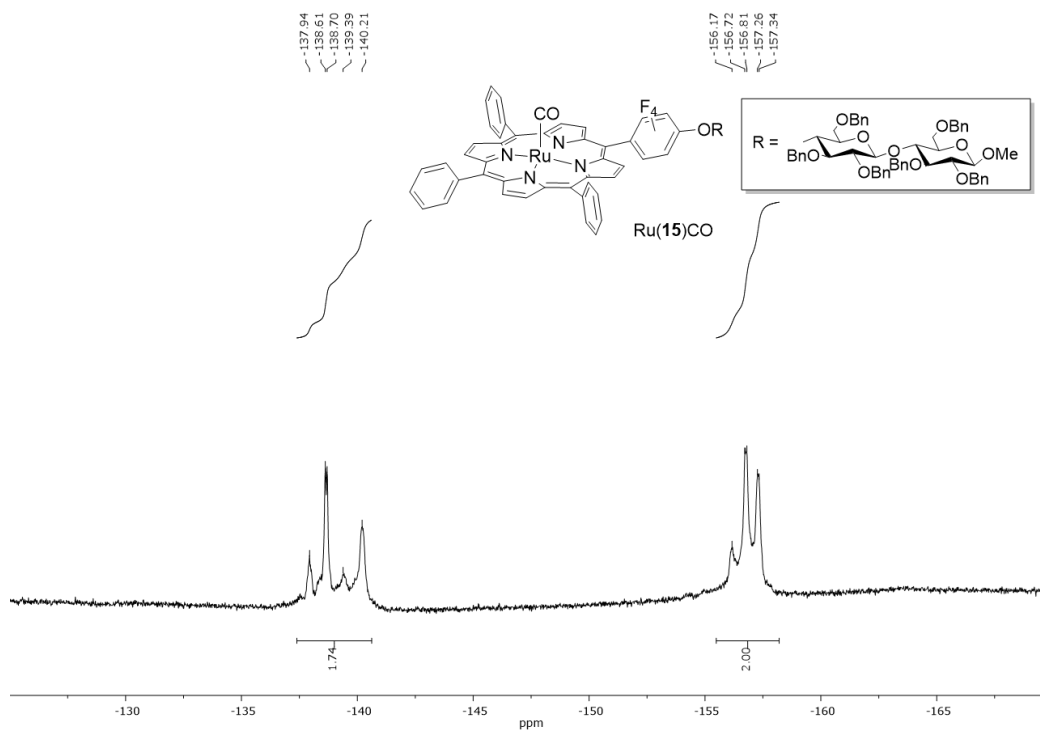
COSY 2D NMR spectrum (400 MHz, CDCl₃, 298 K) of Zn(19)

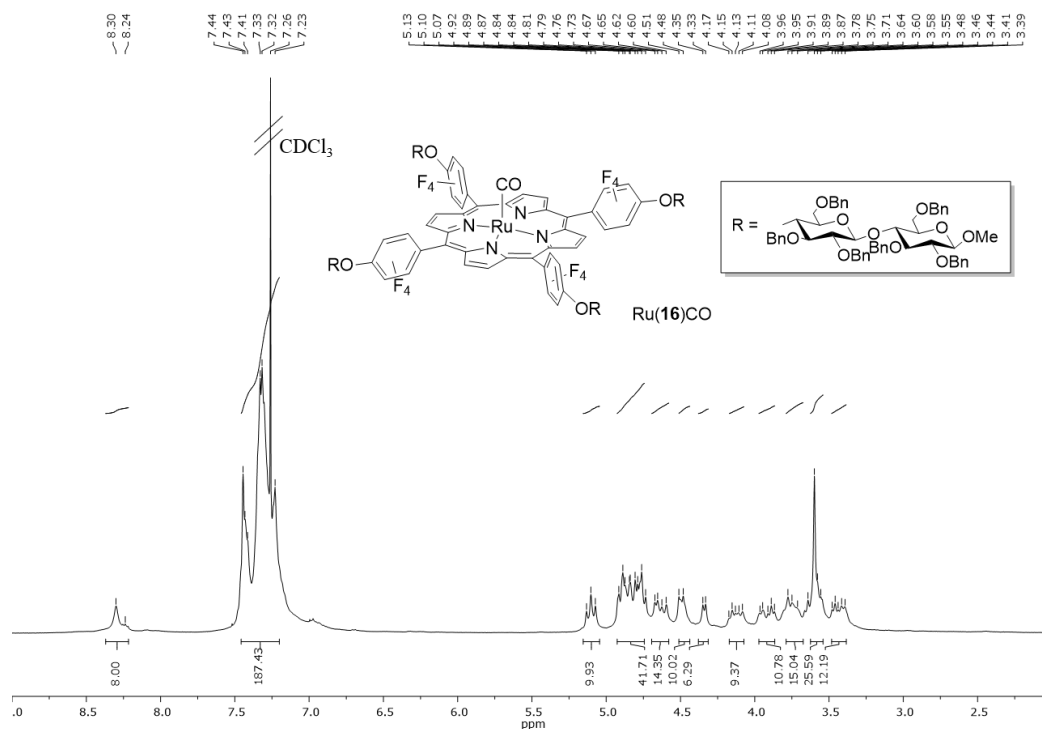
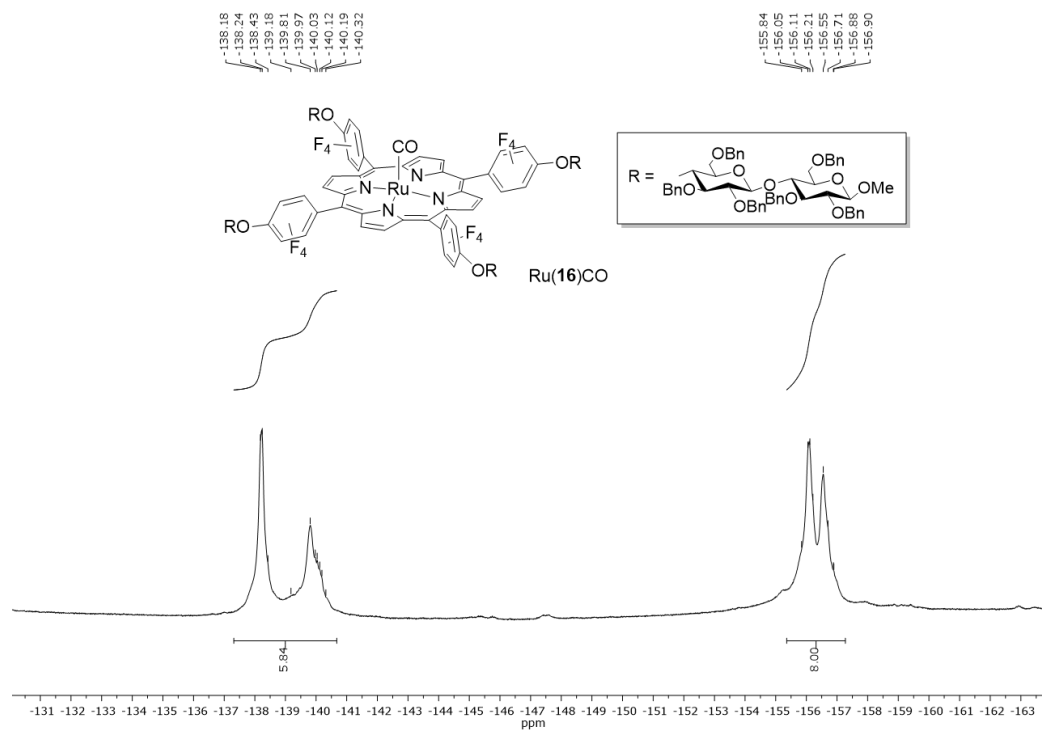


¹H NMR spectrum (300 MHz, CDCl₃, 298 K) of Ru(F₅TTP)CO

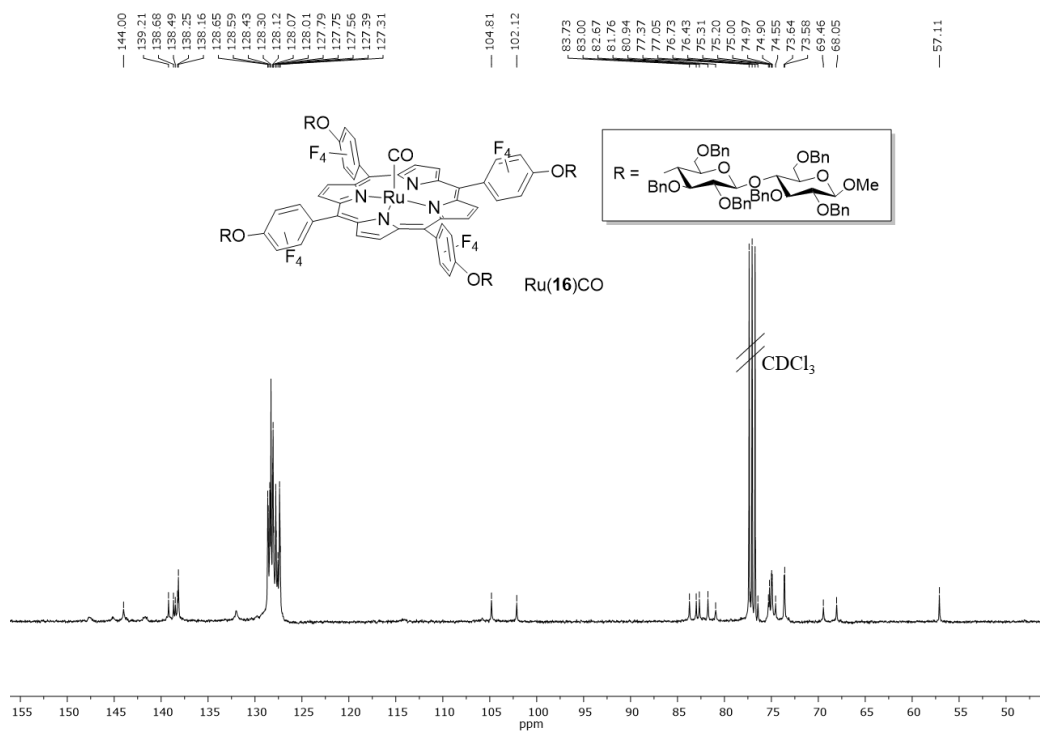


^{19}F NMR spectrum (282 MHz, CDCl_3 , 298 K) of $\text{Ru}(\text{F}_5\text{TPP})\text{CO}$  ^{13}C NMR spectrum (75 MHz, CDCl_3 , 298 K) of $\text{Ru}(\text{F}_5\text{TPP})\text{CO}$ 

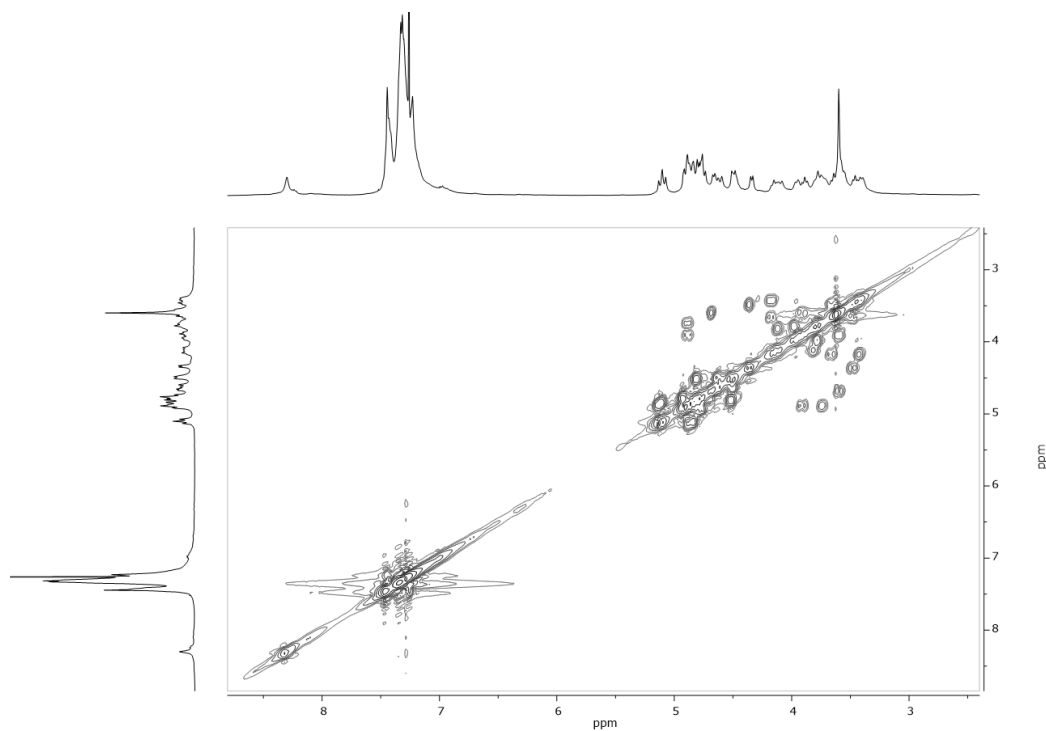
^1H NMR spectrum (300 MHz, CDCl_3 , 298 K) of Ru(15)CO ^{19}F NMR spectrum (282 MHz, CDCl_3 , 298 K) of Ru(15)CO

^1H NMR spectrum (400 MHz, CDCl_3 , 298 K) of Ru(16)CO ^{19}F NMR spectrum (376 MHz, CDCl_3 , 298 K) of Ru(16)CO

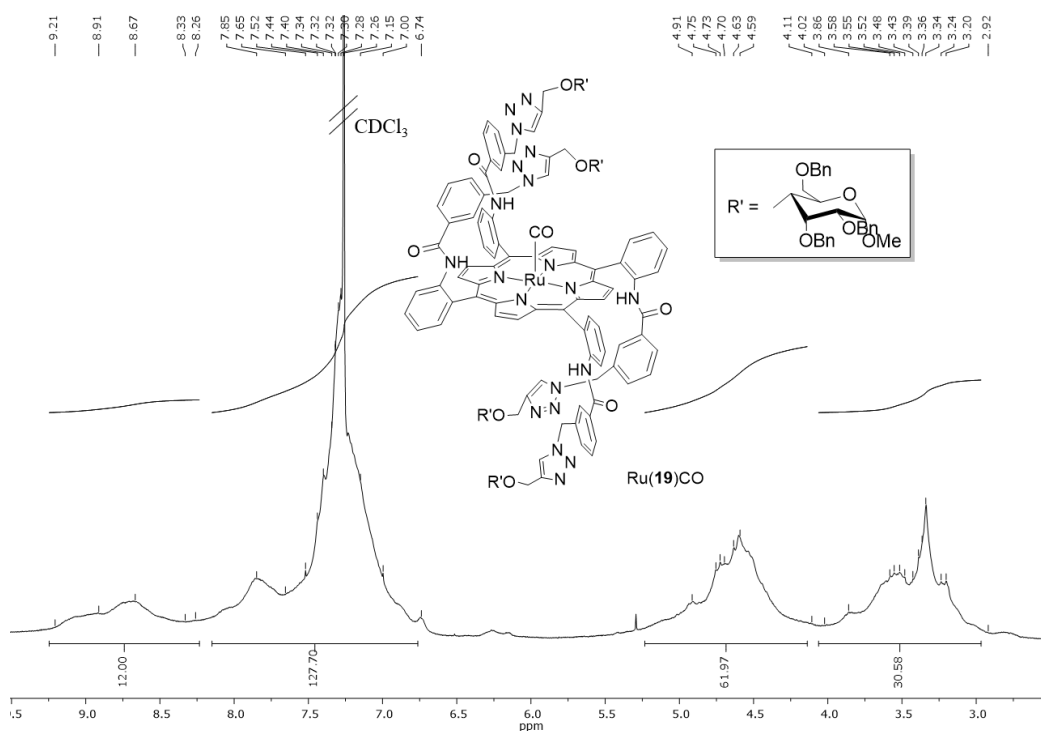
^{13}C NMR spectrum (100 MHz, CDCl_3 , 298 K) of Ru(16)CO



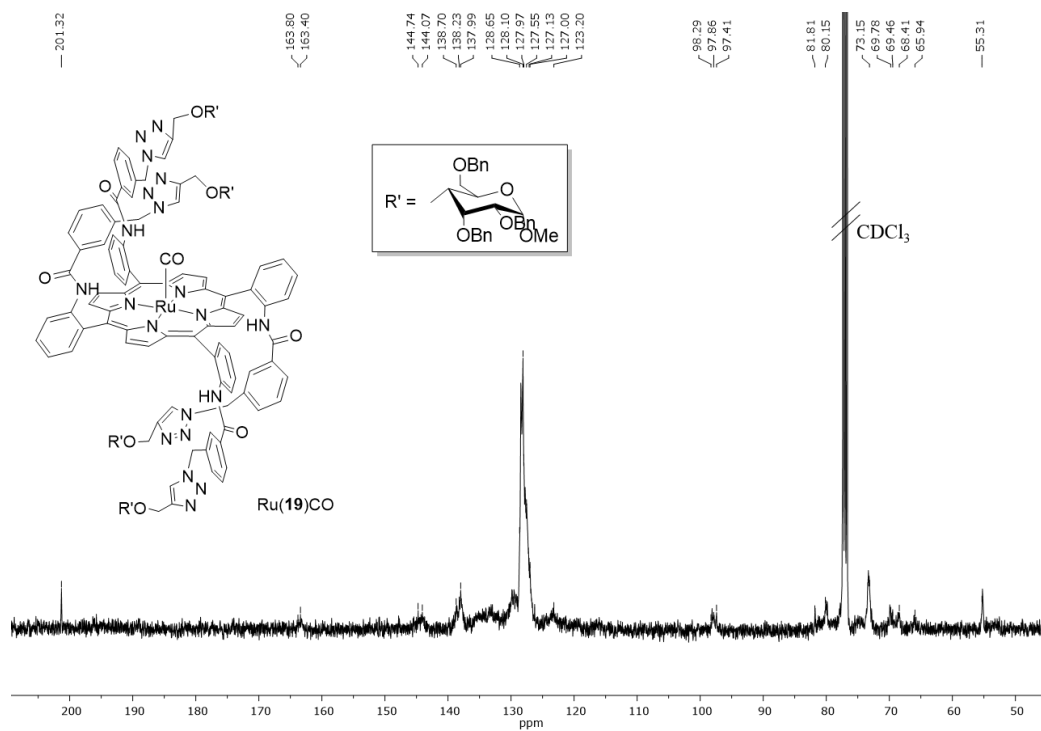
COSY 2D NMR spectrum (300 MHz, CDCl_3 , 298 K) of Ru(16)CO

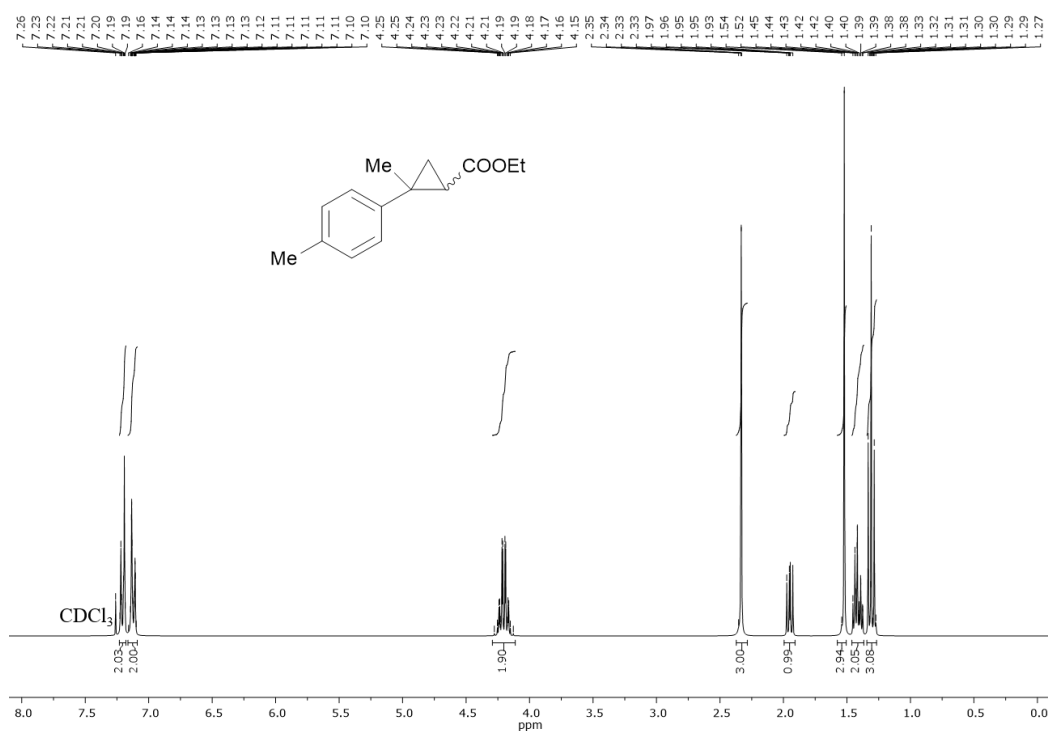
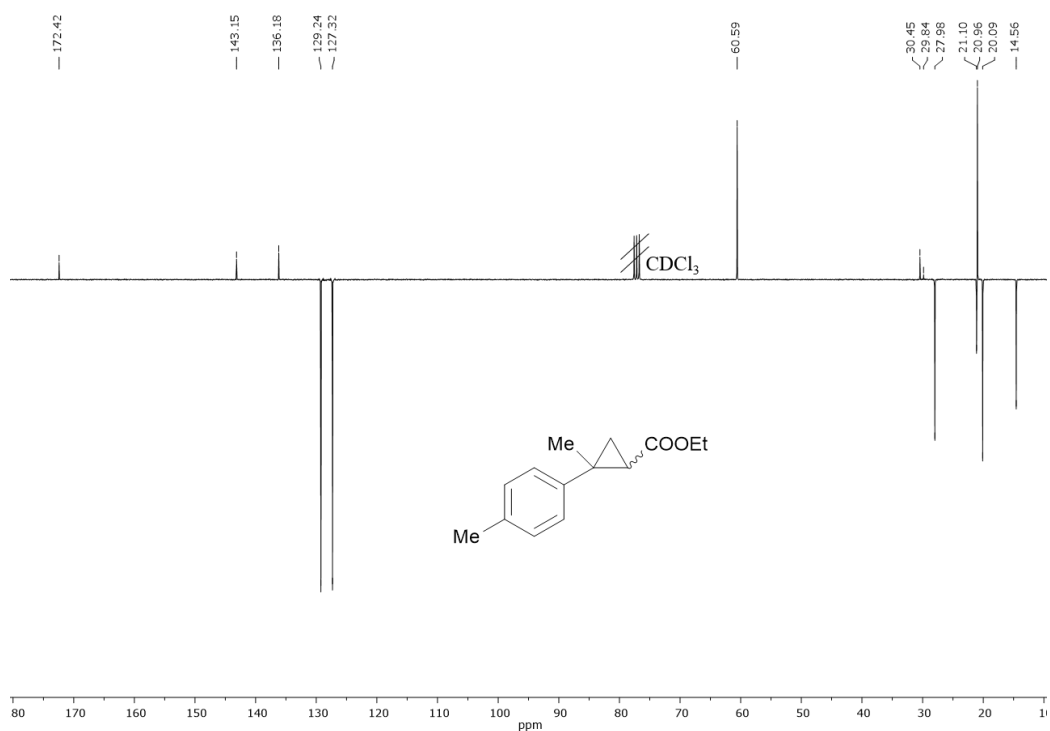


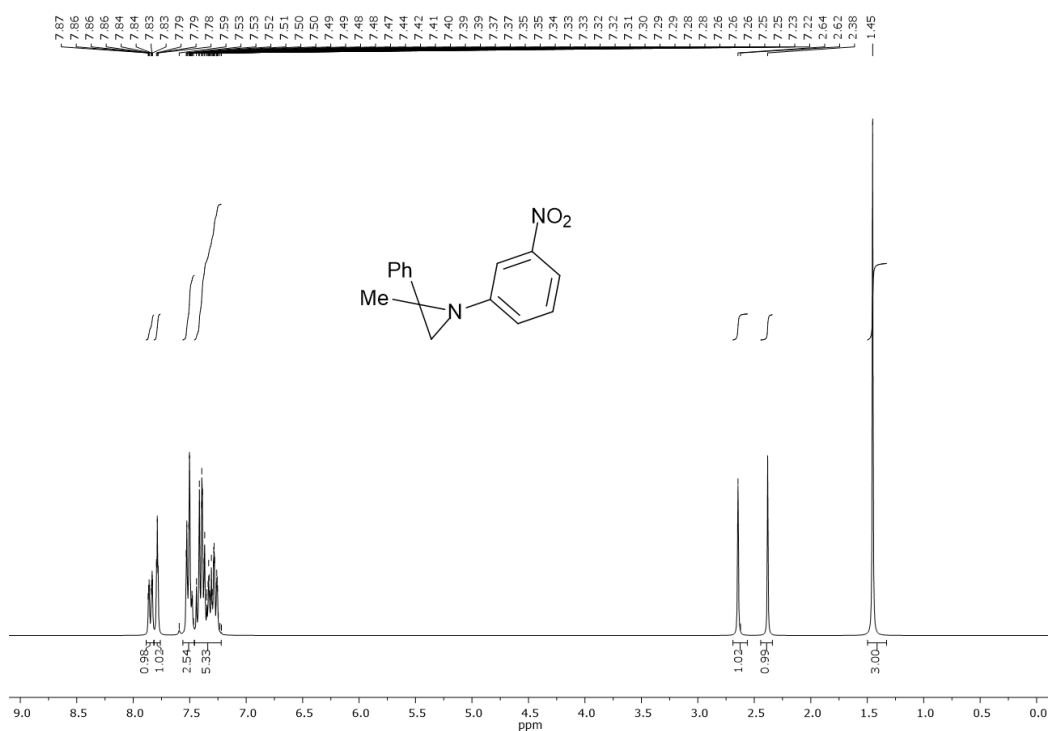
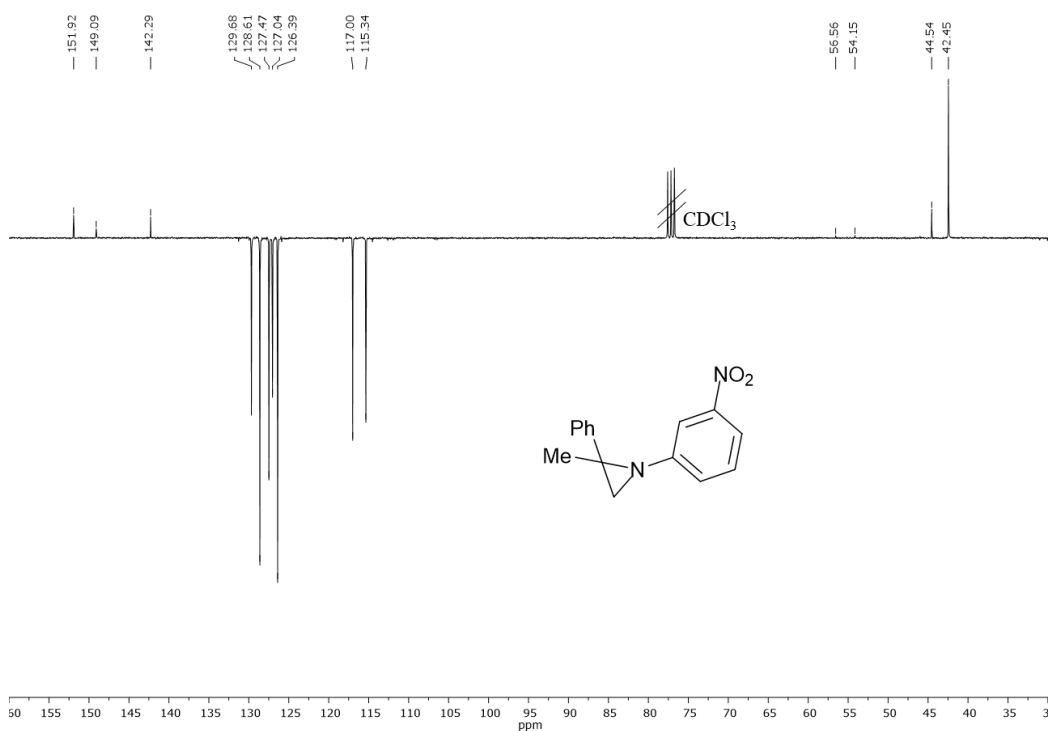
^1H NMR spectrum (400 MHz, CDCl_3 , 298 K) of Ru(19)CO



^{13}C NMR spectrum (100 MHz, CDCl_3 , 298 K) of Ru(19)CO



^1H NMR spectrum (300 MHz, CDCl_3 , 298 K) of *trans* ethyl-2-methyl-(4-methylphenyl) cyclopropane carboxylate (26) **^{13}C NMR spectrum (75 MHz, CDCl_3 , 298 K) of *trans* ethyl-2-methyl-(4-methylphenyl) cyclopropane carboxylate (26)**

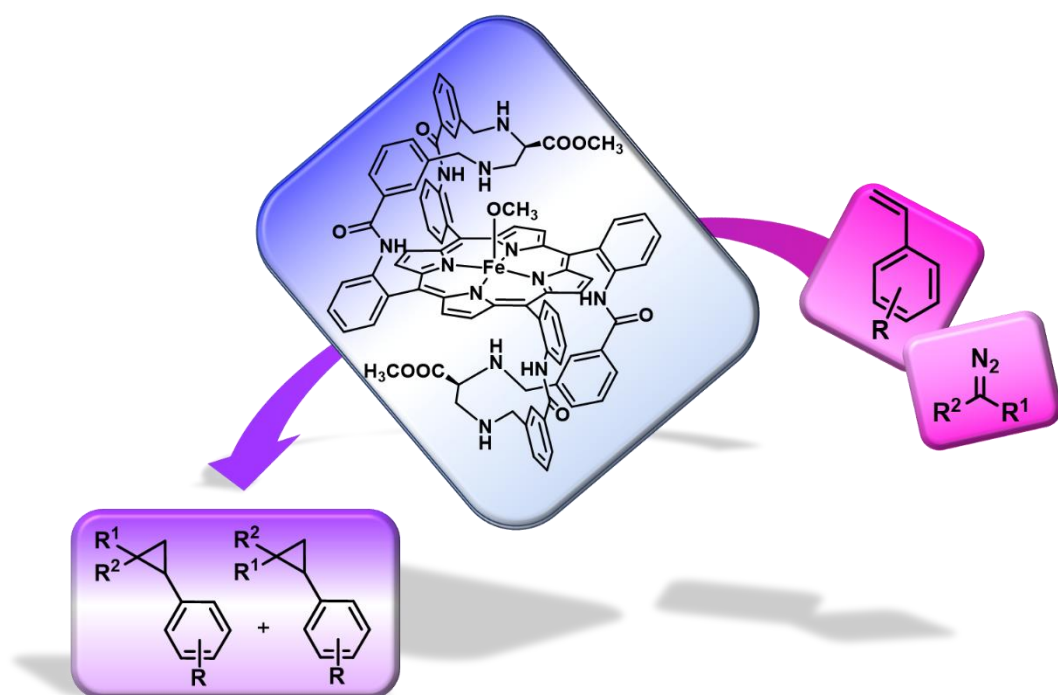
¹H NMR spectrum (300 MHz, CDCl₃, 298 K) of 2-methyl-1-(3-nitrophenyl)-2-phenylaziridine (34)**¹³C NMR spectrum (75 MHz, CDCl₃, 298 K) of 2-methyl-1-(3-nitrophenyl)-2-phenylaziridine (34)**

5. References

- (1) Linhardt, R. J.; Bazin, H. G. Fraser-Reid, B. O., Tatsuta, K., Thiem, J., Eds.; Springer Berlin Heidelberg: Berlin, Heidelberg, **2001**, 53–61.
- (2) Nikitjuka, A.; Jirgensons, A. *Chem. Heterocycl. Compd.* **2014**, *49* (11), 1544–1559.
- (3) Ethirajan, M.; Chen, Y.; Joshi, P.; Pandey, R. K. *Chem. Soc. Rev.* **2011**, *40* (1), 340–362.
- (4) Garcia, G.; Hammerer, F.; Poyer, F.; Achelle, S.; Teulade-Fichou, M.-P.; Maillard, P. *Bioorg. Med. Chem.* **2013**, *21* (1), 153–165.
- (5) Singh, S.; Aggarwal, A.; Bhupathiraju, N. V. S. D. K.; Arianna, G.; Tiwari, K.; Drain, C. M. *Chem. Rev.* **2015**, *115* (18), 10261–10306.
- (6) Achelle, S.; Couleaud, P.; Baldeck, P.; Teulade-Fichou, M. P.; Maillard, P. *European J. Org. Chem.* **2011**, *7*, 1271–1279.
- (7) Singh, S.; Aggarwal, A.; Bhupathiraju, N. V. S. D. K.; Arianna, G.; Tiwari, K.; Drain, C. M. *Chem. Rev.* **2015**, *115* (18), 10261–10306.
- (8) Lupu, M.; Maillard, P.; Mispelster, J.; Poyer, F.; Thomas, C. D. *Photochem. Photobiol. Sci.* **2018**, *17* (11), 1599–1611.
- (9) Diéguez, M.; Pàmies, O.; Claver, C. *Chem. Rev.* **2004**, *104* (6), 3189–3216.
- (10) Henderson, A. S.; Bower, J. F.; Galan, M. C. *Org. Biomol. Chem.* **2016**, *14* (17), 4008–4017.
- (11) Vilain-Deshayes, S.; Robert, A.; Maillard, P.; Meunier, B.; Momenteau, M. *J. Mol. Catal. A Chem.* **1996**, *113* (1), 23–34.
- (12) Vilain-Deshayes, S.; Maillard, P.; Momenteau, M. *J. Mol. Catal. A Chem.* **1996**, *113* (1), 201–208.
- (13) Zhang, X.-B.; Guo, C.-C.; Xu, J.-B.; Yu, R.-Q. *J. Mol. Catal. A Chem.* **2000**, *154* (1), 31–38.
- (14) Ho, C. M.; Zhang, J. L.; Zhou, C. Y.; Chan, O. Y.; Yan, J. J.; Zhang, F. Y.; Huang, J. S.; Che, C. M. *J. Am. Chem. Soc.* **2010**, *132* (6), 1886–1894.
- (15) Tseberlidis, G.; Zardi, P.; Caselli, A.; Cancogni, D.; Fusari, M.; Lay, L.; Gallo, E. *Organometallics* **2015**, *34* (15), 3774–3781.
- (16) Mackie, I. D.; Röhring, J.; Gould, R. O.; Pauli, J.; Jäger, C.; Walkinshaw, M.; Potthast, A.; Rosenau, T.; Kosma, P. *Carbohydr. Res.* **2002**, *337* (2), 161–166.
- (17) Auras, B. L.; De Lucca Meller, S.; da Silva, M. P.; Neves, A.; Cocca, L. H. Z.; De Boni, L.; da Silveira, C. H.; Iglesias, B. A. *Appl. Organomet. Chem.* **2018**, *32* (5), e4318.
- (18) Lindsey, J. S.; Wagner, R. W. *J. Org. Chem.* **1989**, *54* (4), 828–836.
- (19) Didier, A.; Michaudet, L.; Ricard, D.; Baveux-Chambenoît, V.; Richard, P.; Boitrel, B. *European J. Org. Chem.* **2001**, *2001* (10), 1926–1927.
- (20) Mereyala, H. B.; Gurralla, S. R.; Mohan, S. K. *Tetrahedron* **1999**, *55* (37), 11331–11342.
- (21) Collman, J. P.; Gagne, R. R.; Reed, C.; Halbert, T. R.; Lang, G.; Robinson, W. T. *J. Am. Chem. Soc.* **1975**, *97* (6), 1427–1439.
- (22) Fantauzzi, S.; Gallo, E.; Caselli, A.; Piangiolino, C.; Ragaini, F.; Cenini, S. *European J. Org. Chem.* **2007**, *2007* (36), 6053–6059.
- (23) Zhang, Y.; Li, J.; Yang, X.; Zhang, P.; Pang, J.; Li, B.; Zhou, H.-C. *Chem. Commun.* **2019**, *55* (14), 2023–2026.
- (24) Davies, H. M. L.; Hansen, T.; Churchill, M. R. *J. Am. Chem. Soc.* **2000**, *122* (13), 3063–3070.
- (25) Pinho e Melo, T. M. V. D. *Organic Azides*. November 20, **2009**, 53–94.

- (26) Kumar, S.; Pathania, A. S.; Satti, N. K.; Dutt, P.; Sharma, N.; Mallik, F. A.; Ali, A. *Eur. J. Med. Chem.* **2015**, *92*, 236–245.
- (27) Chen, Y.; Zhang, X. P. *J. Org. Chem.* **2004**, *69* (7), 2431–2435.
- (28) Sreenilayam, G.; Moore, E. J.; Steck, V.; Fasan, R. *ACS Catal.* **2017**, *7* (11), 7629–7633.
- (29) Castano, B.; Gallo, E.; Cole-Hamilton, D. J.; Dal Santo, V.; Psaro, R.; Caselli, A. *Green Chem.* **2014**, *16* (6), 3202–3209.
- (30) Fantauzzi, S.; Gallo, E.; Rose, E.; Raoul, N.; Caselli, A.; Issa, S.; Ragaini, F.; Cenini, S. *Organometallics* **2008**, *27* (23), 6143–6151.
- (31) Chen, Y.; Zhang, X. P. *J. Org. Chem.* **2007**, *72* (15), 5931–5934.

Chapter III: Hybrid *bis*-strapped porphyrin



1. Introduction

The synergic effect of biomolecules and organometallic complexes emerged as a prominent tool for the development of new efficient hybrid systems for different applications in medical and material science. Therefore, it is not surprising that during the last 20 years a big number of porphyrin-aminoacid/peptide conjugates have been synthesised and studied as models of metalloenzymes and heme-proteins¹⁻⁵. Great attention has been devoted on these hybrid systems due to their possible use as regio- and enantioselective catalysts. In this context, several chiral porphyrins showing complex and sophisticated structures were developed to reproduce the enzyme functions and their chiral properties. Nevertheless, the main challenge for chemists is the production of efficient and chiral catalysts in an easy, efficient and economical way. For these reasons the research community focused the attention on the introduction of small chiral moieties onto the porphyrin ring in order to mimic the enzyme activities and selectivities.

1.1. Single and double-face porphyrins

The most common way to obtain enzyme-type porphyrin ligands involves the attachment of chiral moieties onto the *meso*-tetra(2-substituted)phenyl porphyrin, which shows four different isomers^{6,7}. The four so-called atropoisomers (α_4 , $\alpha_3\beta$, $\alpha_2\beta_2$, $\alpha\beta$) have different configurations according to the orientation of the *ortho*-substituents (Figure 1). In most cases, each side of the porphyrin ring must be selectively derivatized to exhibit different functionalities.

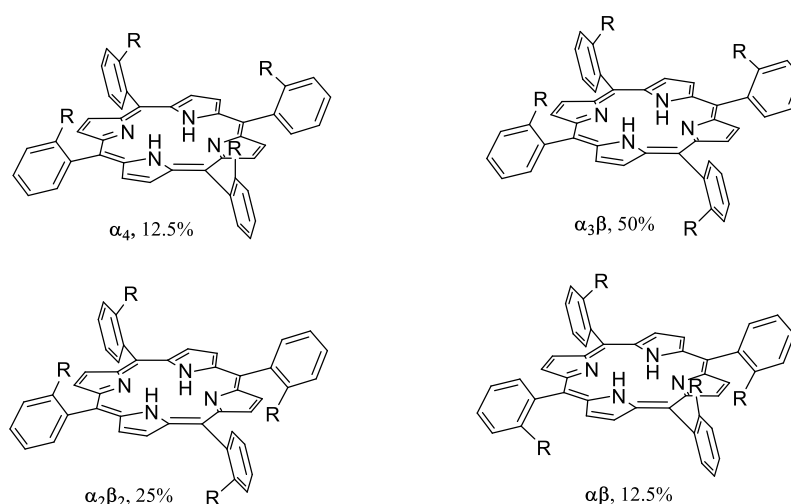


Figure 1: Statistically distribution of the four atropoisomers of *meso*-tetra(2-substituted)phenyl porphyrin

The selective functionalization of the porphyrin atropoisomers can afford different types of ligands. The modification of the α_4 atropoisomer, which shows all the *ortho* substituents above the porphyrins plane, gives the so-called ‘single-face’ porphyrins. The “picket fence”⁸ and “picnic basket”⁹ porphyrins are the

first two examples reported for these kind of single-face ligands (Figure 2). Both porphyrins derive from the same atropoisomer (α_4) but they show different structures and reactivities. The “picket fence” porphyrins have an open structure which work as counterpart of natural systems in the oxo transfer reactions due to its capacity to reduce the formation of the inactive μ -oxo dimer⁸. The “picnic basket” porphyrins instead show a close structure in which one linker closes the two arms of the porphyrin ring. This porphyrins work as efficient ligands for the enantioselective epoxidation of alkenes¹⁰ but the presence of one chiral face is responsible for the approach of substrates on the opposite open achiral side. The undesired substrate approach can be hampered by the introduction of anionic ligands which force the substrate approach towards the chiral porphyrin face by coordinating the metal ion on the opposite open achiral side. On the other hand, the functionalization of one porphyrin face with coordinative groups requires complex and expensive synthetic procedures, which make the picnic basket porphyrins be undesired for industrial applications.

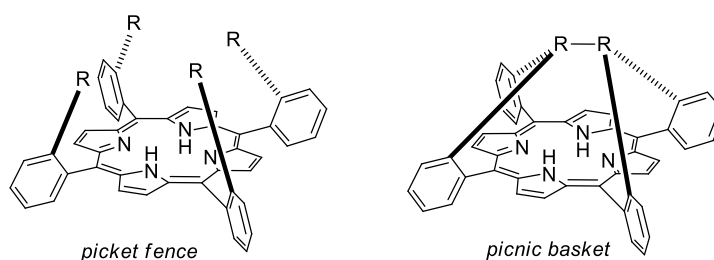


Figure 2: Schematic view of single face porphyrins: picket fence and picnic basket

To overcome the problems related to the single face porphyrins, the so-called double-face generation was developed. These types of porphyrins can be divided in three main classes (depending on the symmetry): D_4 -symmetric, D_2 -symmetric and C_2 -symmetric porphyrins (Figure 3)¹¹.

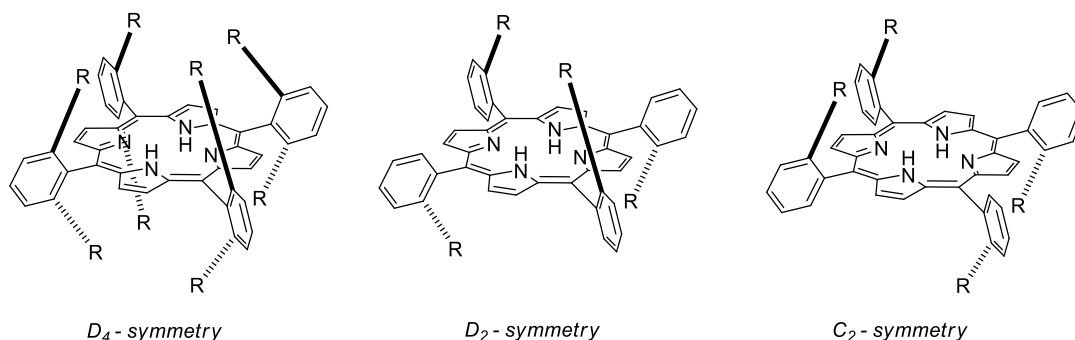


Figure 3: Schematic view of double face porphyrins: D_4 , D_2 and C_2

D_4 -symmetric porphyrins are generally synthesised from the *meso*-tetra(2,2'-disubstituted)phenyl porphyrin. The eight functional *ortho*-positions can be opportunely modified to afford favourable active sites on both porphyrins faces. Even if the desired ligand is obtained in low yields after several reaction

steps, the absence of atropoisomers makes the purification procedures easier than those of other double-face porphyrin ones. Nowadays, D_4 -symmetric porphyrins are widely used with different metals and for several catalytic applications such as oxidation, cyclopropanation and amination reactions¹².

D_2 -symmetric porphyrins derive from the functionalization of the $\alpha\beta$ atropoisomer of the *meso-tetra*(2-substituted)phenyl porphyrin. The corresponding metal complexes were tested in several reactions obtaining good results in term of yields and enantioselectivities¹³. All the data reported up to now clearly indicate that the catalytic performances of these complexes are strongly dependent on the synergic action between the active metal and the ligand periphery. In addition, as reported by Kodadek and co-workers^{14,15}, the substituent steric hinderance plays a fundamental role. The styrene epoxidation performed in presence of manganese $\alpha\beta$ *meso-tetra*[(*R*)-1,1'-binaphth-2-yl] porphyrin complex afforded the desired compound in a very good yield and selectivity. Worse results were observed replacing the binaphthyl group with a more hindered one. These data suggest that certain surrounding bulk degrees are necessary to achieve selectivity, but too hindered systems may easily result less efficient.

The functionalization of $\alpha_2\beta_2$ atropoisomer affords C_2 -symmetric porphyrins which can be used for the synthesis of metal chiral catalysts. This ligand family show bulky substituents on the porphyrin plane and a simultaneous free access to the active site. As the case of D_2 -symmetric porphyrin complexes, the catalytic activity depends on the chiral substituent size and on their distance from the active site. A rigid structure of the C_2 -symmetric ligand affords the desired products with good enantioselectivities and low yields due to the disadvantageous substrate access. On the one hand, the yield and the substrate access can be improved increasing the distance between the substituents and the active metal. On the other hand, the higher structure flexibility is responsible for a lower chiral induction. The same result can be obtained using very bulky groups. As a matter of fact, better catalytic performances can be obtained using less hindered arrangements. These considerations suggest the importance of modifying the porphyrin ring balancing the chiral substituents size and distance.

1.2. *Bis*-strapped porphyrins as ligand for carbene transfer reactions

In 2002, Rose and co-worker reported the first synthesis of a C_2 -symmetric chiral *bis*-binaphthyl porphyrin ligand (**39**) called *bis*-strapped porphyrin (Figure 4)¹⁶. The ligand shows two binaphthyl (BINAP) groups attached on the four picks of the $\alpha_2\beta_2$ atropoisomer of *meso*-tetrakis(2-aminophenyl)porphyrin (TAPPH₂). The corresponding iron (III) complex was employed in cyclopropanation reaction affording the desired cyclopropanes in modest yields and enantioselectivities. The obtained complex also showed good activity in enantioselective alkenes epoxidation, demonstrating the BINAP group ability to discriminate the prochiral faces of alkenes¹⁷.

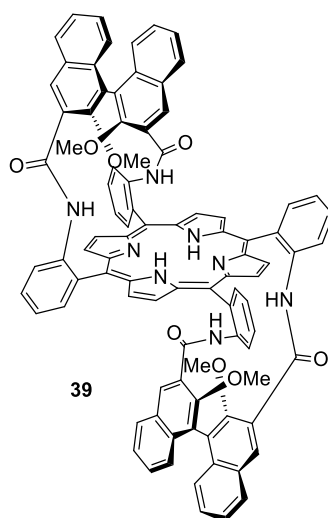


Figure 4: C_2 -symmetric chiral *bis*-binaphthyl porphyrin

E. Gallo, E. Rose and co-workers reported the catalytic activity of Co(**39**) towards the cyclopropanation of styrenes¹⁸. The best result was obtained in the cyclopropanation of α -methylstyrene by EDA in the presence of *N*-methyl imidazole (NMI) as the co-catalyst. The desired cyclopropane was obtained with a *cis/trans* diastereoselectivity of 34:66 and 90% *ee* of the *cis*-diastereomer. Theoretical conformational studies of the cobalt complex were done by L. Toma and co-workers to explain the low degree of the stereocontrol¹⁹. The authors suggested the formation of active carbene species in which NMI and the carbene ethyl group are the two axial ligands of the metal ion. The modelling of this active intermediate revealed that the cavity formed by the binaphthyl group is not large enough to accommodate the carbene ethyl group. In fact, it is positioned outside of the cavity and shows a high degree of freedom, responsible of the low chiral discrimination. Then, the CH_2 linkers of **39** were replaced by benzylic moieties in order to rigidify the ligand structure and increase the cavity dimension. The obtained chiral porphyrin **40** (Scheme 1) was employed for the synthesis of the iron(III) complex which was able to promote the alkene cyclopropanations with good yields (up to 98%) and *trans*-diastereoselectivities (up to 99:1)²⁰. The best result in term of enantiocontrol was obtained in the cyclopropanation of α -methylstyrene (86% *ee*). A general decrease of the stereocontrol was observed using high sterically hindered starting alkenes. Theoretical calculations of the involved carbene species demonstrated that the three-dimensional structure of the ligand can efficiently interact with the alkene substrate giving high reaction diastereoselectivities. On the other hand, the enantiocontrol can be disappointing because of the distance between the chiral substituents and the porphyrin plane.

the synthesis of the corresponding iron (III) complexes²². The gained catalytic data confirmed that the diastereoselectivity is led by the totem porphyrin achiral portion. Unfortunately, the presence of aminoacidic substituents was disadvantaged in terms of stereocontrol and the desired products were obtained in modest enantioselectivities.

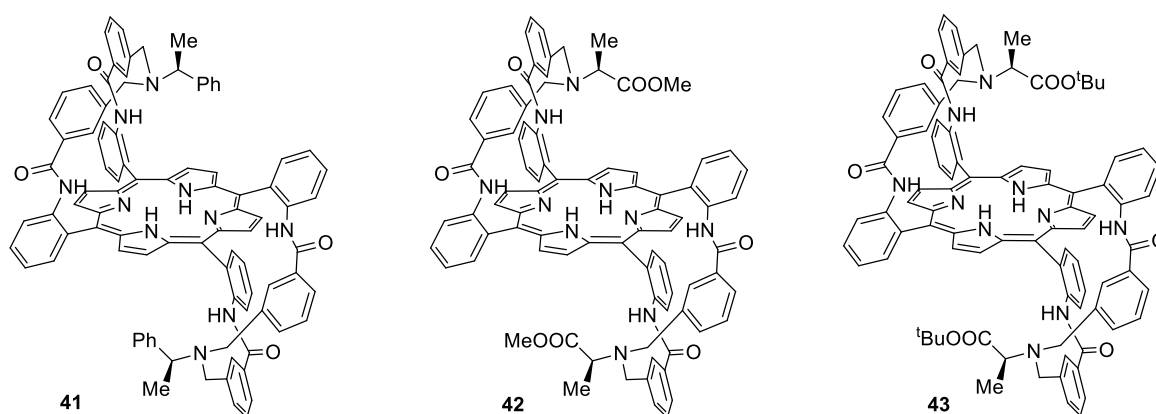


Figure 6: Chiral *bis*-strapped porphyrins **41-43**

According to theoretical investigations, the enantiocontrol loss was due to the different conformations assumed by the porphyrin ligand in free states and in transition states. The free ligand adopts bent conformations in which the chiral moieties are close to the porphyrin ring. Conversely, the two chiral hats are pushed away from the metal centre in the transition state in order to accommodate the substrate. The chiral moieties movement is in fact responsible for a lower enantioselectivity. All the data collected up to now have suggested that the ligand flexibility should be limited to force the chiral substituents to remain close to the porphyrin plane in order to optimise the catalytic performances.

2. Discussion

Considering the *bis*-strapped porphyrin totem structures and the ability of their iron(III) complexes to promote carbene transfer reactions, a new bio-inspired ligand was synthesised by the conjugation of the USCl porphyrin and the *L*-2,3-diaminopropionic acid (DAP). The obtained iron(III) complex was tested in cyclopropanation reactions in order to evaluate the effect of an aminoacid bridge on the reaction diastereo- and enantioselectivity.

2.1. Preliminary studies

DAP is a small and strong unnatural aminoacid arising from the lysine family (Figure 7). According to the parent lysine, the presence of two reactive amines and one carboxylic group makes the aminoacidic residue suitable for a range of functionalizations.

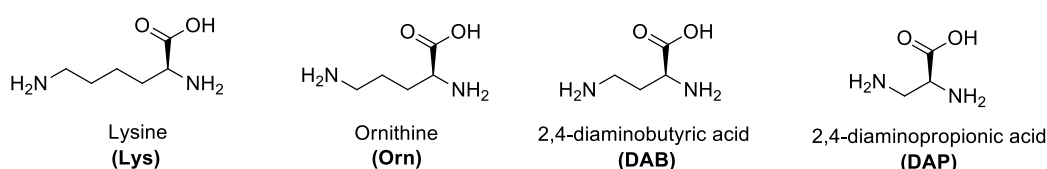
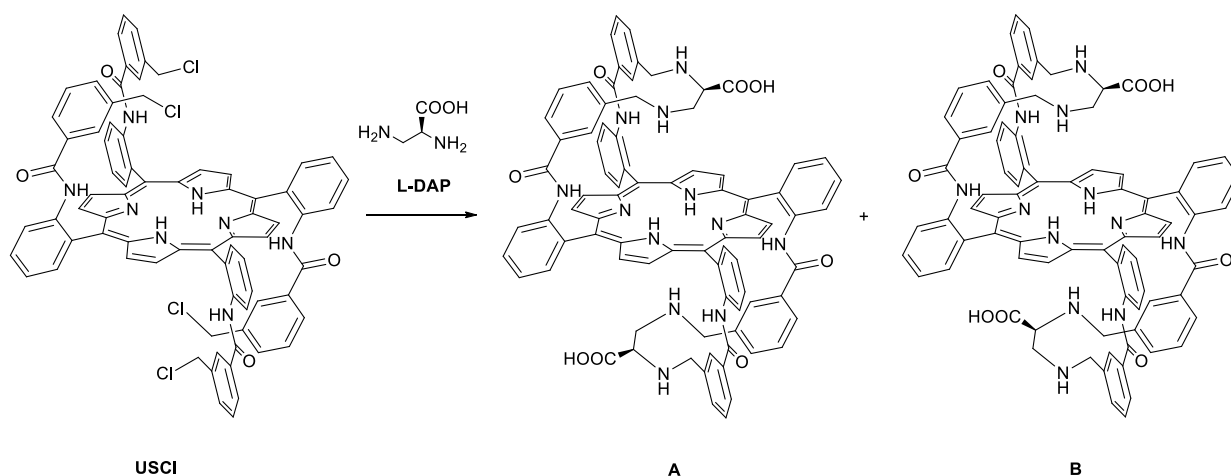


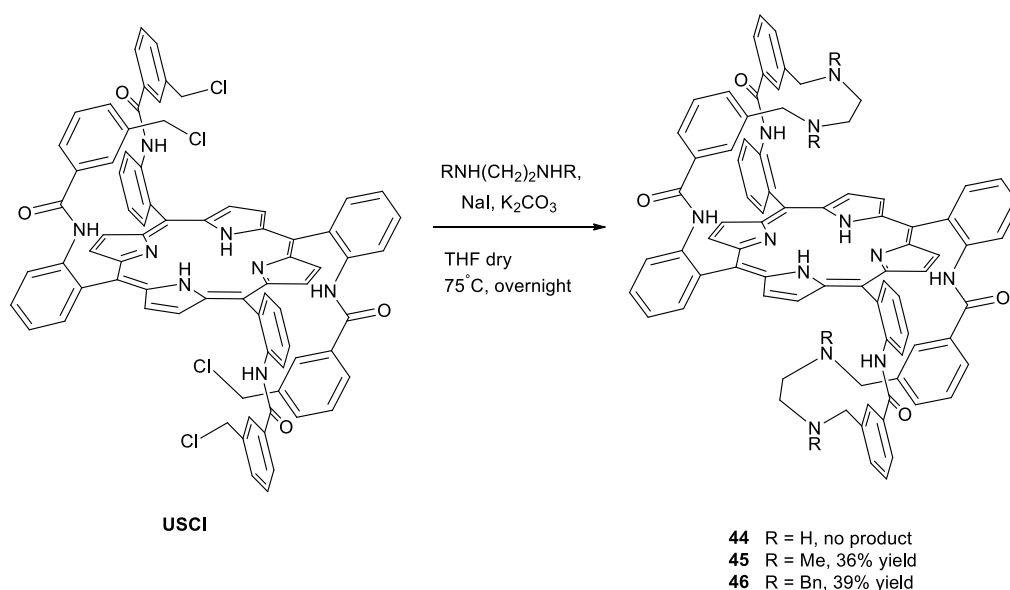
Figure 7: Lysine and its derivatives

The reaction between DAP and USCl porphyrin can afford two different regioisomers (A and B in scheme 2) depending on the disposition of amine groups attached on the porphyrin ring. Both *bis*-strapped ligands show two chiral cavities and two carboxylic groups suitable for the anchoring to hydrophilic chain or solid surfaces.



Scheme 2: Reaction between USCl and DAP

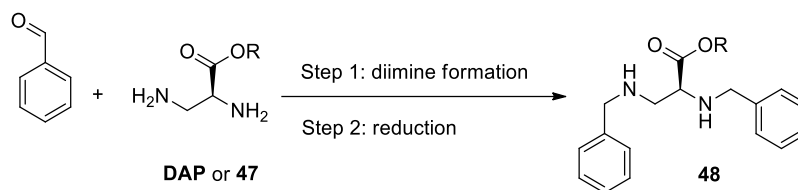
In order to study the feasibility of the reaction described above, USCl porphyrin was reacted with $\text{NH}_2\text{-(CH}_2\text{)}_2\text{-NH}_2$. Unfortunately, the corresponding porphyrin **44** was not isolated in a pure form due to its high polarity, which prevented an easy purification by standard chromatographic techniques. Thus, the reactivity of $\text{RNH-(CH}_2\text{)}_2\text{-NHR}$ molecules, which show benzylic or methylic substituents on the nitrogen amino functionalities, was tested. As reported in Scheme 3, the reaction performed better when $\text{R} = \text{Bn}$ rather than $\text{R} = \text{Me}$. These results suggested that the two additional rings can be efficiently formed using a bridge of two carbon atoms. It is important to notice that the presence of substituents on the nitrogen amine atoms is necessary to decrease the polarity of the corresponding *bis*-strapped porphyrin and the number of possible side products.



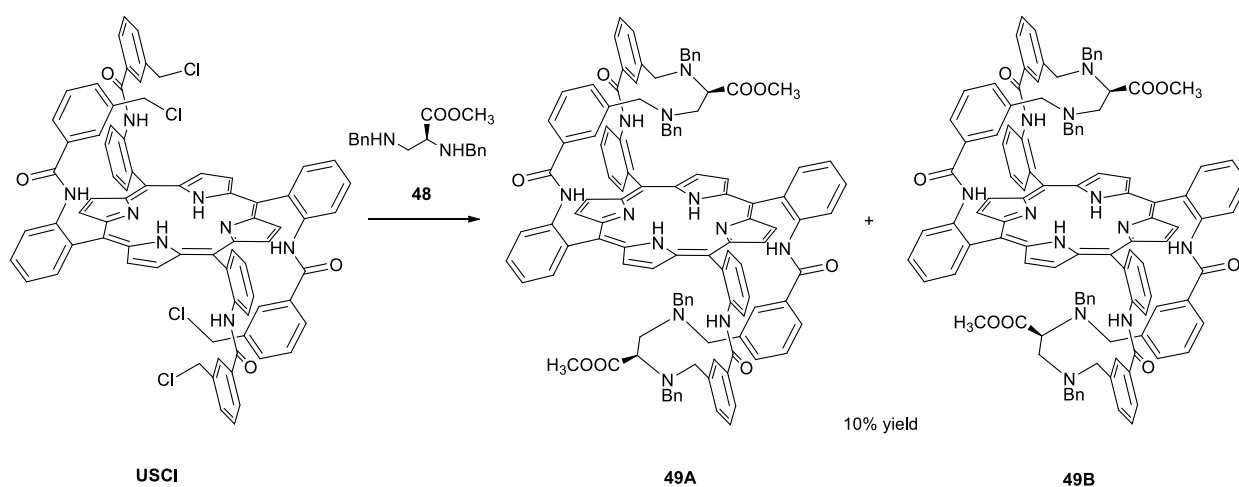
Scheme 3: Reaction between USCl and different substituted ethylenediamines

Considering the preliminary results achieved by reacting USCl with $\text{RNH-(CH}_2\text{)}_2\text{-NHR}$, a great effort was devoted to substitute the amino functionalities of the DAP residue with two benzylic groups by a reductive amination reaction (Table 1). DAP amino acid and the corresponding methyl ester **47** were tested but unfortunately the dibenzyl amino acid **48** was obtained in a very low yield. The consecutive reaction with the USCl porphyrin formed the corresponding *bis*-strapped porphyrin **49** in the low yield of 10% and as a mixture of the two regioisomers **49A** and **49B** (Scheme 4).

As it was difficult to achieve *bis*-strapped porphyrin which shows benzylic substituents on the two nitrogen atoms of the bridge, the attention was turned on the use of unprotected DAP amino acid as the starting material.

Table 1: Synthesis of **48** by reductive amination reaction

entry	R	Solvent	Base	Reducing agent	Reaction time (step 1 + step 2)	yield (%)
1	H	MeOH	DIPEA	NaBH ₄	6h + 4h	-
2	H	MeOH/H ₂ O	-	NaBH ₄	6h + 4h	-
3	CH ₃	MeOH/H ₂ O	-	NaBH ₄	6h + overnight	-
4	CH ₃	DCM dry (step1) MeOH (step 2)	TEA	NaBH ₄	15h + 4h	10
5	CH ₃	DCM dry/MeOH	TEA	NaBH ₄	15h + overnight	12
6	CH ₃	DCM dry/MeOH dry	TEA	NaBH ₄	15h + overnight	12
7	CH ₃	DCM dry	TEA	NaBH(OAc) ₃	15h + 24h	9
8	H	THF	TEA	NaBH(OAc) ₃	48h	-
9	H	DCE	TEA	NaBH(OAc) ₃	48h	-

**Scheme 4:** Synthesis of the mixture of **49A** and **49B**

Due to the absence of benzylic groups onto the amino functionalities, different *bis*-strapped porphyrin species can be obtained, showing different symmetries. In fact, the unprotected DAP amino acid can react with the porphyrin ligand forming two types of bridged substituents, usually called straps. The *mono*- or *di*-alkylation of the DAP amine groups is responsible for the formation of straps C and D (Figure 8). The strap C shows the monoalkylation of both amine groups of DAP and the strap D shows the dialkylation of only one amine.

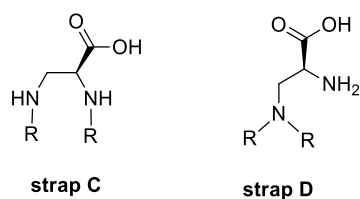


Figure 8: Possible straps formed with DAP

Depending on the strap type, different isomers of the desired *bis*-strapped porphyrin can be formed. The possible products can be distinguished by NMR techniques due to the presence of different β pyrrolic proton patterns, according to the considerations about the symmetry showed in figure 9.

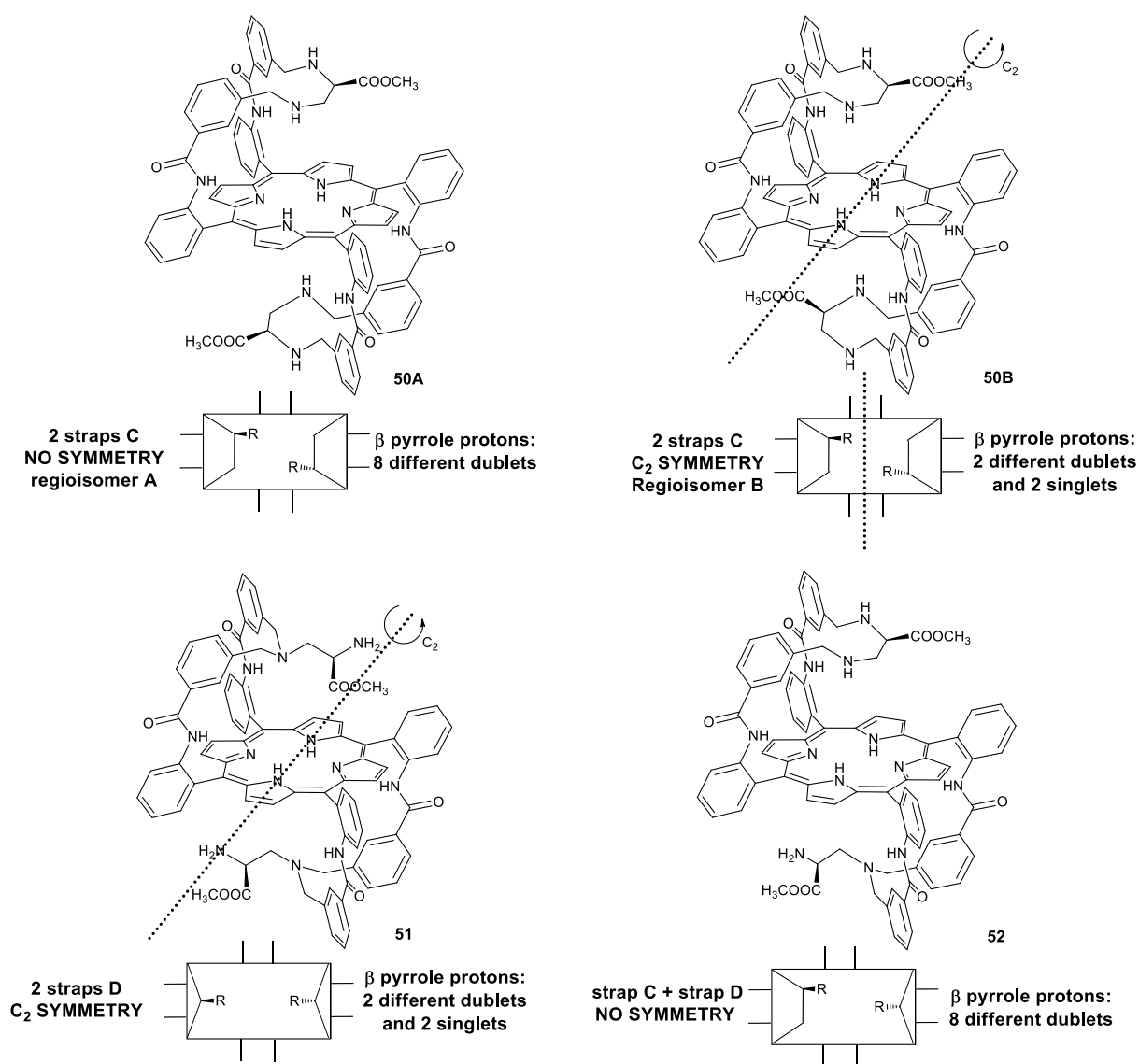


Figure 9: Symmetry considerations and β pyrrolic protons pattern of the possible *bis*-strapped isomers

The ^1H NMR spectrum of the reaction between USCl and **47** (DAP aminoacid methyl ester) revealed the presence of numerous tetrapyrrolic NH groups at very high fields. This observation, along with different β pyrrole proton signals, indicated the presence of several conformations of the ligand skeleton.

The **50B** regioisomer of the desired *bis*-strapped porphyrin was isolated in 10% of yield and characterised by NMR spectroscopy. The ^1H NMR of the isolated compound showed a clear pattern for the β pyrrolic protons that indicates the presence of symmetry in the analysed molecule. In addition, the deuterium exchange with D_2O revealed the presence of two different NH signals of the strap, which can be reconducted to the strap C (Figure 10).

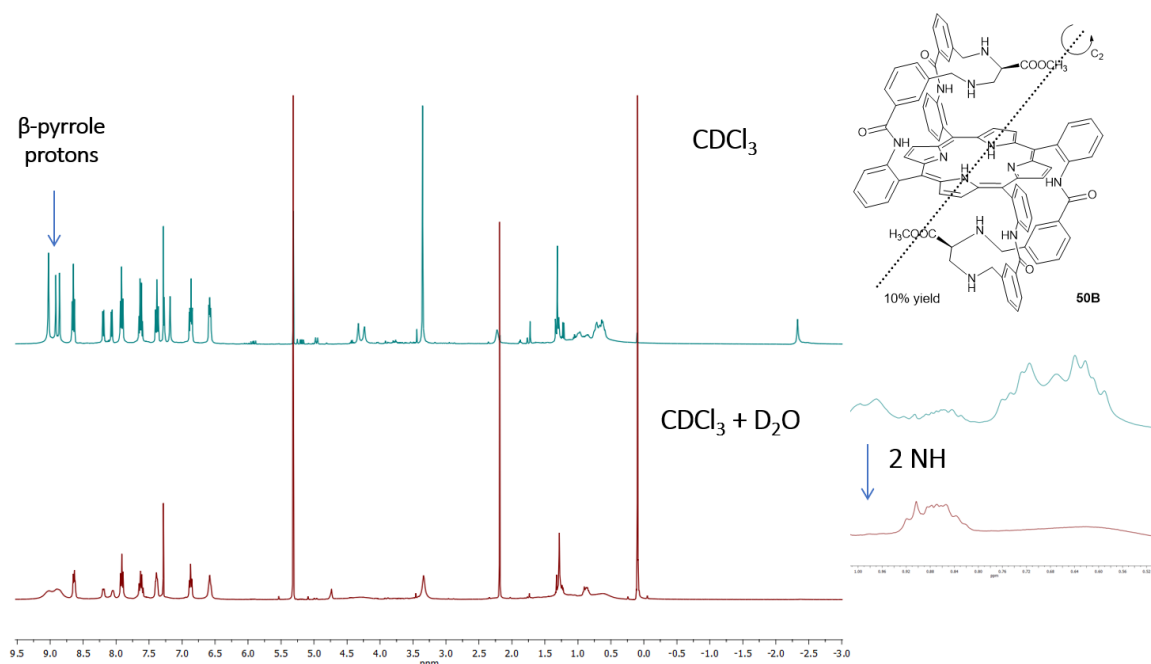


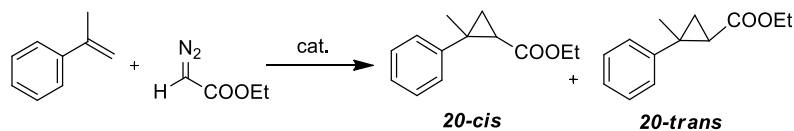
Figure 10: ^1H NMR spectra of **50B**

2.2. Hybrid *bis*-strapped ligand for alkenes cyclopropanation

The new hybrid *bis*-strapped ligand **50B** was used to synthesise the corresponding iron(III) complex, which was tested for promoting the cyclopropanation reactions. Catalytic conditions were firstly optimised in the model reaction between α -methylstyrene and EDA in order to increase the yield and diastereoselectivity. Different catalytic loadings, temperatures and add-on mode of EDA were evaluated. The data showed in table 2 indicate that $\text{Fe}(\mathbf{50B})\text{OMe}$ was very active in promoting the cyclopropanation reaction forming **20** in 99% yield and a *trans/cis* ratio of 89:11 (entry 8, table 2). Unfortunately, not good results were obtained in terms of enantioselectivity and *trans*-**20** was obtained only with 30% *ee*. The lack of enantioselectivity can be reconducted to the mobility of the DAP aminoacid which probably is not enough rigid to induce enantiocontrol. The activity of the

Fe(**50B**)OMe was evaluated with different styrenes affording all the desired cyclopropanes in quantitative yields and very high diastereoselectivities (up to 99:1) (Table 3).

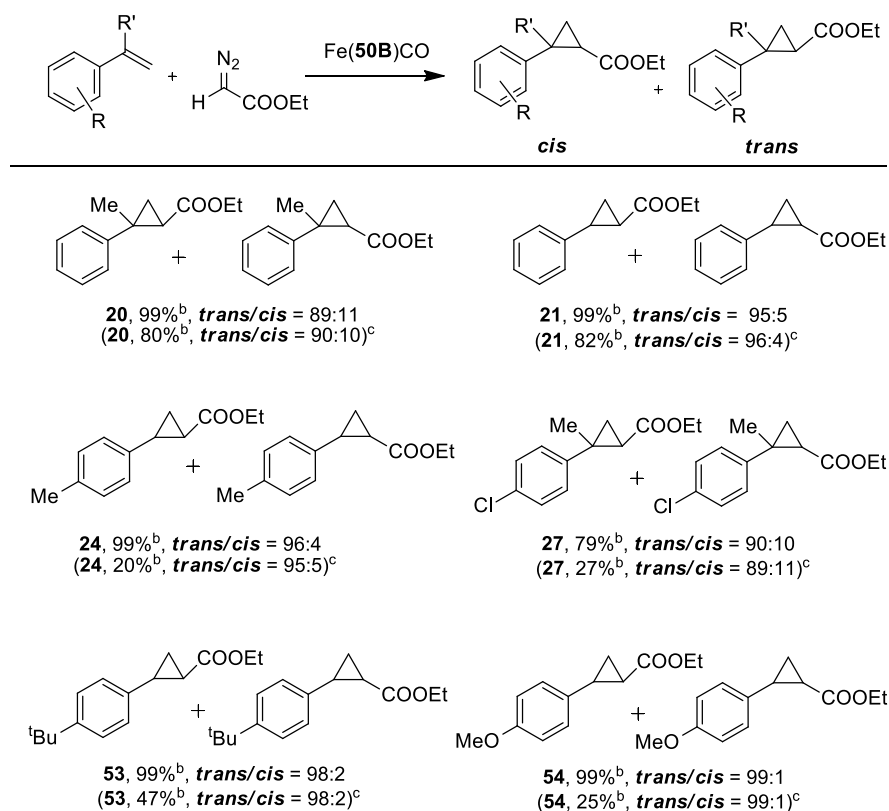
Table 2: Synthesis of **20** catalysed by Fe(**50B**)OMe



entry	cat/EDA/styrene	Temperature (°C)	EDA addition	yield (%) ^b	<i>trans/cis</i> ^b
1	1:1100:1000	25	one-pot	39	90:10
2	1:1100:1000	25	slow	81	90:10
3	1:1100:1000	-80	slow	27	75:25
4	1:1100:1000	-50	slow	33	82:12
5	1:1100:1000	-30	slow	58	70:30
6	1:1100:1000	0	slow	31	85:15
7	1:1100:4000	25	slow	79	89:11
8	1:1100:4000	25	slow	99	89:11
9	1:11000:40000	25	slow	80	90:10

^bDetermined by ¹H NMR spectroscopy using 2,4-dinitrotoluene as the internal standard.

Table 3: Synthesis of compounds **20**, **21**, **24**, **27**, **53** and **54** catalysed by Fe(**50B**)OMe



^aReactions were stirred in toluene for 2 h at 25°C by using Fe(**50B**)OMe/EDA/styrene = 1:1100:4000. ^bDetermined by ¹H NMR spectroscopy using 2,4-dinitrotoluene as the internal standard. ^cFe(**50B**)OMe/EDA/styrene = 1:10000:40000.

The obtained data showed that electronic and steric properties of the starting styrene don't affect the catalytic performances. In addition, the very good results in terms of diastereoselectivities confirm the concept of "totem" ligand in which the achiral C_2 symmetrical component is responsible for the diastereocontrol.

The above described cyclopropanations were also tested with a lower catalyst loading (0.001% mol) and very good results were achieved in forming compounds **20** and **21**, respectively in 80% and 82% of yields and with diastereoselectivities up to 96:4. On the other hand, lower yields were obtained using *para*-substituted styrenes due to the lower conversion of starting-diazo-reagents.

3. Conclusion

In conclusion, the synthesis and catalytic activity of a new iron *bis*-strapped porphyrin is reported. One specific regioisomer of the desired porphyrin ligand was isolated and completely characterised. The collected catalytic data established the ability of the iron (III) complex to promote cyclopropanation reactions with very high yields and diastereoselectivities, according to the previous reported concept of totem porphyrins. Future theoretical studies on the active carbene species involved in the catalytic reaction could be useful to clarify the causes of the low enantiocontrol.

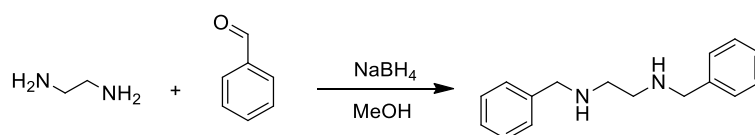
In addition, the presence of carboxylic groups on the porphyrin strap makes the synthesised hybrid ligand suitable for the conjugation with long water soluble chains, like PEG, in order to perform catalytic reaction in biphasic systems.

4. Experimental section

General conditions: Unless otherwise specified, all reactions were carried out under nitrogen atmosphere employing standard Schlenk techniques and vacuum-line manipulations. All the solvents were dried by using standard procedures and stored under nitrogen atmosphere. All the other starting materials were commercial products and used as received. NMR spectra were recorded at room temperature either on a Bruker Avance 300-DRX, operating at 300 MHz for ^1H , at 75 MHz for ^{13}C and at 282 MHz for ^{19}F , or on a Bruker Avance 400-DRX spectrometers, operating at 400 MHz for ^1H , 100 MHz for ^{13}C and 376 MHz for ^{19}F . Chemical shifts (ppm) are reported relative to TMS. The ^1H -NMR signals of the compounds described in the following were attributed by 2D NMR techniques. Assignments of the resonance in ^{13}C -NMR were made by using the APT pulse sequence, HSQC and HMBC techniques. Infrared spectra were recorded on a Varian Scimitar FTS 1000 spectrophotometer. UV/Vis spectra were recorded on an Agilent 8453E instrument. MALDI-TOF spectra were acquired either on a Bruker Daltonics Microflex or on a Bruker Daltonics Autoflex III TOF/TOF at C.I.G.A, University of Milan. High resolution MS (HR-MS) spectra were obtained on a Bruker Daltonics ICR-FTMS APEX II at C.I.G.A, University of Milan. Microanalysis was performed on a Perkin Elmer 2400 CHN Elemental Analyzer instrument.

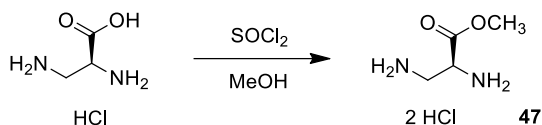
4.1. Synthesis of organic precursors

4.1.1. Synthesis of *N,N'*-dibenzylethane-1,2-diamine



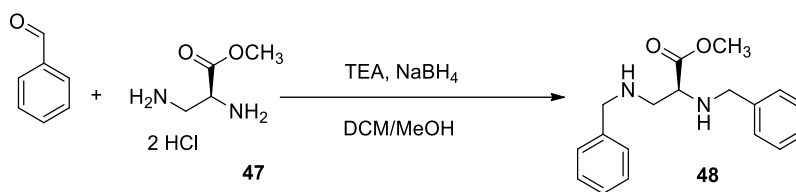
Benzaldehyde (3.0 mL, 3.00×10^{-2} mol) and ethylenediamine (1.0 mL, 1.50×10^{-2} mol) were dissolved under nitrogen in CH_3OH (50.0 mL). The reaction mixture was stirred overnight at room temperature, then NaBH_4 (1.70 g, 4.50×10^{-2} mol) was slowly added at 0°C . The reaction mixture was refluxed for four hours until the complete consumption of the starting ethylenediamine was observed by TLC (SiO_2 , $\text{CH}_2\text{Cl}_2/\text{CH}_3\text{OH} = 95:5$). The solvent was evaporated to dryness under vacuum and the residue was dissolved in CH_2Cl_2 (30.0 mL). The organic phase was extracted three times with H_2O , then dried over Na_2SO_4 and filtered. The solvent was evaporated to dryness under vacuum to yield a yellow oil (3.00 g, 83%). The collected analytical data are in accordance with those reported in literature²³.

^1H NMR (400 MHz, CDCl_3): δ 7.32 – 7.30 (m, 10H, H_{Ar}), 3.77 (s, 4H, H_{CH_2}), 2.76 (s, 4H, H_{CH_2}), 1.54 (br, 2H, H_{NH}).

4.1.2. Synthesis of (S)-methyl 2,3-diaminopropanoate (**47**)

Diaminopropionic acid hydrochloride (110.0 mg, 7.55×10^{-4} mol) was dissolved in CH_3OH (2.0 mL) and stirred for 30 min at room temperature. Then, SOCl_2 (0.11 mL, 1.51×10^{-3} mol) was slowly added at 0°C and the reaction mixture was refluxed for 12 hours. At the end of the reaction the solvent was evaporated to dryness under vacuum and the residue was washed several times with CH_3Cl to yield a white solid (134.0 mg, 93%). The collected analytical data are in accordance with those reported in literature²⁴.

$^1\text{H NMR}$ (400 MHz, D_2O): δ 4.59 – 4.56 (m, 1H, H_{CH}), 3.69 – 3.55 (m, 2H, H_{CH_2}), 3.03 (s, 3H, H_{CH_3}).

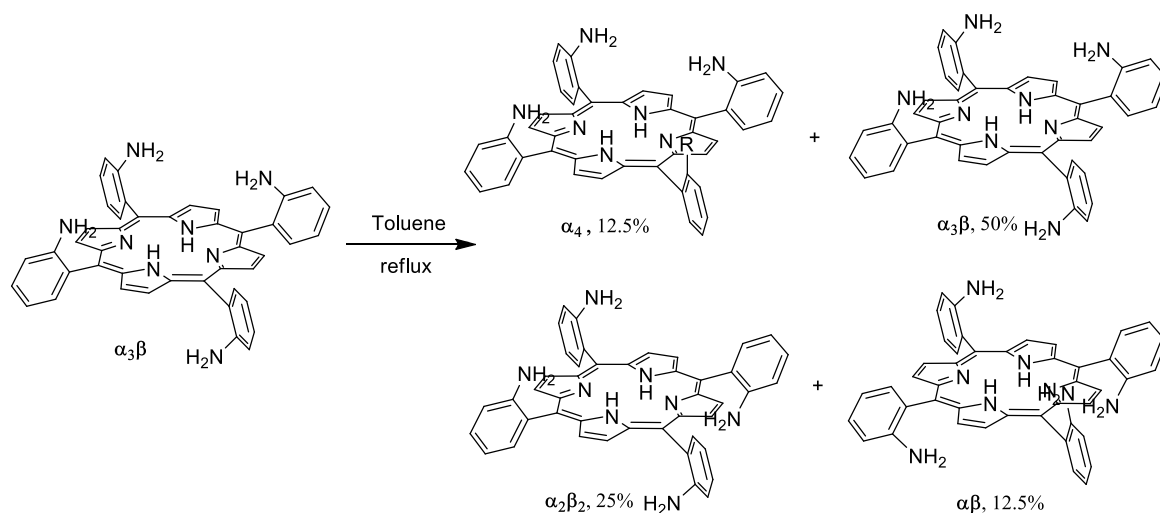
4.1.3. Synthesis of (S)-methyl 2,3-bis(benzylamino)propanoate (**48**)

Benzaldehyde (0.56 mL, 5.26×10^{-4} mol) and **47** (50.0 mg, 2.63×10^{-4} mol) were dissolved under nitrogen in CH_2Cl_2 (3.0 mL). The reaction mixture was cooled at 0°C and TEA (0.73 mL, 5.26×10^{-4} mol) was slowly added in a period of three hours. After the addition, the reaction mixture was stirred for 15 hours until the formation of the diimine intermediate was observed by $^1\text{H NMR}$. Then, NaBH_4 (45.0 mg, 1.18×10^{-3} mol) was slowly added at 0°C and the mixture was stirred at room temperature until the complete consumption of the starting reagents was observed by TLC (SiO_2 , $\text{CH}_2\text{Cl}_2/\text{CH}_3\text{OH} = 95:5$). The solvent was evaporated to dryness under vacuum and the residue was purified by flash chromatography (SiO_2 , gradient elution from CH_2Cl_2 to $\text{CH}_2\text{Cl}_2/\text{CH}_3\text{OH} 90:10$) to yield a yellow oil (22.0 mg, 12%).

$^1\text{H NMR}$ (400 MHz, CDCl_3): δ 7.46 – 7.18 (m, 10H, H_{Ar}), 3.87 (d, $J = 13.0$ Hz, 1H, H_{CH_2}), 3.77 (d, $J = 2.5$ Hz, 2H, H_{CH_2}), 3.75 (s, 3H, H_{CH_3}), 3.69 (d, $J = 12.9$ Hz, 1H, H_{CH_2}), 3.53 – 3.48 (m, 1H, H_{CH}), 2.92 (dd, $J = 12.0, 4.7$ Hz, 1H, H_{CH_2}), 2.79 (dd, $J = 12.0, 7.5$ Hz, 1H, H_{CH_2}), 2.01 (br, 2H, H_{NH}).

4.2. Synthesis of porphyrin ligands

4.2.1. Synthesis of $\alpha_2\beta_2$ *o*-TAPPH₂ by atropoisomerization reaction

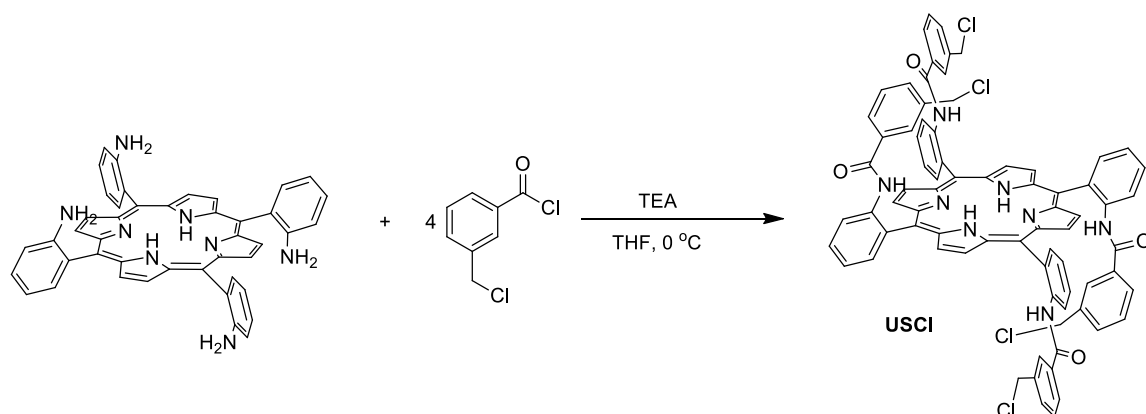


$\alpha_3\beta$ *o*-TAPPH₂ (6.00 g, 8.89×10^{-3} mol) was dissolved in toluene (1.80 L) and the solution was refluxed at 80°C for 12 hours. The solvent was evaporated to dryness under vacuum and the residue was purified by flash chromatography.

The four atropoisomers were separated by flash chromatography (SiO₂, 15 μ m, gradient elution with CH₂Cl₂ and CH₃OH) with CH₂Cl₂ for $\alpha\beta$ (12.5%), 0.5% CH₃OH for $\alpha_2\beta_2$ (25%), 3% CH₃OH for $\alpha_3\beta$ (50%) and 5% CH₃OH for α_4 (12.5%). The collected analytical data are in accordance with those reported in literature²⁵.

¹H NMR (400 MHz, CDCl₃) $\alpha_2\beta_2$ *o*-TAPPH₂: δ 8.92 (s, 8H, H _{β pyrr}), 7.86 (d, $J = 7.4$ Hz, 4H, H_{Ar}), 7.26 (t, $J = 7.8$ Hz, 4H, H_{Ar}), 7.18 (t, $J = 7.4$ Hz, 4H, H_{Ar}), 7.14 (d, $J = 8.1$ Hz, 2H, H_{Ar}), 3.58 (s, 8H, NH₂), -2.65 (s, 2H, NH_{pyrr}).

4.2.2. Synthesis of USCl porphyrin

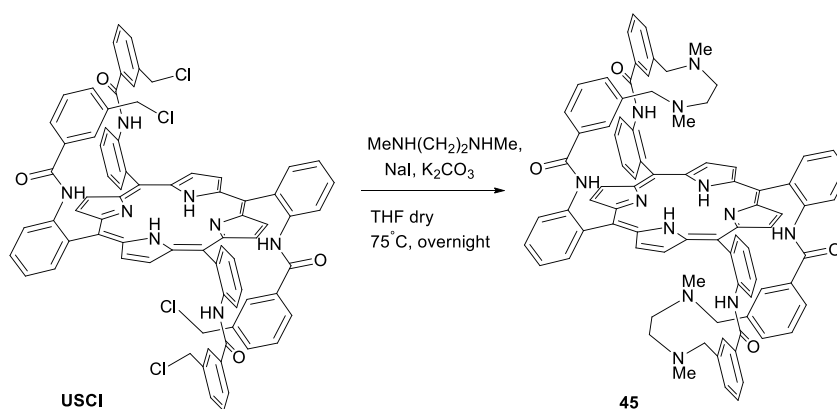


The $\alpha_2\beta_2$ *o*-TAPPH₂ (730.0 mg, 1.08×10^{-3} mol) was dissolved in fresh distilled THF (36.5 mL) at room temperature followed by the addition of TEA (1.25 mL, 8.66×10^{-3} mol). The dark solution was cooled

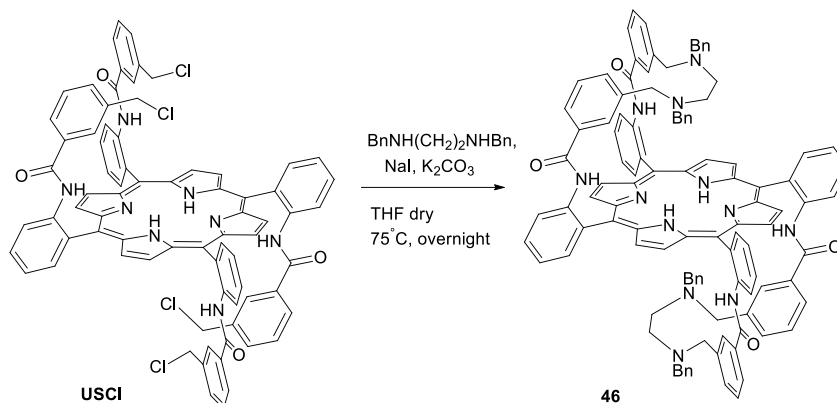
to 0°C and 3-(chloromethyl)benzoyl chloride (0.98 mL, 6.48×10^{-3} mol) was added dropwise. The solution was stirred for 45min and then CH₃OH was added to quench the reaction. The solvent was removed under reduced pressure and the crude was purified by flash chromatography (SiO₂, 15 μm, gradient elution from CH₂Cl₂ to CH₂Cl₂/CH₃OH = 99.5:0.5) to yield a purple solid (900.0 mg, 68%). The collected analytical data are in accordance with those reported in literature²⁵.

¹H NMR (400 MHz, CDCl₃): δ 8.96 (d, $J = 4.1$ Hz, 8H, H_{βpyrr}), 8.86 (d, 4H, $J = 8.4$ Hz, H_{Ar}), 8.04 (d, $J = 6.3$ Hz, 4H, H_{Ar}), 7.90 (t, $J = 7.3$ Hz, 4H, H_{Ar}), 7.62 (s, 4H, H_{NH}), 7.58 (t, $J = 8.0$ Hz, 4H, H_{Ar}), 6.71 (d, $J = 7.7$ Hz, 4H, H_{Ar}), 6.54 – 6.42 (m, 8H, H_{Ar}), 6.36 (t, $J = 7.7$ Hz, 4H, H_{Ar}), 3.54 – 3.46 (m, 8H, H_{CH2}), -2.55 ppm (s, 2H, NH_{pyrr}).

4.2.3. Synthesis of porphyrin 45

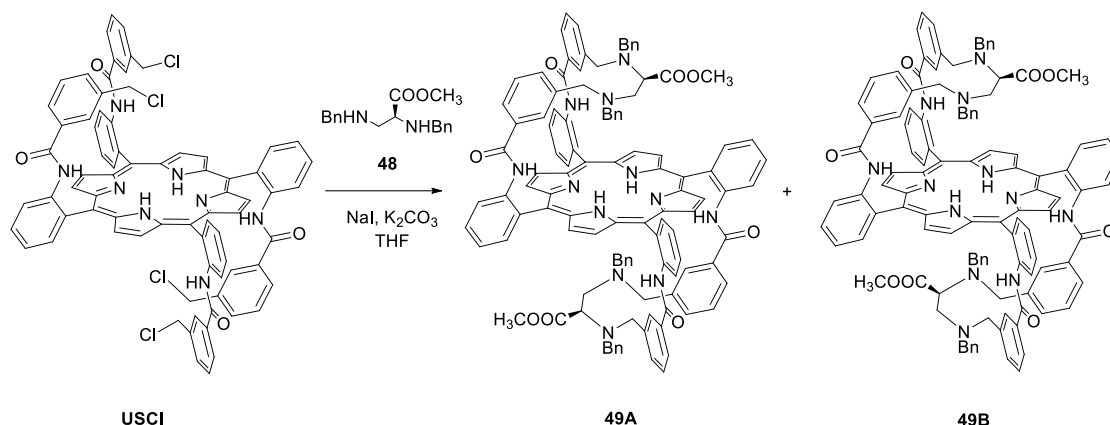


N,N'-dimethylethane-1,2-diamine (0.13 mL, 1.16×10^{-4} mol), NaI (58.0 mg, 3.88×10^{-4} mol) and K₂CO₃ (107.0 mg, 7.76×10^{-4} mol) were added to a THF (50.0 mL) solution of USCl porphyrin (50.0 mg, 3.88×10^{-4} mol). The solution was refluxed at 75°C for 10 hours until the complete consumption of the starting porphyrin was observed by TLC (SiO₂, CH₂Cl₂/CH₃OH = 95:5). The solvent was removed under reduced pressure and the residue was dissolved in CH₂Cl₂ (15.0 mL). The organic phase was extracted three times with H₂O, then dried over Na₂SO₄ and filtered. The solvent was evaporate to dryness and the crude was purified by flash chromatography (SiO₂, 15 μm, gradient elution from CH₂Cl₂ to CH₂Cl₂/CH₃OH = 90:10) to yield a purple solid containing the product (20.0 mg, 36%). Compound **45** wasn't isolated in a pure form.

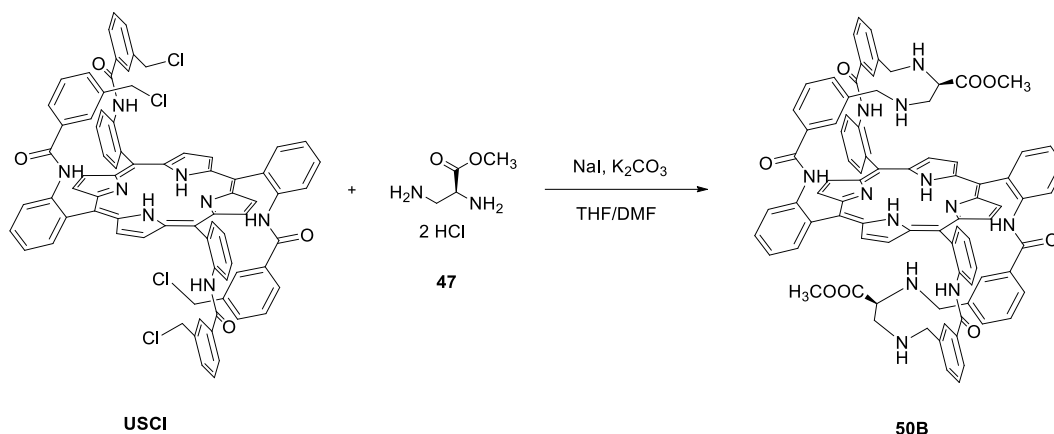
4.2.4. Synthesis of porphyrin **46**

N,N'-dibenzylethane-1,2-diamine (28.0 mg, 1.16×10^{-4} mol), NaI (58.0 mg, 3.88×10^{-4} mol) and K_2CO_3 (107.0 mg, 7.76×10^{-4} mol) were added to a THF (50.0 mL) solution of **USCl** porphyrin (50.0 mg, 3.88×10^{-5} mol). The solution was refluxed at 75°C for 12 hours until the complete consumption of the starting porphyrin was observed by TLC (SiO_2 , $\text{CH}_2\text{Cl}_2/\text{CH}_3\text{OH} = 95:5$). The solvent was removed under reduced pressure and the residue was dissolved in CH_2Cl_2 (15.0 mL). The organic phase was extracted three times with H_2O , then dried over Na_2SO_4 and filtered. The solvent was evaporated to dryness and the crude was purified by flash chromatography (SiO_2 , 15 μm , gradient elution from CH_2Cl_2 to $\text{CH}_2\text{Cl}_2/\text{CH}_3\text{OH} = 95:5$) to yield the purple solid **46** (25.0 mg, 39%).

$^1\text{H NMR}$ (400 MHz, CDCl_3 , 298 K): δ 9.07 (s, 4H, $\text{H}_{\beta\text{pyrr}}$), 8.99 (s, 4H, $\text{H}_{\beta\text{pyrr}}$), 8.90 (dd, $J = 8.4, 1.2$ Hz, 4H, H_{Ar}), 7.91 (td, $J = 8.0, 1.6$ Hz, 4H, H_{Ar}), 7.85 (dd, $J = 7.6, 1.6$ Hz, 4H, H_{Ar}), 7.53 – 7.44 (m, 8H, H_{Ar}), 7.13 (dd, $J = 5.0, 1.9$ Hz, 12H, H_{Ar}), 7.01 (d, $J = 7.6$ Hz, 4H, H_{NH}), 6.85 – 6.63 (m, 16H, H_{Ar}), 5.47 (s, 4H, H_{Ar}), 2.52 (d, $J = 13.6$ Hz, 4H, H_{CH_2}), 2.28 – 2.14 (m, 10H, $\text{H}_{\text{CH}_2} + \text{H}_{\text{solvent}}$), 1.59 (br, 4H, H_{NH}), 1.42 (d, $J = 13.9$ Hz, 4H, H_{CH_2}), 0.69 (q, $J = 5.4, 4.9$ Hz, 4H, H_{CH_2}), 0.38 (d, $J = 7.9$ Hz, 4H, H_{CH_2}), -2.38 (s, 2H, NH_{pyrr}). **$^{13}\text{C NMR}$** (100 MHz, CDCl_3 , 298 K): δ 134.62, 131.41, 130.33, 128.21, 128.00, 125.85, 124.74, 123.45, 121.33, 57.89, 56.63, 49.32, 44.81, 32.02, 29.47. **HR-MS** (MALDI): m/z ($\text{C}_{108}\text{H}_{94}\text{N}_{12}\text{O}_4$) calcd. 1622.74, found [M] 1622.4.

4.2.5. Synthesis of porphyrin **49**

NaI (58.0 mg, 3.88×10^{-4} mol), K_2CO_3 (107.0 mg, 7.76×10^{-4} mol) and **48** (23.0 mg, 7.76×10^{-5} mol), were added to a THF (50.0 mL) solution of **USCI** porphyrin (50.0 mg, 3.88×10^{-5} mol). The solution was refluxed at 75°C for 10 hours until the complete consumption of the starting porphyrin was observed by TLC (SiO_2 , $CH_2Cl_2/CH_3OH = 95:5$). The solvent was removed under reduced pressure and the residue was dissolved in CH_2Cl_2 (5.0 mL). The crude was precipitated with heptane (20.0 mL), collected in a filter and then was purified by flash chromatography (SiO_2 , 15 μm , gradient elution from CH_2Cl_2 to $CH_2Cl_2/CH_3OH = 90:10$) to yield a purple solid containing the product (11.0 mg, 10%). Compound **49** wasn't isolated in a pure form.

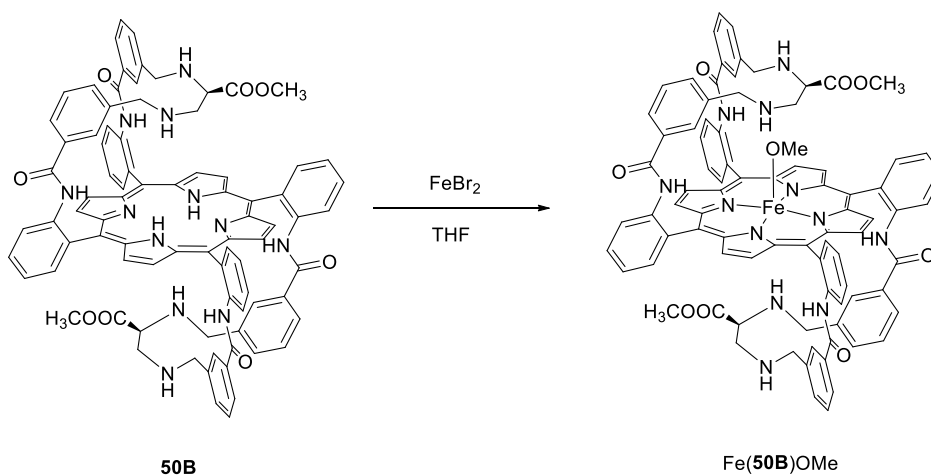
4.2.6. Synthesis of porphyrin **50B**

NaI (0.87 g, 5.82×10^{-3} mol), K_2CO_3 (1.60 g, 1.16×10^{-2} mol) and **47** (0.29 g, 1.55×10^{-3} mol), were added to a THF/DMF (450.0/50.0 mL) solution of **USCI** porphyrin (0.50 g, 3.88×10^{-4} mol). The solution was refluxed at 75°C for three hours until the complete consumption of the starting porphyrin was observed by TLC (SiO_2 , $CH_2Cl_2/CH_3OH = 95:5$). The solvent was removed under reduced pressure and the residue was dissolved in CH_2Cl_2 (10.0 mL). The compound was precipitated with heptane (50.0 mL), collected in a filter and then was purified by flash chromatography (SiO_2 , 15 μm , gradient elution from CH_2Cl_2 to $CH_2Cl_2/CH_3OH = 95:5$) to yield the purple solid **50B** (0.06 g, 10%).

¹H NMR (400 MHz, CDCl₃, 298 K): δ 9.03 (s, 4H, H_{βpyrr}), 8.88 (d, *J* = 23.0 Hz, 4H, H_{βpyrr}), 8.64 (t, *J* = 7.88 Hz, 4H, H_{Ar}), 8.19 (d, *J* = 6.60 Hz, 2H, H_{Ar}), 8.07 (d, *J* = 8.18 Hz, 2H, H_{Ar}), 7.91 (t, *J* = 8.34 Hz, 4H, H_{Ar}), 7.62 (q, *J* = 7.2 Hz, 4H, H_{Ar}), 7.38 (t, *J* = 8.22 Hz, 4H, H_{Ar}), 7.28 (s, 2H, H_{NH}), 7.20 (s, 2H, H_{NH}), 6.86 (td, *J* = 7.7, 3.9 Hz, 4H, H_{Ar}), 6.62 – 6.53 (m, 4H, H_{Ar}), 4.30 (s, 2H, H_{Ar}), 4.21 (s, 2H, H_{Ar}), 3.35 (s, 6H, H_{CH₃}), 2.29 – 2.14 (m, 2H, H_{CH₂}), 1.29 (s, 2H, H_{CH₂}), 1.06 – 0.84 (m, 6H, H_{NH} + H_{CH₂} + H_{solvents}), 0.82 – 0.60 (m, 10H, H_{CH₂} + H_{CH} + H_{solvents}), -2.32 (s, 2H, NH_{pyrr}). **¹³C NMR** (100 MHz, CDCl₃, 298 K): δ 134.45, 134.15, 131.52, 131.30, 130.73, 127.32, 124.82, 124.79, 124.36, 57.47, 57.27, 57.29, 53.81, 52.54, 52.12, 36.40, 33.84, 30.11, 27.18. **HR-MS** (MALDI): *m/z* (C₈₄H₇₀N₁₂O₈) calcd. 1376.54, found [M] 1376.8.

4.3. Synthesis of porphyrin complex

4.3.1. Synthesis of Fe(50B)OMe

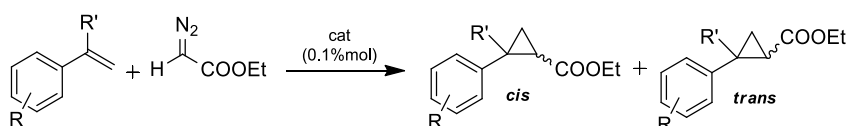


FeBr₂ (158.0 mg, 7.28 x 10⁻⁴ mol) was added to a THF (20.0 mL) solution of **50B** (50.0 mg, 3.64 x 10⁻⁵ mol) under nitrogen. The solution was refluxed at 75°C for 5 hours until the complete consumption of the starting porphyrin was observed by TLC (Al₂O₃, CH₂Cl₂/CH₃OH = 95:5). The solvent was evaporated to dryness under vacuum and the residue purified by chromatography (Al₂O₃, eluent CH₂Cl₂/CH₃OH 90:10) to yield the brown solid Fe(**50B**)OMe (58.0 mg, 96%).

LR-MS (ESI): *m/z* (C₈₅H₇₁FeN₁₂O₉) calcd. 1459.48; found [M-OMe] 1428.62. **Elemental analysis** calc. for C₈₅H₇₁FeN₁₂O₉: calcd. C, 69.91; H, 4.90; N, 11.51; found C, 70.35; H, 5.17; N, 11.19.

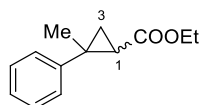
4.4. Synthesis of cyclopropanes

General catalytic procedure for the synthesis of cyclopropanes



Method A: In a typical run, the catalyst (6.79×10^{-7} mol) was dissolved in 2.0 mL of dry toluene before adding the alkene (3.39×10^{-4} mol) and the diazo compound (7.47×10^{-4} mol) by a syringe pump under nitrogen. The reaction was stirred for 2 hours at 25°C. The solution was then evaporated to dryness and the reaction crude was analysed by $^1\text{H-NMR}$ spectroscopy using 2,4-dinitrotoluene as the internal standard. *Method B:* the procedure illustrated for method A was followed using 6.79×10^{-7} mmol of catalyst, 3.39×10^{-2} mol of alkene and 6.79×10^{-3} mol of diazo compound.

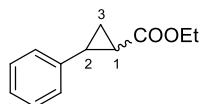
4.4.1. Synthesis of *trans*-ethyl-2-methyl-2-phenylcyclopropanecarboxylate(20)



The general catalytic procedure for the synthesis of cyclopropanes was followed using α -methylstyrene and EDA. The collected analytical data are in accordance with those reported in literature²⁶.

$^1\text{H NMR}$ (300 MHz, CDCl_3): δ 7.31 (d, 4H, $J = 4.4$ Hz, H_{Ar}), 7.22 (m, 1H, H_{Ar}), 4.20 (q, 2H, $J = 7.1$ Hz, $\text{H}_{\text{CH}_2\text{Et}}$), 1.97 (dd, 1H, $J = 8.2, 6.1$ Hz, H^1), 1.54 (s, 3H, H_{CH_3}), 1.49 – 1.39 (m, 2H, H^3), 1.31 (t, 3H, $J = 7.1$ Hz, $\text{H}_{\text{CH}_3\text{Et}}$).

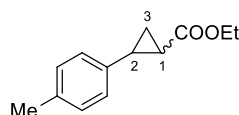
4.4.2. Synthesis of *trans*-ethyl-2-phenylcyclopropanecarboxylate (21)



The general catalytic procedure for the synthesis of cyclopropanes was followed using styrene and EDA. The collected analytical data are in accordance with those reported in literature²⁶.

$^1\text{H NMR}$ (300 MHz, CDCl_3): δ 7.09 – 7.31 (m, 5H, H_{Ar}), 4.17 (q, 2H, $J = 7.2$ Hz, $\text{H}_{\text{CH}_2\text{Et}}$), 2.57 – 2.52 (m, 1H, H^2), 1.94 – 1.90 (m, 1H, H^1), 1.64 – 1.60 (m, 1H, H^3), 1.35-1.30 (m, 1H, H^3), 1.28 (t, 3H, $J = 7.2$ Hz, $\text{H}_{\text{CH}_3\text{Et}}$).

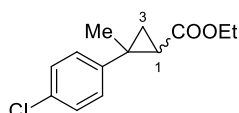
4.4.3. Synthesis of *trans*-ethyl-2-(4-methylphenyl)cyclopropane carboxylate (24)



The general catalytic procedure for the synthesis of cyclopropanes was followed using 4-methylstyrene and EDA. The collected analytical data are in accordance with those reported in literature²⁷.

$^1\text{H NMR}$ (400 MHz, CDCl_3): δ 7.10 (d, 2H, $J = 7.9$ Hz, H_{Ar}), 7.01 (d, 2H, $J = 8.1$ Hz, H_{Ar}), 4.18 (q, 2H, $J = 7.1$ Hz, $\text{H}_{\text{CH}_2\text{Et}}$), 2.53 – 2.48 (m, 1H, H^2), 2.32 (s, 3H, H_{CH_3}), 1.86 (m, 1H, H^1), 1.58 (m, 1H, H^3), 1.28 (t, 3H, $J = 7.1$ Hz, $\text{H}_{\text{CH}_3\text{Et}}$), 1.27 (m, 1H, H^3).

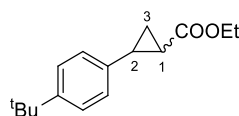
4.4.4. Synthesis of *trans*-ethyl-2-methyl-(4-chlorophenyl)cyclopropane carboxylate (27)



The general catalytic procedure for the synthesis of cyclopropanes was followed using 4-chloro- α -methylstyrene and EDA. The collected analytical data are in accordance with those reported in literature²¹.

$^1\text{H NMR}$ (400 MHz, CDCl_3): δ 7.26 (q, 4H, $J = 8.5$ Hz, H_{Ar}), 4.26 – 4.18 (m, 2H, $\text{H}_{\text{CH}_2\text{Et}}$), 1.94 (dd, 1H, $J = 8.3, 6.1$ Hz, H^1), 1.52 (s, 3H, H_{CH_3}), 1.47 (m, 1H, H^3), 1.39 (dd, 1H, $J = 8.4, 4.8$ Hz, H^3), 1.32 (t, 3H, $J = 7.1$ Hz, $\text{H}_{\text{CH}_3\text{Et}}$).

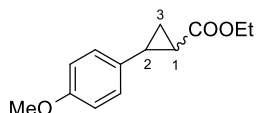
4.4.5. Synthesis of *trans*-ethyl 2-(4-(*tert*-butyl)phenyl)cyclopropanecarboxylate (53)



The general catalytic procedure for the synthesis of cyclopropanes was followed using 4-*tert*-butylstyrene and EDA. The collected analytical data are in accordance with those reported in literature²¹.

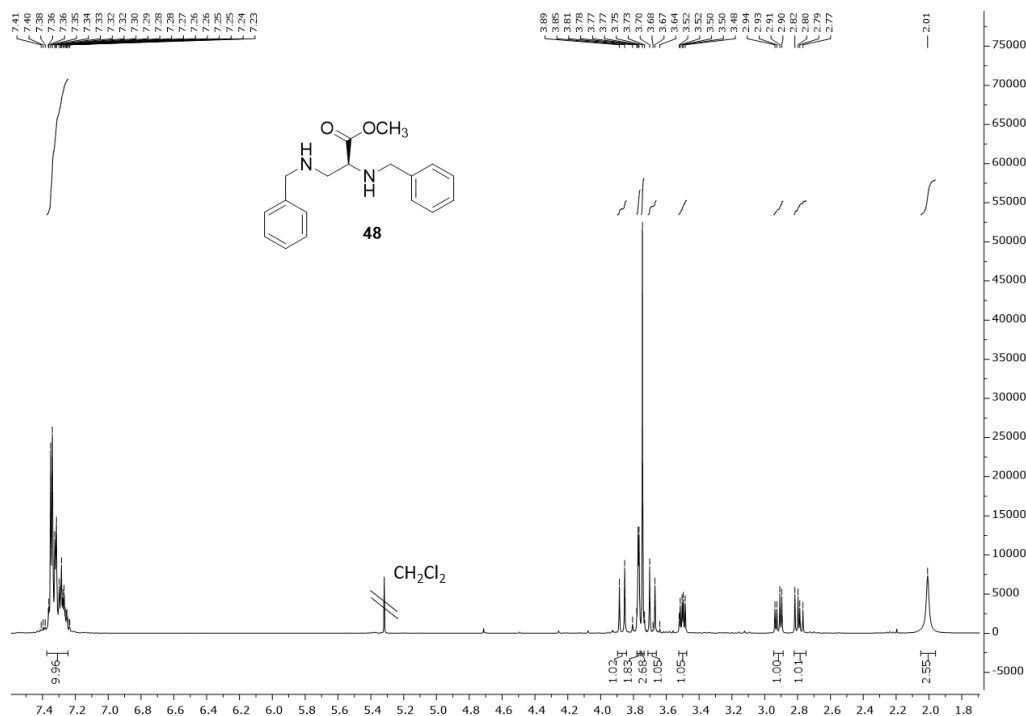
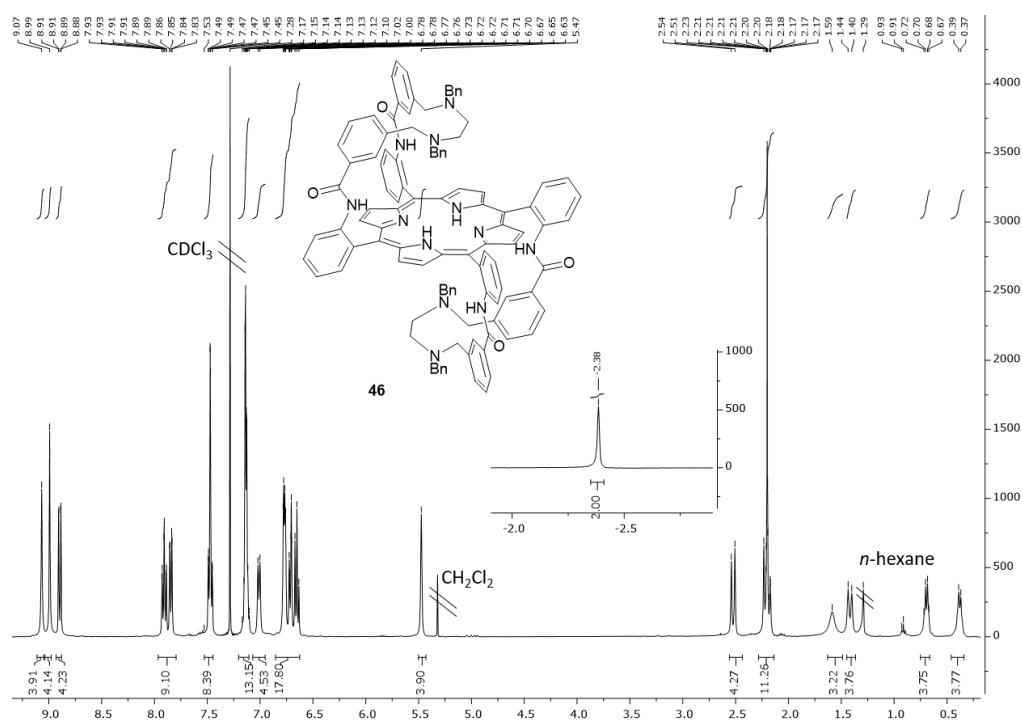
$^1\text{H NMR}$ (300 MHz, CDCl_3): δ 7.34 (d, 2H, $J = 8.5$ Hz, H_{Ar}), 7.05 (d, 2H, $J = 8.4$ Hz, H_{Ar}), 4.21 (q, 2H, $J = 7.1$ Hz, $\text{H}_{\text{CH}_2\text{Et}}$), 2.55 – 2.49 (m, 1H, H^1), 1.91 – 1.88 (m, 1H, H^2), 1.64 – 1.61 (m, 1H, H^3), 1.33 (s, 9H, H_{tBu}), 1.29 (t, $J = 7.1$ Hz, 3H, $\text{H}_{\text{CH}_3\text{Et}}$), 1.32 – 1.28 (m, 1H, H^3).

4.4.6. Synthesis of *trans*-ethyl 2-(4-methoxyphenyl)cyclopropanecarboxylate (54)

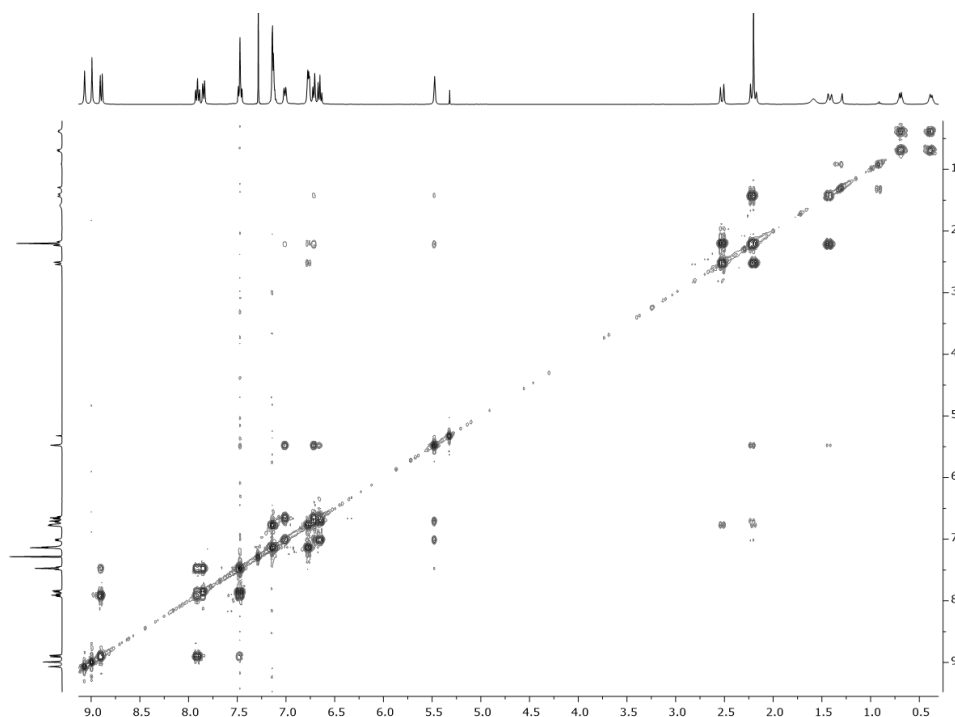


The general catalytic procedure for the synthesis of cyclopropanes was followed using 4-methoxystyrene and EDA. The collected analytical data are in accordance with those reported in literature²¹.

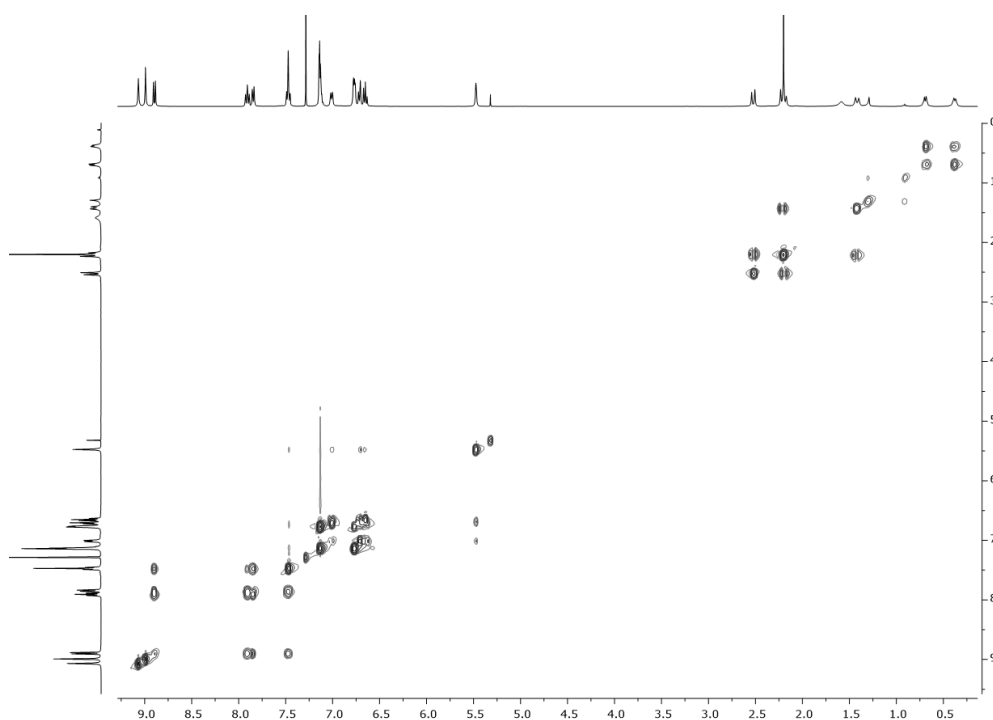
$^1\text{H NMR}$ (300 MHz, CDCl_3): δ 7.02 (d, 2H, $J = 8.7$ Hz, H_{Ar}), 6.80 (d, 2H, $J = 8.7$ Hz, H_{Ar}), 4.15 (q, 2H, $J = 7.1$ Hz, $\text{H}_{\text{CH}_2\text{Et}}$), 3.78 (s, 3H, H_{OMe}), 2.50 – 2.44 (m, 1H, H^1), 1.82 – 1.80 (m, 1H, H^2), 1.64 – 1.53 (m, 1H, H^3), 1.27 (t, $J = 7.1$ Hz, 3H, $\text{H}_{\text{CH}_3\text{Et}}$), 1.28 – 1.25 (m, 1H, H^3).

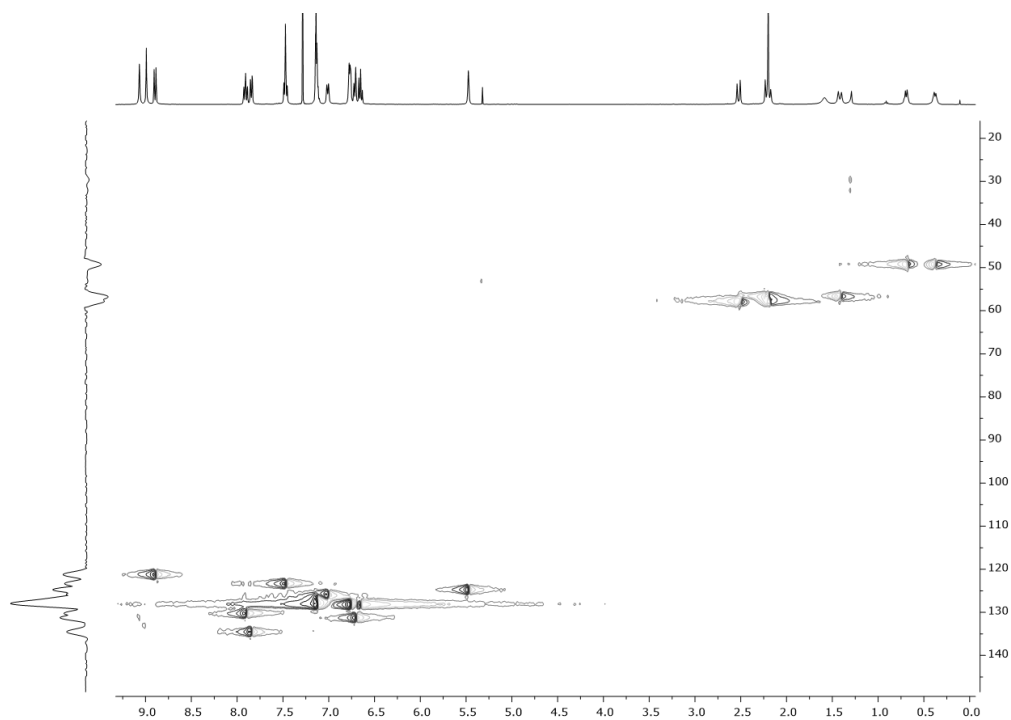
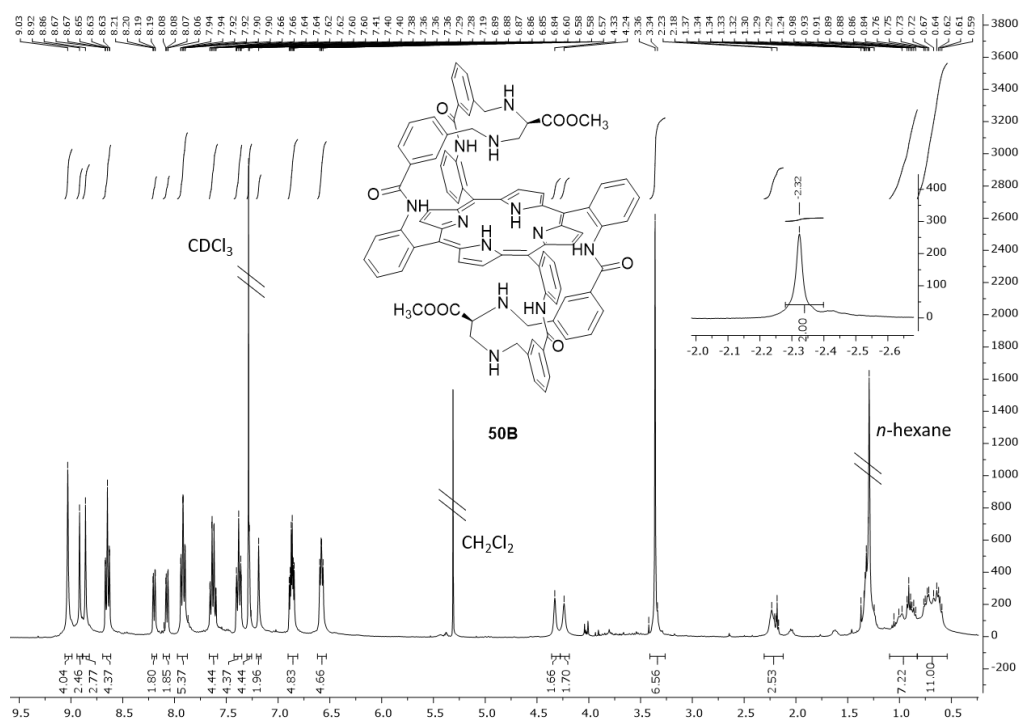
4.5. ^1H -NMR and 2D NMR of isolated compounds ^1H NMR spectrum (400 MHz, CDCl_3 , 298 K) of 48 ^1H NMR spectrum (400 MHz, CDCl_3 , 298 K) of porphyrin 46

COSY 2D NMR spectrum (400 MHz, CDCl₃, 298 K) of porphyrin 46

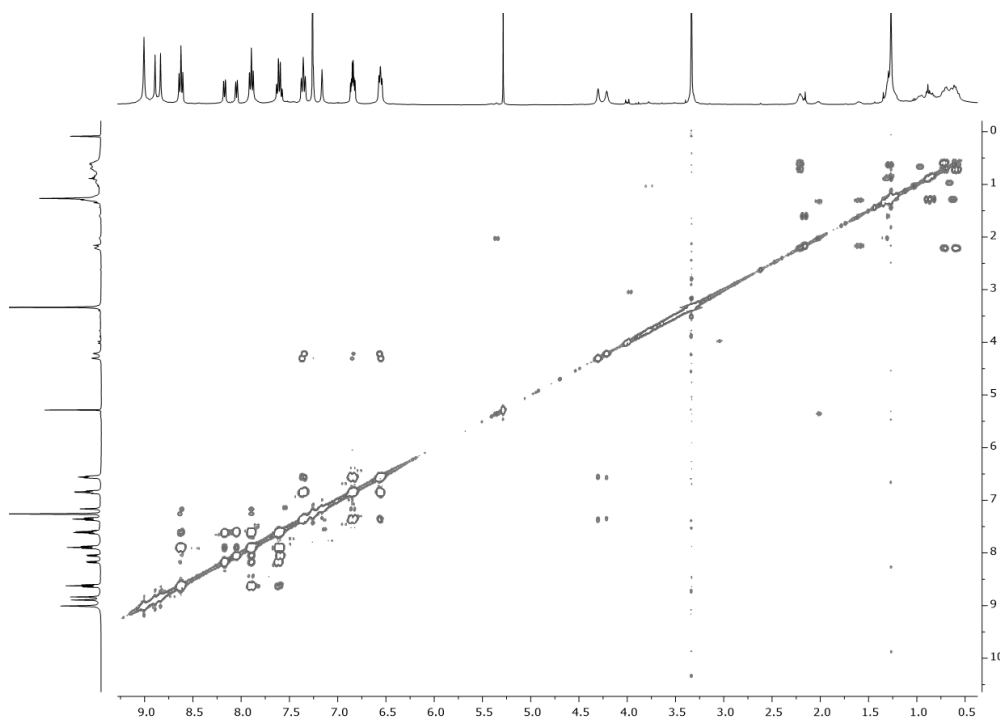


TOCSY 2D NMR spectrum (400 MHz, CDCl₃, 298 K) of porphyrin 46

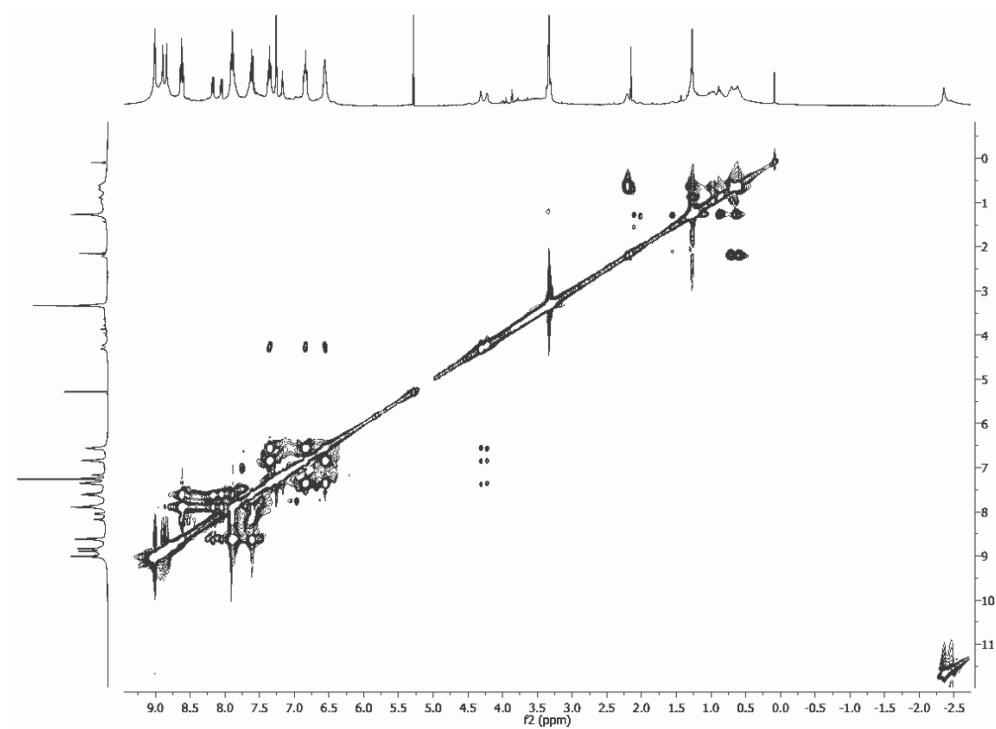


HSQC 2D NMR spectrum (400 MHz, CDCl₃, 298 K) of porphyrin 46¹H NMR spectrum (400 MHz, CDCl₃, 298 K) of porphyrin 50B

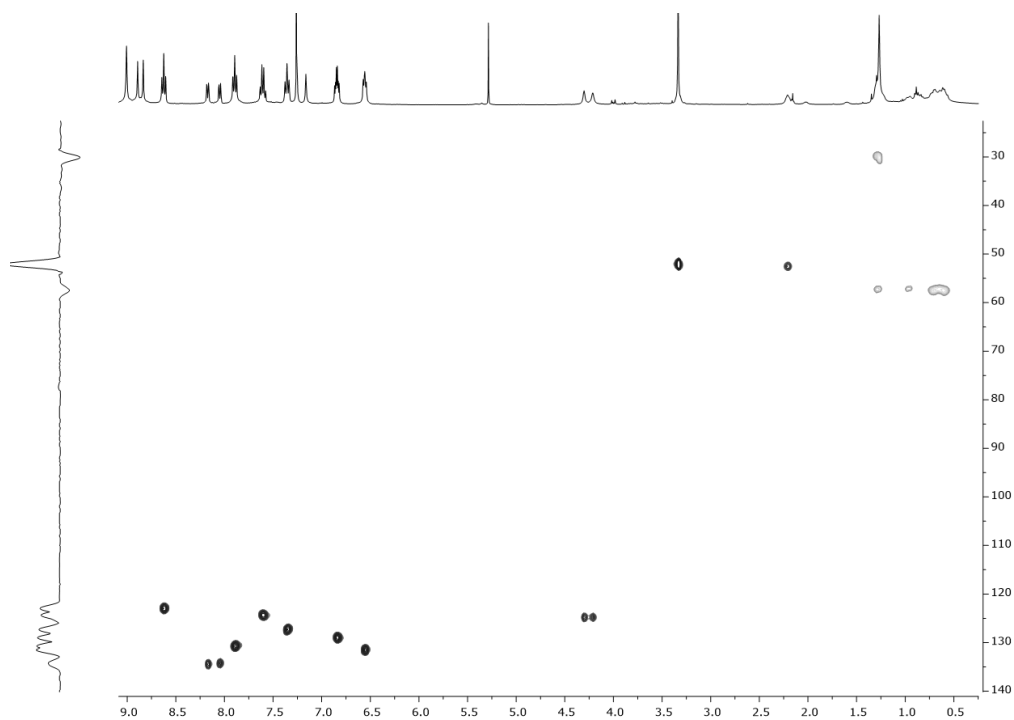
COSY 2D NMR spectrum (400 MHz, CDCl₃, 298 K) of porphyrin 50B



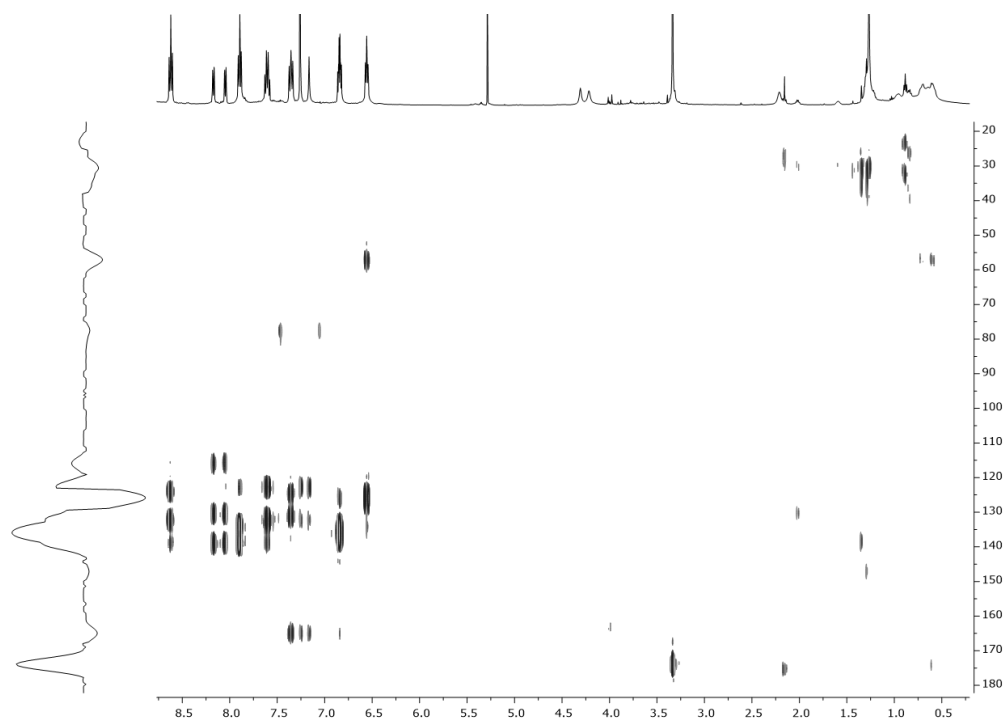
TOCSY 2D NMR spectrum (400 MHz, CDCl₃, 298 K) of porphyrin 50B



HSQC 2D NMR spectrum (400 MHz, CDCl₃, 298 K) of porphyrin 50B



HMBC 2D NMR spectrum (400 MHz, CDCl₃, 298 K) of porphyrin 50B

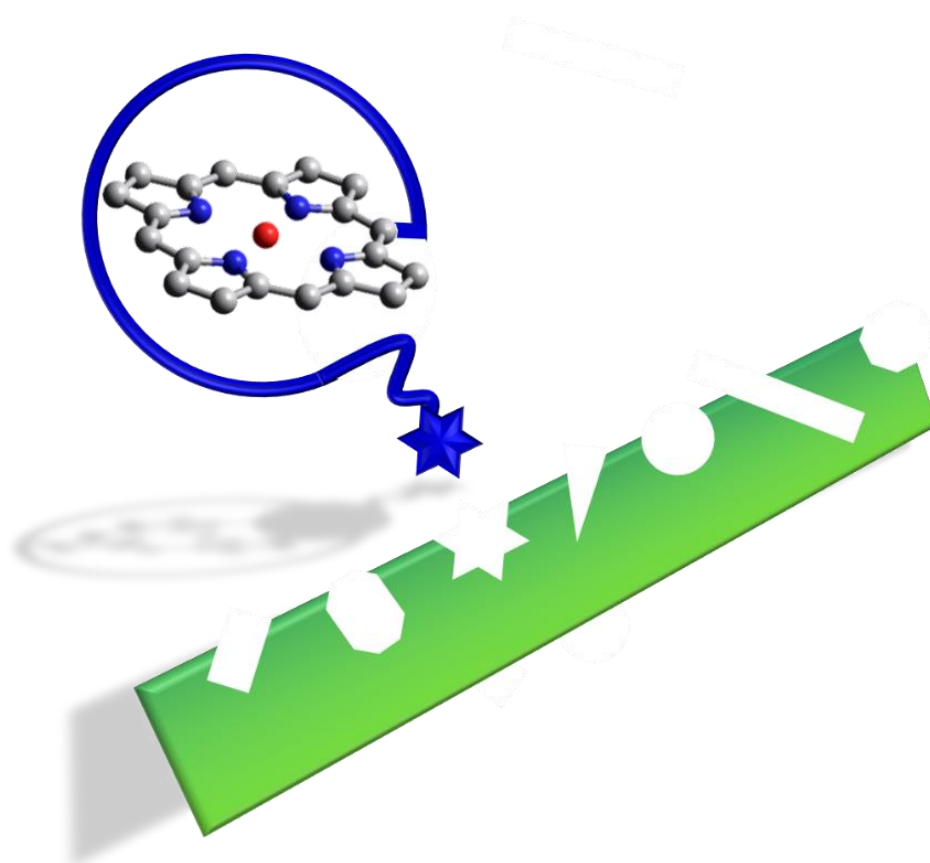


5. References

- (1) Lombardi, A.; Nastri, F.; Marasco, D.; Maglio, O.; De Sanctis, G.; Sinibaldi, F.; Santucci, R.; Coletta, M.; Pavone, V. *Chem. – A Eur. J.* **2003**, *9* (22), 5643–5654.
- (2) Kovaric, B. C.; Kokona, B.; Schwab, A. D.; Twomey, M. A.; de Paula, J. C.; Fairman, R. *J. Am. Chem. Soc.* **2006**, *128* (13), 4166–4167.
- (3) Giuntini, F.; Alonso, C. M. A.; Boyle, R. W. *Photochem. Photobiol. Sci.* **2011**, *10* (5), 759–791.
- (4) Biscaglia, F.; Gobbo, M. *Pept. Sci.* **2018**, *110* (5), e24038.
- (5) Perez-Rizquez, C.; Rodriguez-Otero, A.; Palomo, J. M. *Org. Biomol. Chem.* **2019**, *17* (30), 7114–7123.
- (6) Rose, E.; Lecas, A.; Quelquejeu, M.; Kossanyi, A.; Boitrel, B. *Coord. Chem. Rev.* **1998**, *178–180*, 1407–1431.
- (7) Tomé, A. C.; Silva, A. M. S.; Alkorta, I.; Elguero, J. *J. Porphyr. Phthalocyanines* **2011**, *15* (01), 1–28.
- (8) Collman, J. P.; Gagne, R. R.; Reed, C.; Halbert, T. R.; Lang, G.; Robinson, W. T. *J. Am. Chem. Soc.* **1975**, *97* (6), 1427–1439.
- (9) Collman, J. P.; Zhang, X.; Wong, K.; Brauman, J. I. *J. Am. Chem. Soc.* **1994**, *116* (14), 6245–6251.
- (10) Collman, J. P.; Zhang, X.; Hembre, R. T.; Brauman, J. I. *J. Am. Chem. Soc.* **1990**, *112* (13), 5356–5357.
- (11) Intrieri, D.; Carminati, D. M.; Gallo, E. *Dalt. Trans.* **2016**, *45* (40), 15746–15761.
- (12) Simonneaux, G.; Le Maux, P. *Coord. Chem. Rev.* **2002**, *228* (1), 43–60.
- (13) Zhang, R.; Yu, W.; Sun, H.; Liu, W.; Che, C. *Chem. Eur. J.* **2002**, *8* (11), 2495–2507.
- (14) Maxwell, J. L.; O'Malley, S.; Brown, K. C.; Kodadek, T. *Organometallics* **1992**, *11* (2), 645–652.
- (15) O'Malley, S.; Kodadek, T. *Organometallics* **1992**, *11* (6), 2299–2302.
- (16) Du, G.; Andrioletti, B.; Rose, E.; Woo, L. K. *Organometallics* **2002**, *21* (21), 4490–4495.
- (17) Rose, E.; Ren, Q.-Z.; Andrioletti, B. *Chem. – A Eur. J.* **2004**, *10* (1), 224–230.
- (18) Fantauzzi, S.; Gallo, E.; Rose, E.; Raoul, N.; Caselli, A.; Issa, S.; Ragaini, F.; Cenini, S. *Organometallics* **2008**, *27* (23), 6143–6151.
- (19) Gallo, E.; Rose, E.; Boitrel, B.; Legnani, L.; Toma, L. *Organometallics* **2014**, *33* (21), 6081–6088.
- (20) Intrieri, D.; Le Gac, S.; Caselli, A.; Rose, E.; Boitrel, B.; Gallo, E. *Chem. Commun.* **2014**, *50* (15), 1811–1813.
- (21) Carminati, D. M.; Intrieri, D.; Caselli, A.; Le Gac, S.; Boitrel, B.; Toma, L.; Legnani, L.; Gallo, E. *Chem. Eur. J.* **2016**, *22* (38), 13599–13612.
- (22) Carminati, D. M.; Intrieri, D.; Le Gac, S.; Roisnel, T.; Boitrel, B.; Toma, L.; Legnani, L.; Gallo, E. *New J. Chem.* **2017**, *41* (13), 5950–5959.
- (23) Dowlati, B.; Othman, M. R.; Ahmad, A.; Safaei, E. *New J. Chem.* **2016**, *40* (6), 5121–5127.
- (24) Alsibai, W.; Hahnenkamp, A.; Eisenblätter, M.; Riemann, B.; Schäfers, M.; Bremer, C.; Haufe, G.; Hölte, C. *J. Med. Chem.* **2014**, *57* (23), 9971–9982.

- (25) Didier, A.; Michaudet, L.; Ricard, D.; Baveux-Chambenoît, V.; Richard, P.; Boitrel, B. *European J. Org. Chem.* **2001**, 2001 (10), 1926–1927.
- (26) Chen, Y.; Zhang, X. P. *J. Org. Chem.* **2004**, 69 (7), 2431–2435.
- (27) Sreenilayam, G.; Moore, E. J.; Steck, V.; Fasan, R. *ACS Catal.* **2017**, 7 (11), 7629–7633.

Chapter IV: Porphyrins for conjugation with macromolecules



1. Introduction

Hybrid systems derived from the conjugation of organometallic complexes and bio-macromolecules represent one of the most interesting approaches to realise efficient catalytic systems that are able to promote chemical processes in sustainable way. Depending on the biosystem, the catalytic process can be performed under homogeneous or heterogeneous conditions. Both approaches can improve the process sustainability avoiding, in the first, case the use of toxic solvents or ensuring the catalyst recover/reuse in the second one. In fact, the use of protein scaffolds as hosts for unnatural organometallic complexes can combine the protein properties (water solubility and chirality) with the high catalytic activity of synthetic catalysts. Instead, the conjugation of metal active species with solid bio-supports can make the realization of bio-compatible heterogeneous systems possible. These ones should be able to combine the advantages of both homogeneous and heterogeneous catalysis. Choosing natural macromolecules which are usually defined as biomass, the process sustainability can be improved not only for the catalytic application of hybrid systems, but also for their synthesis. In this context, β -lactoglobulin proteins and bio-cellulose represent the best candidates for the development of bio-inspired water soluble or heterogeneous catalysts.

1.1. B-lactoglobulines as host proteins

B-lactoglobulins (β -LG)¹⁻³ are small whey proteins derived from milk processing. They are present in the milk of ruminants, non-ruminants and marsupials but they are absent in humans.

β -LG proteins can be found in several genetic variants and the most common ones are the A and B types. Both variants contain 162 amino acids, in which four cysteine (Cys) residues are involved in the formation of disulphide bonds and the only free cysteine (Cys121) is considered a potential site for chemical modification. The two β -LG variants differ for the aminoacidic residues located in positions 64 and 118. β -LG A has an aspartic acid residue in position 64 and a valine residue at position 118, while variant B has glycine and alanine in these positions, respectively.

The aminoacidic sequence of β -LG fold up into 8-stranded, antiparallel β -barrel with a 3-turn α -helix on the outer surface and a ninth β -strand flanking the first strand. The β -barrel structure, usually called calyx, is a conical motif in which one sheet is formed by the A-D β -strands and the second one is formed by the E-H strands. All the β -strands are connected by different types of loops. Short loops connect the strands at the closed end of the calyx; longer and more flexible loops are instead located on the open end (Figure 1). The central cavity of the calyx arrangement represents the protein binding site. The access to this site is driven by the loops conformation. In particular, the EF loop acts as a gate over the binding site. At low pH, it is in a “closed” conformation which inhibits the molecule binding. On the contrary, at high pH it is “open” and permits the ligand penetration into the hydrophobic channel.

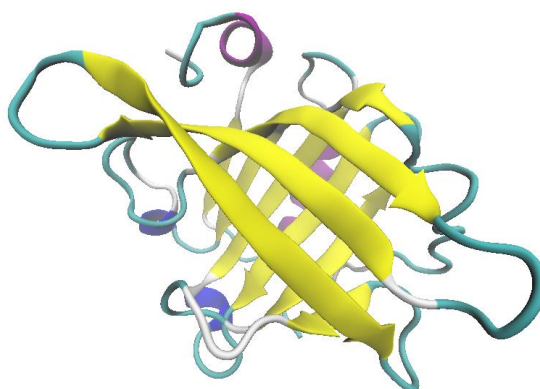


Figure 1: β -lactoglobulin protein (PDB: 3BLG)

Extensive studies were performed on the structural and physicochemical properties of β -LGs but the proteins biological function still seems to be unclear. Data reported up to now show that β -LGs are involved in the hydrophobic nutrients transport because of their ability to bind molecule like retinol⁴, vitamin D^{5,6}, fatty acids^{3,4}, phenolic compounds⁷ and cholesterol⁶. The hydrophobic channel and the Cys121 residue represent those two possible binding sites of β -LGs. Thus, the conjugation with organometallic complexes can be performed by following two different approaches, either thanks to the high number of hydrophobic interactions inside the channel or by a covalent bond with the changeable free Cys residue.

Very few examples on the use of these proteins as hosts for unnatural metal complexes are reported. Banse et al. reported the synthesis of an hybrid metalloenzyme derived from the covalent grafting of a nonheme Fe(II) polyazadentate complex on the β -LG protein⁸. The covalent linkage of the iron complex efficiently occurred and specifically at the Cys121 residue because of the presence of a pentadentate L_5^2 ligand functionalized with a maleimide group (**53**, figure 2). The so-obtained artificial metalloenzyme showed activity towards the oxidation of thioanisole by hydrogen peroxide yielding phenylmethylsulfoxide as the sole product with an enantiomeric excess up to 20 %. The investigation of the reaction mechanism, performed in absence of thioanisole, showed the formation of a high-spin $Fe^{III}(H_2O_2)$ intermediate which was identified as the active oxidizing species of the catalytic sulfoxidation reaction.

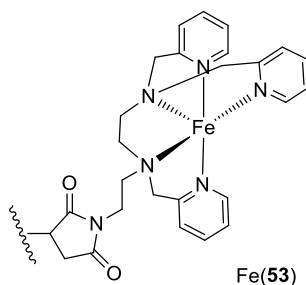


Figure 2: Fe(II) polyazadentate complex on the β -LG protein

Using a different binding approach, Salmain et al prepared a new hybrid metalloenzyme that was able to promote the asymmetric transfer hydrogenation of aryl ketones⁹. Preliminary studies were performed using organometallic complexes functionalized with several fatty acid moieties, which were suitable for the interaction with the β -LG hydrophobic channel (Figure 3).

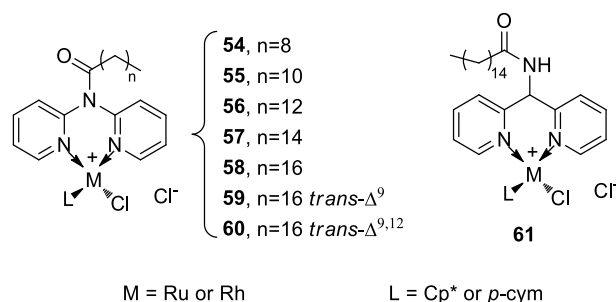


Figure 3: Ruthenium and rhodium complexes conjugated with β -LG

All the tested Ru/Rh complexes showed activity towards the activated aryl ketone-transfer hydrogenation in neat water using formate as the hydrogen source. Even if different efficiencies were obtained according to the metal, the fatty acid length and the catalyst structure, all the complexes preferentially promoted the formation of the (*R*)-enantiomer. The best result in terms of enantioselectivity (32% *ee*) was obtained by employing the **58** rhodium complex which shows a cyclopentadienyl (Cp*) as the ancillary ligand. The promising results prompt the authors to study the activity of hybrid β -LG metalloenzymes modified with half-sandwich organometallic complexes (Figure 4)¹⁰.

The synthesised bio-hybrid catalysts promoted the aryl ketones-asymmetric transfer hydrogenation in water at a much faster rate than that observed by using the complexes alone. Full conversions of the starting materials were observed, the desired products were obtained in good yields and with an *ee* of 86 % using the most selective bio-hybrid **62**. In addition, the authors pointed out the fundamental role of the histidine residue (His146), which was probably involved in the coordination and activation of the ruthenium-bio-hybrid-complex.

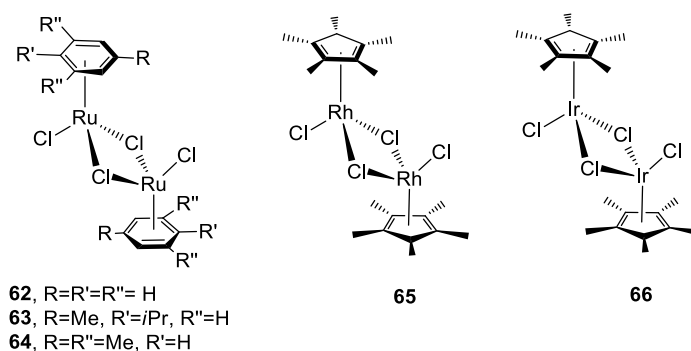


Figure 4: Half sandwich complexes conjugated with β -LG

The above-mentioned examples of β -LG proteins used as bio-scaffolds for asymmetric catalysis confirm the promising future of these proteins as starting materials for the development of new and efficient artificial metalloenzymes for catalytic applications.

1.2. Bio-cellulose as solid support

The employment of heterogeneous systems for catalytic applications may solve problems relating to homogeneous catalysts, which are usually due to difficulties in the catalyst recycling and the final product separation. Even if heterogeneous catalysts present a higher chemical stability than homogeneous ones, the lower catalytic activity and higher reaction temperatures required often represent an obstacle for their large application.

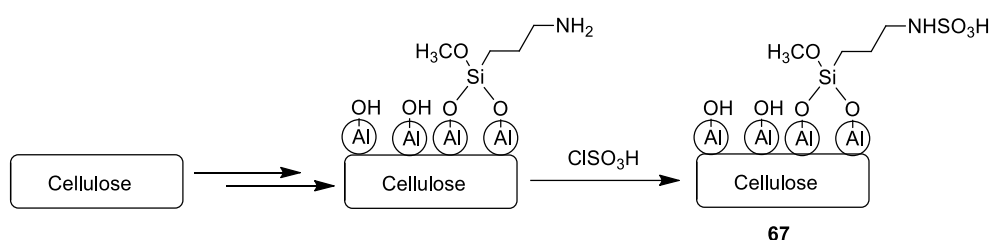
To overcome these impediments, the best choice can be the combination of the efficiency of homogenous systems with the heterogenous ones advantages by anchoring homogenous catalysts onto solid eco-compatible supports.

Few examples are reported about homogenous systems covalently anchored on naturally abundant, cheap, chemically and mechanically high stable solid supports¹¹⁻¹⁴. Thus, the scientific community is continuously working on developing new bio-renewable functional materials, which can ensure a better sustainability to the entire process. Regarding this aspect, bio-cellulose is one of the most interesting resources due to its wide natural abundance, biocompatibility, nontoxicity, reactivity, and low-cost¹⁵. The unique well-defined structure¹⁶ and the presence of primary and secondary alcohol functions, with different reactivity, make cellulose an essential support that can be modified by introducing organocatalysts or metal complexes.

Cellulose has been used in several applications fields¹⁷⁻²⁰, including packaging, construction, materials, cosmetics and clothing. It is extensively used as solid support for the development of medical equipment but its use as heterogenous catalyst has been still limited. Even if the main emphasis is on the use of cellulose nanocrystals as substrate for metal containing nano-catalysts, some examples of the

immobilization of active catalytic species on the cellulose surface are reported and few of them concern the covalent anchoring of active catalysts.

In 2017, Helavi et al reported the synthesis of organocatalytic active species anchored on functionalised cellulose²¹. The heterogenous catalyst was prepared grafting chlorosulfonic acid on the amino-functionalised surface of cellulose (Scheme 1). The hybrid organocatalytic system **67** showed high activity in the synthesis of several symmetrical and unsymmetrical 1,4-dihydropyridines (1,4-DHPs). High conversions, short reaction times and very good yields were obtained under sustainable experimental conditions. The robustness and reusability of the heterogenous system were confirmed reusing the catalyst for three times without a significant decrease in the desired product yield.



Scheme 1: Sulphamic acid anchored on cellulose

In the same year, Sarkar et al. tested the cellulose as solid support for transition metal catalysts¹¹. They reported the synthesis of a supported *poly*-(amidoxime) Pd(II) complex that was able to promote the Mizoroki-Heck reaction. The obtained heterogenous catalyst **68** (Figure 5) efficiently promoted the Mizoroki-Heck coupling reaction of activated and inactivated aryl halides and arenediazonium tetrafluoroborate salts with a variety of alkenes. The supported Pd(II) complex was also recycled for several successive catalytic cycles without a significant decrease in catalytic performances.

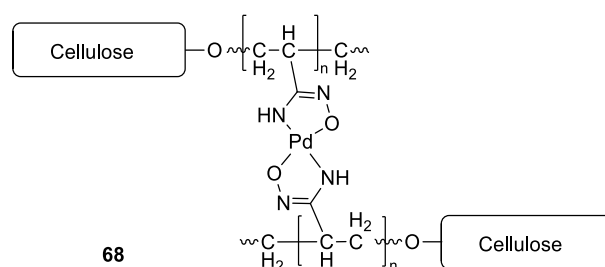
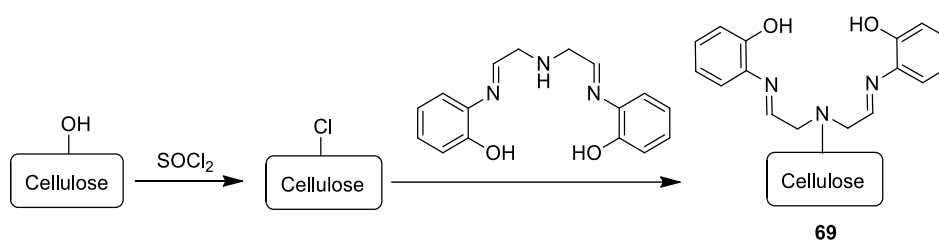


Figure 5: Cellulose supported *poly*-(amidoxime) Pd(II) complex

Both examples show the applicability of cellulose as solid support after the surface modification with functional groups and spacers suitable for the anchoring of active species. These modifications usually require long synthetic procedures depending on the desired final structure and rigidity.

Cellulose-supported catalysts, that don't need specific spacers or structural reinforcements, can be easily obtained as reported by Jia et al.¹³. They synthesised a metal-free cellulose based Schiff-base heterogeneous catalyst (**69**) with the substitution of cellulose hydroxylic groups with chloride atoms which reacted with the desired ligand (Scheme 2) yielding the active material. The heterogeneous material was applied as catalyst for the synthesis of cyclic carbonates by carbon dioxide cycloaddition to epoxides. The heterogeneous catalyst showed high reactivity towards a series of epoxides and it was effectively reused for five consequent runs without a significant loss in the catalytic activity.



Scheme 2: Cellulose supported Schiff-base ligand

The above-mentioned examples confirm the cellulose potentialities as a solid support for catalytic applications in order to combine homogeneous catalysts efficiency with the recyclability of heterogeneous ones.

1.3. A₃B-type porphyrins

Metal porphyrin complexes are remarkably able to promote catalytic transformations with high regio- and stereoselectivities. Thus, they are suitable candidates for the development of bio-inspired and solid supported catalysts for sustainable applications. Among all the porphyrin ligands, A₃B-type porphyrins are the most interesting species to design hybrid catalysts derived from β -LGs and cellulose. The chosen bio-scaffold structures require that the designed ligand has at least one functional group able to react with the cellulose surface or able to interact with the hydrophobic channel of β -LG. A₃B-type porphyrins satisfy this request because of the presence both of one catalytically active component and one adjustable linker that can be modified as needed (Figure 6).

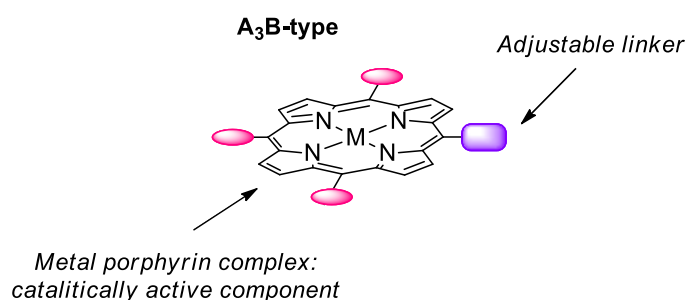
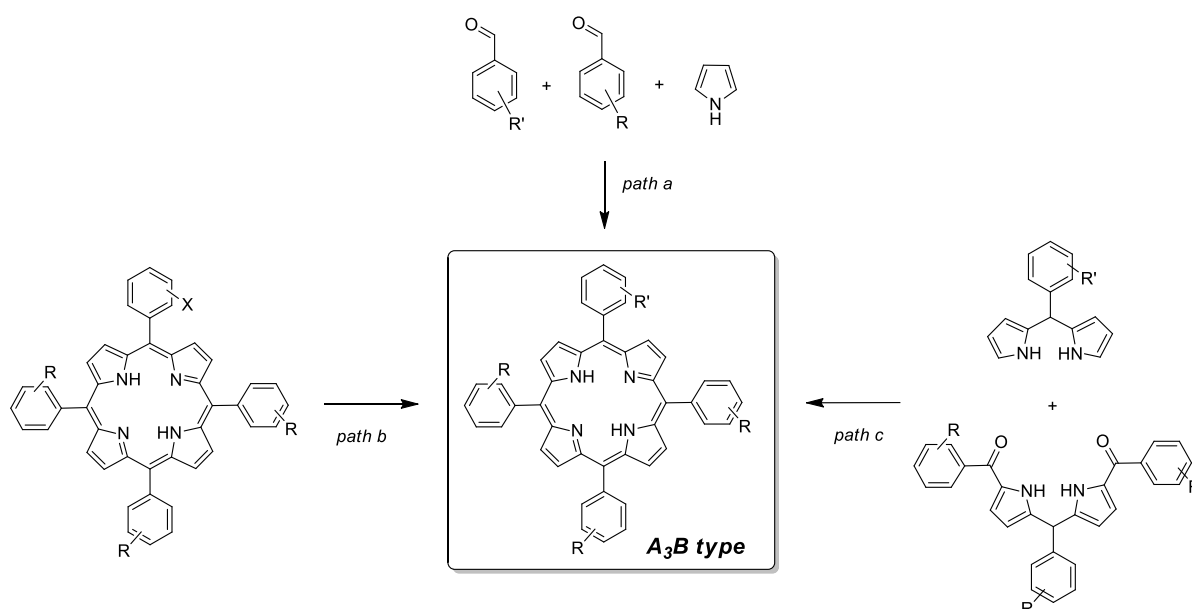


Figure 6: A₃B-type porphyrins

The synthetic strategy of *mono-meso*-substituted porphyrins depends on different substituents pattern²²⁻²⁴. The routes employed can be summarised in three typologies (Scheme 3) that become more elaborate as the number of different substituents increases.



Scheme 3: Approaches for the synthesis of A₃B-type porphyrins

The most known way for the synthesis of A₃B-porphyrins is the reaction of pyrrole and two opportunely functionalised aldehydes (*path a*, scheme 3). This procedure usually affords a statistical mixture of the possible substituted products which can be separated by chromatography. The lengthy purification step gives small quantities of the desired porphyrin. For these reasons this strategy is not often employed when the starting aldehydes are expensive or require long and difficult functionalization procedures. In this case an alternative approach could be the synthesis of structurally complex A₃B-porphyrins starting from *mono*-substituted ligands which can be easily synthesised (*path b*, scheme 3). *Mono*-substituted porphyrins, which show halogenated or amino moieties can be considered as ideal precursors for the

Chapter IV: Porphyrins for conjugation with macromolecules

introduction of different spacers by nucleophilic substitutions. The last possible strategy is the “2+2” route that requires the synthesis of two opportunely functionalised dipyrromethanes (*path c*, scheme 3). This approach usually affords the desired porphyrin in low yields which are however satisfactory when the target compounds are inaccessible by other means.

2. Discussion

Considering the applicability of cellulose and β -lactoglobulins as bio-scaffolds for the synthesis of sustainable hybrid catalysts, different A_3B -porphyrins suitable for the bio-conjugation were designed and synthesised. Preliminary studies were performed in the anchoring on cellulose and in the use of the corresponding iron (III) hybrid material as a heterogenous catalyst for cyclopropanation reactions.

2.1. Synthesis of A_3B -porphyrins

In order to develop metal porphyrin complexes supported on cellulose, different ligands containing reactive groups like fluoride (F_5TPPH_2), carboxylic (**70**) and amino groups (**71-72**) onto the *para* position of one phenyl ring of the porphyrin skeleton, were synthesised. Ligand **73** was designed and synthesised with a long aliphatic chain that can be accommodated inside the three-dimensional structure of β -lactoglobulin protein by hydrophobic interactions (Figure 7).

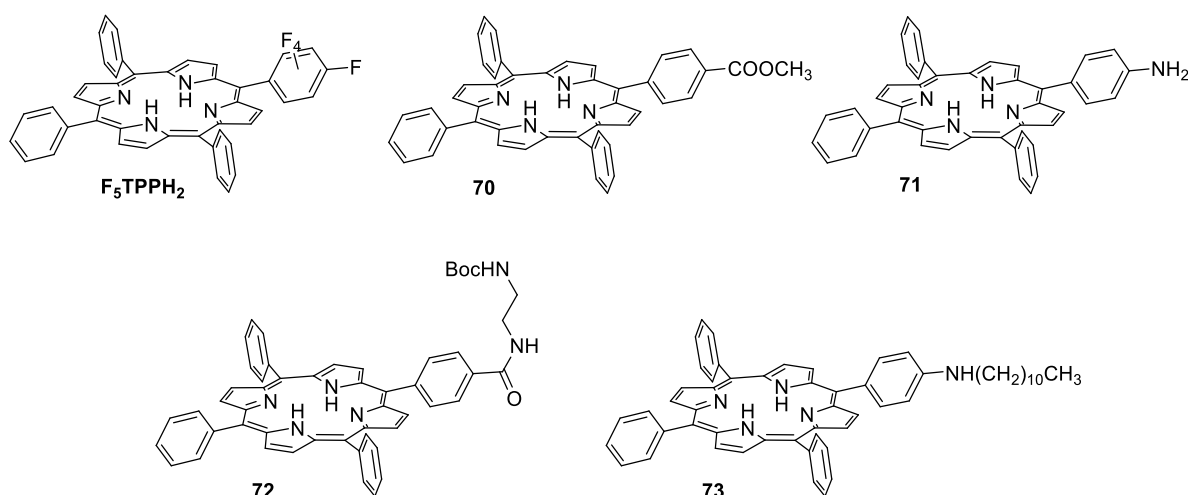
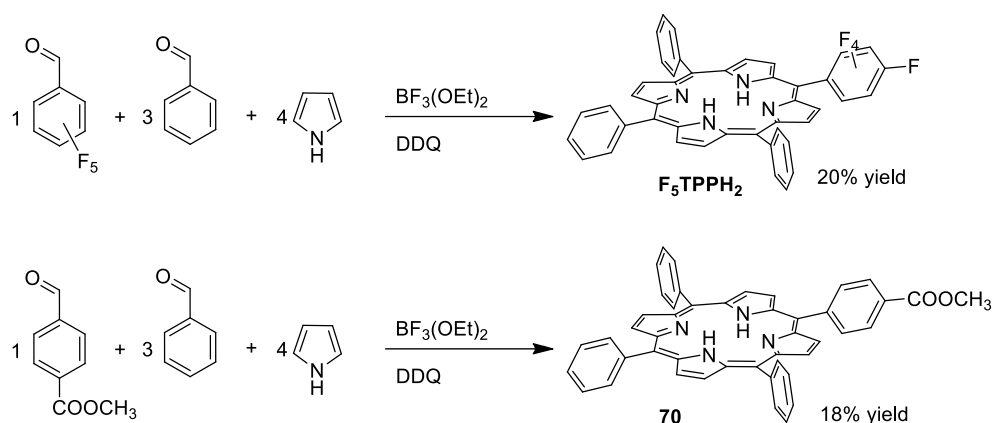


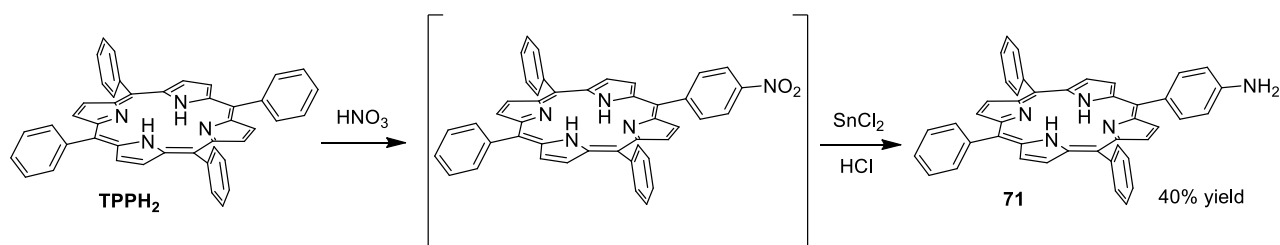
Figure 7: A_3B -type porphyrins synthesised

A_3B -type porphyrin ligands showed in figure 7 were synthesised adopting different synthetic strategies, depending on the introduced functional groups. F_5TPPH_2 and ligand **70** were synthesised adopting a typical Lindsay's methodology, reacting pyrrole with three equivalents of benzaldehyde and one of substituted benzaldehyde. The two ligands were purified by standard chromatographic techniques and they were obtained respectively in 20% and 18% of yield (Scheme 4).



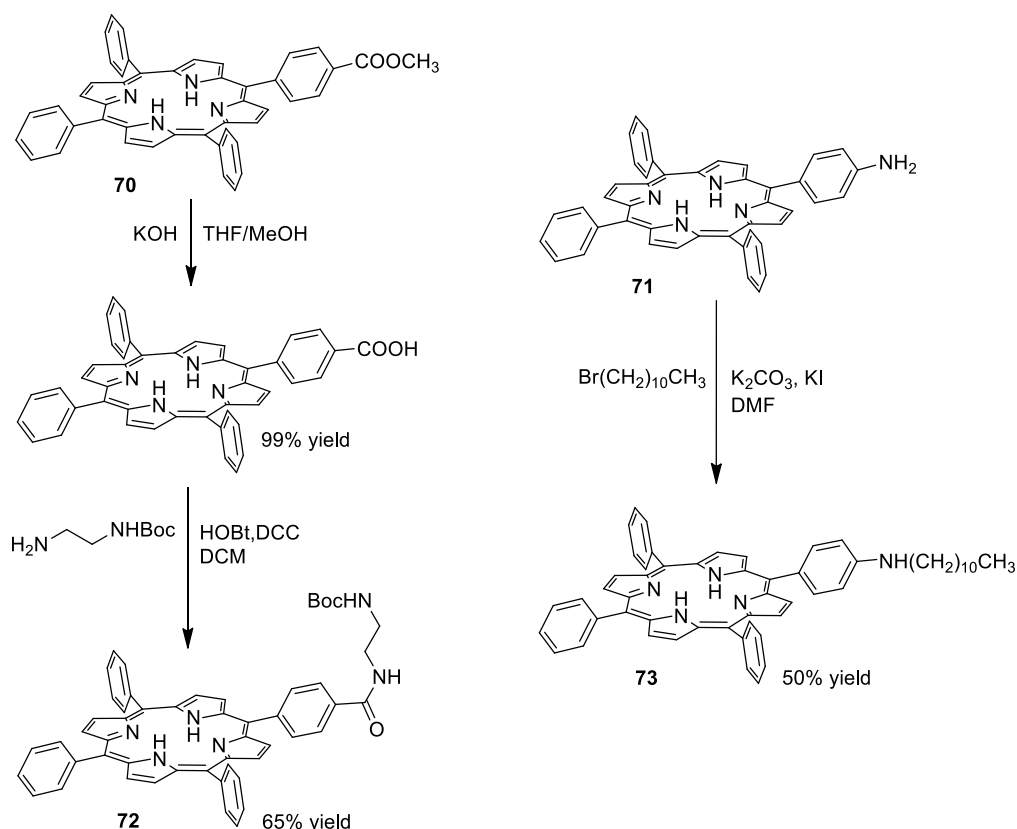
Scheme 4: Synthesis of **F₅TPPH₂** and **70**

A different approach was adopted in the case of the synthesis of porphyrin **71** which was obtained by *mono*-functionalization of the unsubstituted **TPPH₂** porphyrin. The slow addition of nitric acid to a **TPPH₂** solution was responsible for the *mono*-substitution of a hydrogen atom in *para* position of the phenyl ring with a nitro group. The so-formed *mono*-nitro intermediate was directly reduced in presence of tin(II) chloride and hydrochloric acid affording the desired ligand **71** in 40% yield (Scheme 5).



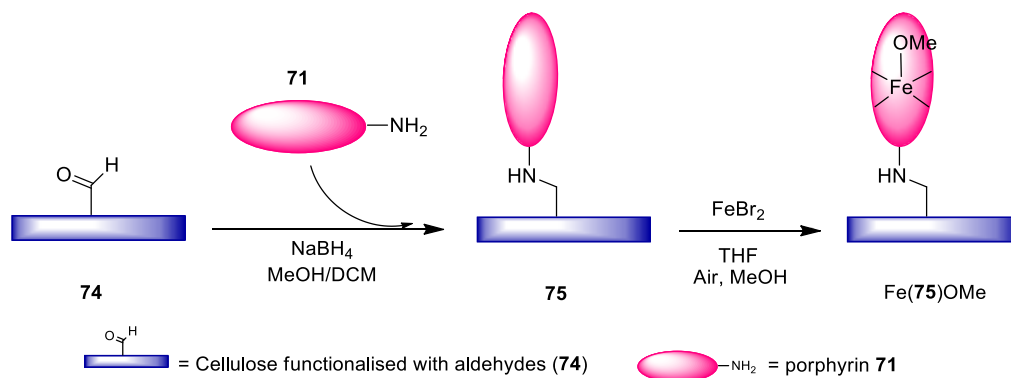
Scheme 5: Synthesis of ligand **71**

The last two *mono*-substituted porphyrins, **72** and **73**, were obtained by modifications of preformed A₃B precursors **70** and **71**. The carboxylic ester of ligand **70** was firstly deprotected in presence of potassium hydroxide giving the corresponding free acid in a quantitative yield. The so-formed porphyrin was reacted with a *mono*-protected ethylenediamine in the presence of condensing agents affording the desired porphyrin **72** in 65% yield. Ligand **73**, which shows a long aliphatic chain, was instead obtained in 50% yield by *N*-alkylation reaction of the amino functionality of porphyrin **71** (Scheme 6).

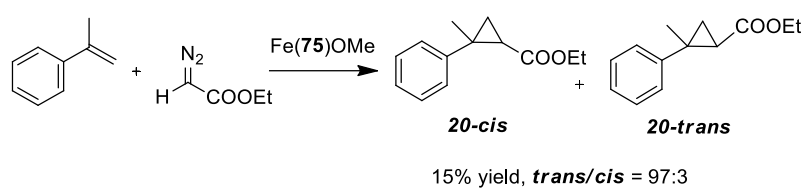


2.2. Preliminary studies with cellulose

Preliminary studies were performed for the conjugation of porphyrin **71** with a cellulose derivative functionalised with aldehyde groups (**74**). The conjugated material was obtained by a reductive amination reaction performed in the presence of sodium borohydride (NaBH_4). The cellulose-supported porphyrin **75** was washed several times with CH_2Cl_2 in order to remove the excesses of free ligand **71**. The obtained material **75** was directly refluxed in THF with an excess of FeBr_2 affording the corresponding iron(III) complex (Scheme 7).



The cellulose derivative **74** and the obtained heterogenous complex Fe(**75**)OMe were tested in the model cyclopropanation reaction between α -methylstyrene and EDA forming cyclopropane **20**. Collected data showed that the unsubstituted cellulose **74** was completely inactive in accordance with the absence of catalytic active species in its structure. On the other hand, Fe(**75**)OMe was able in promoting the synthesis of cyclopropane **20** in 15% yield with a *trans*-diastereoselectivity of 97:3 (Scheme 8). The promising result confirmed the iron porphyrin anchorage on the cellulose surface and suggested the potential use of the conjugated heterogeneous catalyst in cyclopropanation reactions.



Scheme 8: Synthesis **20** catalysed by Fe(**75**)OMe

3. Conclusion

In conclusion, the synthesis of several A₃B-porphyrins suitable for the conjugation with proteins and cellulose is reported. The preliminary studies on the synthesis of heterogenous bio-catalysts show the possibility to covalently anchor porphyrin ligands on the cellulose surface. The catalytic data established the ability of cellulose-supported iron (III) complex in promoting the α -methylstyrene cyclopropanation with a modest yield and very good diastereoselectivity. Future characterizations of the hybrid material could be useful to optimise the heterogenous catalyst structure and its catalytic performances.

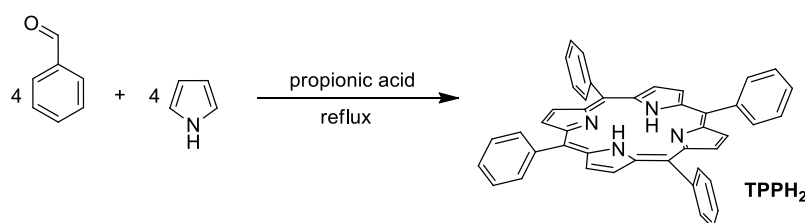
Considering the high activity of metal porphyrin complexes to promote carbene and nitrene transfer reactions, the obtained data represent a starting point to obtain a new generation of catalysts which can be employed for the synthesis of several fine chemicals through sustainable synthetic methodologies.

4. Experimental section

General conditions: Unless otherwise specified, all reactions were carried out under nitrogen atmosphere employing standard Schlenk techniques and vacuum-line manipulations. All the solvents were dried by using standard procedures and stored under nitrogen atmosphere. All the other starting materials were commercial products and used as received. NMR spectra were recorded at room temperature either on a Bruker Avance 300-DRX, operating at 300 MHz for ^1H , at 75 MHz for ^{13}C and at 282 MHz for ^{19}F , or on a Bruker Avance 400-DRX spectrometers, operating at 400 MHz for ^1H , 100 MHz for ^{13}C and 376 MHz for ^{19}F . Chemical shifts (ppm) are reported relative to TMS. The ^1H -NMR signals of the compounds described in the following were attributed by 2D NMR techniques. Assignments of the resonance in ^{13}C -NMR were made by using the APT pulse sequence, HSQC and HMBC techniques. Infrared spectra were recorded on a Varian Scimitar FTS 1000 spectrophotometer. UV/Vis spectra were recorded on an Agilent 8453E instrument. MALDI-TOF spectra were acquired either on a Bruker Daltonics Microflex or on a Bruker Daltonics Autoflex III TOF/TOF at C.I.G.A, University of Milan. High resolution MS (HR-MS) spectra were obtained on a Bruker Daltonics ICR-FTMS APEX II at C.I.G.A, University of Milan. Microanalysis was performed on a Perkin Elmer 2400 CHN Elemental Analyzer instrument.

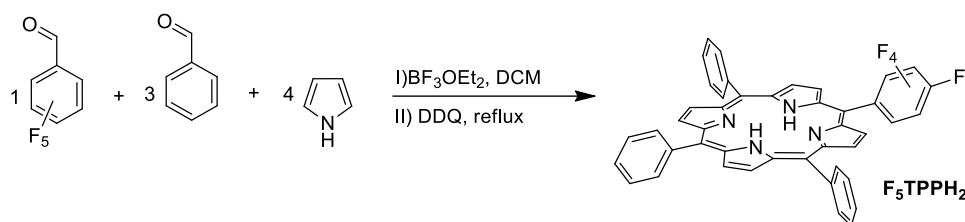
4.1. Synthesis of porphyrin ligands

4.1.1. Synthesis of TPPH₂



Benzaldehyde (36.5 mL, $3.60 \cdot 10^{-1}$ mol) was dissolved in propionic acid (500 mL) under air. The colourless mixture was heated to 50°C , then a solution of distilled pyrrole (25.0 mL, $3.60 \cdot 10^{-1}$ mol) in propionic acid (30.0 mL) was added dropwise in about 10 minutes. The resulting mixture was refluxed for 2 hours. During this period, the mixture turned to red at first, then to deep black. The reaction mixture was allowed to cool at RT and the formation of crystalline violet precipitate was observed. The dark suspension was filtered, washed with methanol (50.0 mL), water (50.0 mL) and again with methanol until the filtrate was clear. The crystalline purple solid was dried *in vacuo* (10.6 g, 19%). The collected analytical data are in accordance with those reported in literature.

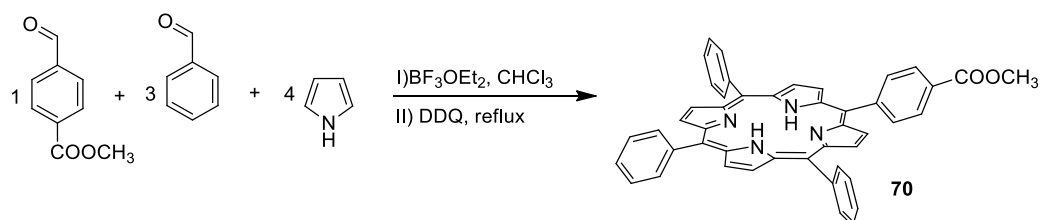
^1H NMR (300 MHz, CDCl_3): δ 8.86 (s, 8H, H_{pyrr}), 8.22 (m, 8H, H_{Ar}), 7.78 (m, 12H, H_{Ar}), -2.74 ppm (s, 2H, NH_{pyrr}).

4.1.2. Synthesis of F₅TPPH₂


Pentafluorobenzaldehyde (0.16 mL, 1.25×10^{-3} mol), benzaldehyde (0.38 mL, 3.75×10^{-3} mol) and pyrrole (0.35 mL, 5.00×10^{-3} mol) were dissolved in CH₂Cl₂ (0.40 L) and BF₃·Et₂O (0.63 mL, 5.00×10^{-4} mol) was added under nitrogen. The reaction was stirred at room temperature overnight and then 2,3-dichloro-5,6-dicyano-1,4-benzoquinone (DDQ) (0.56 mg, 2.51×10^{-3} mol) was added. The reaction mixture was refluxed for 12 hours. At the end of the reaction TEA was added and the solvent was evaporated to dryness. The crude was purified by flash chromatography (SiO₂, gradient elution from *n*-hexane to *n*-hexane/CH₂Cl₂ = 85:15) to yield a purple solid (180.0 mg, 21%). The collected analytical data are in accordance with those reported in literature²⁵.

¹H NMR (300 MHz, CDCl₃): δ 9.01 (d, *J* = 4.8 Hz, 2H, H_{βpyrr}), 8.92 (s, 4H, H_{βpyrr}), 8.85 (d, *J* = 4.6 Hz, 2H, H_{βpyrr}), 8.27 (m, 6H, H_{Ar}), 7.79 (m, 9H, H_{Ar}), -2.66 (s, 2H, NH_{pyrr}).

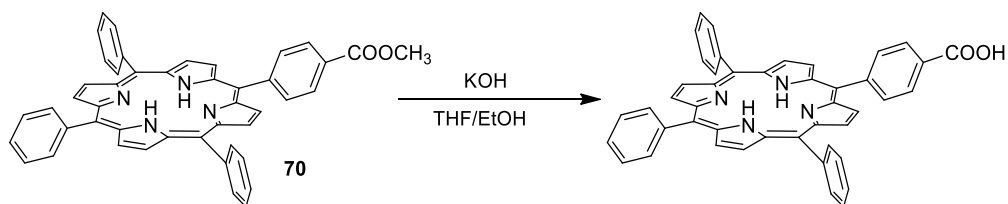
4.1.3. Synthesis of porphyrin 70



Methyl 4-formylbenzoate (206.0 mg, 1.25×10^{-3} mol), benzaldehyde (0.38 mL, 3.75×10^{-3} mol) and pyrrole (0.35 mL, 5.00×10^{-3} mol) were dissolved in CH₃Cl (0.50 L) and BF₃·Et₂O (0.63 mL, 5.00×10^{-4} mol) was added under nitrogen. The reaction was stirred at room temperature overnight and then 2,3-dichloro-5,6-dicyano-1,4-benzoquinone (DDQ) (0.56 mg, 2.51×10^{-3} mol) was added. The reaction mixture was refluxed for 2 hours. At the end of the reaction TEA was added and the solvent was evaporated to dryness. The crude was purified by flash chromatography (SiO₂, gradient elution from *n*-hexane to *n*-hexane/CH₂Cl₂ = 80:20) to yield a purple solid (120.0 mg, 16%). The collected analytical data are in accordance with those reported in literature²⁶.

¹H NMR (300 MHz, CDCl₃): δ 8.90 – 8.79 (m, 8H, H_{βpyrr}), 8.46 (d, *J* = 7.9 Hz, 2H, H_{Ar}), 8.33 (d, *J* = 7.9 Hz, 2H, H_{Ar}), 8.24 (dd, *J* = 7.4, 2.0 Hz, 6H, H_{Ar}), 7.79 (td, *J* = 8.0, 5.6 Hz, 9H, H_{Ar}), 4.14 (s, 3H, H_{OCH3}), -2.75 (s, 2H, NH_{pyrr}).

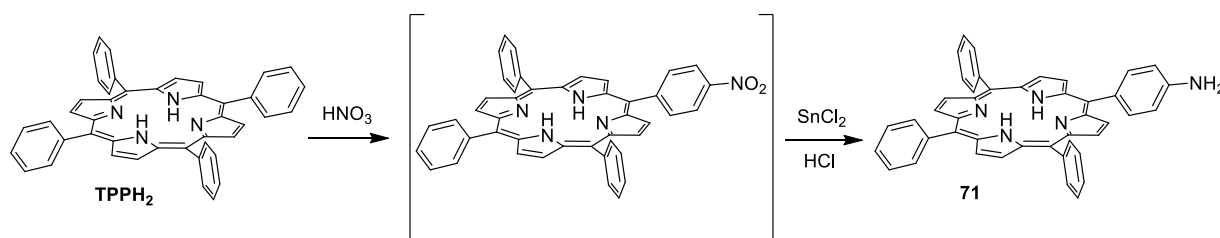
4.1.4. Deprotection of porphyrin 70



Porphyrin **70** (140.0 mg, 2.11×10^{-4} mol) was dissolved in THF (30.0 mL) and ethanol (15.0 mL) was added under nitrogen. Then, 20.0 mL of a KOH solution in water (2 M) was added and the mixture was stirred at room temperature overnight. At the end of the reaction the solvent was evaporated to dryness and a solution of HCl (1 M) was added dropwise until to pH = 7. CH_2Cl_2 was added and the organic phase was washed with water (3 x 30 mL), dried over Na_2SO_4 and filtered. The solvent was evaporated to dryness to yield a purple solid (120.0 mg, 99 %). The collected analytical data are in accordance with those reported in literature²⁷.

$^1\text{H NMR}$ (300 MHz, CDCl_3): δ 8.88 – 8.75 (m, 8H, $\text{H}_{\beta\text{pyrr}}$), 8.50 (d, $J = 7.9$ Hz, 2H, H_{Ar}), 8.30 (d, $J = 7.9$ Hz, 2H, H_{Ar}), 8.20 (dd, $J = 7.4, 2.0$ Hz, 6H, H_{Ar}), 7.80 (td, $J = 8.0, 5.6$ Hz, 9H, H_{Ar}), -2.73 (s, 2H, NH_{pyrr}).

4.1.5. Synthesis of porphyrin 71

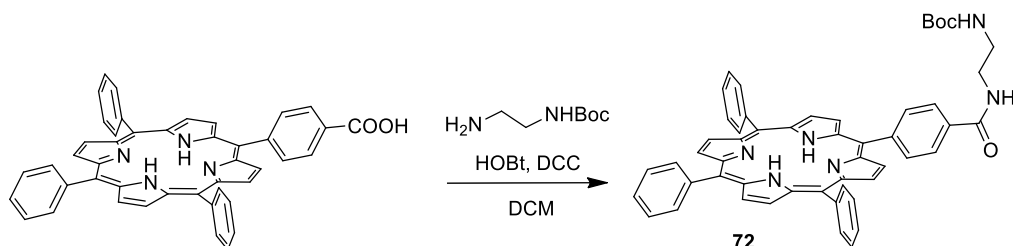


TPPH₂ (1.00 g, 1.63×10^{-3} mol) was dissolved in dry CH_2Cl_2 (150 mL). Nitric acid 65% (2.11 mL, 3.08×10^{-2} mol) was slowly added at 0°C , over a 2 h period. The reaction mixture was stirred until the complete consumption of the starting porphyrin was observed by TLC (SiO_2 , n -hexane/ CH_2Cl_2 = 50:50). The solution was washed with a saturated solution of NaHCO_3 (3×150 mL) and then with water (3×150 mL). The mixture was dried over Na_2SO_4 , filtered and the solvent was evaporated to dryness. Then, the crude was dissolved in HCl 37% (35.0 mL) and tin chloride (1 g, 5.25×10^{-3} mol) was added. The solution was refluxed for 12 hours. At the end of the reaction the mixture was neutralized by adding aqueous ammonia and washed with CH_2Cl_2 (5×150.0 mL), dried over Na_2SO_4 and filtered. The solvent was evaporated to dryness and the crude was purified by flash chromatography (SiO_2 , gradient elution from n -hexane/ CH_2Cl_2 = 80:20 to n -hexane/ CH_2Cl_2 = 20:80) to yield a purple solid (0.42 g, 40%).

$^1\text{H NMR}$ (300 MHz, CDCl_3 , 298 K) δ 8.93 (d, $J = 4.8$ Hz, 2H, $\text{H}_{\beta\text{pyrr}}$), 8.82 (s, 6H, $\text{H}_{\beta\text{pyrr}}$), 8.21 (d, $J = 7.6$ Hz, 6H, H_{Ar}), 7.98 (d, $J = 8.2$ Hz, 2H, H_{Ar}), 7.74 (d, $J = 6.2$ Hz, 9H, H_{Ar}), 7.03 (d, $J = 8.2$ Hz,

2H, H_{Ar}), 3.97 (s, 2H, NH), -2.75 (s, 2H, NH_{pyrr}). ¹³C NMR (75 MHz, CDCl₃, 298 K) δ 146.44, 142.71, 142.66, 136.03, 134.97, 132.81, 131.42, 128.06, 127.06, 121.31, 120.38, 120.14, 114.17, 113.85. **LR-MS** (ESI): m/z (C₄₄H₃₁N₅) calcd. 629.26; found [M+H]⁺ 630.98. **Elemental Analysis** calc. for C₄₄H₃₁N₅: C, 83.92; H, 4.96; N, 11.12; found: C, 83.08; H, 4.72; N, 10.86.

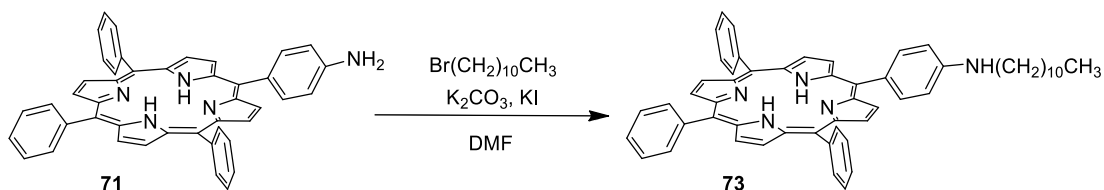
4.1.6. Synthesis of porphyrin 72



N-Boc-ethylenediamine (95.0 mg, 5.94 x 10⁻⁴ mol), HOBt (80.0 mg, 5.92 x 10⁻⁴ mol) and DCC (130.0 mg, 5.94 x 10⁻³ mmol) were added to a CH₂Cl₂ (140.0 mL) solution of the deprotected porphyrin (130.0 mg, 1.98 x 10⁻⁴ mol). The reaction was stirred at room temperature for 24 hours until the complete consumption of the starting porphyrin was observed by TLC (SiO₂, CH₂Cl₂/CH₃OH/TEA= 95:4:1). The solvent was evaporated to dryness and the crude was purified by flash chromatography (SiO₂, gradient elution from CH₂Cl₂/TEA= 99:1 to CH₂Cl₂/CH₃OH/TEA= 90:9:1) to yield a purple solid (90.0 mg, 65 %). The collected analytical data are in accordance with those reported in literature²⁷.

¹H NMR (400 MHz, CDCl₃, 298 K) δ 8.84 – 8.78 (m, 8H, H_{βpyrr}), 8.29 – 8.20 (m, 10H, H_{Ar}), 7.75 (s, 9H, H_{Ar}), 7.53 (s, 1H, NH), 5.07 (s, 1H, NH), 3.74 (s, 2H, H_{CH2}), 3.56 (s, 2H, H_{CH2}), 1.49 (s, 9H, H_{Boc}), -2.78 (s, 2H, NH_{pyrr}). **LR-MS** (ESI): m/z (C₅₂H₄₄N₆O₃) calcd. 800.35; found [M+H]⁺ 801.67

4.1.7. Synthesis of porphyrin 73

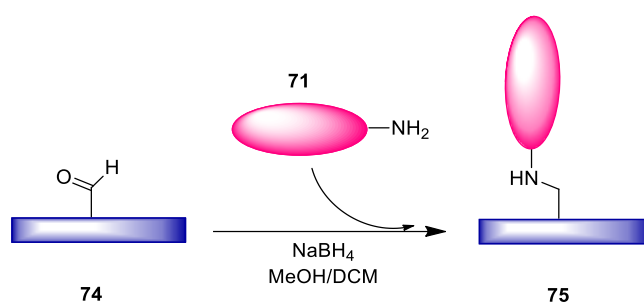


K₂CO₃ (352.0 mg, 2.21 x 10⁻³ mol), KI (423.0 mg, 2.23 x 10⁻³ mol) and 1-bromoundecane (0.57 mL, 2.24 x 10⁻³ mmol) were added to a DMF (140.0 mL) solution of porphyrin **71** (140.0 mg, 2.23 x 10⁻³ mol) under nitrogen. The reaction mixture was refluxed for 7 hours until the complete consumption of the starting porphyrin was observed by TLC (SiO₂, *n*-hexane/CH₂Cl₂= 50:50). The solvent was evaporated to dryness and the crude was dissolved with CH₂Cl₂ (50.0 mL) and washed with water (3 x 50.0 mL), dried over Na₂SO₄ and filtered. The solvent was evaporated to dryness and the crude was purified by flash chromatography (SiO₂, gradient elution from *n*-hexane to *n*-hexane/CH₂Cl₂= 50:50) to yield a purple solid (130.0 mg, 50 %).

¹H NMR (400 MHz, CDCl₃, 298 K) δ 9.06 (d, *J* = 4.8 Hz, 2H, H_{βpyrr}), 8.93 (s, 6H, H_{βpyrr}), 8.31 (dq, *J* = 8.1, 2.7 Hz, 6H, H_{Ar}), 8.15 – 8.01 (m, 2H, H_{Ar}), 7.81 (dd, *J* = 7.0, 2.9 Hz, 9H, H_{Ar}), 7.02 – 6.93 (m, 2H, H_{Ar}), 3.96 (s, 1H, NH), 3.37 (t, *J* = 7.1 Hz, 2H, H_{CH2}), 1.86 – 1.83 (m, 2H, H_{CH2}), 1.62 – 1.30 (m, 18H, H_{CH2}), 0.99 (t, *J* = 6.5 Hz, 3H, H_{CH3}), -2.59 (s, 2H, NH_{pyrr}). **¹³C NMR** (100 MHz, CDCl₃, 298 K) δ 148.15, 142.43, 135.92, 134.64, 127.69, 126.71, 121.49, 120.01, 119.66, 111.03, 111.03, 44.23, 29.79, 29.69, 29.66, 29.64, 14.22. **LR-MS** (ESI): *m/z* (C₅₅H₅₂N₅) calcd. 784.43; found [M+H]⁺ 784.54

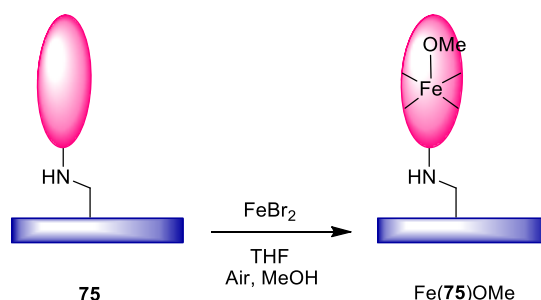
4.2. Synthesis of solid supported catalyst

4.2.1. Synthesis of solid supported porphyrin **75**



Cellulose **74** (100.0 mg) was suspended in CH₃OH (45.0 mL) and a solution of porphyrin **71** (50.0 mg, 7.51 × 10⁻⁵ mol) in CH₂Cl₂ (5.0 mL) was added under nitrogen. The mixture was stirred overnight at room temperature, then NaBH₄ (1.70 g, 7.51 × 10⁻⁵ mol) was slowly added at 0°C. The resulting suspension was stirred for five days at room temperature. At the end of the reaction the solid was filtered and washed with CH₂Cl₂ until to obtain a colourless solution. The obtained solid was dried *in vacuo* (100.0 mg) and used for the next step without further purification.

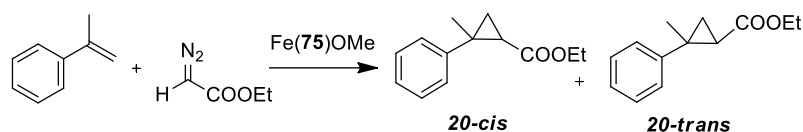
4.2.2. Synthesis of solid supported Fe(**75**)OMe



FeBr₂ (50.0 mg, 3.18 × 10⁻⁵ mol) was added to a THF (20.0 mL) suspension of **75** (50.0 mg) under nitrogen. The solution was refluxed at 75°C for 5 hours. At the end of the reaction the solid was filtered and washed with CH₃OH until to obtain a colourless solution. The obtained solid was dried *in vacuo* (50.0 mg) and used for the cyclopropanation reaction without further purification.

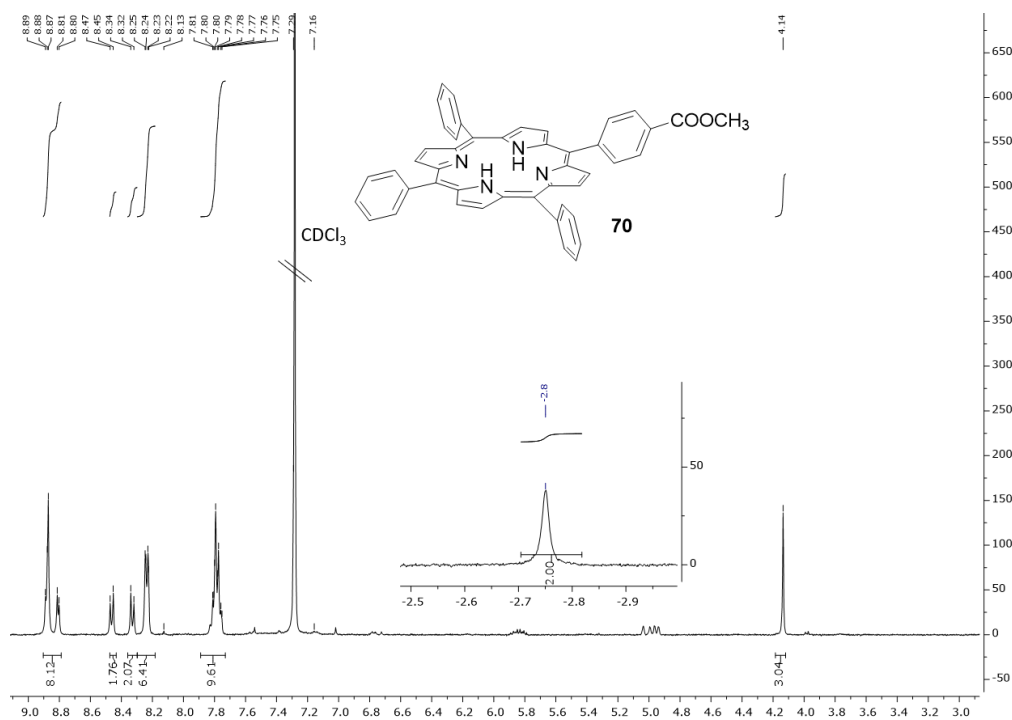
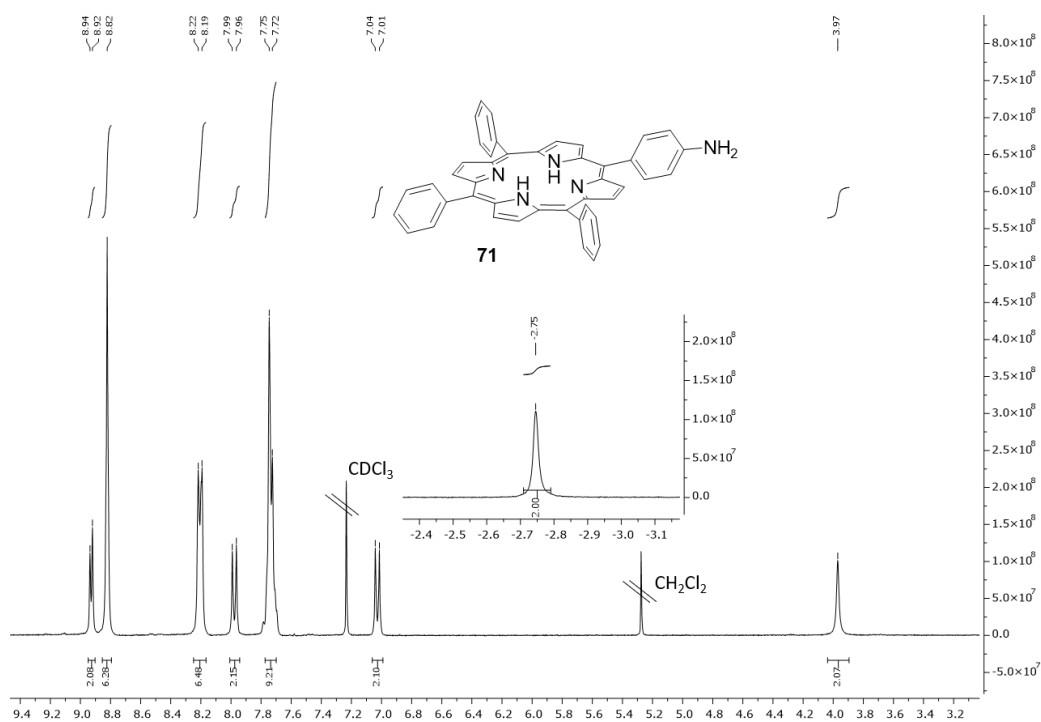
4.3. Synthesis of cyclopropane

Catalytic procedure for the synthesis of cyclopropane 20

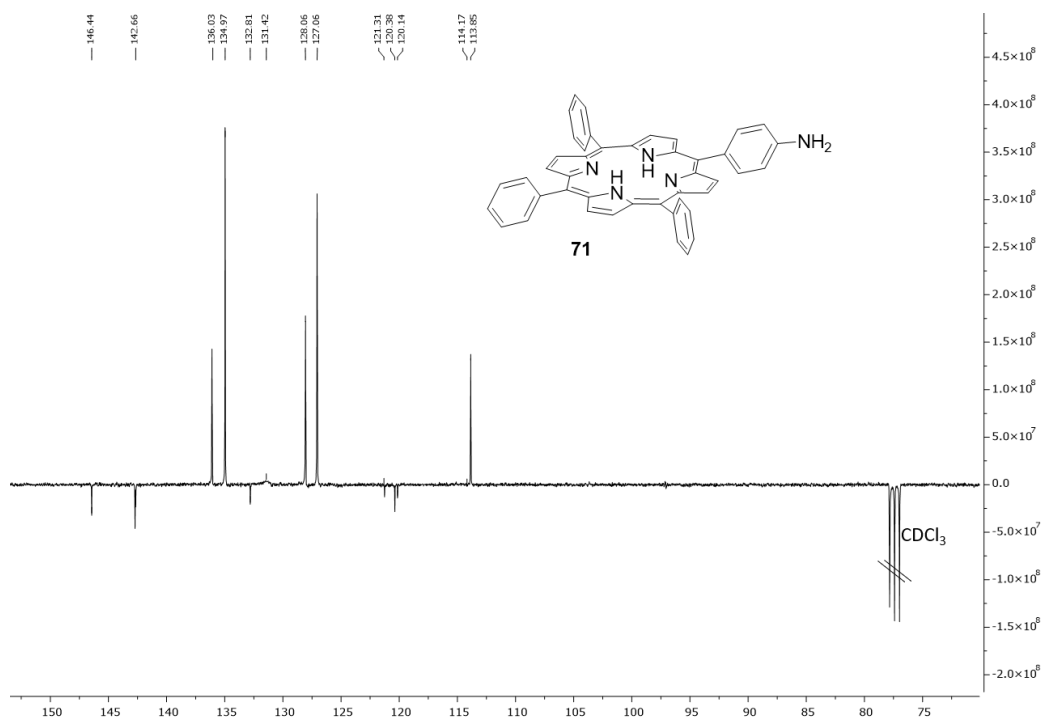


The solid-supported Fe(75)OMe was suspended in 5.0 mL of dry toluene before adding the α -methylstyrene (3.39 mmol) and EDA (7.47×10^{-1} mmol) under nitrogen. The reaction was stirred for 2 hours at 25°C. The solution was filtered and the solid-supported catalyst was washed three times with toluene (3 x 3.0 mL). The solvent was evaporated to dryness and the reaction crude was analysed by $^1\text{H-NMR}$ spectroscopy using 2,4-dinitrotoluene as the internal standard (15% yield, *trans/cis* = 97:3). The collected analytical data are in accordance with those reported in literature²⁸.

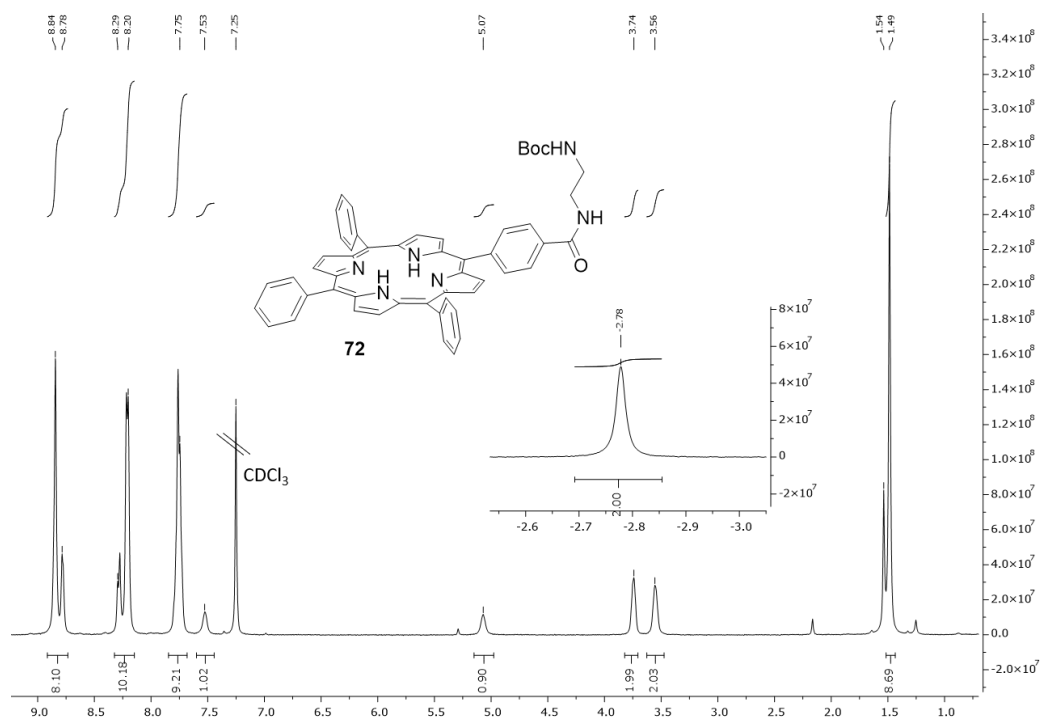
$^1\text{H NMR}$ (300 Hz, CDCl_3): δ 7.31 (d, 4H, $J = 4.4$ Hz, H_{Ar}), 7.22 (m, 1H, H_{Ar}), 4.20 (q, 2H, $J = 7.1$ Hz, $\text{H}_{\text{CH}_2\text{Et}}$), 1.97 (dd, 1H, $J = 8.2, 6.1$ Hz, H^1), 1.54 (s, 3H, H_{CH_3}), 1.49 – 1.39 (m, 2H, H^3), 1.31 (t, 3H, $J = 7.1$ Hz, $\text{H}_{\text{CH}_3\text{Et}}$).

4.4. ^1H -NMR and ^{13}C -NMR of isolated compounds ^1H NMR spectrum (300 MHz, CDCl_3 , 298 K) of porphyrin 70 ^1H NMR spectrum (300 MHz, CDCl_3 , 298 K) of porphyrin 71

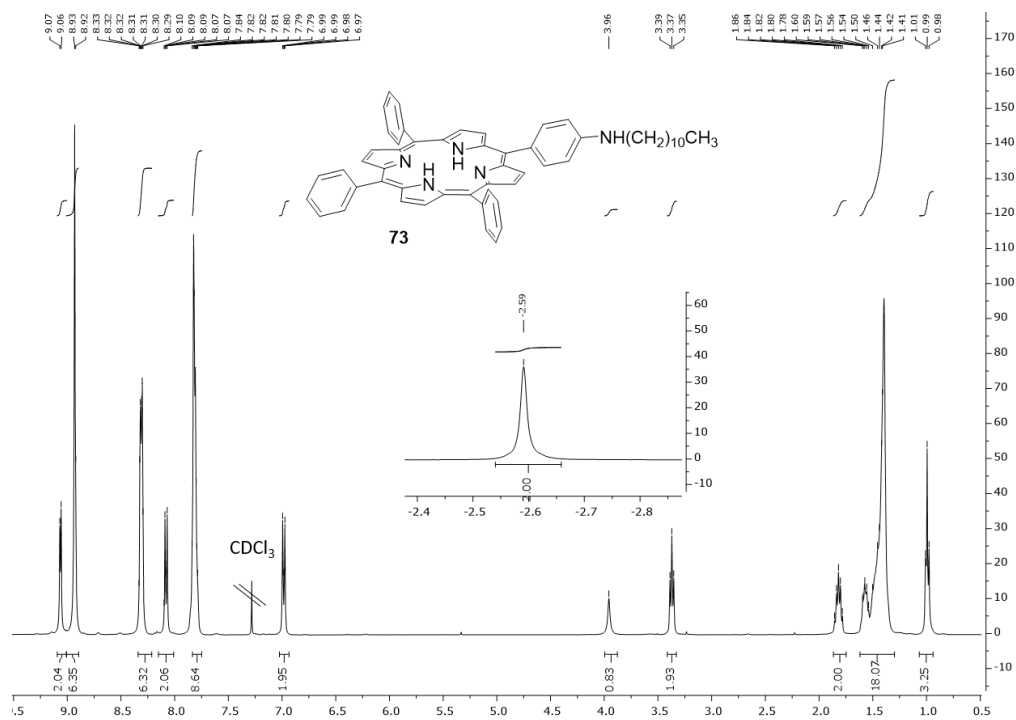
^{13}C NMR spectrum (75 MHz, CDCl_3 , 298 K) of porphyrin 71



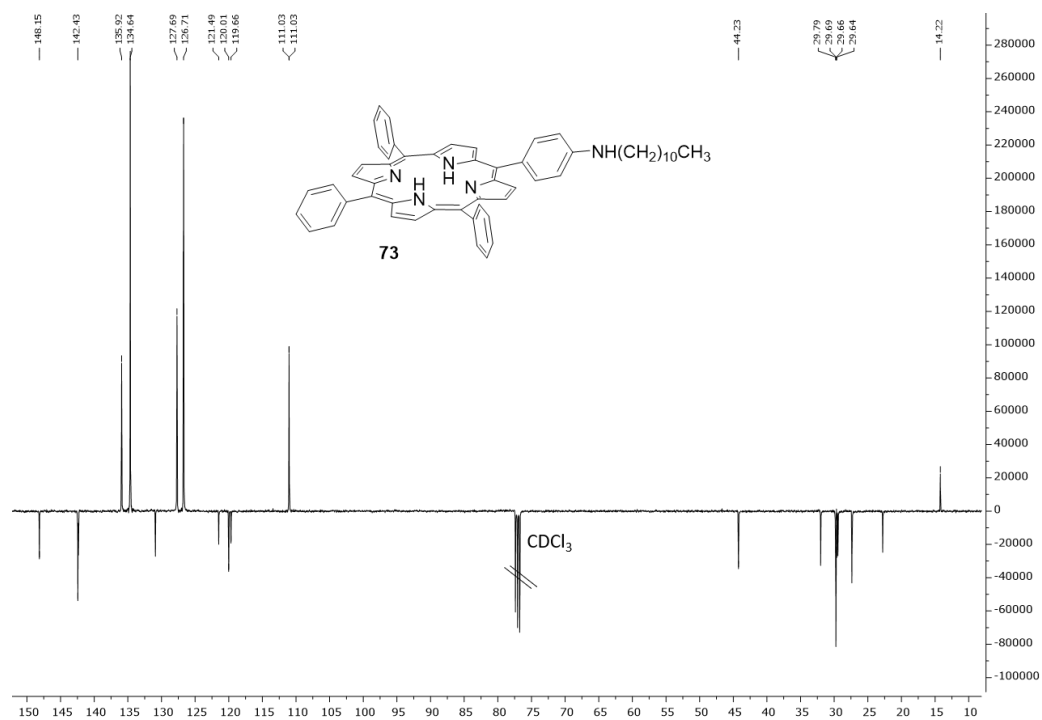
^1H NMR spectrum (400 MHz, CDCl_3 , 298 K) of porphyrin 72



¹H NMR spectrum (400 MHz, CDCl₃, 298 K) of porphyrin 73



¹³C NMR spectrum (100 MHz, CDCl₃, 298 K) of porphyrin 73

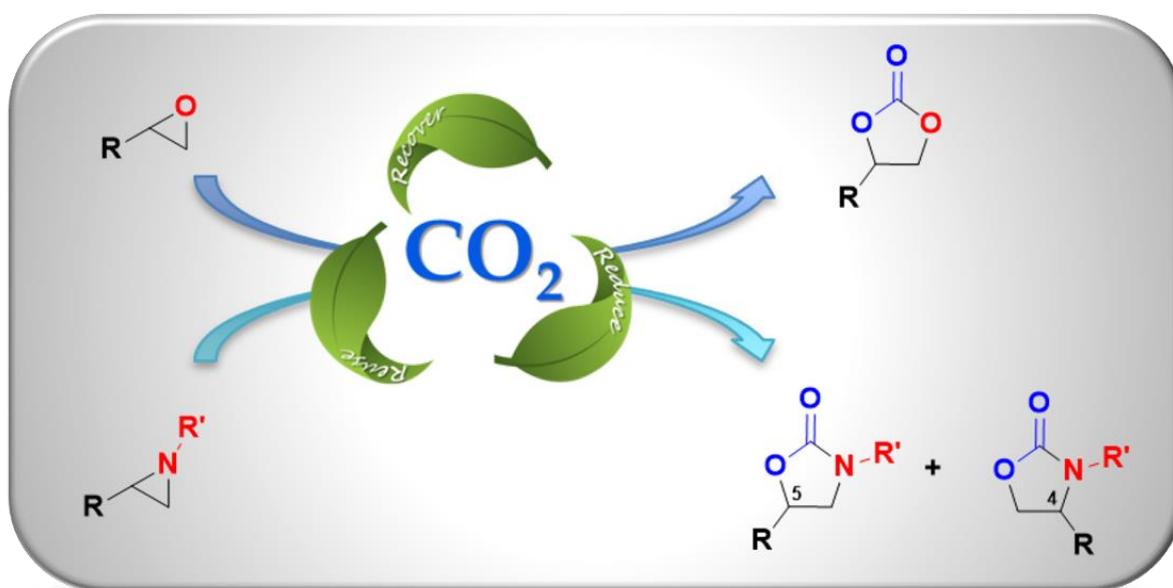


5. References

- (1) Sawyer, L. Fox, P. F., McSweeney, P. L. H., Eds.; Springer US: Boston, MA, **2003**; 319–386.
- (2) Kontopidis, G.; Holt, C.; Sawyer, L. *J. Dairy Sci.* **2004**, *87* (4), 785–796.
- (3) Le Maux, S.; Bouhallab, S.; Giblin, L.; Brodkorb, A.; Croguennec, T. *Dairy Sci. Technol.* **2014**, *94* (5), 409–426.
- (4) Pérez, M. D.; Calvo, M. *J. Dairy Sci.* **1995**, *78* (5), 978–988.
- (5) Forrest, S. A.; Yada, R. Y.; Rousseau, D. *J. Agric. Food Chem.* **2005**, *53* (20), 8003–8009.
- (6) Wang, Q.; Allen, J. C.; Swaisgood, H. E. *J. Dairy Sci.* **1997**, *80* (6), 1054–1059.
- (7) Riihimäki, L. H.; Vainio, M. J.; Heikura, J. M. S.; Valkonen, K. H.; Virtanen, V. T.; Vuorela, P. M. *J. Agric. Food Chem.* **2008**, *56* (17), 7721–7729.
- (8) Buron, C.; Sénéchal-David, K.; Ricoux, R.; Le Caër, J. P.; Guérineau, V.; Méjanelle, P.; Guillot, R.; Herrero, C.; Mahy, J. P.; Banse, F. *Chem. - A Eur. J.* **2015**, *21* (34), 12188–12193.
- (9) Chevalley, A.; Cherrier, M. V; Fontecilla-Camps, J. C.; Ghasemi, M.; Salmain, M. *Dalt. Trans.* **2014**, *43* (14), 5482–5489.
- (10) de Jesús Cázares-Marinero, J.; Przybylski, C.; Salmain, M. *Eur. J. Inorg. Chem.* **2018**, *2018* (12), 1383–1393.
- (11) Islam, S.; Rahman, L.; Mohd, M.; Sarkar, S. M. *J. Clean. Prod.* **2017**, *149*, 1045–1050.
- (12) Karhale, S.; Bhenki, C.; Rashinkar, G.; Helavi, V. **2017**, 5133–5141.
- (13) Chen, S.; Pudukudy, M.; Yue, Z.; Zhang, H.; Zhi, Y.; Ni, Y.; Shan, S.; Jia, Q. *Ind. Eng. Chem. Res.* **2019**, *58*, 17255–17265.
- (14) Rodrigues, D. M.; Hunter, L. G.; Bernard, F. L.; Rojas, M. F.; Vecchia, F. D. *Catal. Letters* **2019**, *149* (3), 733–743.
- (15) Sharip, N. S.; Ariffin, H. *Mater. Today Proc.* **2019**, *16*, 1959–1968.
- (16) Heinze, T. In *Cellulose Chemistry and Properties: Fibers, Nanocelluloses and Advanced Materials*; Rojas, O. J., Ed.; Springer International Publishing: Cham, **2016**; 1–52.
- (17) de Oliveira Barud, H. G.; da Silva, R. R.; da Silva Barud, H.; Tercjak, A.; Gutierrez, J.; Lustri, W. R.; de Oliveira, O. B.; Ribeiro, S. J. L. *Carbohydr. Polym.* **2016**, *153*, 406–420.
- (18) Ullah, H.; Santos, H. A.; Khan, T. *Cellulose* **2016**, *23* (4), 2291–2314.
- (19) Picheth, G. F.; Pirich, C. L.; Sierakowski, M. R.; Woehl, M. A.; Sakakibara, C. N.; de Souza, C. F.; Martin, A. A.; da Silva, R.; de Freitas, R. A. *Int. J. Biol. Macromol.* **2017**, *104*, 97–106.
- (20) Bethke, K.; Palantöken, S.; Andrei, V.; Roß, M.; Raghuvanshi, V. S.; Kettemann, F.; Greis, K.; Ingber, T. T. K.; Stückrath, J. B.; Valiyaveetil, S.; et al. *Adv. Funct. Mater.* **2018**, *28* (23), 1800409.
- (21) Karhale, S.; Bhenki, C.; Rashinkar, G.; Helavi, V. *New J. Chem.* **2017**, *41* (12), 5133–5141.
- (22) Rao, P. D.; Dhanalekshmi, S.; Littler, B. J.; Lindsey, J. S. *J. Org. Chem.* **2000**, *65* (22), 7323–7344.
- (23) Ryppa, C.; Senge, M. O.; Hatscher, S. S.; Kleinpeter, E.; Wacker, P.; Schilde, U.; Wiehe, A. *Chem. - A Eur. J.* **2005**, *11* (11), 3427–3442.
- (24) Lindsey, J. S. *Acc. Chem. Res.* **2010**, *43* (2), 300–311.

- (25) Auras, B. L.; De Lucca Meller, S.; da Silva, M. P.; Neves, A.; Cocca, L. H. Z.; De Boni, L.; da Silveira, C. H.; Iglesias, B. A. *Appl. Organomet. Chem.* **2018**, 32 (5), e4318.
- (26) Zhao, X.; Yuan, L.; Zhang, Z. Q.; Wang, Y. S.; Yu, Q.; Li, J. *Inorg. Chem.* **2016**, 55 (11), 5287–5296.
- (27) Ni, Y.; Puthenkovilakom, R. R.; Huo, Q. *Langmuir* **2004**, 20 (7), 2765–2771.
- (28) Chen, Y.; Zhang, X. P. *J. Org. Chem.* **2004**, 69 (7), 2431–2435.

Chapter V: Ruthenium porphyrins for CO₂ cycloaddition to three-membered ring compounds



Parts of this chapter have been published and are reproduced here from:

D. Carminati, E. Gallo, **C. Damiano**, A. Caselli and D. Inrieri, "Ruthenium Porphyrin-Catalyzed Synthesis of Oxazolidin-2-ones by Cycloaddition of CO₂ to Aziridines", *Eur. J. Inorg. Chem.*, 2018, 48, 5258-5262. DOI:10.1002/ejic.201801208

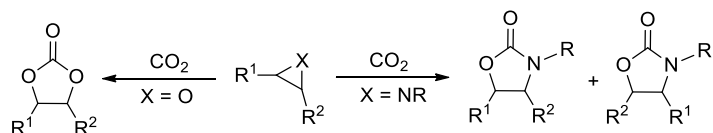
1. Introduction

Academic, industrial and scientific communities are working together to meet the needs of a society that is increasingly focused on environment-friendly chemical processes. The objective is to replace the linear-economic-synthesis of fine chemicals, based on the 'Take-Make-Consume-Throw away' philosophy, with circular-economic-procedures which are *Restorative and/or Regenerative* by intention and design (Figure 1).



Figure 1: Linear economy vs circular economy

Circular economic procedures can be adapted to the chemical valorisation of carbon dioxide (CO₂). Its over-production is responsible of several environmental concerns. High interest has been focused towards some strategies for the Carbon Capture and Utilization (CCU)^{1,2} of CO₂ because of its applicability as starting material for the synthesis of several organic compounds. Indeed, CO₂ can be employed as an eco-friendly and renewable C1 building block to synthesise cyclic carbonates^{3,4} and oxazolidinones⁵ by the 100% atom-efficient cycloaddition of CO₂ to epoxides and aziridines, respectively (Scheme 1).

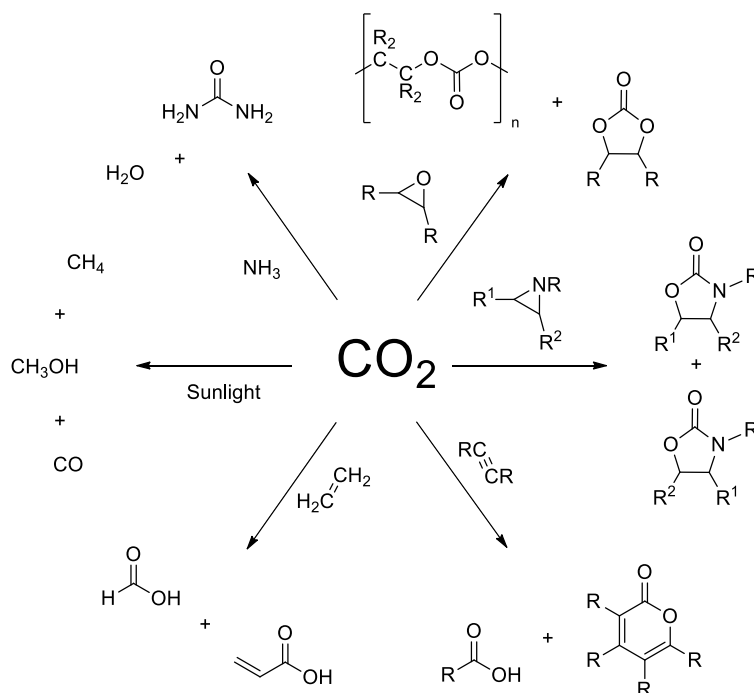


Scheme 1: CO₂ cycloaddition to epoxides and aziridines

1.1. CO₂ as renewable C1 building block

CO₂ is the major overproduced green-house gas by chemical and energy supply industries, power plants and transportation sectors. Because of its role in polluting⁶ and global warming⁷, many efforts have been focused on reducing its amount in the atmosphere and in the research for efficient methods to transfer it into fine chemicals⁸.

Carbon dioxide is an ideal and attractive C1 source in organic synthesis due to its abundance, ready availability, non-toxicity and recyclability. Unfortunately, it is a very stable compound and its activation usually requires extremely reactive compounds, highly reactive catalysts and drastic conditions of temperature and pressure⁹⁻¹². However, carbon dioxide has a strong affinity to nucleophiles and electron-donating reagents due to the carbonyl carbon electron deficiency. In fact, it can react with protonic and polar reagents, including alcohols, ketals, esters and amines, to produce carbonate, carbamate, and urea derivatives. The catalytic coupling of CO₂ with small-ring heterocycles, such as epoxides, has drawn significant attention to the creation of polycarbonates/polycarbamates¹³ and/or cyclic carbonates/carbamates¹⁴ which are biodegradable plastic materials, widely used in materials industries. Otherwise, the CO₂ cycloaddition to aziridines affords oxazolidin-2-ones which are active moieties of several antibacterial and antimicrobial compounds¹⁵ and they are extensively used as chiral auxiliaries in asymmetric synthetic reactions¹⁶. Another interesting pathway, especially in terms of sustainability, is the photocatalytic reduction of CO₂ to CO, methane or methanol in which the activation energy is generated by sunlight (Scheme 2)^{17,18}.



Scheme 2: CO₂ as C1 source in organic synthesis

All these carbon dioxide activations overcome the high stability of CO₂ by chemical reactions with high reactive molecules. Unfortunately, the only use of reactive substrates is not enough to obtain high added-value compounds in efficient and sustainable way. These reasons prompt the scientific community to move on the use of catalytic systems that are able to optimize the process sustainability, avoiding the use of toxic reagents, high temperatures and pressures. Among all the catalytic systems developed during the years (heterogeneous, homogeneous, organo- and organometallic), metal porphyrin complexes represent the most promising tools because of their ability to reduce the activation energy required for the CO₂ transformations¹⁹. This makes the conversion of this “inert” gas into useful molecules possible.

1.2. Mechanism of CO₂ cycloaddition to epoxides and aziridines

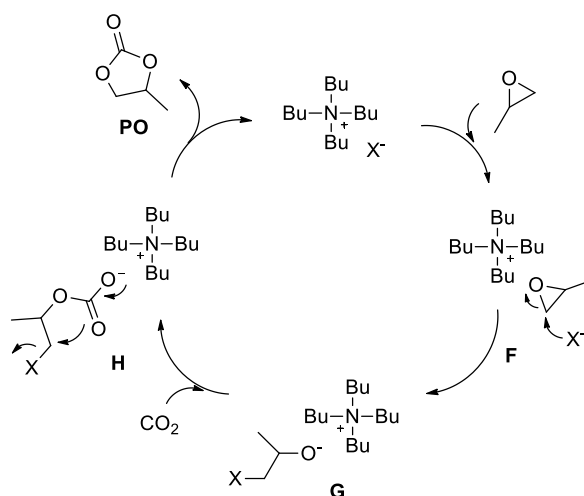
Carbon dioxide is a linear and non-polar molecule containing two polar C=O bonds with two sets of orthogonal π orbitals. CO₂ exhibits several coordination sites and a great variety of coordination modes in its complexes. The carbon atom (LUMO orbitals) has a Lewis acid character and it can be described as an electrophilic center, whereas the oxygens (HOMO orbitals) are weak Lewis bases described as nucleophilic centers. Due to this electronic structure, the CO₂ catalytic transformations usually require a simultaneous acid – base activation^{20–22}.

Among all the metal-mediated CO₂ transformations, the synthesis of cyclic carbonates by CO₂ cycloaddition to epoxides represents the most studied and better known reaction.

From a theoretical point of view, as reported by Ema et al., this reaction could be performed in presence of sole nucleophilic species²³. DFT calculations on the synthesis of propylene carbonate (**PO**) catalysed by TBAX (TBA = tetrabutyl ammonium cation, X = Cl⁻, Br⁻, I⁻) showed that the halide atom can open the epoxide ring thanks to the interaction of the TBA⁺ cation with the epoxide oxygen atom (**F**). The so-formed intermediate **G** can react with CO₂ and the rearrangement of intermediate **H** can afford the desired cyclic carbonate **PO** (Scheme 3).

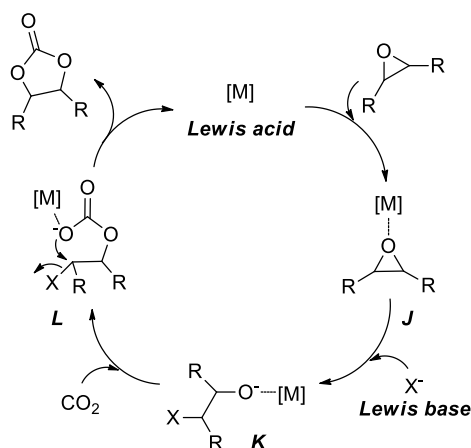
Despite this, several metal complexes were tested for the CO₂ cycloaddition to epoxides and the most efficient systems show the coexistence of transition metals and nucleophilic species. Indeed, the metal ion (M) works as a Lewis acid while the nucleophile (X⁻) is the Lewis base. The published data show that the cooperative action of Lewis acidic metals and Lewis bases is extremely important to improve the reaction yields and sustainability.

Chapter V: Ruthenium porphyrins for CO₂ cycloaddition to three-membered ring compounds



Scheme 3: Mechanism of TBAX-catalysed CO₂ cycloaddition to epoxides simulated by DFT

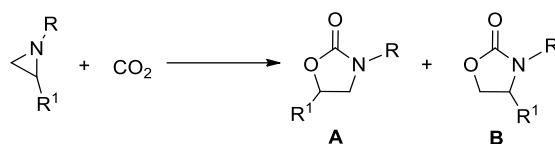
The suggested catalytic cycle of the metal-mediated CO₂ cycloaddition starts with the coordination of the epoxide oxygen atom to the metal. This first step affords the intermediate **J** which is necessary to allow the nucleophilic Lewis base (X⁻) to attach to the activated three-membered ring. The obtained intermediate **K** is very reactive towards CO₂ and forms the species **L** that, thanks to a ring-closure reaction, generates the desired cyclic carbonate and restores the original metal catalyst (Scheme 4)¹⁹.



Scheme 4: Mechanism of metal catalysed CO₂ cycloaddition to epoxides

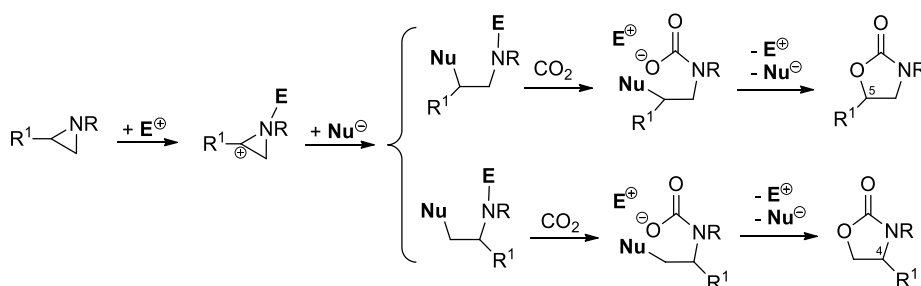
Even if aziridines are structurally analogous to epoxides, the CO₂ cycloaddition to these heterocycles has not yet been adequately investigated. The CO₂ coupling to epoxides generates only one corresponding cyclic carbonate, while the CO₂ cycloaddition to aziridine molecules can produce two different regioisomers, conventionally called A and B (Scheme 5). The ring opening reaction can take place on two inequivalent carbon atoms and the two regioisomers can be formed in a ratio strongly dependent on the catalyst nature.

Chapter V: Ruthenium porphyrins for CO₂ cycloaddition to three-membered ring compounds



Scheme 5: Regioisomers derived from the CO₂ coupling to aziridines

Analogously to the epoxides, electrophilic (**E**) and nucleophilic (**Nu**) species are required for the insertion of CO₂ into aziridine rings. The most probable mechanism provides the coordination of **E** to the aziridine nitrogen atom, in order to promote the ring opening reaction by the nucleophilic species. The so-formed intermediate can react with CO₂ yielding the desired oxazolidin-2-one. The 5-substituted oxazolidin-2-ones are usually formed as the prevalent regioisomer, due to the preferred nucleophilic attachment on the most substituted aziridine carbon atom (Scheme 6).



Scheme 6: CO₂ cycloaddition to aziridines mechanism

Regarding the metal-catalysed CO₂ cycloaddition to aziridines, the only mechanism reported up to now has been proposed by H. Ji and co-workers²⁴. They studied the model reaction of 1-butyl-2-phenyl aziridine with CO₂ using the bifunctional porphyrin system **IL-ZnTPP** (Figure 2).

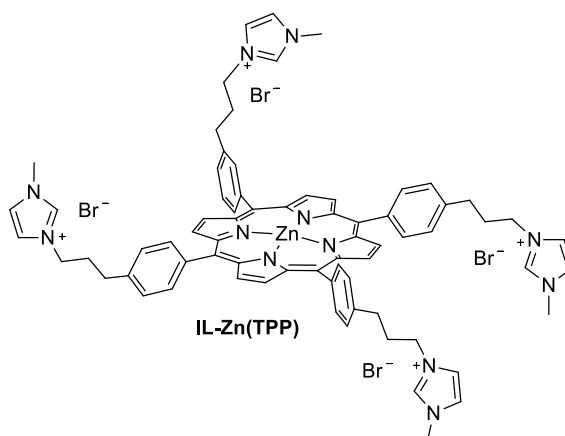
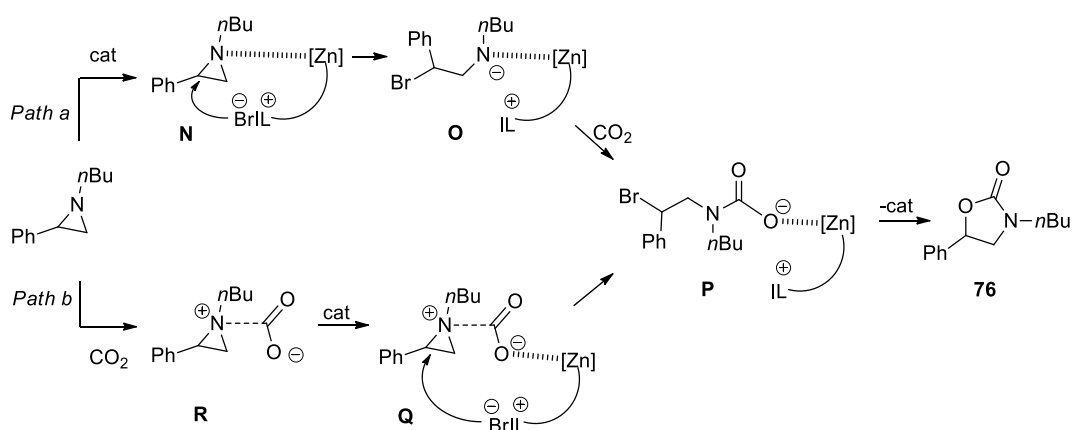


Figure 2: Bifunctional complex IL-Zn(TPP)

Chapter V: Ruthenium porphyrins for CO₂ cycloaddition to three-membered ring compounds

The authors suggested two different mechanistic pathways for the IL-Zn(TPP)-catalysed synthesis of **76** (Scheme 7). Both mechanisms provide the formation of the intermediate **P** that yields the desired oxazolidinone by a ring-closing reaction. The *path a* is very similar to the metal-catalysed synthesis of cyclic carbonates. The first step is the coordination of aziridine to the Lewis acid zinc metal and the formation of intermediate **N** which is followed by the nucleophilic attack of bromide ion to the substituted aziridine carbon atom forming **O**. The consecutive reaction of intermediate **O** with CO₂ generates zinc alkoxide **P** which evolves into the corresponding oxazolidinone by a ring-closing reaction. Considering the Lewis basicity of aziridine molecules, the alternative *path b* shows the formation of the CO₂-aziridine adduct **R**. This species can coordinate IL-Zn(TPP) compound by the oxygen atom of CO₂ yielding intermediate **Q**. Next, an intramolecular nucleophilic reaction yields the intermediate **P** which forms the desired 5-substituted oxazolidinone as its major product and restores the catalytic species permitting the cycle to restart.



Scheme 7: CO₂ cycloaddition to aziridines mechanism, catalysed by IL-Zn(TPP)

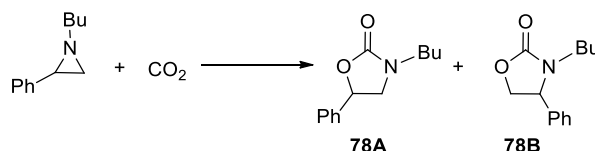
2. Discussion

Considering the metal porphyrin complexes ability to promote CO₂ transformations, a ruthenium *bis-imido* porphyrin was employed as catalyst for CO₂ cycloaddition to aziridines and epoxides. The catalyst robustness and its role in the synthesis of several cyclic carbonates were evaluated. Preliminary studies on the reaction mechanism were also performed in order to shade some light on the role of the nitrogen *imido* atom.

2.1. CO₂ cycloaddition to aziridines

As already reported in a previous PhD thesis, ruthenium *bis-imido* porphyrins are able to promote the regioselective cycloaddition of CO₂ to aziridines to form oxazolidinones. Among all the tested catalysts, Ru(TPP)(NAr)₂ (Ar = 3,5(CF₃)₂C₆H₃) (**77**) showed high activity towards several *N*-alkyl aziridines affording the desired oxazolidinones in yields up to 96% and **A/B** ratio up to 99:1 (previous reported data are summarised in table 1).

In order to study the catalyst robustness, the model reaction between CO₂ and 1-butyl-2-phenylaziridine (Scheme 8) was performed for three consecutive times in the presence of 1% mol of **77** and 10% mol of tetrabutyl ammonium chloride (TBACl).

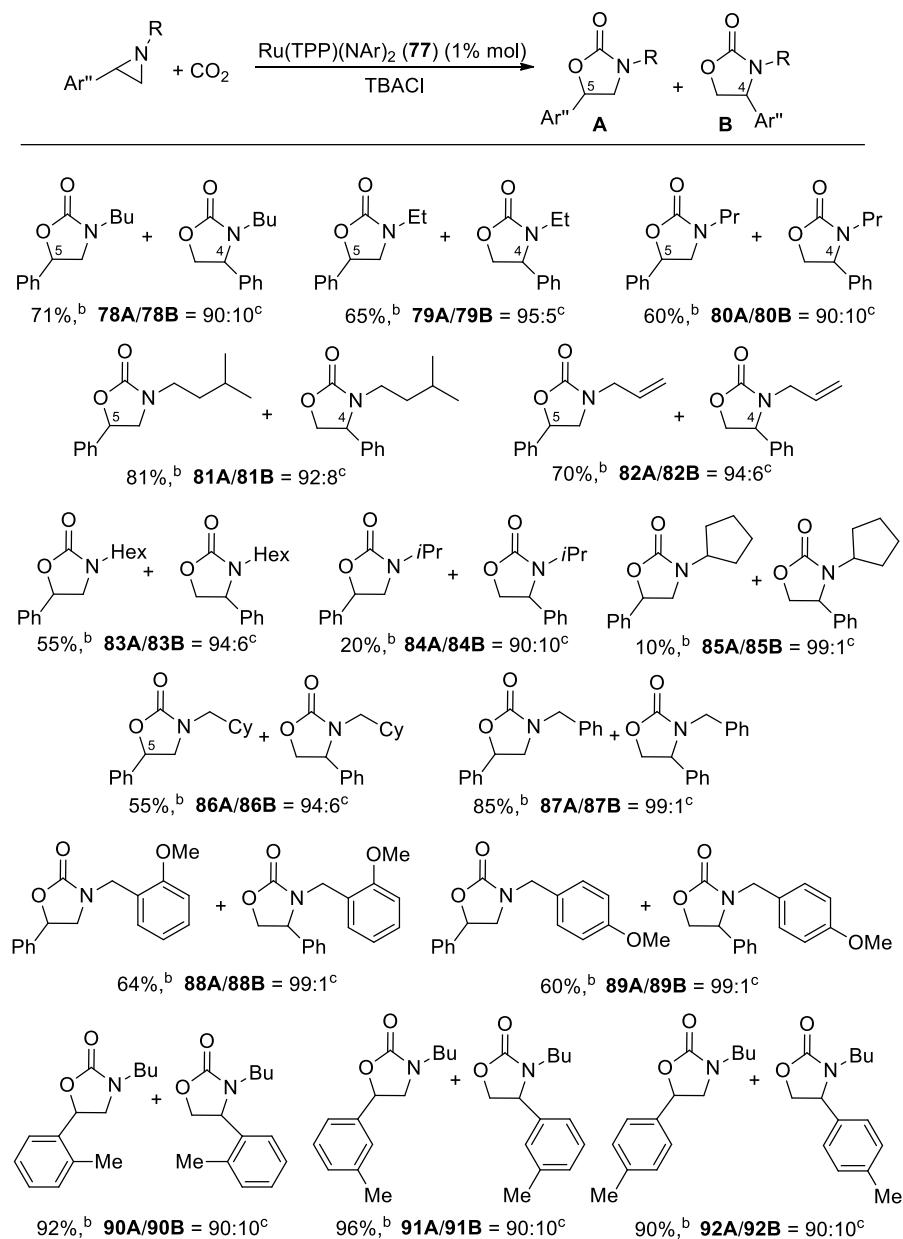


Scheme 8: Model reaction between CO₂ and 1-butyl-2-phenylaziridine

Each reaction was run for 6 hours at 100°C and, after checking that the aziridine conversion was > 95%, a same amount of 1-butyl-2-phenylaziridine was added before recharging the autoclave with 0.6 MPa of CO₂. At the end of three runs, the ¹H NMR analysis revealed the formation of corresponding oxazolidinone-2-ones in 70% yield and good regioselectivity (**78A/78B** = 90:10), indicating that Ru(TPP)(NAr)₂ retains its catalytic activity for at least three consecutive catalytic reactions.

Chapter V: Ruthenium porphyrins for CO₂ cycloaddition to three-membered ring compounds

Table 1: Synthesis of compounds **78-92** catalysed by **77**

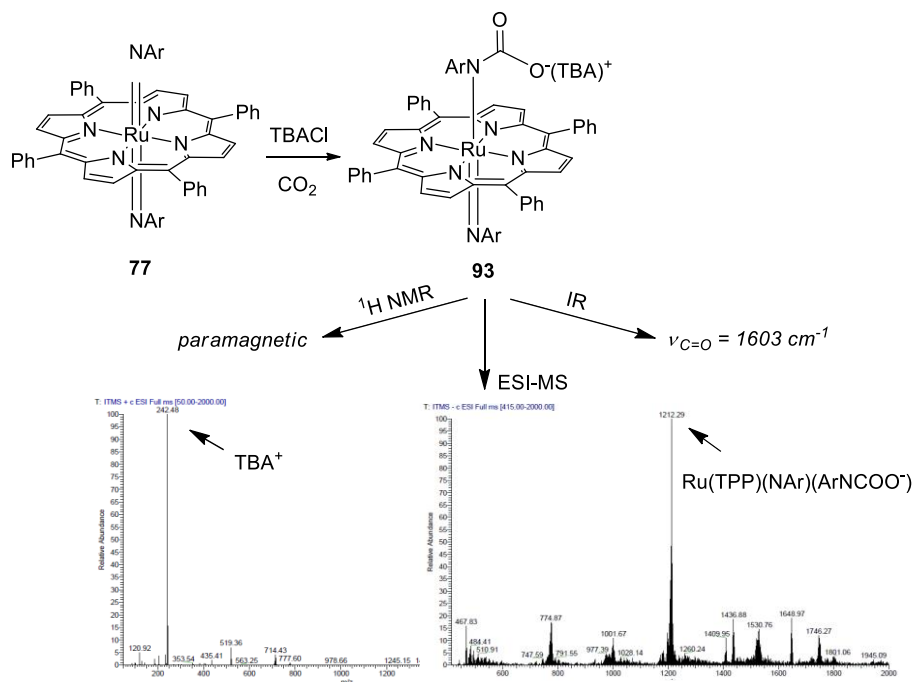


^a Reaction conditions: Ru(TPP)(NAr)₂/TBACl/aziridine = 1:10:100 (Ar = 3,5-(CF₃)₂C₆H₃). Reactions were performed in a steel autoclave for 6 h at 100°C and 0.6 MPa of CO₂. ^b Isolated yields. ^c Determined by ¹H NMR spectroscopy using 2,4-dinitrotoluene as the internal standard.

The reaction between Ru(TPP)(NAr)₂ and CO₂ was performed in the presence of only TBACl in order to shed some light on the catalytic mechanism. The ESI-MS spectroscopic analysis of the crude revealed the formation of a new ruthenium species, Ru(TPP)(NAr)(ArNCOO⁻TBA⁺) (**93**), inactive in the catalytic process and with paramagnetic properties, as revealed by ¹H NMR spectroscopic analysis. The crude containing the new complex was also analysed by IR spectroscopy that showed the presence of

Chapter V: Ruthenium porphyrins for CO₂ cycloaddition to three-membered ring compounds

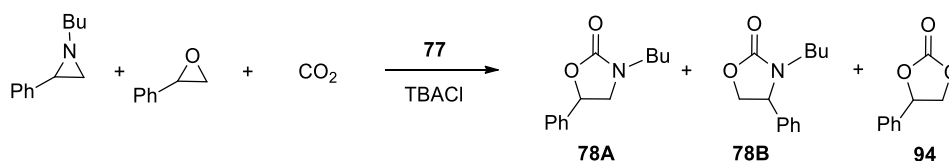
the C=O stretching at 1603 cm⁻¹ (Scheme 9). The formation of complex **93** suggests the direct interaction of CO₂ with the nitrogen imido atom of **77** which shows a very high electron density due to the presence of ruthenium, as indicated by a previous DFT study.



Scheme 9: Formation and characterization of complex **93**

2.2. CO₂ cycloaddition to epoxides

Considering the ability of Ru(TPP)(NAr)₂ (**77**) to promote the CO₂ cycloaddition to aziridines, the competitive reaction between aziridines and epoxides was evaluated. Using the same catalytic conditions of CO₂ coupling to aziridines, 2-phenyloxirane and 1-butyl-2-phenylaziridine were reacted with CO₂ in presence of 1% mol of **77** and 10% mol of TBACl (Scheme 10). Collected data revealed the higher efficiency of complex **77** in forming the cyclic carbonate **94** (99% yield) than the oxazolidinone **78** (20% yield), according to the greater reactivity shown by epoxides compared to that of aziridines.



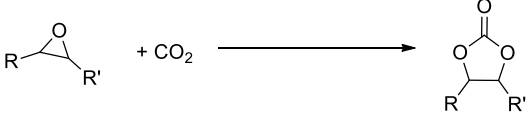
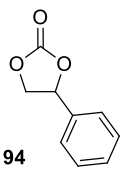
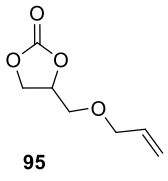
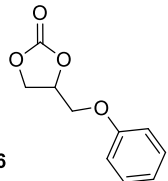
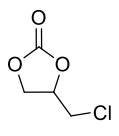
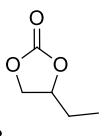
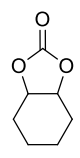
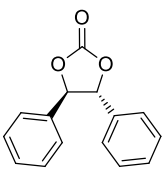
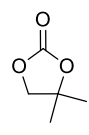
Scheme 10: Competition between aziridines and epoxides in the CO₂ coupling catalysed by **77**

Chapter V: Ruthenium porphyrins for CO₂ cycloaddition to three-membered ring compounds

The good result obtained in forming **94** prompted us to test the catalytic performances of Ru(TPP)(NAr)₂ (**77**) in the CO₂ cycloaddition to epoxides. Due to the chance to promote the cyclic carbonates synthesis in the sole presence of TBACl, the catalytic activity of **77** was compared with those of TBACl alone in order to establish the catalyst role (Table 2). Very good results were obtained in the synthesis of different cyclic carbonates showing the catalyst **77** positive effect on the reaction selectivity.

As reported in table 2, some cyclic carbonates (**94**, **96** and **97**) can be easily synthesised with the use of the sole TBACl because of the very high reactivity of starting epoxides. The high reactivity is often responsible of various by-products formation, like polymeric compounds, which decreases the reaction selectivity. In this contest, the Ru(TPP)(NAr)₂ complex (**77**) has proven to be an efficient catalyst able to increase the cyclic carbonates yields (up to 99%) avoiding the formation of side-products (products **95** and **98**).

Table 2: Synthesis of compounds **94-101**

		
 94	 95	 96
TBACl: 81% ^b conv., 95% ^b sel. 77 + TBACl: 100% ^b conv., 99% ^b sel.	TBACl: 91% ^b conv., 63% ^b sel. 77 + TBACl: 100% ^b conv., 99% ^b sel.	TBACl: 100% ^b conv., 84% ^b sel. 77 + TBACl: 100% ^b conv., 94% ^b sel.
 97	 98	 99
TBACl: 100% ^b conv., 99% ^b sel. 77 + TBACl: 100% ^b conv., 99% ^b sel.	TBACl: 100% ^b conv., 27% ^b sel. 77 + TBACl: 100% ^b conv., 65% ^b sel.	TBACl: 100% ^b conv., 9% ^b sel. 77 + TBACl: 100% ^b conv., 17% ^b sel.
 100	 101	
TBACl: 10% ^b conv., 99% ^b sel. 77 + TBACl: 15% ^b conv., 99% ^b sel.	TBACl: 100% ^b conv., 14% ^b sel. 77 + TBACl: 100% ^b conv., 15% ^b sel.	

^aReactions were performed in a steel autoclave for 8 h at 100°C and 0.6 MPa of CO₂. ^bDetermined by ¹H NMR spectroscopy using 2,4-dinitrotoluene as the internal standard.

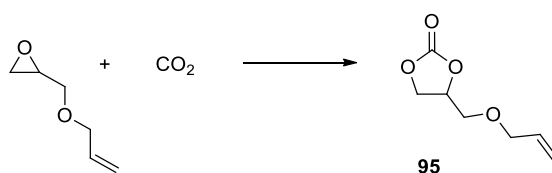
Chapter V: Ruthenium porphyrins for CO₂ cycloaddition to three-membered ring compounds

Despite the use of **77** as a catalyst, low yields were observed in the synthesis of cyclic carbonates **99-101**. The low selectivity in the formation of **99** can be justified by the high propensity of the starting epoxide to polymerize in presence of CO₂. On the contrary, the low yield of **101** was strongly dependent on the low boiling point of the epoxydic precursor which can be easily removed from the reaction mixture during the solvent evaporation distorting the conversion value. A different argument concerns the product **100** in which the steric hinderance of the two phenyl groups can disadvantage the epoxide ring-opening reaction preventing the coupling of CO₂.

Similarly to the aziridines case, the robustness of **77** was tested through a model reaction (Scheme 11) performed for three consecutive times. The model product **95** was obtained in 99% yield after three consecutive runs indicating the high reusability of the catalyst **77**.

2.3. Hypothesis of the CO₂ cycloaddition mechanism

Different experiment were performed on the model reaction between 2-((allyloxy)methyl)oxirane and CO₂ (Scheme 11) in order to shed some light on the role of Ru(TPP)(NAr)₂ (**77**) in the CO₂ cycloaddition to epoxides and aziridines.



Scheme 11: Model reaction between CO₂ and 2-((allyloxy)methyl)oxirane

As previously discussed, Ru(TPP)(NAr)₂ complex (**77**) was an efficient catalyst for the synthesis of cyclic carbonates even if some of these products can be prepared with the sole TBACl. In addition, complex **77** reacts with CO₂ and TBACl forming the species Ru(TPP)(NAr)(ArNCOO⁻TBA⁺) (**93**) (Scheme 9) which shows the nitrogen *imido* atom interaction with carbon dioxide.

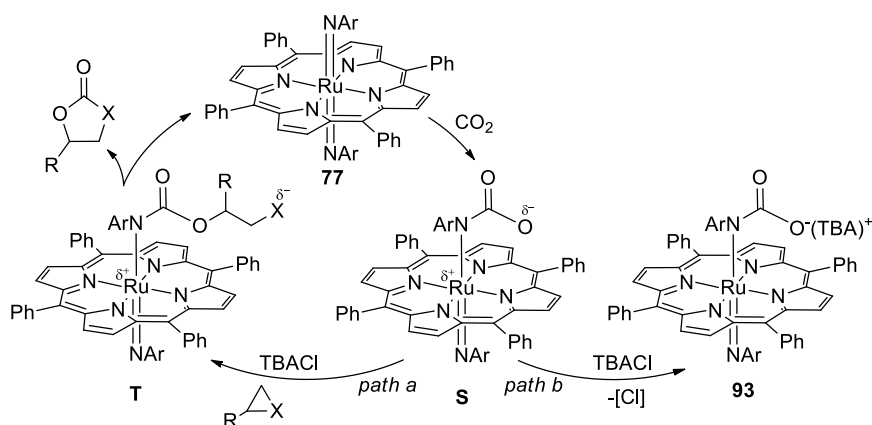
In order to clarify the reaction mechanism, complex **93** was tested as catalyst in the model reaction reported in scheme 11. The observed inactivity in forming **95** suggests that complex **93** is the decomposition product of other active species formed during the catalytic cycle.

All the reactions are usually carried out in a molar ratio **77**/TBACl = 1:10, these catalytic conditions makes it difficult to determinate if the catalytic active species is the ruthenium complex or the TBACl salt. To elucidate this aspect, the model reaction was performed with the ratio **77**/TBACl/epoxide = 2:1:100. Under these conditions it can be assumed that all the TBACl reacts with **77** forming a catalytically active species which evolves into complex **93** at the end of the reaction. The reaction carried out under these conditions occurred in higher yield (93%) than the one performed in the

Chapter V: Ruthenium porphyrins for CO₂ cycloaddition to three-membered ring compounds

presence of TBACl alone (57%) suggesting the possible formation of an adduct from the reaction of CO₂ with **77** and consequently the active role of the ruthenium species in the catalytic cycle. Conversely, the model reaction didn't occur in presence of the sole ruthenium complex **77** suggesting that the TBACl salt is necessary for the epoxide ring-opening reaction.

The obtained results, both in the CO₂ cycloaddition to epoxides and aziridines, allowed to hypothesise a mechanism in which the first step is the interaction of CO₂ with the nitrogen *imido* atom of complex **77** (Scheme 12) forming the intermediate **S**. Complex **S** could attack the three-membered ring, activated by the TBACl salt, yielding the intermediate **T** (*path a*, Scheme 12). The ring-closure reaction of intermediate **T** can afford the desired product regenerating the active catalyst **77**. Complex **S** could also react with TBACl forming the inactive species **93** by a not yet clarified side-reaction mechanism (*path b*, Scheme 12).



Scheme 12: Proposed mechanism for the CO₂ cycloaddition to three-membered ring compounds

3. Conclusion

In conclusion, the activity of Ru(TPP)(NAr)₂ complex was evaluated towards the CO₂ cycloaddition to aziridines and epoxides. The catalyst showed high selectivity both in the CO₂ coupling to aziridines and epoxides. Collected data gave more information about the catalyst robustness and the *imido* functionalities role in the CO₂ activation. Preliminary studies on the reaction mechanism suggested the direct interaction of carbon dioxide with the nitrogen *imido* during the first reaction step. Future kinetics and DFT studies on the reaction between *bis-imido* complexes and CO₂ could be useful to completely understand the reaction mechanism.

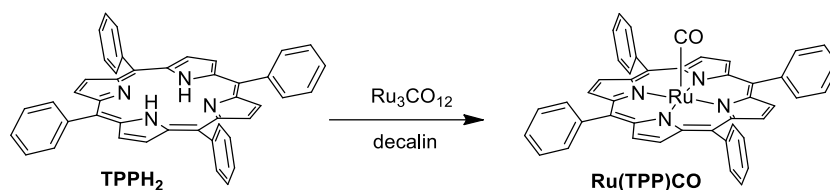
Considering the high activity of ruthenium porphyrin complexes to promote alkene aziridination reactions, the obtained data represent a starting point to test a catalyst that is able to promote the synthesis of oxazolidinones in a two-steps one-pot reaction in order to afford added value compounds in efficient and sustainable way.

4. Experimental section

General conditions: Unless otherwise specified, all reactions were carried out under nitrogen atmosphere employing standard Schlenk techniques and vacuum-line manipulations. All the solvents were dried by using standard procedures and stored under nitrogen atmosphere. All the other starting materials were commercial products and used as received. NMR spectra were recorded at room temperature either on a Bruker Avance 300-DRX, operating at 300 MHz for ¹H, at 75 MHz for ¹³C and at 282 MHz for ¹⁹F, or on a Bruker Avance 400-DRX spectrometers, operating at 400 MHz for ¹H, 100 MHz for ¹³C and 376 MHz for ¹⁹F. Chemical shifts (ppm) are reported relative to TMS. The ¹H-NMR signals of the compounds described in the following were attributed by 2D NMR techniques. Assignments of the resonance in ¹³C-NMR were made by using the APT pulse sequence, HSQC and HMBC techniques. Infrared spectra were recorded on a Varian Scimitar FTS 1000 spectrophotometer. UV/Vis spectra were recorded on an Agilent 8453E instrument. MALDI-TOF spectra were acquired either on a Bruker Daltonics Microflex or on a Bruker Daltonics Autoflex III TOF/TOF at C.I.G.A, University of Milan. High resolution MS (HR-MS) spectra were obtained on a Bruker Daltonics ICR-FTMS APEX II at C.I.G.A, University of Milan. Microanalysis was performed on a Perkin Elmer 2400 CHN Elemental Analyzer instrument.

4.1. Synthesis of ruthenium complexes

4.1.1. Synthesis of Ru(TPP)CO

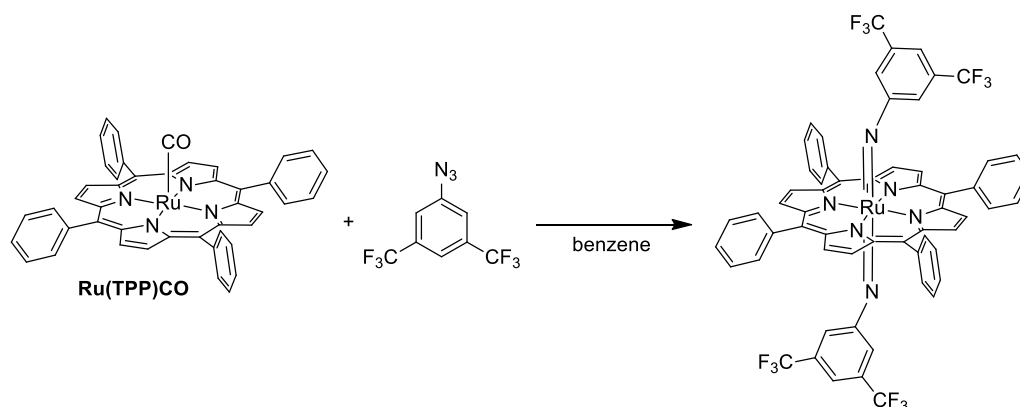


Ru₃(CO)₁₂ (0.626 g, 9.80 x 10⁻¹ mol) and TPPH₂ (1.23 g, 2.00 x 10⁻³ mol) were suspended in dry decalin (60.0 mL). The reaction mixture was refluxed for 7 hours until the complete consumption of the starting porphyrin was observed by TLC (SiO₂, *n*-hexane/CH₂Cl₂ = 80:20). The solvent was evaporated to dryness under vacuum and the residue purified by flash chromatography (silica gel, 60 μm, starting from hexane/CH₂Cl₂ 8:2 to CH₂Cl₂). The Ru(TPP)CO fraction was evaporated to dryness and dried *in vacuo* at 120°C. The product was obtained as a purple crystalline solid (1.09 g, 73%). The collected data are in accordance with those reported in literature²⁵.

¹H NMR (300 MHz, CDCl₃): δ 8.68 (s, 8H, H_{βpyr}), 8.22 (m, 4H, H_{Ar}), 8.11 (m, 4H, H_{Ar}), 7.75 – 7.72 (m, 12H, H_{Ar}).

Chapter V: Ruthenium porphyrins for CO₂ cycloaddition to three-membered ring compounds

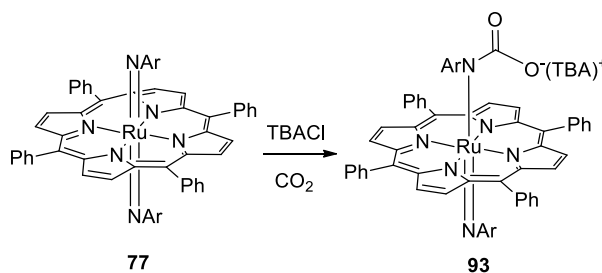
4.1.2. Synthesis of Ru(TPP)(NAr)₂ (Ar = 3,5-(CF₃)₂C₆H₃) (77)



3,5-Bis(trifluoromethyl)phenyl azide (0.154 g, 6.06 x 10⁻³ mol) was added to a benzene (30.0 mL) suspension of Ru(TPP)CO (0.150 g, 2.02 x 10⁻⁴ mol). The resulting dark mixture was refluxed for three hours observing the complete consumption of Ru(TPP)CO by TLC (Al₂O₃, *n*-hexane/CH₂Cl₂ 1:1). The solution was concentrated to about 5 mL and hexane (20.0 mL) was added. A crystalline violet solid was collected by filtration and dried *in vacuo* (0.165 g, 70%). The collected data are in accordance with those reported in literature²⁶.

¹H NMR (300 MHz, CDCl₃): δ 8.87 (s, 8H, H_{βpyrr}), 8.08 (d, 8H, *J*=6.9 Hz, H_{Ar}), 7.83 – 7.76 (m, 12H, H_{Ar}), 6.60 (s, 2H, H_{Ar}), 2.66 (s, 4H, H_{Ar}).

4.1.3. Synthesis of Ru(TPP)(NAr)(ArNCOO⁻TBA⁺) (Ar = 3,5-(CF₃)₂C₆H₃) (93)



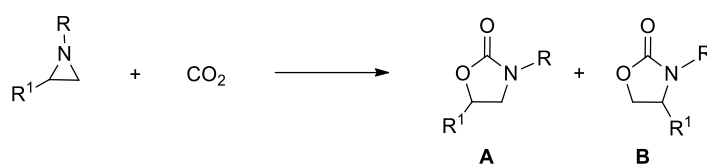
In a 100 mL glass liner equipped with a screw cap and a glass wool, tetrabutyl ammonium chloride (120.0 mg, 4.32 x 10⁻⁴ mol) was added to a benzene (15.0 mL) solution of Ru(TPP)(NAr)₂ (100.0 mg, 8.64 x 10⁻⁵ mol). The reaction mixture was cooled with liquid nitrogen and the flask was transferred into a stainless-steel autoclave, three vacuum-nitrogen cycles were performed and 0.6 MPa of CO₂ was charged at room temperature. The autoclave was placed in a preheated oil bath at 100°C and stirred for 6 hours, then it was cooled at room temperature and slowly vented. The solvent was evaporated to dryness and the crude was washed with H₂O (3 x 10.0 mL) in order to remove the TBACl excess. Toluene (20.0 mL) was added to the solid and the suspension was refluxed for removing water as an

Chapter V: Ruthenium porphyrins for CO₂ cycloaddition to three-membered ring compounds

azeotropic mixture. The toluene suspension was evaporated to dryness and the solid resulted to be a mixture of different ruthenium species containing **93** as revealed by the ESI-MS analysis. The ¹H NMR spectroscopy in CD₃OD disclosed the presence of paramagnetic species and the IR (ATR) spectrum showed the C=O stretching at 1603 cm⁻¹. *m/z* (ESI) 242.48 [M⁺]; 1212.29 [M⁻]. Unfortunately, any attempt to isolate **93** in a pure form has failed up to now.

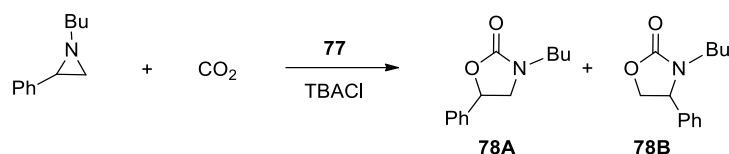
4.2. Synthesis of oxazolidin-2-ones

General catalytic procedure for the synthesis of oxazolidinones



In a 100 mL glass liner equipped with a screw cap and a glass wool, tetrabutyl ammonium chloride (14.2 mg, 5.13 x 10⁻⁵ mol) and aziridine (5.13 x 10⁻⁴ mol) were added to a benzene (2.50 mL) solution of catalyst (5.13 x 10⁻⁶ mol). The reaction mixture was cooled with liquid nitrogen and the flask was transferred into a stainless-steel autoclave, three vacuum-nitrogen cycles were performed and 0.6 MPa of CO₂ was charged at room temperature. The autoclave was placed in a preheated oil bath at 100°C and stirred for 6 hours, then it was cooled at room temperature and slowly vented. The solvent was evaporated to dryness and the crude was analyzed by ¹H NMR and then purified by flash chromatography (SiO₂, 60 μm, *n*-hexane/AcOEt = 8:2).

4.2.1. Synthesis of 3-butyl-5-phenyloxazolidin-2-one (**78**)



The general catalytic procedure was followed using *N*-butyl-phenyl aziridine as reagent to obtain a yellowish oil. The collected data are in accordance with those reported in literature²⁷.

¹H NMR (300 MHz, CDCl₃) **78A**: δ 7.42 – 7.28 (m, 5H, H_{Ar}), 5.49 (t, 1H, *J* = 8.0 Hz, H_{CH}), 3.92 (t, 1H, *J* = 8.8 Hz, H_{CH2}), 3.43 (t, 1H, *J* = 8.0 Hz, H_{CH2}), 3.38 – 3.23 (m, 2H, H_{CH2}), 1.58 – 1.51 (m, 2H, H_{CH2}), 1.40 – 1.31 (m, 2H, H_{CH2}), 0.94 (t, 3H, *J* = 6.8 Hz, H_{CH3}).

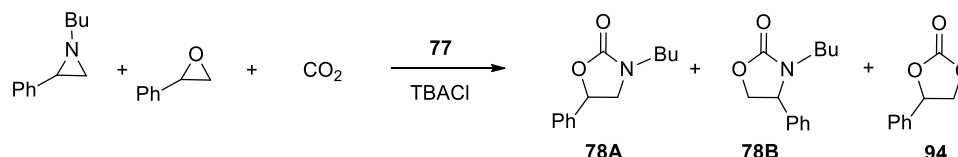
4.2.2. Recycle of the catalyst Ru(TPP)(NAr)₂ (Ar = 3,5-(CF₃)₂C₆H₃) (**77**)

The general catalytic procedure was followed using *N*-butyl-phenyl aziridine as reagent. The consumption of the aziridine was monitored by TLC analysis (*n*-hexane/AcOEt = 80:20). After the

Chapter V: Ruthenium porphyrins for CO₂ cycloaddition to three-membered ring compounds

consumption of the starting material, *N*-butyl-phenyl aziridine was added again to the catalytic mixture for two more consecutive times. The NMR analysis of the crude revealed 70% of global yield and **78A/78B** ratio of 90:10.

4.3. Competitive reaction between aziridines and epoxides



In a 100 mL glass liner equipped with a screw cap and a glass wool, tetrabutyl ammonium chloride (4.7 mg, 1.72 x 10⁻⁵ mol), *N*-butyl-phenyl aziridine (34.0 μL, 1.72 x 10⁻⁴ mol) and 2-phenyloxirane (20.0 μL, 1.72 x 10⁻⁴ mol) were added to a benzene (2.0 mL) solution of catalyst **77** (2.0 mg, 1.72 x 10⁻⁶ mol). The reaction mixture was cooled with liquid nitrogen and the flask was transferred into a stainless-steel autoclave, three vacuum-nitrogen cycles were performed and 0.6 MPa of CO₂ was charged at room temperature. The autoclave was placed in a preheated oil bath at 100°C and stirred for 6 hours, then it was cooled at room temperature and slowly vented. The solvent was evaporated to dryness and the crude was analyzed by ¹H NMR with 2,4-dinitrotoluene as the internal standard. The NMR analysis of the crude revealed 99% of yield of **94** and 20% of yield of **78**. The collected data are in accordance with those reported in literature.

¹H NMR (300 MHz, CDCl₃) **78A**: δ 7.42 – 7.28 (m, 5H, H_{Ar}), 5.49 (t, 1H, *J* = 8.0 Hz, H_{CH}), 3.92 (t, 1H, *J* = 8.8 Hz, H_{CH₂}), 3.43 (t, 1H, *J* = 8.0 Hz, H_{CH₂}), 3.38 – 3.23 (m, 2H, H_{CH₂}), 1.58 – 1.51 (m, 2H, H_{CH₂}), 1.40 – 1.31 (m, 2H, H_{CH₂}), 0.94 (t, 3H, *J* = 6.8 Hz, H_{CH₃})²⁷.

¹H NMR (300 MHz, CDCl₃) **94**: δ 7.47 – 7.34 (m, 5H, H_{Ar}), 5.67 (t, *J* = 8.0 Hz, 1H, H_{CH}), 4.79 (t, *J* = 8.4 Hz, 1H, H_{CH₂}), 4.33 (t, *J* = 8.0 Hz, 1H, H_{CH₂})²⁸.

4.4. Synthesis of cyclic carbonates

General catalytic procedure for the synthesis of cyclic carbonates



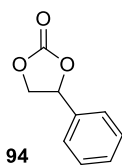
Method A: In a 100 mL glass liner equipped with a screw cap and glass wool, tetrabutyl ammonium chloride (9.71 x 10⁻⁵ mol) and the epoxide (9.71 x 10⁻⁴ mol) in a molar ratio = 10/100 were dissolved in THF (3.3 mL). The reaction mixture was cooled with liquid nitrogen and the flask was transferred into a stainless-steel autoclave, three vacuum-nitrogen cycles were performed and 0.6 MPa of CO₂ was

Chapter V: Ruthenium porphyrins for CO₂ cycloaddition to three-membered ring compounds

charged at room temperature. The autoclave was placed in a preheated oil bath at 100°C and stirred for 8 hours, then it was cooled at room temperature and slowly vented. The solvent was evaporated to dryness and the crude was analysed by ¹H NMR with 2,4-dinitrotoluene as the internal standard.

Method B: the procedure illustrated for method A was repeated by using Ru(TPP)(NAr)₂ (Ar = 3,5-(CF₃)₂C₆H₃) (**77**) (5.14 x 10⁻⁶ mol), tetrabutyl ammonium chloride (5.14 x 10⁻⁵ mol) and the epoxide (5.14 x 10⁻⁴ mol) in the molar ratio = 1/10/100 and benzene (3.3 mL) as the reaction solvent.

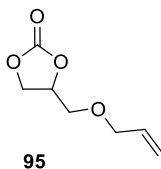
4.4.1. Synthesis of 4-phenyl-1,3-dioxolan-2-one (**94**)



The general catalytic procedure was followed using 2-phenyloxirane as reagent. The collected data are in accordance with those reported in literature.

¹H NMR (300 MHz, CDCl₃): δ 7.47 – 7.34 (m, 5H, H_{Ar}), 5.67 (t, *J* = 8.0 Hz, 1H, H_{CH}), 4.79 (t, *J* = 8.4 Hz, 1H, H_{CH₂}), 4.33 (t, *J* = 8.0 Hz, 1H, H_{CH₂})²⁸.

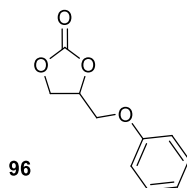
4.4.2. Synthesis of 4-((allyloxy)methyl)-1,3-dioxolan-2-one (**95**)



The general catalytic procedure was followed using 2-((allyloxy)methyl)oxirane as reagent. The collected data are in accordance with those reported in literature²⁹.

¹H NMR (300 MHz, CDCl₃): δ 6.00 – 5.86 (m, 1H, H, H_{CH}), 5.31 – 5.21 (m, 2H, H_{CH₂}), 4.86 – 4.75 (m, 1H, H, H_{CH}), 4.50 (t, *J* = 8.3 Hz, 1H, H_{CH₂}), 4.43 – 4.36 (m, 1H, H_{CH₂}), 4.07 (d, *J* = 4.6 Hz, 2H, H_{CH₂}), 3.71 – 3.59 (m, 2H, H_{CH₂}).

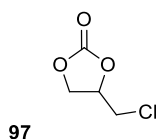
4.4.3. Synthesis of 4-(phenoxyethyl)-1,3-dioxolan-2-one (96)



The general catalytic procedure was followed using 2-(phenoxyethyl)oxirane as reagent. The collected data are in accordance with those reported in literature²⁸.

¹H NMR (300 MHz, CDCl₃): δ 7.30 (t, *J* = 8.3 Hz, 2H, H_{Ar}), 7.01 (t, *J* = 7.3 Hz, 1H, H_{Ar}), 6.92 (d, *J* = 7.9 Hz, 2H, H_{Ar}), 5.06 – 4.99 (m, 1H, H_{CH}), 4.64 – 4.58 (m, 1H, H_{CH2}), 4.54 – 4.50 (m, 1H, H_{CH2}), 4.28 – 4.09 (m, 2H, H_{CH2}).

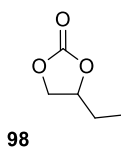
4.4.4. Synthesis of 4-(chloromethyl)-1,3-dioxolan-2-one (97)



The general catalytic procedure was followed using 2-(chloromethyl)oxirane as reagent. The collected data are in accordance with those reported in literature²⁸.

¹H NMR (400 MHz, CDCl₃): δ 5.09 – 4.89 (m, 1H, H_{CH}), 4.61 (t, *J* = 8.5 Hz, 1H, H_{CH2}), 4.45 – 4.38 (m, 1H, H_{CH2}), 3.75 (d, *J* = 5.1 Hz, 2H, H_{CH2}).

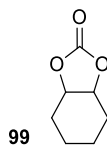
4.4.5. Synthesis of 4-ethyl-1,3-dioxolan-2-one (98)



The general catalytic procedure was followed using 2-ethyloxirane as reagent. The collected data are in accordance with those reported in literature²⁹.

¹H NMR (400 MHz, CDCl₃): δ 4.66 – 4.60 (m, 1H, H_{CH}), 4.46 (t, *J* = 8.2 Hz, 1H, H_{CH2}), 3.98 (t, *J* = 8.0 Hz, 1H, H_{CH2}), 1.60 – 1.66 (m, 2H, H_{CH2}), 0.97 (t, *J* = 7.4 Hz, 3H, H_{CH3}).

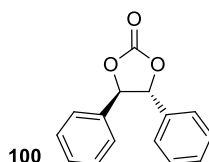
4.4.6. Synthesis of hexahydrobenzo[*d*][1,3]dioxol-2-one (99)



The general catalytic procedure was followed using 7-oxabicyclo[4.1.0]heptane as reagent. The collected data are in accordance with those reported in literature²⁹.

¹H NMR (400 MHz, CDCl₃): δ 4.69 – 4.64 (m, 2H, H_{CH}), 1.91 – 1.79 (m, 2H, H_{CH₂}), 1.72 – 1.50 (m, 4H, H_{CH₂}), 1.48 – 1.33 (m, 2H, H_{CH₂}).

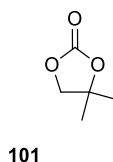
4.4.7. Synthesis of (4*R*,5*R*)-4,5-diphenyl-1,3-dioxolan-2-one (100)



The general catalytic procedure was followed using 2,3-diphenyloxirane as reagent. The collected data are in accordance with those reported in literature²⁹.

¹H NMR (300 MHz, CDCl₃): δ 7.51 – 7.45 (m, 6H, H_{Ar}), 7.35 – 7.36 (m, 4H, H_{Ar}), 5.44 (s, 2H, H_{CH}).

4.4.8. Synthesis of 4,4-dimethyl-1,3-dioxolan-2-one (101)



The general catalytic procedure was followed using 2,2-dimethyloxirane. The collected data are in accordance with those reported in literature²⁹.

¹H NMR (400 MHz, CDCl₃): δ 4.13 (s, 2H, H_{CH₂}), 1.91 (s, 6H, H_{CH₃}).

4.4.9. Recycle of the catalyst Ru(TPP)(NAr)₂ (Ar = 3,5-(CF₃)₂C₆H₃) (77)

The general catalytic procedure was followed using 2-((allyloxy)methyl)oxirane as reagent. The consumption of the aziridine was monitored by TLC analysis (*n*-hexane/AcOEt = 80:20). After the consumption of the starting material, 2-((allyloxy)methyl)oxirane was added again to the catalytic mixture for two more consecutive times. The NMR analysis of the crude revealed 99% of global yield of compound **95**.

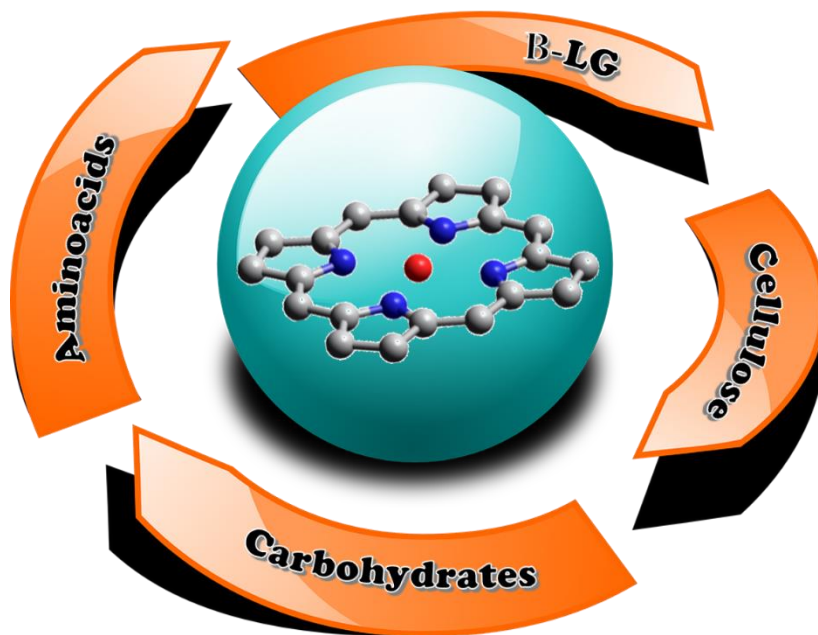
5. References

- (1) Aresta, M.; Dibenedetto, A.; Angelini, A. *Chem. Rev.* **2014**, *114* (3), 1709–1742.
- (2) Aresta, M.; Dibenedetto, A.; Quaranta, E. *J. Catal.* **2016**, *343*, 2–45.
- (3) Tenhumberg, N.; Büttner, H.; Schäffner, B.; Kruse, D.; Blumenstein, M.; Werner, T. *Green Chem.* **2016**, *18* (13), 3775–3788.
- (4) Büttner, H.; Steinbauer, J.; Wulf, C.; Dindaroglu, M.; Schmalz, H. G.; Werner, T. *ChemSusChem* **2017**, *10* (6), 1076–1079.
- (5) Nale, D. B.; Rana, S.; Parida, K.; Bhanage, B. M. *Appl. Catal. A Gen.* **2014**, *469*, 340–349.
- (6) Kim, J.-Y.; Kang, D.-J.; Lee, T.; Kim, K.-R. *Biogeosciences* **2014**, *11* (9), 2443–2454.
- (7) He, M.; Sun, Y.; Han, B. *Angew. Chemie Int. Ed.* **2013**, *52* (37), 9620–9633.
- (8) Alper, E.; Yuksel Orhan, O. *Petroleum* **2017**, *3* (1), 109–126.
- (9) Cokoja, M.; Bruckmeier, C.; Rieger, B.; Herrmann, W. A.; Kühn, F. E. *Angew. Chemie - Int. Ed.* **2011**, *50* (37), 8510–8537.
- (10) Omae, I. *Coord. Chem. Rev.* **2012**, *256* (13–14), 1384–1405.
- (11) Razali, N. A. M.; Lee, K. T.; Bhatia, S.; Mohamed, A. R. *Renew. Sustain. Energy Rev.* **2012**, *16* (7), 4951–4964.
- (12) Liu, Q.; Wu, L.; Jackstell, R.; Beller, M. *Nat. Commun.* **2015**, *6*, 1–15.
- (13) Langanke, J.; Wolf, A.; Peters, M. Styring, P., Quadrelli, E. A., Armstrong, K. B. T.-C. D. U., Eds.; Elsevier: Amsterdam, **2015**; 59–71.
- (14) Riemer, D.; Hirapara, P.; Das, S. *ChemSusChem* **2016**, *9* (15), 1916–1920.
- (15) Michalska, K.; Karpiuk, I.; Król, M.; Tyski, S. *Bioorg. Med. Chem.* **2013**, *21* (3), 577–591.
- (16) Heravi, M. M.; Zadsirjan, V.; Farajpour, B. *RSC Adv.* **2016**, *6* (36), 30498–30551.
- (17) Habisreutinger, S. N.; Schmidt-Mende, L.; Stolarczyk, J. K. *Angew. Chemie Int. Ed.* **2013**, *52* (29), 7372–7408.
- (18) Yamazaki, Y.; Takeda, H.; Ishitani, O. *J. Photochem. Photobiol. C Photochem. Rev.* **2015**, *25*, 106–137.
- (19) Intrieri, D.; Damiano, C.; Sonzini, P.; Gallo, E. *J. Porphyr. Phthalocyanines* **2019**, *23*, 3–24.
- (20) Shaikh, R. R.; Pornpraprom, S.; D’Elia, V. *ACS Catal.* **2018**, *8* (1), 419–450.
- (21) Liang, J.; Huang, Y.-B.; Cao, R. *Coord. Chem. Rev.* **2019**, *378*, 32–65.
- (22) Kamphuis, A. J.; Picchioni, F.; Pescarmona, P. P. *Green Chem.* **2019**, *21* (3), 406–448.
- (23) Ema, T.; Fukuhara, K.; Sakai, T.; Ohbo, M.; Bai, F.-Q.; Hasegawa, J. *Catal. Sci. Technol.* **2015**, *5* (4), 2314–2321.
- (24) Chen, Y.; Luo, R.; Yang, Z.; Zhou, X.; Ji, H. *Sustain. Energy Fuels* **2018**, *2* (1), 125–132.
- (25) Rillema, D. P.; Nagle, J. K.; Barringer, L. F.; Meyer, T. J. *J. Am. Chem. Soc.* **1981**, *103* (1), 56–62.

Chapter V: Ruthenium porphyrins for CO₂ cycloaddition to three-membered ring compounds

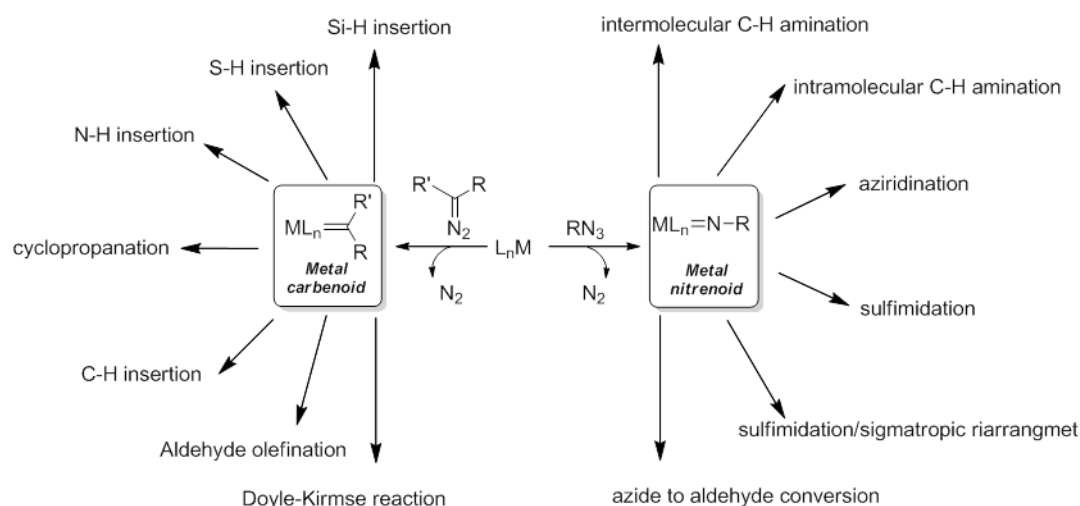
- (26) Fantauzzi, S.; Gallo, E.; Caselli, A.; Ragaini, F.; Casati, N.; MacChi, P.; Cenini, S. *Chem. Commun.* **2009**, 26, 3952–3954.
- (27) Du, Y.; Wu, Y.; Liu, A.-H.; He, L.-N. *J. Org. Chem.* **2008**, 73 (12), 4709–4712.
- (28) Clegg, W.; Harrington, R. W.; North, M.; Pasquale, R. *Chem. – A Eur. J.* **2010**, 16 (23), 6828–6843.
- (29) Steinbauer, J.; Spannenberg, A.; Werner, T. *Green Chem.* **2017**, 19 (16), 3769–3779.

Summary



Chapter I: General introduction

The chemical industry is ever more focused on the development of sustainable and selective procedures for the synthesis of high-added value fine chemicals, in order to meet the demand in society for environment-friendly chemical processes. The metal-catalysed carbene and nitrene transfer reactions have proved to be an excellent strategy to achieve the goal, due to their ability to form C-C, C-N and C-heteroatom bonds with high stereo- and regioselectivities. In addition, the good choice of the carbene and nitrene precursors can increase the reaction sustainability and the atom efficiency, as when diazo compounds and azides were used as starting materials thanks to the formation of molecular nitrogen as the only by-product of the reaction (Scheme 1).



Scheme 1: Metal-catalysed carbene and nitrene transfer reactions

Among all the metal-catalysed carbene and nitrene transfer reactions, the formation of three-membered ring compounds, such as cyclopropanes and aziridines, is a very attractive topic due to their use as building blocks in organic chemistry and their biological and/or pharmaceutical activity. Considering the catalytic activity of metal porphyrin complexes in promoting cyclopropanation and aziridination reactions of alkenes, the following PhD thesis aims to develop a new class of hybrid catalysts which are able to mediate carbene and nitrene transfer reactions under mild experimental conditions. In order to confer chiral recognition properties and modulate the catalyst properties, the conjugation of metal porphyrin complexes with bio-scaffolds such as carbohydrates, amino acids, cellulose and β -lactoglobulins was studied.

Chapter II: Glycoconjugated porphyrins

Carbohydrates are natural chiral, polyhydroxylated compounds which play critical roles in several biological processes, including the energy storage, cellular communications and recognitions, and the immune system maintenance. Glycoporphyrins, derived from the conjugation of porphyrin rings with

sugar units, are efficient photosensitizers extensively used in photodynamic therapy (PDT) and they are desirable ligands for organometallic synthesis.

To assess how different glycosylated porphyrin ligands can influence the catalytic activity of corresponding ruthenium and iron complexes, different *meso* glycosyl-conjugated porphyrins were synthesised. The number and position of carbohydrate units on the porphyrin skeleton play an important role in determining the ligand chemo-physical properties. *Mono* and *tetra*-glycosylated porphyrins were synthesised and the corresponding iron and ruthenium complexes (Figure 1) were tested as catalysts of cyclopropanation and aziridination reactions.

In the model cyclopropanation reaction between α -methylstyrene and EDA, Fe(III)(porphyrin)OMe complexes showed higher activity than Ru(II)(porphyrin)CO derivatives and obtained data indicated the strong dependence of the reaction diastereoselectivity on the ligand structure. Among all the iron complexes which were tested as cyclopropanation catalysts, Fe(**15**)OMe complex was chosen to study the reaction scope by testing different styrenes in view of the good compromise between the synthetic accessibility of synthesizing it and reaction productivity (yields and diastereoselectivities). All the desired cyclopropanes were obtained in very good yields (up to 80%) and *trans*-diastereoselectivities (up to 98:2).

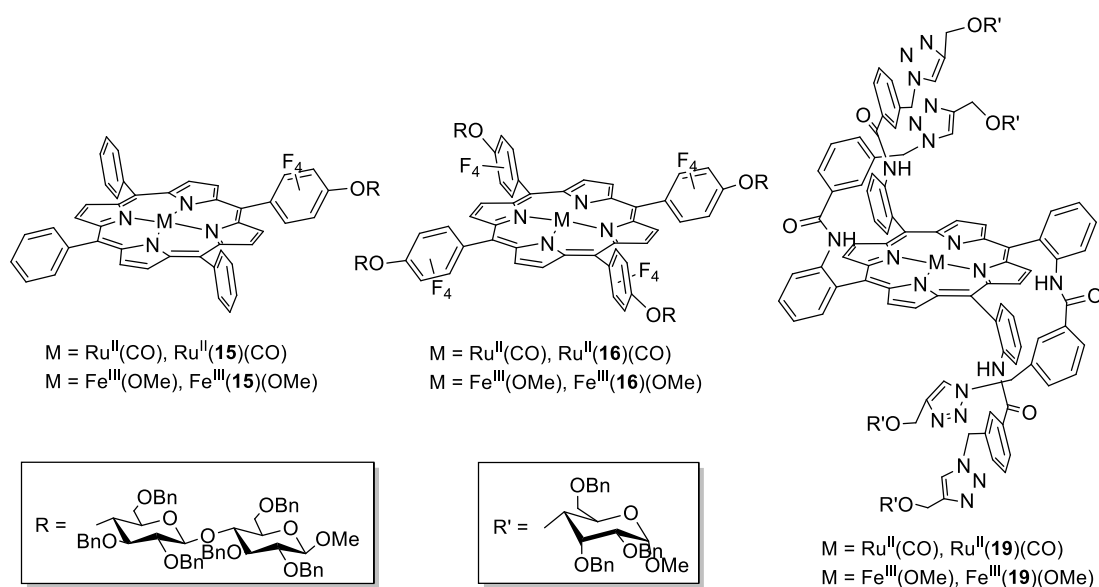


Figure 1: Iron(III) and ruthenium(II) glycoporphyrin complexes

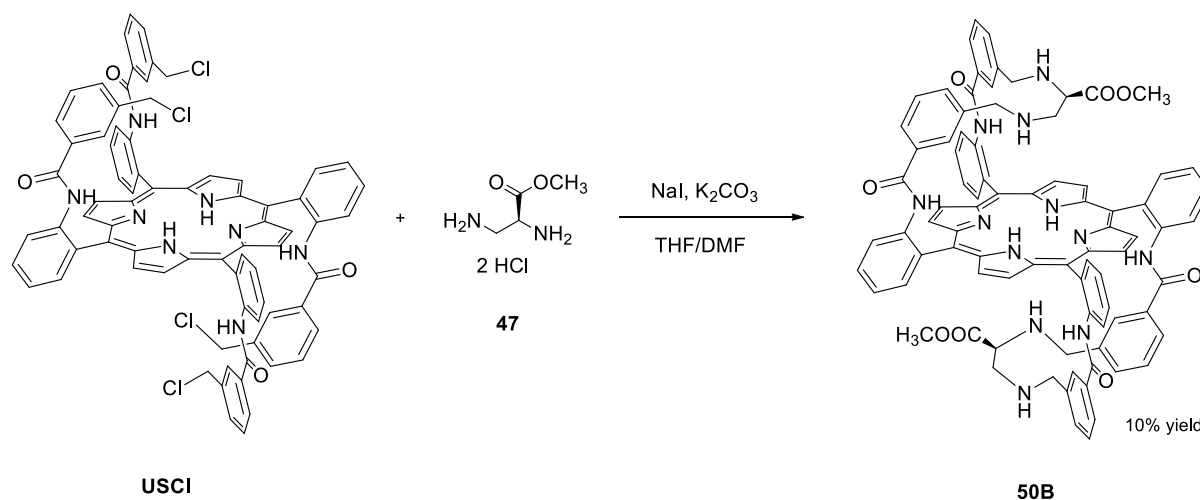
The obtained iron and ruthenium glycoporphyrin complexes were also tested in the model aziridination reaction between α -methylstyrene and 3,5-*bis*-(trifluoromethyl)phenylazide. Unfortunately, Fe(III)(porphyrin)OMe complexes didn't catalyse the aziridination reaction but the desired product was obtained in a very good yield (83%) in the presence of Ru(**15**)CO. The latter catalyst was used to study the reactivity of α -methylstyrene towards different aryl azides and the obtained data indicated the ability of Ru(**15**)CO to promote the aziridination of azides showing different electronic and steric nature. Low

yields were obtained in the presence of coordinating methoxy groups which can be responsible for the catalyst deactivation.

Obtained results showed the applicability of Fe(**15**)OMe and Ru(**15**)CO as catalysts for the synthesis of three-membered ring compounds and the amphiphilic nature of ligand **15** can be suitable, after deprotection of the saccharide units, to perform catalytic reactions in biphasic systems.

Chapter III: Hybrid *bis*-strapped porphyrin

The second biomolecules class that has been studied in this thesis consists of aminoacidic residues. In order to synthesise new bio-inspired catalysts, the conjugation of $\alpha_2\beta_2$ USCl porphyrin with the DAP aminoacid was studied. The desired product can be formed as a mixture of two different regioisomers. A similar ligand was obtained by reacting USCl porphyrin with the methyl ester of DAP aminoacid (Scheme 1). The presence of different porphyrin derivatives was revealed by the ^1H NMR analysis where several tetrapyrrolic NH signals, as well as different β -pyrrole proton signals, were detected at very high fields indicating the presence of different conformations of the ligand skeleton. The **50B** regioisomer of the desired *bis*-strapped porphyrin was isolated in 10% yield and characterized by NMR spectroscopy. The new ligand was used to synthesise the corresponding iron(III) complex, which was tested to promote the cyclopropanation reaction.



Scheme 1: Synthesis of *bis*-strapped porphyrin **50B**

In the optimised conditions, the Fe(**50B**)OMe complex was very active in promoting the reaction between α -methylstyrene and EDA, forming the desired cyclopropane in 99% yield and a *trans/cis* ratio of 90:10. Considering the very good result obtained in the model reaction, the catalytic performance of Fe(**50B**)OMe was tested in the presence of different substituted alkenes. Very good results were achieved in terms of yields (up to 99%) and diastereoselectivities (up to 99:1). Under the optimized catalytic

conditions, the desired cyclopropanes were formed in quantitative yields; lower yields were observed by using 0.001 mol % of Fe(**50B**)OMe due to the low conversion of the starting diazo compound.

Obtained data showed the applicability of Fe(**50B**)OMe as an efficient catalyst for carbene transfer reactions. In addition, the presence of carboxylic groups on the porphyrin strap makes the synthesised hybrid ligand suitable for the conjugation with long water soluble chains, like PEG, in order to perform catalytic reaction in biphasic systems.

Chapter IV: Porphyrins for conjugation with macromolecules

Besides the conjugation of porphyrin ligands with small bio-scaffolds, like sugars and aminoacids, new *mono*-substituted porphyrins were designed and synthesized (Figure 2) for their conjugation with cellulose and β -lactoglobuline proteins. In order to develop metal porphyrin complexes supported on cellulose, ligands **71** and **72**, with amino groups onto the *para* position of one porphyrin ring phenyl group, were synthesized. Ligand **73** was synthesized with a long aliphatic chain that can be accommodated inside the three-dimensional structure of β -lactoglobulin protein by hydrophobic interactions.

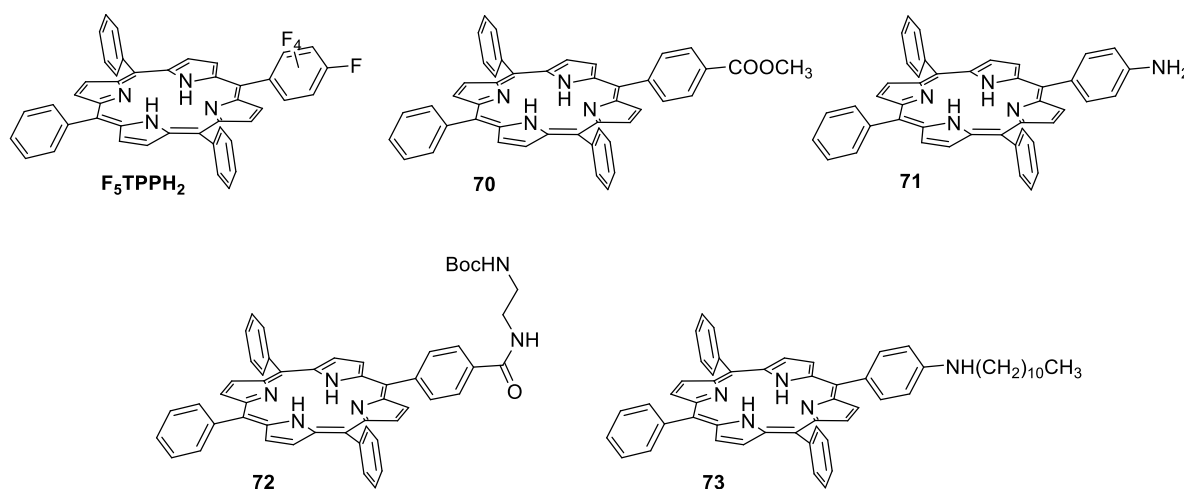


Figure 2: *Mono*-substituted porphyrins synthesised

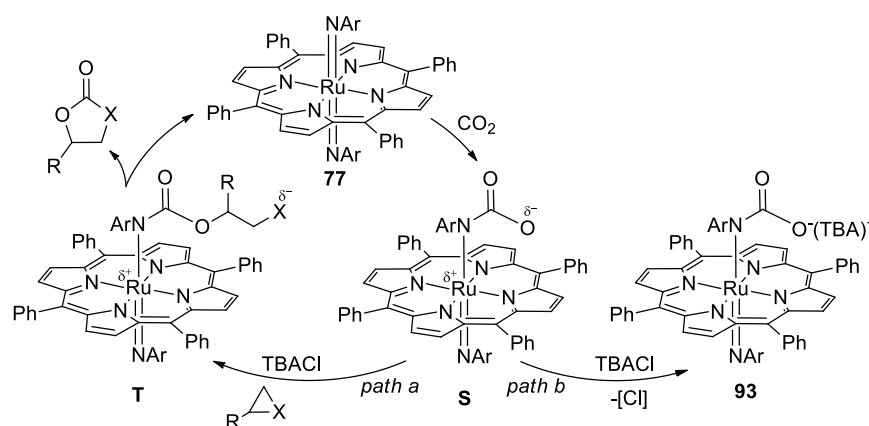
Preliminary studies were performed for the conjugation of porphyrin **71** with a cellulose derivative functionalised with aldehyde groups. The conjugated material was obtained by a reductive amination reaction and then reacted with FeBr₂ affording the corresponding iron(III) complex. Preliminary tests as cyclopropanation catalyst revealed the ability of the cellulose-based iron catalyst to promote the reaction between α -methylstyrene and EDA, forming the desired cyclopropane in 15% yield and a *trans/cis* ratio of 97:3.

The promising result suggested the potential use as cyclopropanation catalyst of the conjugated heterogeneous species. Considering that metal porphyrin complexes show high activity in promoting

carbene and nitrene transfer reactions, the obtained data represent a starting point to develop a new generation of catalysts which can be employed for the synthesis of several fine chemicals through sustainable synthetic methodologies.

Chapter V: Ruthenium porphyrins for CO₂ cycloaddition to three-membered ring compounds

For developing sustainable and selective procedures for the synthesis of high-added value fine chemicals, a part of the PhD thesis was devoted to the study of the CO₂ cycloaddition to three membered ring compounds in the presence of metal porphyrin complexes. Ruthenium *bis-imido* porphyrins were able to catalyse the regioselective cycloaddition of CO₂ to aziridines to form oxoazolidinones, as reported in a previous PhD work. The catalytic performances of Ru(TPP)(NAr)₂ (Ar = 3,5-(CF₃)₂C₆H₃) (**77**) were also tested in the CO₂ cycloaddition to epoxides. Very good results were obtained in the synthesis of different cyclic carbonates and the formation of the ruthenium species, Ru(TPP)(NAr)(ArNCOO⁻TBA⁺) (**93**), suggested the fundamental role of *imido-axial* ligand in activating CO₂. The results, achieved in the CO₂ cycloaddition of both epoxides and aziridines, suggested a mechanism in which the interaction of CO₂ with the nitrogen imido atom is the first step of the reaction (Scheme 3). This hypothesis is supported by the very high electron density on the nitrogen atom due to the linkage with ruthenium, as indicated by a previous DFT study. Future kinetics and DFT studies of the reaction between *bis-imido* complexes and CO₂ could be useful to shed some light on the reaction mechanism.



Scheme 3. Proposed mechanism for the CO₂ cycloaddition to three-membered ring compounds

Considering the high activity of ruthenium porphyrin complexes to promote alkene aziridination reactions, the obtained data are the starting point to develop a catalytic system in which the same catalyst can be able to promote both the synthesis of aziridines and their transformation into oxazolidinones in a two-steps one-pot reaction which affords added value compounds in an efficient and sustainable way.

List of publications

1. **C. Damiano**, D. Intrieri, S. Le Gac, B. Boitrel and E. Gallo, “Hybrid bis-strapped porphyrin complexes: efficient catalysts for promoting cyclopropanation reactions” submitted to *Eur. J. Chem*
2. **C. Damiano**, P. Sonzini, D. Intrieri and E. Gallo, “Synthesis of cyclic carbonates by ruthenium(VI)bis-imido porphyrin/TBACl-catalysed reaction of epoxide with CO₂”, *J. Porphyrins Phthalocyanines*, accepted
3. D. Intrieri, D. M. Carminati, P. Zardi, **C. Damiano**, G. Manca, E. Gallo and C. Mealli, “Indoles from Alkynes and Aryl Azides. Scope and Theoretical Assessment of Ruthenium Porphyrin-Catalyzed Reactions”, *Chem. Eur. J.*, accepted
4. **C. Damiano**, S. Gadolini, D. Intrieri, L. Lay, C. Colombo and E. Gallo, “Iron and Ruthenium Glycoporphyrins: Active Catalysts for the Synthesis of Cyclopropanes and Aziridines”, *Eur. J. Inorg. Chem.*, article in press [DOI:10.1002/ejic.201900829](https://doi.org/10.1002/ejic.201900829)
5. D. Intrieri, **C. Damiano**, P. Sonzini and E. Gallo, “Porphyrin-based homogeneous catalysts for the CO₂ cycloaddition to epoxides and aziridines”, *J. Porphyrins Phthalocyanines*, **2019**, 23, 3-24. [DOI:10.1142/S1088424619300015](https://doi.org/10.1142/S1088424619300015)
6. D. Carminati, E. Gallo, **C. Damiano**, A. Caselli and D. Intrieri, “Ruthenium Porphyrin-Catalyzed Synthesis of Oxazolidin-2-ones by Cycloaddition of CO₂ to Aziridines”, *Eur. J. Inorg. Chem.*, **2018**, 48, 5258-5262. [DOI:10.1002/ejic.201801208](https://doi.org/10.1002/ejic.201801208)
7. D. Intrieri, **C. Damiano**, S. Rizzato, R. Paolesse, M. Venanzi, D. Monti, M. Savioli, M. Stefanelli and E. Gallo, “Sensing of Diclofenac by a Porphyrin-based Artificial Receptor” *New J. Chem.*, **2018**, 42, 15778–15783. [DOI:10.1039/C8NJ02737D](https://doi.org/10.1039/C8NJ02737D)
8. **C. Damiano**, D. Intrieri and E. Gallo, “Aziridination of alkenes promoted by Iron or Ruthenium complexes”, *Inorganica Chimica Acta*, **2017**, 470, 51-67. [DOI:10.1016/j.ica.2017.06.032](https://doi.org/10.1016/j.ica.2017.06.032)

